New Targeting Opportunities in Isocitrate Dehydrogenase (IDH)-Wildtype Glioblastoma

By

Elvis Martinez -Jaramillo, M.D., M.Sc.

Department of Pathology

McGill University

Montreal, Canada

December 2023

A thesis submitted to McGill University in partial fulfillment of the requirements of the degree of Doctor of Philosophy

TABLE OF CONTENTS

ABSTRACT

Isocitrate Dehydrogenase (IDH)-wildtype Glioblastoma (GBM) is the most common and aggressive malignant primary brain tumour in adults, it has a very poor prognosis with a median survival of 14.6 months. Several mechanisms account for the dismal outcome including: (i) The activation of epidermal growth factor receptor (EGFR)-induced pathways in 40–60% of primary GBMs contributes to faulty DNA repair mechanisms. EGFR variant III (EGFRvIII), the most common mutation, results in a ligand-independent and constitutively active receptor and more aggressive disease; (ii) An imbalance in reactive oxygen species (ROS) and antioxidants. The antioxidant systems involving thioredoxin (Trx) and glutathione (GSH) play a key role in regulating the intracellular redox balance to protect cells from ROS-induced damage. To keep the redox balance and survive after therapy, cancer cells increase their antioxidant systems to counteract their augmented ROS levels. Consequently, redox regulation represents a potential therapeutic target to overcome drug-induced resistance in cancer. Thioredoxin Reductase 1 (TrxR1) is part of the Trx system, and it can decrease the level of ROS. High levels of TrxR1 are correlated with cancer progression in many malignancies.

Auranofin is an FDA- approved drug for rheumatoid arthritis, it is very well tolerated, it crosses the blood brain barrier (BBB) and primarily targets TrxR1 leading to ROS increase. We hypothesized that auranofin as a ROS inducer might sensitize GBM cells to the cytotoxicity of EGFR inhibitors. ZR2002 is a single combi-molecule designed to target EGFR with its tyrosine kinase inhibitor moiety while inflicting DNA damage to overcome the protective effect of EGFR-induced DNA repair. ZR2002 induces high levels of DNA damage with concomitant inhibition of EGFR-mediated MAPK/ERK and PI3K/AKT signaling pathways. ZR2002 had significantly

higher cytotoxic activity than Temozolomide (TMZ) or gefitinib (clinically approved tyrosine kinase inhibitor), it crossed the BBB and significantly increased survival in highly aggressive intracranial mouse models of GBM.

Auranofin, gefitinib, and ZR2002 were assessed in U87MG, U87EGFRwt, and U87EGFRvIII GBM cell lines. All cell lines treated with ZR2002 experienced cytotoxic effects at very low concentrations. The combination index for auranofin and gefitinib indicated synergistic effects at different ratios of their respective IC_{50s}, while this was not the case for auranofin and ZR2002.

Auranofin produced cytotoxic effects at very low concentrations and reduced the clonogenic potential. The cell death mechanism found was apoptosis which occurred in a dose-dependent manner. Although auranofin increased EGFR phosphorylation, the phosphorylation of AKT was significantly decreased. While auranofin did not decrease TrxR expression, it significantly reduced TrxR activity in the three cell lines using low concentration. Auranofin increased ROS levels in all cell lines and N-acetylcysteine (NAC), a ROS scavenger prevented its cytotoxic effect, suggesting the main mechanism of action of auranofin is the elevation of ROS. The results using a combination approach with auranofin provide the proof-of- concept to implement a new strategy to overcome drug resistance in GBM patients. Using GBM cell lines isogenic for EGFRwt and EGFRvIII, we provide the first evidence that auranofin equally decreased their viability and clonogenic potential through an ROS-dependent mechanism. We further demonstrate that auranofin together with L- buthionine sulfoximine (L-BSO) produces synergistic lethality in GBM cells irrespective of the subtype of EGFRwt and EGFRvIII overexpression. These findings reveal EGFRwt and EGFRvIII as potential vulnerabilities for Trx/GSH co-targeting in GBM.

RÉSUMÉ

Le glioblastome de type sauvage (GBM) à isocitrate déshydrogénase (IDH) est la tumeur cérébrale maligne primitive la plus courante et la plus agressive chez les adultes, il a un très mauvais pronostic avec une survie médiane de 14,6 mois. Plusieurs mécanismes expliquent ce résultat lamentable, notamment : (i) L'activation des voies induites par le récepteur du facteur de croissance épidermique (EGFR) dans 40 à 60 % des GBM primaires contribue à des mécanismes défectueux de réparation de l'ADN. La variante III de l'EGFR (EGFRvIII), la mutation la plus courante, aboutit à un récepteur indépendant du ligand et constitutivement actif et à une maladie plus agressive ; (ii) Un déséquilibre entre les espèces réactives de l'oxygène (ROS) et les antioxydants. Les systèmes antioxydants impliquant la thiorédoxine (Trx) et le glutathion (GSH) jouent un rôle clé dans la régulation de l'équilibre rédox intracellulaire afin de protéger les cellules des dommages induits par les ROS. Pour maintenir l'équilibre redox et survivre après le traitement, les cellules cancéreuses augmentent leurs systèmes antioxydants pour contrecarrer l'augmentation des niveaux de ROS. Par conséquent, la régulation redox représente une cible thérapeutique potentielle pour vaincre la résistance induite par les médicaments dans le cancer. La thiorédoxine réductase 1 (TrxR1) fait partie du système Trx et peut diminuer le niveau de ROS. Des niveaux élevés de TrxR1 sont corrélés à la progression du cancer dans de nombreuses tumeurs malignes.

L'auranofine est un médicament approuvé par la FDA pour le traitement de la polyarthrite rhumatoïde. Il est très bien toléré, il traverse la barrière hémato-encéphalique (BHE) et cible principalement TrxR1, entraînant une augmentation des ROS. Nous avons émis l'hypothèse que l'auranofine, en tant qu'inducteur de ROS, pourrait sensibiliser les cellules GBM à la cytotoxicité des inhibiteurs de l'EGFR. ZR2002 est une molécule combinée unique conçue pour cibler l'EGFR

avec son fragment inhibiteur de tyrosine kinase tout en infligeant des dommages à l'ADN pour surmonter l'effet protecteur de la réparation de l'ADN induite par l'EGFR. ZR2002 induit des niveaux élevés de dommages à l'ADN avec une inhibition concomitante des voies de signalisation MAPK/ERK et PI3K/AKT médiées par l'EGFR. Le ZR2002 avait une activité cytotoxique significativement plus élevée que le témozolomide (TMZ) ou le géfitinib (inhibiteur de la tyrosine kinase cliniquement approuvé), il a traversé la BHE et a significativement augmenté la survie dans des modèles murins intracrâniens très agressifs de GBM.

L'auranofine, le géfitinib et le ZR2002 ont été évalués dans les lignées cellulaires U87MG, U87EGFRwt et U87EGFRvIII GBM. Toutes les lignées cellulaires traitées avec ZR2002 ont présenté des effets cytotoxiques à de très faibles concentrations. L'indice de combinaison de l'auranofine et du géfitinib a indiqué des effets synergiques à différents rapports de leurs IC50 respectives, alors que ce n'était pas le cas pour l'auranofine et le ZR2002.

L'auranofine produit des effets cytotoxiques à de très faibles concentrations et réduit le potentiel clonogénique. Le mécanisme de mort cellulaire découvert était l’apoptose, qui se produisait de manière dose-dépendante. Bien que l'auranofine ait augmenté la phosphorylation de l'EGFR, la phosphorylation de l'AKT a été significativement diminuée. Bien que l'auranofine n'ait pas diminué l'expression de TrxR, elle a considérablement réduit l'activité de TrxR dans les trois lignées cellulaires en utilisant une faible concentration. L'auranofine a augmenté les niveaux de ROS dans toutes les lignées cellulaires et la N-acétylcystéine (NAC), un piégeur de ROS, a empêché son effet cytotoxique, ce qui suggère que le principal mécanisme d'action de l'auranofine est l'élévation des ROS. Les résultats utilisant une approche combinée avec l'auranofine fournissent la preuve de concept pour mettre en œuvre une nouvelle stratégie visant à vaincre la résistance aux médicaments chez les patients atteints de GBM. En utilisant des lignées cellulaires

GBM isogéniques pour EGFRwt et EGFRvIII, nous fournissons la première preuve que l'auranofine diminue également leur viabilité et leur potentiel clonogénique par le biais d'un mécanisme dépendant des ROS. Nous démontrons en outre que l'auranofine et la L-butthionine sulfoximine (L-BSO) produisent une létalité synergique dans les cellules GBM, quel que soit le sous-type de surexpression d'EGFRwt et d'EGFRvIII. Ces résultats révèlent EGFRwt et EGFRvIII comme vulnérabilités potentielles pour le co-ciblage Trx/GSH dans GBM.

ACKNOWLEDGEMENTS

I would like to express my sincere gratitude to all those who have supported and encouraged me throughout my doctoral journey. First and foremost, I would like to thank my supervisor Dr. Carlos Telleria, for their invaluable guidance, expertise, and patience during the research process. I would like to extend my heartfelt gratitude to my former supervisor, Dr. Siham Sabri, for their indispensable guidance, expertise, and unwavering support throughout my research. Their extensive knowledge and invaluable insights have been instrumental in helping me overcome challenges and achieve my objectives.

I am also indebted to the members of my Advisor committee members, Dr. Carolyn Baglole and Dr. Sabah Hussein, for their insightful feedback and constructive criticism. Their expertise in their respective fields has been invaluable in shaping this research. I am grateful to Dr. Bertrand Jean-Claude, Dr. Bassam Abdulkarim, Julie Schmitt, Alicia Goyeneche who generously gave their time and shared their experiences and support for this research.

I would like to express my gratitude to Dr. Edith Zorychta and Hua Ling for their exceptional support and dedication.

My colleagues, Fatemeh Jamali, Katherine Lan, Monisha Bagchi, Aymane Deiri, Zeinab Shariff, Rehka Raveendrakumar, Leonardo Jurado, Sara Teimouri, Prisca Bustamante, Constanza Martínez, Sabrina Ritch, Mahbuba Subeha, Rob Dube, Farah Abdalbari, Rewati Prakash, Ben Forgie, and Naya El Mokbel have been an endless source of inspiration, supporting me during difficult times and celebrating my successes with me.

I would like to thank Salvador Flores and Ivan Martinez for their advice and conversations. I thank Hugo Cere, who always helped me when working late, saving me often with dinner and

coffee. Thank Fannie C. Lemieux, who not only helped me and allowed me to live in a perfect and cozy place in Montreal during my PhD journey but also taught me about the unlimited aspects of life in Montreal and Canada. I am grateful to them for their unyielding friendships and camaraderie.

The unwavering faith, support, and encouragement of my family Fina, Brayant, Karisma, Ivan, Renata, and Alison have been a constant source of motivation and inspiration throughout my doctoral studies. I am grateful for their belief in me.

I am grateful to The Mexican National Council for Science and Technology (CONACYT) Scholarship (#493862) and Fonds de recherche du Québec - Santé (FRQS) (#277270), and Department of Pathology of McGill University for their financial assistance.

Finally, I would like to acknowledge the individuals who have passed away during my PhD training. My grandmother who left us during pandemic, my stepfather and Carlos cleaner of McGill who were cancer fighters. Although they are no longer with us, their impact on my life and my research will never be forgotten. Their absence is deeply felt, and I am grateful for the time I had with them.

Thank you all for your invaluable support and encouragement throughout my doctoral journey.

CONTRIBUTION TO ORIGINAL KNOWLEDGE

1. In this study, we report different targeting strategies to overcome compensatory mechanisms in the context of EGFR wild type or EGFRvIII overexpression in glioblastoma. Aberrant expression of EGFR is highly relevant, as EGFR alterations have recently been used as a molecular criterion that is diagnostic in GBM despite the absence of malignant histological features. The frequency of amplification and overexpression is linked to the aggressive behaviour and dismal prognosis for this group of patients.
2. Auranofin/L-BSO combination treatment has potent synergistic cytotoxicity against GBM cell lines with aberrant EGFR expression through a ROS-dependent mechanism. This combination induced downregulation of AKT and EGFR in U87EGFRvIII cells; these effects were less evident in U87EGFRwt cells, which could explain the slightly less sensitivity to the treatment combination. However, the combination of auranofin/L-BSO effectively killed U87MG, U87EGFRwt and U87EGFRvIII cells, rendering a synergistic combination index in all cells. These results suggest that targeting TrxR and GSH pathways is a promising strategy for treating EGFR-driven GBM tumours. We do not discard other off-targeted mechanisms, and pleiotropic effects might be involved in this potent combination. Additional studies are warranted to investigate co-targeting Trx and GSH antioxidant systems as a therapeutic strategy in GBM.
3. Antagonistic effects were observed in the combination of auranofin and ZR2002 when treating U87MG, U87EGFRwt and U87EGFRvIII cells, despite both drugs being very potent as single treatments. Although cytotoxic effects were evident in the simultaneous drug co-treatment, the drug interaction analysis showed largely antagonistic and minor additive effects. Whether direct drug-drug interaction or opposite downstream signalling

pathways are the mechanisms responsible remains unknown. A significant decrease in vitality was observed during the first 24 hours of sequential treatment with ZR2002 for two or four hours of pretreatment, followed by 72 hours treatment of auranofin. These suggest that some drug incompatibilities may occur when auranofin and ZR2002 are used simultaneously, and to overcome this issue, a sequential drug combination strategy may lead to more efficient results.

4. Synergistic effects *in vitro* were also evident in the combination treatment of auranofin and gefitinib in U87MG, U87EGFRwt and U87EGFRvIII cells. This finding is interesting as both drugs are FDA-approved, and assessing the combination's efficacy in clinical trials could be easier to perform. This also encourages evaluating new generations of tyrosine kinase inhibitors that may lead to potentiation/sensitizing effects in GBM. Additional studies are warranted to investigate this strategy combination preclinically *in vivo* and in clinical trials.
5. A combi-molecule strategy, where two active moieties of different drugs with distinct mechanisms of action are constructed in a single molecule, was assessed in two cancer cell models. JS440 possesses gefitinib and PRIMA-1^{Met} components while JS470 has moieties of Olaparib and PRIMA-1^{Met}; the combi-molecules JS440 and JS470 did not demonstrate superior cytotoxic effects in comparison to their corresponding individual drugs added in equimolar concentrations in GMB and ovarian cancer cells, respectively. Compared to the ZR2002 combi-molecule, which has demonstrated a low IC_{50} in different cancer cells, the combi-molecules JS440 and JS470 do not have a DNA-alkylating mechanism, which suggests targeting DNA is still a relevant mechanism that combi-molecules need to include to maximize lethality.

CONTRIBUTION OF AUTHORS

This doctoral thesis is the product of original research conducted by Elvis Martinez-Jaramillo, under the supervision of Dr. Carlos Telleria. The thesis adheres to the traditional format and follows the *Guideline for Thesis Preparation from McGill University.*

Elvis Martinez-Jaramillo performed, organized, and analyzed every experiment described in this thesis, with the guidance of Dr. Siham Sabri, Dr. Carlos Telleria, Dr. Alicia Goyeneche and Dr. Zorychta. Fatemeh Jamali helped this work with Figure 3.11E for the analysis of TCGA data correlation.

LIST OF FIGURES

CHAPTER 1

LIST OF TABLES

LIST OF ABBREVIATIONS

$^1O_2$	Singlet oxygen
7-AAD	7-aminoactinomycin D
AAAIR	Annual Age-Adjusted Incidence Rate
AAPA	2-acetylamino-3-[4-(2-acetylamino-2-carboxyethylsulfanylthiocarbonylamino)phenylthiocarbamoylsulfanyl]propionic acid
ABC	ATP-binding cassette
ADC	Antibody-drug conjugated form
AED	Anti-epileptic drugs
AIC	5-amino-imidazole-4-carboxamide
AKT	Protein kinase B (PKB)
ALL	Acute lymphoblastic leukemia
AML	Acute myeloid leukemia
APL	Acute promyelocytic leukemia
APNG	Alkylpurine-DNA-N-glycosylase
AQPs	Aquaporins/peroxiporins
AR	Amphiregulin
AREs	Antioxidant responsive elements
ASK1	Apoptosis signal-regulated kinase 1
ATCC	American Type Culture Collection
ATM	Ataxia telangiectasia mutated
ATP	Adenosine triphosphate
ATR	Ataxia telangiectasia and Rad3-related protein
AU	Auranofin
Bax	BCL2 Associated X, Apoptosis Regulator
BBB	Blood-brain barrier
BCA	Bicinchoninic acid
BER	Base excision repair
BEV	Bevacizumab

BRAF	B-Raf proto-oncogene, serine/threonine kinase
BRCA	Breast cancer gene
BTICs	Brain-tumor initiating (stem) cells
BZ	Bortezomib
CAR T	Chimeric antigen receptor T
CAT	Catalase
Cat	Catalog
Cbl	Casitas B-lineage Lymphoma
CBTRUS	Central Brain Tumor Registry of the United States
CCR	Canadian Cancer Registry
CDK	Cyclin dependent kinase
CDKN2	Cyclin-dependent kinase inhibitor 2
CGGA	Chinese Glioma Genome Atlas
CHOP	C/EBP Homologous Protein
CHORDC1	Cysteine and Histidine Rich Domain Containing 1
CI	Combination index
CLL	Chronic lymphocytic leukemia
CM-H2DCFDA	2',7'-dichlorodihydrofluorescein diacetate
CML	Chronic myelogenous leukemia
CNS	Central Nervous System
CO_2	Carbon dioxide
CO_3•-	Carbonate radical anion
COX-2	Cyclooxygenase-2
CSCs	Cancer stem cells
CUSP9v3	Coordinated Undermining of Survival Paths combining 9 repurposed non-oncological drugs with metronomic temozolomide-version 3
Cys	Cysteine
DAPI	4′,6-diamidino-2-phenylindole
DDR	DNA damage response
DEVD	DNA-binding peptide; substrate for caspase-3

DHE	Dihydroethidium
DMEM	Dulbecco's Modified Eagle Medium
DMF	Dimethylfumarate
DMSO	Dimethyl sulfoxide
DNA	Deoxyribonucleic acid
DNA-PK	DNA-dependent protein kinase
DSBs	Double-strand breaks
DTNB	5,5'-dithiobis (2-nitrobenzoic) acid
DTT	Dithiothreitol
DUBs	Deubiquitinases
EA	Ethacrynic acid
EC	Endothelial cells
EC_{50}	50% of the maximum cytotoxic effect
ECD	Extracellular domain
ecDNA	Extrachromosomal DNA
ECL	Enhanced chemiluminescence
ECM	Extracellular matrix
EGF	Epidermal growth factor
EGFR	Epidermal growth factor receptor
EGFRvIII	EGFR variant III
EGFRwt	EGFR wildtype
em	Emission
EORTC	European Organization for Research and Treatment of Cancer
EPR	Epiregulin
ER	Endoplasmic reticulum
ERK	Extracellular signal-regulated kinase
ETC	Electron transport chain
ex	Excitation
FACS	Fluorescence activating cell sorting
FADD	Fas-associated death domain

FBS	Fetal Bovine Serum
FDA	US Food and Drug Administration
FGFR	Fibroblast growth factor receptor
FISH	Fluorescence in situ hybridization
GADD45A	Growth arrest and DNA-damage-inducible alpha
GBM	Glioblastoma
GEF	Gefitinib
GFAP	Glial fibrillary acidic protein
GOF	Gain-of-function
GPx	Glutathione peroxidase
GPX1	Glutathione Peroxidase 1
Grb2	Growth Factor Receptor Bound Protein 2
GRP78	Glucose-Regulated Protein 78
GSC	Glioblastoma stem cells
GSH	Glutathione
GSR	Glutathione-disulfide reductase/glutathione reductase
GSSG/GSSH	Glutathione disulfide
GST	Glutathione S-transferase
GTP	Guanine triphosphate
Gy	Gray
h	Hours
H2AX	Histone variant H2AX
H_2O_2	Hydrogen Peroxide
HCl	Hydrochloric Acid
HDAC	Histone deacetylases
HEPES	4-(2-hydroxyethyl)-1-piperazine ethane sulfonic acid
HER	Human epidermal growth factor receptor
HGSOC	High-Grade Serous Ovarian Cancer
HIF	Hypoxia inducible factor
HOCl	Hypochlorous acid

HR	Homologous recombination
HRP	Horseradish peroxidase
HSR	Homogeneous staining regions
IC_{50}	Half-maximal inhibitory concentration
IDH	Isocitrate dehydrogenase
IGFR	Insulin-like growth factor receptor
IgG	Immunoglobulin G
IHC	Immunohistochemical
iJM	Intracellular juxtamembrane domain
IL	Interleukin
iNOS	Inducible nitric oxide synthase
IR	Ionizing radiation
JAK	Janus kinase
kDa	Kilodaltons
Keap1	Kelch like ECH-associated protein 1
KILLER/DR5	Death receptor 5
KPS	Karnofsky Performance Scale
L-BSO	L-buthionine-sulfoximine
LGG	Low Grade Glioma
LigIII	Ligase III
LOH	Loss of heterozygosity
L-PAM	Melphalan
mAbs	Monoclonal antibodies
MAPK	Mitogen-activated protein kinase
MDM2	Mouse double minute 2 homolog
Met	Mesenchymal-epithelial transition factor
MGd	Motexafin gadolinium
MGMT	O-6-methylguanine-DNA methyltransferase
min	Minutes
MMP	Mitochondrial transmembrane potential

MMR	Mismatch repair
MQ	Methylene quinuclidinone
MRI	Magnetic resonance imaging
MSO	Methionine sulfoximine
MTIC	5-(3-methyltriazen-1-yl) imidazole-4-carboxamide
mTOR	Mammalian target of rapamycin
MTT	3-(4,5-dimethylthiazol-2-yl)-2,5-diphenyltetrazolium bromide
mutp53	Mutant p53
MVP	Microvascular proliferation
n.s.	Non-significant
NAC	N-acetylcysteine
NAD	Nicotinamide adenine dinucleotide
NADPH	Nicotinamide adenine dinucleotide phosphate
NANO	The Neurologic Assessment in Neuro-Oncology
NCCN	The National Comprehensive Cancer Network
NCICCTG	National Cancer Institute of Canada Clinical Trials Group
NCT	The (USA) National Clinical Trial number
NER	Nucleotide excision repair
NF1	Neurofibromatosis type 1
NF-κB	Nuclear factor kappa-light-chain-enhancer of activated B cells
NHAs	Normal human astrocytes
NHEJ	Non-homologous end-joining
NO•	Nitric oxide
NO_2•	Nitrogen dioxide
NONO	Non-POU domain-containing octamer-binding protein
NOX	NADPH Oxidase
NRF2	Nuclear factor erythroid 2–related factor 2
NSCLC	Non-small-cell lung cancer
O_2•-	Superoxide radical anion
OD	Optical density

OH•	Hydroxyl radical
OLIG2	Oligodendrocyte transcription factor 2
ONOO−/ONOOH	Peroxynitrite
OS	Overall survival
OXPHOS	Oxidative phosphorylation
$p21^{Waf1/Cip1}$	Cyclin-dependent kinase inhibitor 1/CDK-interacting protein 1
P3Cy5	Phycoerythrin-Cyanine5
PAGE	Polyacrylamide gel electrophoresis
PARG	Poly (ADP-ribose) glycohydrolase
PARP	Poly(ADP-ribose) polymerase
PBS	Phosphate Buffered Saline
PCNA	Proliferating cell nuclear antigen
PDGF	Platelet-derived growth factor
PDGFR	Platelet-derived growth factor receptor
PE	Phycoerythrin
PE	Phosphatidyl ethanolamine
PeCy5	PE-Cyanine®5
PFA	Paraformaldehyde
PFS	Progression free survival
PI	Propidium iodide
PI3K	Phosphoinositide 3-kinase
PIP_2	Phosphatidyl-4,5-diphosphate
PIP_3	Phosphatidyl-3,4,5-triphosphate
PIP_3	Phosphatidylinositol (3,4,5)-trisphosphate
PKB	Protein kinase B
PKC	Protein kinase C
PL	Piperlongumine
PLC	Phospholipase C
PMSF	Phenylmethylsulphonyl fluoride
PNS	Peripheral nervous system

polβ	Polymerase beta
Prim	PRIMA-1^{MET}
PRIMA-1^{MET}	p53 reactivation and induction of massive apoptosis
Prx2	Peroxiredoxin 2
PS	Phosphatidylserine
PTEN	Phosphatase and tensin homolog
PTPs	Protein tyrosine phosphatases
PUMA	The p53 upregulated modulator of apoptosis
PVDF	Polyvinylidene fluoride
RAD51	DNA repair protein RAD51 homolog 1
Ras	Rat sarcoma virus (protein)
RB	Retinoblastoma
RING	Really Interesting New Gene
RNA	Ribonucleic acid
RO•	Alkoxyl radical
ROO•	Peroxyl radical
ROS	Reactive oxygen species
RPMI	Roswell Park Memorial Institute
RT	Radiation therapy
RTK	Receptor tyrosine kinase
SAS	Sulfasalazine
SDS	Sodium dodecyl sulfate
SEM	Standard error of the mean
SH2	Src homology 2
SK	Small-conductance Ca2+-activated K+
SNP	Single nucleotide polymorphism
SOD	Superoxide dismutase
SOS	Son of Sevenless
SSA	Sulfosalicylic Acid
SSBs	Single-strand breaks

STAT	Signal transducer and activator of transcription
TBS	Tris-Buffered Saline
TBST	Tris-buffered saline 0.1% Tween 20
TCGA	The Cancer Genome Atlas
TERT	Telomerase reverse transcriptase
TGF-α	Transforming growth factor-alpha
TGX	Tris-Glycine eXtended
TK	Tyrosine kinase
TKIs	Tyrosine kinase inhibitors
TM	Transmembrane region
TMZ	Temozolomide
TNB	2-nitro-5-thiobenzoate
Trx	Thioredoxin
TrxR	Thioredoxin reductase
TTF	Tumor treating fields
TUNEL	Terminal deoxynucleotidyl transferase dUTP nick end labeling
TUSC2	Tumour Suppressor Candidate 2
Txnip	Thioredoxin interacting protein
Tyr	Tyrosine
UBA1	Ubiquitin like modifier activating enzyme 1
UPR	Unfolded protein response
USPs	Ubiquitin-specific proteases
VEGF	Vascular endothelial growth factor receptor
VEGFR	Vascular endothelial growth factor receptor
WB	Western Blot
WHO	World Health Organization
Wt	Wild-type
XBP1	X-box binding protein 1
XRCC1	X-ray repair cross-complementing protein 1

z-devd-fmk	Benzyloxycarbonyl-Asp(OMe)-Glu(OMe)-Val-Asp(OMe)-fluoromethylketone
ZR	ZR2002
z-vad-fmk	Benzyloxycarbonyl-Val-Ala-Asp(OMe)-fluoromethylketone
γ-GCL/γGCS/GCLC	Gamma-glutamylcysteine synthetase

Chapter 1 - LITERATURE REVIEW

1.1. Overview of glioblastoma (GBM)

Gliomas are the most common malignant primary brain tumors in adults comprising a vast array of diseases. Among these, Glioblastoma CNS WHO grade 4 (GBM; previously known as Glioblastoma multiforme) is the most aggressive and the most frequent primary tumor of the central nervous system in adults (median age at diagnosis, 65 years) [1, 2]. The 2021 World Health Organization classification requires both histological and molecular diagnoses for GBM, now defined as a high-grade glioma harboring wild-type isocitrate dehydrogenase (IDH1 and IDH2) genes [1, 2]. GBM are characterized by rapid progression and a dismal prognosis with a median survival of less than 15-18 months from the initial diagnosis [3-6], thus underscoring the pressing need for the development of more effective therapeutic approaches [7].

Over the past two decades, the introduction of temozolomide in conjunction with radiotherapy and surgical resection has not substantially improved the life expectancy of patients with GBM, prompting the need for new therapeutic opportunities. The current standard-of-care involves maximal safe surgical resection, fractionated radiation therapy, and concurrent/adjuvant temozolomide [8-10].

Large-scale studies such as The Cancer Genome Atlas (TCGA) and the Chinese Glioma Genome Atlas (CGGA) revealed significant inter-tumoral heterogeneity (heterogeneity between tumors) [11-14] when classifying GBM based on grouping the transcriptional profile into subtypes (proneural, classical, and mesenchymal) [14, 15], each with distinct aggressiveness and treatment responses. Subsequent research using single-cell sequencing revealed significant intra-tumoral heterogeneity and temporal changes in driver mutations between paired primary and recurrent GBM tumours [16]. Precision oncology analyses based on a limited number of targets have struggled to address this complexity. Understanding the mechanisms behind molecular

heterogeneity is crucial for developing effective therapeutic strategies and overcoming drug resistance [17].

1.2. Epidemiology and outcome of GBM

The Central Brain Tumor Registry of the United States (CBTRUS) Statistical Report 2016-2020 showed the average Annual Age-Adjusted Incidence Rate (AAAIR) of all malignant brain and other Central Nervous System (CNS) tumors was 6.94/100,000 persons. The CBTRUS also found the most common of all malignant CNS tumour histopathology was GBM (50.9%), having an incidence rate of 3.27/100,000 population, with occurrence in males: 4.09 (4.05-4.14) being higher than females: 2.55 (2.52-2.58) [18]. The most commonly diagnosed histopathologies in older ages were GBM, meningiomas, and tumours of the pituitary (median age of 66, 67, and 51 years, respectively) [18].

The five-year relative survival rate following diagnosis of a malignant brain and other CNS tumors was 35.7%, being highest in persons aged 0-14 years (75.0%) and 15-39 years (71.9%) in comparison to those aged 40+ years (21.1%) [18]. These statistics were obtained using criteria from 2016 World Health Organization (WHO) Classification of Tumours of the Central Nervous System (WHO-CNS4).

In Canada, glioblastoma has been the most commonly diagnosed neuroepithelial tumour with an AAAIR 2010-2017 of 4.01/100,000 (excluding Quebec, where data is not collected by the Canadian Cancer Registry (CCR) due to the lack of an agreement on data sharing), and glioblastoma had the most unfavourable prognoses, with median survival times of <2.5 years [19].

Regarding all brain tumors, various studies have confirmed that ionizing radiation exposure to the head and neck is a risk factor, while a history of atopic diseases such as allergies, asthma,

eczema, and hay fever is a protective factor [20]. It is worth noting that most patients with glioblastoma do not have a family history of cancer, but about 5% of all gliomas are familial.

1.3. GBM diagnosis and WHO classification of CNS tumors

The nervous system is anatomically divided into the central nervous system (CNS), which includes the brain and spinal cord, and peripheral nervous system (PNS), which consists of the sensory and motor nerves that connect the brain and spinal cord to the rest of the body. Within the CNS, neurons are accompanied by other cells that are vital for normal function. Glial cells support nerve cells in a variety of ways, supplying energy and nutrients and they help maintain the blood-brain barrier. Glial cell tumors, called gliomas, are classified according to the type of cell involved. Astrocytoma is the most common type of glioma, it develops from the star-shaped astrocytes which have multiple roles, including the regulation of blood flow, homeostasis of extracellular fluid, concentration of ions and neurotransmitters, energy provision, regulation of synapse function, and synaptic remodeling [21]. Oligodendrogliomas are a less frequent type of glioma that develop from the fried egg-shaped glial cells called oligodendrocytes, which promote electrical transmission by surrounding nerve fibers in the CNS [22]. Glioblastoma is the most malignant form of astrocytoma [23, 24].

Glioblastomas are typically identified when their rapid growth leads to symptoms, such as seizures, worsening headaches, neurological problems, alterations in mental status, and indicators of increased intracranial pressure, as they may displace or infiltrate brain structures [25]. Clinical information and radiological findings can help narrow down potential diagnoses. GBM may be diagnosed using magnetic resonance imaging (MRI) with contrast enhancement, which displays the tumor as a mass with necrotic tissue and surrounding non-enhancing signal abnormalities, such as edema and infiltrative tumor. Other features may include hemorrhage, cystic changes, or

multicentric enhancement. However, differentiating images from metastasis, lower-grade gliomas, and lymphomas can be challenging. Non-neoplastic neurological conditions like abscesses or demyelinating lesions may also have a similar appearance. MRI is helpful for surgical planning as it shows the tumor and its surrounding structures. Additionally, functional MRI can be used to plan the optimal surgical trajectory for eloquent location of tumors, improving patient survival [20].

The importance of molecular mechanisms in classifying glial neoplasms has become increasingly recognized, going beyond traditional histologic diagnosis for evaluating prognosis and treatment options. Molecular characteristics are now considered to have a more significant relationship with glioma biology than histologic features [26].

By extending diagnostic capabilities beyond histology alone, the introduction of the WHO classification system and the rise of immunohistochemistry has led to increased accuracy in diagnosis. Molecular surrogates have further expanded the use of immunohistochemistry in providing valuable information. Since this tumor is infamous for its histologic and cytologic heterogeneity, which is reflected in its original name, "multiforme" many histological subtypes and patterns have been recognized, including gliosarcoma, giant cell, small cell, granular cell, epithelioid, and primitive neuronal component, with similar prognosis. A detailed description of these variants has recently been published [27]. GBM is often distinguished by the presence of mitotic activity, as well as prominent or even "glomeruloid" (due florid/clustered appearance) microvascular proliferation (MVP) and/or necrosis as shown in **Figure. 1.3.1**. MVP refers to the presence of multilayered microvessels with endothelial cells and pericytes in the vessel walls displaying hypertrophy and hyperplasia, respectively [26]. Necrosis in these tumors frequently

appears as irregular, serpiginous areas encompassed by densely packed, radially oriented tumor cells, a phenomenon known as "pseudopalisading necrosis"[28].

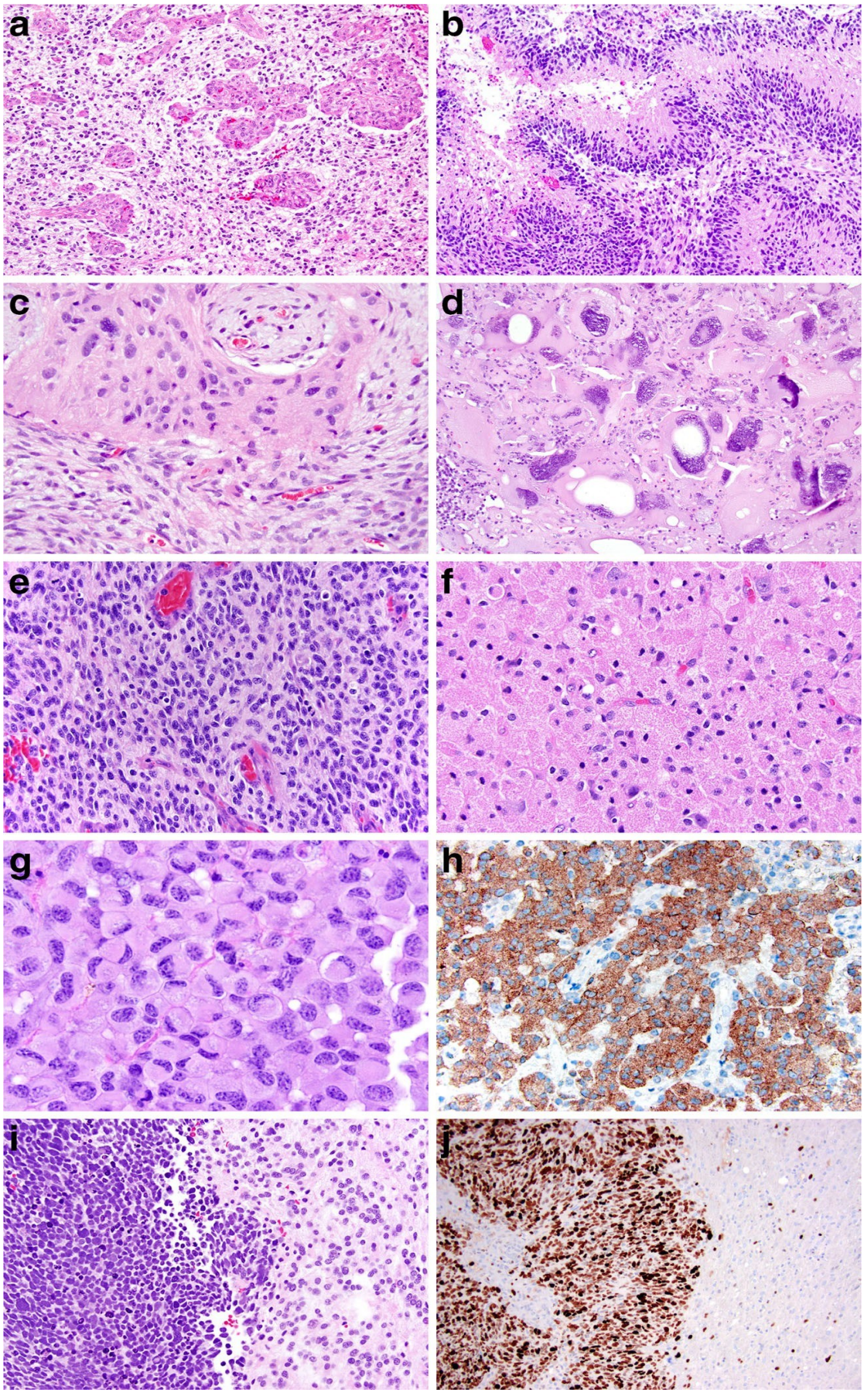
a
b
c
d
e
f
g
h
i
j

Figure. 1.3.1. Glioblastoma histological features. (a) Glomeruloid microvascular proliferation (MVP) and (b) pseudopalisading necrosis, characterized by a garlandlike arrangement of hypercellular tumor nuclei lining up around irregular foci of tumor necrosis containing pyknotic nuclei. GBM morphology variants include: (c) Gliosarcoma; its most frequent form of mesenchymal metaplasia, shows alternated islands of glial component (fibrillary cells, upper half of image) and sarcomatous component (densely packed, fusiform/spindled cell, lower half of image). (d) Giant cell GBM which contains numerous multinucleated pleomorphic giant cells, (e) Small cell GBM, has oval monomorphic nuclei, mimicking oligodendroglioma. (f) Granular cell GBM deceptively bland appearing, with abundant clear to granular eosinophilic cytoplasm, mimicking macrophages. (g) Epithelioid GBM has closely packed large eosinophilic cells with prominent nucleoli eccentric nuclei, high mitotic activity, along with microvascular proliferation and focal necrosis; around half of them are positive for (h) $BRAF^{V600E}$ mutation. (i) GBM with primitive neuronal component; sharply demarcated hypercellular clones (left side), arising within a diffuse glioma (right side), it is characterized by high nuclear/cytoplasmic ratio, nuclear molding (conformity of adjacent cell nuclei to one another), mitotic activity, apoptotic bodies and highly positive to (j) Ki-67 nuclear protein. Typically, they are losses of glial markers including glial fibrillary acidic protein (GFAP) or oligodendrocyte transcription factor 2 (OLIG2), and gains of neuronal marker expression, such as synaptophysin. Adapted from Ref. [29]

The World Health Organization (WHO) Classification of CNS Tumours (the WHO Blue Books) serves as a globally recognized diagnostic resource for identifying tumours [30]. **The 2021 WHO Classification of Tumors of CNS Tumours (2021 WHO)** (**Figure 1.3.2)** is the most recent update and includes molecular criteria that allow for a diagnosis of GBM [31]. The 2021 WHO incorporates new molecular data into the classification and grading of many entities based on molecular alterations including DNA methylation in refining and defining certain entities. These key molecular features have important implications beyond conventional histomorphology for diagnostic, clinical practice, impact of treatment strategies, and the interpretation of clinical trials.

Category	Gliomas, glioneuronal tumours and neuronal tumours						Choroid plexus tumours	Embryonal tumours		Pineal tumours	Mesenchymal/ Non-Meningothelial Tumours	Tumours of the sellar region
Family	Adult-type diffuse gliomas	Paediatric-type high-grade diffuse gliomas	Paediatric-type low-grade diffuse gliomas	Circumscribed astrocytic gliomas	Glioneuronal and neuronal tumours	Ependymal tumours		Medullo-blastoma	Other CNS Embryonal tumours		Uncertain differentiation	
Types	Astrocytoma, IDH-mutant	Diffuse midline glioma, H3 K27-altered	Diffuse astrocytoma, *MYB*- or *MYBL1*-altered	High-grade astrocytoma with piloid features	Diffuse glioneuronal tumor with oligodendroglioma-like features and nuclear clusters (DGONC)	Supratentorial ependymoma, *ZFTA* fusion–positive	Choroid plexus papilloma	MB, WNT-activated	CNS neuroblastoma, *FOXR2*–activated	Desmoplastic myxoid tumor of the pineal region, *SMARCB1*-mutant	Intracranial mesenchymal tumor, *FET-CREB* fusion positive (provisional type)	Pituitary blastoma
	Oligodendro-glioma, IDH-mutant and 1p/19q-codeleted	Diffuse hemispheric glioma, H3 G34-mutant	Polymorphous low-grade neuroepithelial tumour of the young (PLNTY)	Pilocytic astrocytoma	Myxoid glioneuronal tumor	Supratentorial ependymoma, *YAP1* fusion–positive	Atypical choroid plexus papilloma	MB, SHH-activated, *TP53* -wildtype	CNS tumour with *BCOR* internal tandem duplication and the provisional type (CNS tumour *BCOR* ITD)	Pineocytoma	CIC-rearranged sarcoma	Adaman-tinomatous cranio-pharyngioma
	Glioblastoma, IDH-wildtype	Diffuse paediatric-type high-grade glioma, H3-wildtype/ IDH-wildtype	Diffuse low-grade glioma, MAPK pathway-altered	Pleomorphic xanthoastro-cytoma	Multinodular and vacuolating neuronal tumor (MVNT)	Posterior fossa group A (PFA) ependymoma	Choroid plexus carcinoma	MB, SHH-activated, *TP53* -mutant	Cribriform neuroepithelial tumour (CRINET)	Pineal parenchymal tumour of intermediate differentiation	Primary intracranial sarcoma, *DICER1* -mutant	Papillary cranio-pharyngioma
		Infant-type hemispheric glioma	Angiocentric glioma	Subependymal giant cell astrocytoma	Diffuse leptomeningeal glioneuronal tumor	Posterior fossa group B (PFB) ependymoma		MB, non-WNT/non-SHH	Atypical teratoid/ rhabdoid tumour (ATRT)	Pineoblastoma	Solitary fibrous tumour	Pituicytoma, granular cell tumour of the sellar region, and spindle cell oncocytoma
				Chordoid glioma	Ganglioglioma	Spinal ependymoma, *MYCN*–amplified		MB, histo-logically defined	Embryonal tumour with multi-layered rosettes (ETMR)	Papillary tumor of the pineal region	Ewing sarcoma	Pituitary adenomas
				Astroblastoma, *MN1* -altered	Desmoplastic infantile ganglioglioma/desmoplastic infantile astrocytoma	Myxopapillary ependymoma			CNS embryonal tumor			Pituitary neuro-endocrine tumour (PitNET)
					Dysembryoplastic neuroepithelial tumor	Subependymoma						
					Papillary glioneuronal tumor							
					Rosette-forming glioneuronal tumor							
					Gangliocytoma							
					Dysplastic cerebellar gangliocytoma							
					Central neurocytoma							
					Extraventricular neurocytoma							
					Cerebellar liponeurocytoma							

Note: for Mesenchymal/Non-meningothelial tumours, only the group of "Uncertain differentiation" is shown.

Figure 1.3.2. Summary of the 2021 WHO classification of CNS tumors; newly identified tumor types are highlighted in grey. Adapted from Ref. [32].

Gliomas are now divided into those occurring primarily in adults “adult-type” or in children “paediatric type”. The tumor grading in the 2021 WHO classification has changed from its 2016 version now employing Arabic numerals instead of Roman numerals (WHO CNS grades 1-4 instead of grades I–IV; corresponding from less to more aggressive behaviour); also, the neoplasms are graded within types rather than across different tumor types [2].

Isocitrate dehydrogenase 1 and 2 (IDH1, IDH2) mutations are among the better prognostic factors in gliomas [33]. Thus, gliomas are grouped as those with and without IDH mutations [30]. In the 2016 WHO classification, IDH1 or IDH2 mutations were included; however, their relevance increased in the 2021 WHO classification for identifying GBM (**Figure 1.3.3**.) GBM is now considered exclusively an IDH1/IDH2-wildtype infiltrating astrocytic glioma in the adult**.** Consequently**,** all IDH-wildtype adult-type diffuse astrocytic gliomas are classified as GBM, IDH-wildtype, WHO CNS grade 4 [2]. On the other hand, the term secondary GBM or GBM IDH-mutant from the 2016 WHO CNS classification (**Figure 1.3.4**), changed its name to astrocytoma, IDH-mutant (despite some aggressive histology, but no GBM behavior).

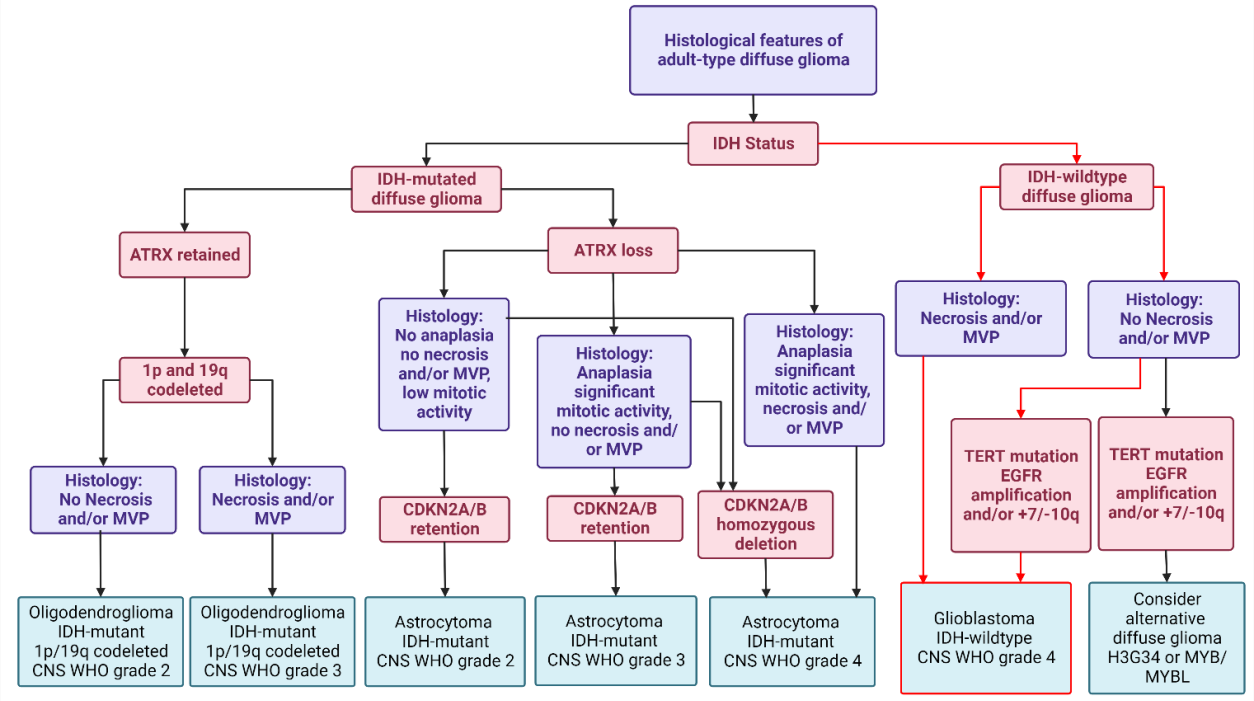

Figure 1.3.3. Algorithm for GBM, IDH-Wildtype diagnosis based on WHO 2021 Classification; MVP: Microvascular proliferation. Created with BioRender.com and adapted from Ref. [34]

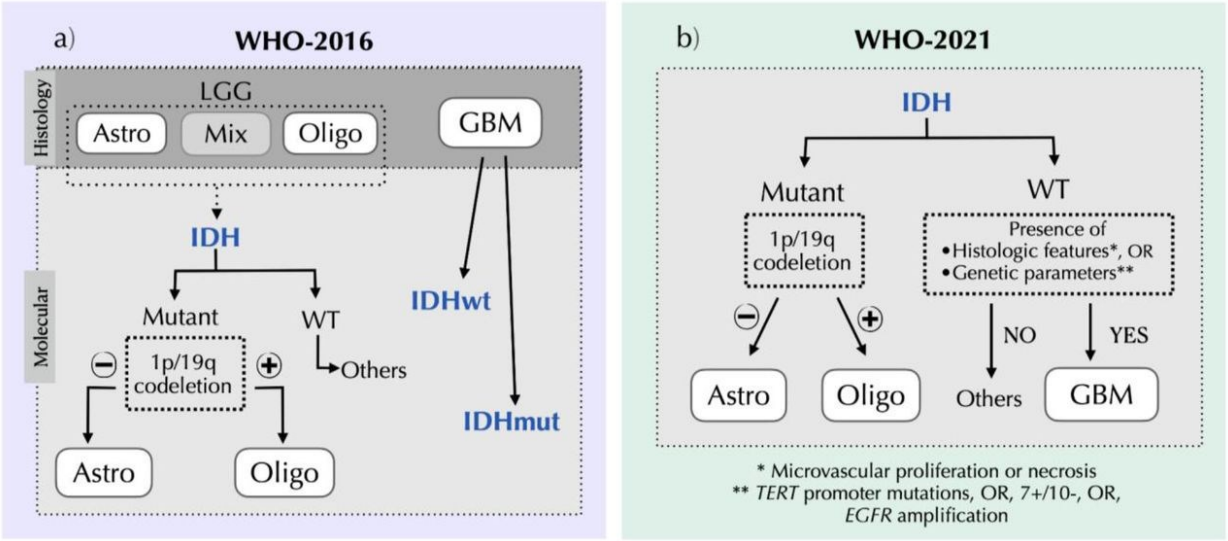

Figure 1.3.4. Simplified diagram showing the adult glioma differences in diagnostic algorithm based on the a) WHO-2016 and b) WHO-2021 guidelines. Astro: Astrocytoma; Oligo: oligodendroglioma; GBM: glioblastoma; LGG: Low Grade Glioma. Adapted from Ref. [35].

Histologically, GBM are characterized by prominent cellular and nuclear atypia, frequent mitotic figures, areas of pseudopalisading necrosis, and vascular proliferation. Although histologic features of tumor necrosis and/or microvascular proliferation contribute to the diagnosis of GBM, they are not required if any of these 3 molecular features are identified: epidermal growth factor receptor (EGFR) amplification or combined chromosome 7 gain and chromosome 10 loss (+7/−10) or telomerase reverse transcriptase (TERT) promoter mutation (hotspots c.-124 (referred to as C228T) and c.-146 (referred to as C250T)). Interestingly, even in the absence of high-grade histopathologic features such as increased mitotic activity, necrosis, or microvascular proliferation, IDH-wildtype infiltrating astrocytic gliomas (which were classified as low-grade gliomas in 2016 WHO classification due to their histological characteristics) with these molecular features behave aggressively like high-grade gliomas with poor overall survival comparable to those GBM IDH-wildtype; this suggests that these tumors represented under-sampled GBM. This change with high clinical impact was proposed in 2018 by a committee of neuropathologists named the Consortium to Inform Molecular and Practical Approaches to CNS Tumor Taxonomy (cIMPACT-NOW), which is the basis for the updated 2021 WHO classification of CNS tumors [36].

Clinically, this revision is significant, as using the 2016 WHO guidelines, IDH-wildtype low grade gliomas with molecular features of glioblastoma had almost the same radiographic and histological findings as IDH-mutant low grade gliomas, making their distinction difficult; now the additional molecular information indicates the correct classification of these tumors facilitating proper treatment [33].

The absence of molecular features of GBM in a diffuse astrocytoma, IDH-wildtype CNS WHO grade 2 or 3, is a rare entity and is not included in the 2021 WHO classification; it is

recommended to conduct further molecular testing to determine its specific diagnosis including BRAF alterations, histone mutations, and methylome profiling [31].

It is important to note that the classification and grading of IDH-mutant astrocytoma has been updated. The terms "diffuse astrocytoma" and "anaplastic astrocytoma" for grades 2 and 3 tumors are no longer used, while a grade 4 designation has been added. The classification is now Astrocytoma, IDH-mutant, CNS WHO grade 2, 3 and 4. Grade 2 and 3 tumors are still determined by increased anaplasia and proliferative activity, while grade 4 can be identified by tumor necrosis, microvascular proliferation, or homozygous loss of CDKN2A and/or CDKN2B. Because a low-grade IDH-mutant astrocytoma can still be designated as grade 4 if it has homozygous deletion of CDKN2A and/or CDKN2B, it is important to test for CDKN2A/B status on all IDH-mutant astrocytomas.

1.4. Intratumor heterogeneity of GBM

Molecular profiling has helped to determine the genes and pathways that are commonly affected in GBM. Furthermore, by analyzing additional factors such as gene expression and DNA methylation across a wide range of tumors, researchers have identified three distinct transcriptional subtypes of GBM [20], each with its own somatic alterations (**Figure 1.4.1**): The **proneural gene expression**/RTK I/LGm6 DNA methylation group is characterized by amplifications of cyclin-dependent kinase 4 (CDK4) and platelet-derived growth factor alpha (PDGFRα). Conversely, the **classical gene expression**/classic-like/RTK II DNA methylation group frequently exhibits EGFR amplifications and homozygous loss of CDKN2A/B. In the **mesenchymal**/mesenchymal-like group, it is common to observe tumors with neurofibromatosis type 1 (NF1) loss and increased infiltration of macrophages. All 3 molecular subgroups have TERT promoter mutations.

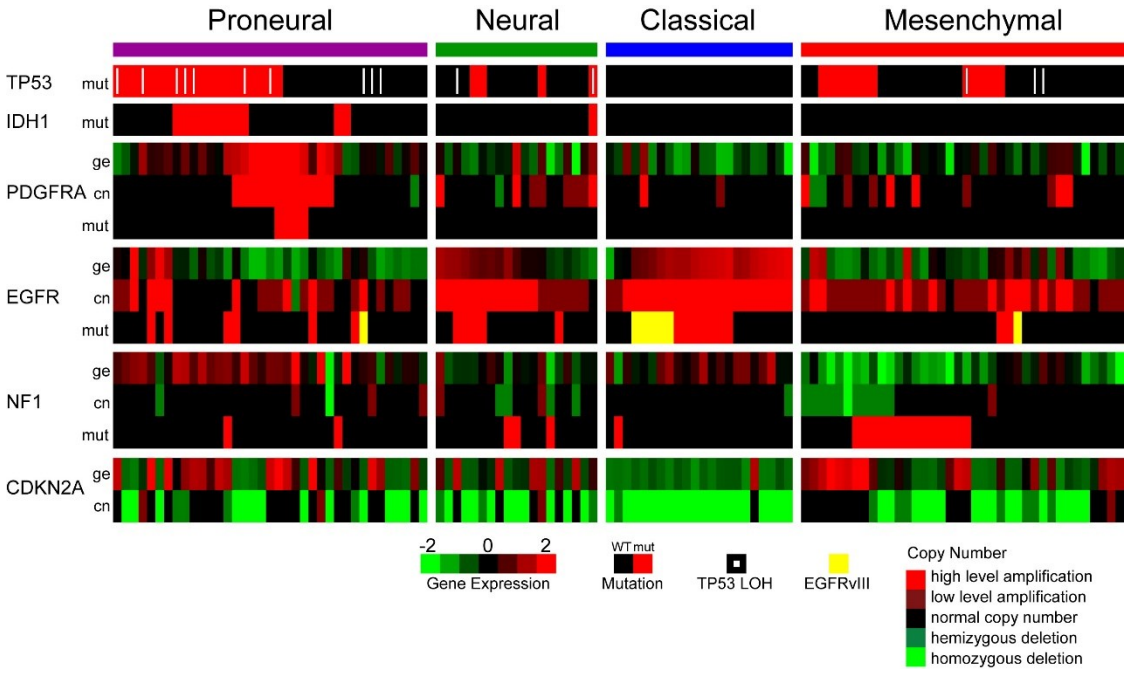

Figure 1.4.1 Overview of genetic expression and genomic changes in molecular subtypes of glioblastomas. The neural subtype was further considered a contamination from normal brain [37]. Adapted from Ref. [15].

The classification system provides a useful tool for research, but its application in the clinical settings remains unclear. Identifying subtypes within certain tumours is difficult due to the presence of multiple subtypes within the same tumour. Furthermore, none of the existing subtypes can predict treatment response. After initial treatment, subclones with unique characteristics, such as DNA mismatch repair deficiency, may emerge. The study of genomic profiling has shed light on the molecular pathogenesis of GBM and has given insight into potential genotype-directed therapies for certain patients. Despite this progress, treatment outcomes for GBM patients have not yet improved [20].

In 2008, The Cancer Genome Atlas (TCGA) group conducted a study on the genomic characterization of GBM. They analyzed 206 specimens of GBM tissue and discovered significant alterations in three core pathways: receptor tyrosine kinase (RTK)/rat sarcoma (RAS)/PI3K, p53,

and RB in approximately 88%, 78%, and 87% of cases, respectively [14, 38]. RTK oncogene mutations like EGFR, PDGFRA, and MET are common in GBM and make them favorable targets for therapy [39]. More than 63% of the 378 GBM cases in the TCGA PanCancer atlas cohort exhibit either amplification or gain of function mutations in at least one of these RTK [14]. The most significant alteration in the RTK/RAS/PI3K pathway was in epidermal growth factor receptor (EGFR) which was altered in 45% of the specimens [38]. This alteration results in the overexpression of EGFR in GBM seen in the classical subtype. The PTEN gene had the most significant inactivating change, affecting 36% of the specimens. This alteration removes the negative feedback to PI3K, leading to an increase in cancer cell growth and a decrease in apoptosis.

Fluorescence in situ hybridization (FISH) studies revealed that some tumors have mosaic amplification of multiple RTK alterations [39]. EGFR and PDGFRA amplifications were present in the main tumor core, while only EGFR amplification was found in the infiltrating tumor edge [40] (**Figure 1.4.2**).

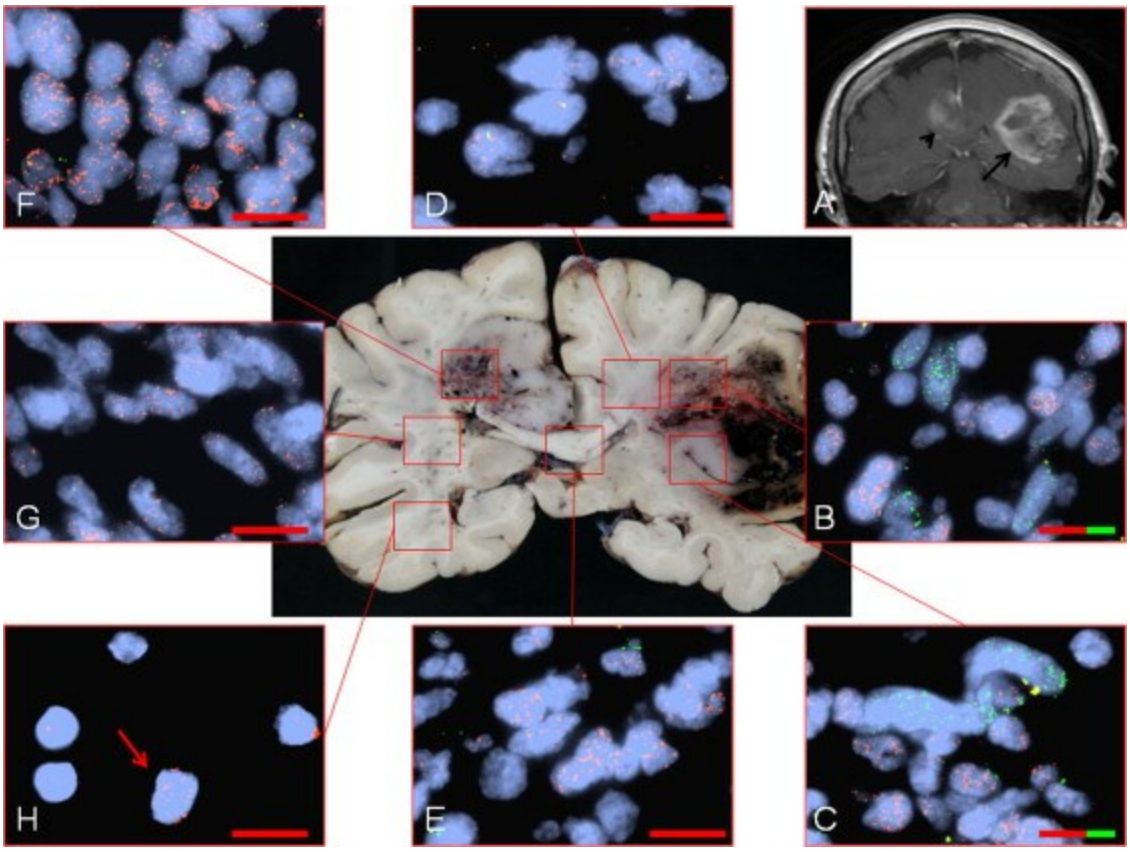

Figure 1.4.2 Autopsy of mosaic GBM case. (A) The MRI with contrast displays a large primary tumor with ring enhancement in the left parietal lobe (arrow) and a smaller secondary lesion in the right cingulate gyrus (arrowhead). (B and C) The main parietal tumor mass shows a mixture of cells with either EGFR (red) or PDGFRA (green) amplification, while the invasive edge of the main tumor (D) and corpus callosum (E) are infiltrated by GBM cells composed exclusively of cells with EGFR amplification. The second mass in the right cingulate gyrus is also composed of EGFR-amplified cells (F), and infiltrates (G) into the white matter of the right temporal lobe (H, arrow). The colors indicate the percentage of EGFR-amplified or PDGFRA-amplified subclones in each section, and the scale bars represent 40 μm. Adapted from Ref. [40].

1.5. Current standard of care of GBM

Treatment in patients involves surgery, radiation, and chemotherapy. However, patients continue to have a poor prognosis despite receiving intense treatment. The progression-free survival rate is only 7-8 months, with a median survival of 14-16 months and, after five years, the overall survival rate is just 9.8% [38]. Clinically, O-6-methylguanine-DNA methyltransferase (MGMT) is used as a predictive factor for treatment decisions. Patients with MGMT-methylated (MGMT-) tumors have higher median overall survival (22-26 months) compared to non-MGMT-methylated (MGMT +) tumors (12-15 months) [38].

Surgery for GBM aims to completely remove the tumor mass, with gross total resection resulting in better outcomes. The goal is to leave the smallest possible residual postoperative volume, which is correlated with survival. Surgical procedures involve the use of various techniques such as stereotactic navigation systems, intraoperative monitoring, and fluorescent dye visualization to maximize extent of resection and minimize risk of new neurologic deficits [20].

After a tumor is removed, GBM is typically treated with radiotherapy (60 Gy in 30 fractions) and concurrent temozolomide (TMZ) (75 mg/m^2/day for six weeks), followed by maintenance TMZ (150–200 mg/m^2/day for five days for six cycles 28-day) [41]. Whether or not to use TMZ depends on the patient's MGMT promoter methylation status.

Tumor treating fields (TTF) are a novel cancer treatment that provides low intensity, intermediate frequency (200 kHZ), alternating electric fields to produce antimitotic effects selective for dividing tumor cells with limited toxicity [42]. The treatment involves wearing a portable device that delivers these electric fields via adhesive patches placed on the skin over the head. Adding TTF during adjuvant TMZ can increase survival rates by a median of 4.9 months with limited toxicity.

Temozolomide is an oral alkylating pro-drug used to treat GBM and astrocytomas, which can permeate the blood-brain barrier (BBB) due to its lipophilic properties. At a physiological pH, TMZ is transformed into the short-lived active compound 5-(3-methyltriazen-1-yl) imidazole-4-carboxamide (MTIC), which is subsequently hydrolyzed to 5-amino-imidazole-4-carboxamide (AIC) and methyldiazolium. The latter reacts with the DNA and releases its methyl group [43]. TMZ modifies DNA or RNA by adding methyl groups to guanine at the N7 and O6 sites, and to adenine at the N3 site [44]. Alkylation of the O6 site on guanine leads to the insertion of a thymine instead of a cytosine opposite to the methylguanine during subsequent DNA replication [43]. It is believed that O6-Methylated guanine lesions trigger the formation of DNA double-strand breaks (DSBs), induce cell cycle arrest at G2/M, and eventually lead to apoptosis through a mechanism that depends on mismatch repair (MMR) [45, 46]. Methylated sites can either remain mutated, be repaired through DNA MMR, be eliminated by base excision repair (BER) with the help of a DNA glycosylase like alkylpurine-DNA-N-glycosylase (APNG) or be demethylated by O6-methylguanine methyltransferase (MGMT). Thus, cancer cells with high levels of MGMT, APNG, and BER proteins are TMZ-resistant. TMZ efficacy is limited due to the fact that at least half of the patients with GBM have high expression of MGMT, or lack of MMR [43]. MGMT promoter methylation is a known response predictor; methylation status can increase by 50% the median survival for GBM patients treated with TMZ, while where there is lack of methylation, TMZ has little or no benefit [20]. Currently, the only predictive biomarker of treatment response to TMZ is MGMT promoter methylation and the loss of the second allele of chromosome 10 [20].

1.6. Medical management and supportive care

Corticosteroids like dexamethasone are administered for peritumoral vasogenic edema symptoms. Dexamethasone alleviates neurologic deficits and signs of increased intracranial

pressure. Low doses are enough for most clinically symptomatic patients. However, corticosteroids may negatively impact patient outcome due to immunosuppression, so they should only be prescribed if patients are experiencing symptoms [20]. About 23% of GBM patients experience seizures at diagnosis and 20% later during disease progression. Anti-epileptic drugs (AED) are needed for patients with seizures, but there is no evidence to support prolonged AED prophylaxis for those patients who have never had a seizure. Guidelines recommend gradually discontinuing AEDs 1-2 weeks after surgery and avoiding long-term prophylaxis. Primary perioperative prophylaxis is not necessary for those who have never had a seizure [20]. Patients with GBM experience cognitive deficits, personality changes, and mood disturbances. Up to 91% of these patients have cognitive deficits before treatment [20]. Clinicians rely on The Neurologic Assessment in Neuro-Oncology (NANO) scale to evaluate the neurologic function of patients with brain tumors. It is used in conjunction with radiographic assessments, patient-reported outcomes, and cognitive testing to obtain a complete evaluation of their overall well-being [47].

Glioblastoma tumours often recur within 7 months of initial therapy; there is no clear standard-of-care for these patients that have a median OS of 24–44 weeks. The National Comprehensive Cancer Network (NCCN) recommends that clinical trials are the preferred option, while surgery may be considered for large lesions [38]. Complete resections offer survival benefits. Systemic therapy (TMZ rechallenge, nitrosoureas, bevacizumab, re-irradiation, and TTF) has not shown to prolong survival. Palliative care is best for poor performance status [20].

1.7. Other treatments

Bevacizumab (BEV) is a humanised monoclonal antibody that targets the vascular endothelial growth factor receptor (VEGF). It was approved in 2009 by the Food and Drug Administration (FDA) for recurrent GBM. It can only cross the BBB where it is disrupted; it

increases progression free survival (PFS) [20] and reduces peritumoral edema and related clinical symptoms and corticosteroid use, but has no long-term survival benefit [38].

Nitrosoureas have good BBB penetration, they were the first line of treatment for GBM before the discovery of TMZ. However, they remain a second-line treatment option due to the induction of bone marrow suppression, liver and renal toxicity, and interstitial lung disease. Nitrosoureas include lomustine, carmustine, and fotemustine; this last one is available in Europe, but it is not approved in the US [20].

1.8. Receptor tyrosine kinases

Receptor tyrosine kinases (RTKs) are the main drivers in cell signaling by serving as receptors for several growth factors, cytokines, and hormones. The RTK family is comprised of several sub-families, including but not limited to fibroblast growth factor receptor (FGFR), insulin-like growth factor receptor (IGFR), vascular endothelial growth factor receptor (VEGFR), hepatocyte growth factor receptor (HGFR), and ErbB [48]. To date there are over 60 RTKs identified [49, 50]. RTKs and the downstream signal transduction pathways are the most well-characterized networks associated with glioma pathogenesis and progression.

Mutations in RTKs are also the most frequent alterations in GBM, namely, copy number variation, structure variation, nucleotide variation, and over-activation of the autocrine growth factor/receptor loop [50, 51]. RTKs cause deregulation of several important pathways, namely, Ras/MAPK, PI3K/Akt/PTEN, PLC gamma/PKC, and Jak/STAT3 [52, 53]. RTKs, including PDGFR, VEGFR, and FGFR, are the most critical signaling molecules involved in tumor angiogenesis [54]. c-Met, also known as mesenchymal-epithelial transition factor, plays a crucial role in migration, therapy resistance, and vasculogenesis [55]. RTKs regulate the expression of

transcription factors such as OLIG2, SOX2, and ZEB, which are relevant to GBM stem cells (GSC) and serve as marker molecules for GSCs. The dynamic changes in the expression of RTKs variants over time and space in tumor entities contribute to the complexity of GBM and the development of therapy resistance following recurrence [56-58].

1.9. Epidermal Growth Factor Receptor

Epidermal growth factor receptor (EGFR) is a receptor tyrosine kinase (RTK) which is activated via extracellular ligand binding, and induces downstream signaling pathways that regulate cell proliferation, differentiation, migration, and survival [59, 60]. The EGF ligand/receptor system plays a crucial role in early embryonic development, wound healing, ion transport, and the regeneration of stem cells in normal tissues like the skin, liver, and gut [61]. Tumor cells can increase their level of EGFR through various mechanisms, one of which is gene amplification. This has been observed in several types of cancer such as breast carcinomas, non-small-cell lung cancer (NSCLC), pancreatic cancer, hepatocellular carcinoma, squamous cell cancer of head and neck and GBM [48, 62-64]. Overexpression of EGFR without gene amplification can also occur due to increased activity of the EGFR promoter or deregulation at the translational and post-translational levels [65]. EGFR is the most commonly RTK in GBM [66] and can be overexpressed, and/or mutated in GBM [67-69]. EGFR gene alterations, including amplification, mutation, rearrangement, and altered splicing have been reported in 57 percent of GBMs [70]. EGFR amplification is one molecular alteration currently used to confirm GBM IDH-wildtype grade 4 diagnosis [2].

The EGFR family comprises four homologous members: ErbB1/human epidermal growth factor receptor 1 (EGFR or HER1), ErbB2/HER2, ErbB3/HER3, and ErbB4/HER4. EGFR was the first member discovered of the four members of this family [64]. The extracellular ligand-

binding site of the EGFR protein comprises four domains: I, II, III, and IV. Following this are the transmembrane region (TM), the intracellular juxtamembrane domain (iJM), the tyrosine kinase (TK) domain, and the carboxyl-terminal tail (carboxy tail) with multiple tyrosine residues. In its unstimulated state, EGFR exists as a monomer [71]. Domains II and IV interact with each other, preventing the interaction of domains I and III, which are responsible for binding the ligand and executing receptor activation. EGFR activation is triggered by ligand binding, which induces receptor dimerization, such as homo-dimerization (EGFR-EFGR) or hetero-dimerization (EGFR with HER2, 3, or 4) [72] leading to a series of structural rearrangements that culminate in the asymmetric alignment of dimers between the two juxtaposed catalytic domains that triggers the transphosphorylation of tyrosine residues by its TK domain (**Figure 1.9.1**). In EGFR wildtype (wt), strong ligands induce symmetrical homo-dimerization and transient signaling, while weak ligands induce asymmetrical homo-dimerization and sustained signaling to promote cellular differentiations [73].

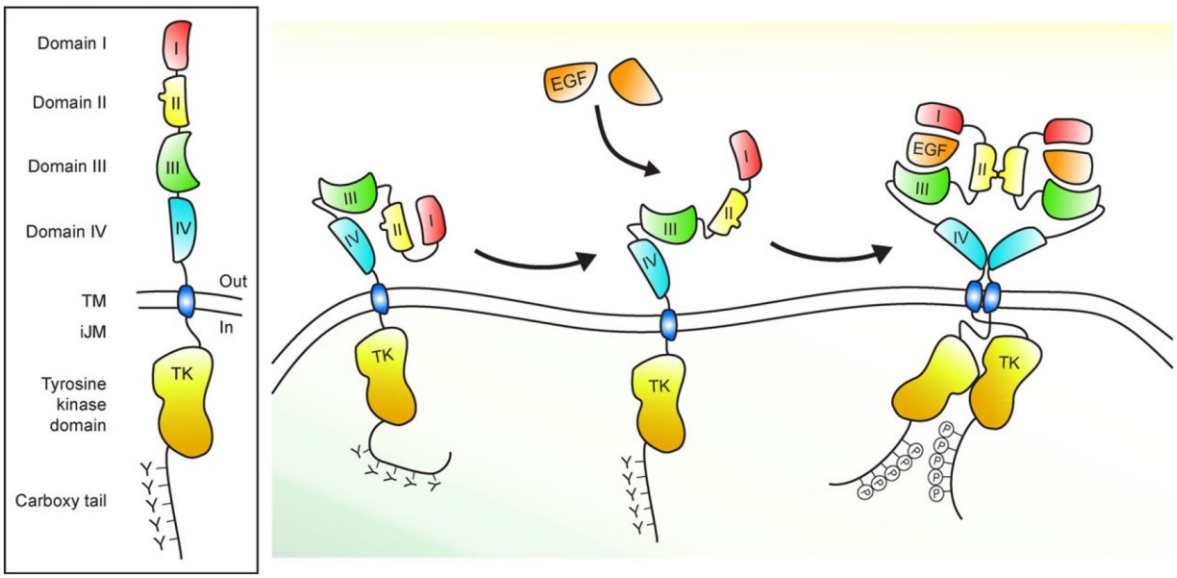

Figure 1.9.1. Structure of EGFR and EGFR-induced receptor activation. Adapted from Ref [71].

The signaling of the family of EGF is regulated by a group of ligands known as EGF-like ligands. The high-affinity ligands for EGFR include transforming growth factor-alpha (TGF-α), betacellulin, EGF, and heparin-binding growth factor, while the low-affinity ligands include epiregulin, amphiregulin, epigen, and neuregulin 2b [71]. The activity of EGFR receptors is suppressed by the accumulation of tyrosine phosphatase when they are not interacting with EGF-like ligands.

1.9.1. Function

EGFR activates multiple signaling pathways, including the Ras/mitogen-activated protein kinase (MAPK)/extracellular signal-regulated kinase (ERK) pathway, the phosphatidylinositol 3-kinase (PI3K)/AKT pathway, the phospholipase C (PLC)/protein kinase C (PKC) signaling cascade, and the signal transducer and activator of transcription (STAT) signaling pathway [74, 75]. EGFR signaling is critical for several cellular functions including survival, proliferation, differentiation, migration, and resistance to apoptosis [74, 76] (**Figure 1.9.1.1**.). In addition to the upregulation of EGFR or gene amplification, the EGFR-mediated pathway can be disrupted by several alternative mechanisms, such as mutations in EGFR, the formation of heterodimers with other ErbB family of proteins, and the excessive production of the receptor's ligands [71].

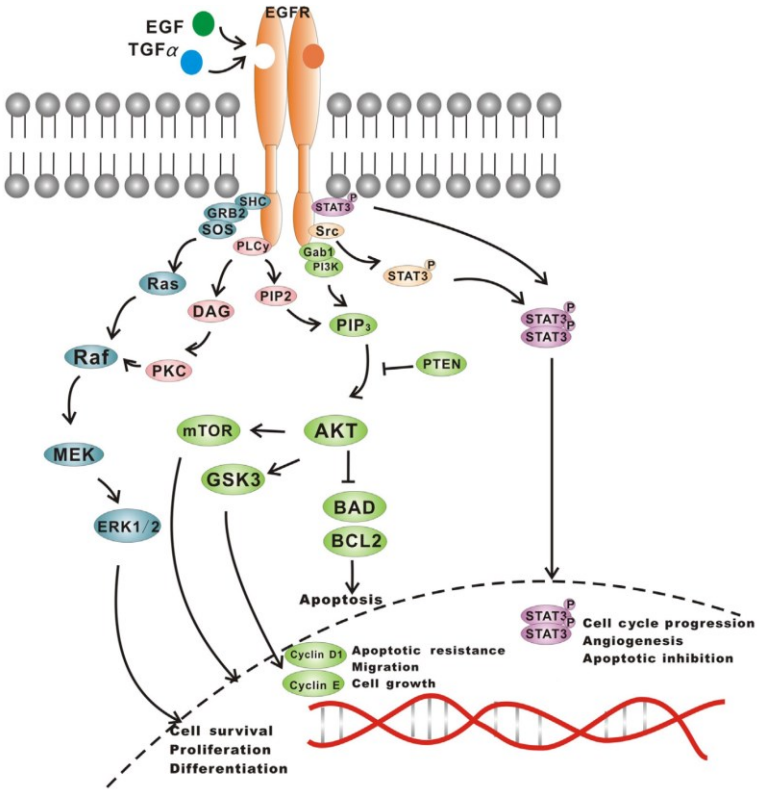

Figure 1.9.1.1. EGFR and downstream signal pathways: (1) RAS/RAF/MEK/ERK, (2) PI3K/AKT and (3) JAK/STAT pathways. Adapted from Ref [77].

1.9.2. EGFRvIII

EGFR mutant deletions in GBM include EGFRvariant I (EGFRvI; deletion of the N-terminal), vII (deletion of exons 14-15), vIII (deletion of exons 2-7), vIV (deletion of exons 25-27), and vV (deletion of exons 25-28) [66, 78]. EGFRvII and EGFRvIII are considered oncogenic [79-81]. EGFRvIII is the most frequent mutant version shown in around 25% of GBM [82, 83]; the deletion of its ECD results in inability to bind to its usual ligands (**Figure 1.9.2.1**) and be weakly constitutively active (comparable to ~10% of ligand activated EGFR wildtype [EGFRwt]), which is sufficient to support growth and promote malignant cell signaling [84, 85]. EGFRvIII preferentially triggers downstream PI3K signaling via AKT phosphorylation (while EGFRwt does mainly via MAPK and STAT3; **Figure 1.9.2.2**) [80, 86], and contributes to chemoradioresistance

[87]. EGFRvIII could also be found in prostate cancer, breast cancer, non-small cell lung carcinoma, ovarian cancer, and head and neck cancer, but not in normal tissue [65]. This variant exhibits reduced phosphorylation levels at Y1045 as compared to EGFRwt, which consequently inhibits its internalization and subsequent degradation via ubiquitination [86].

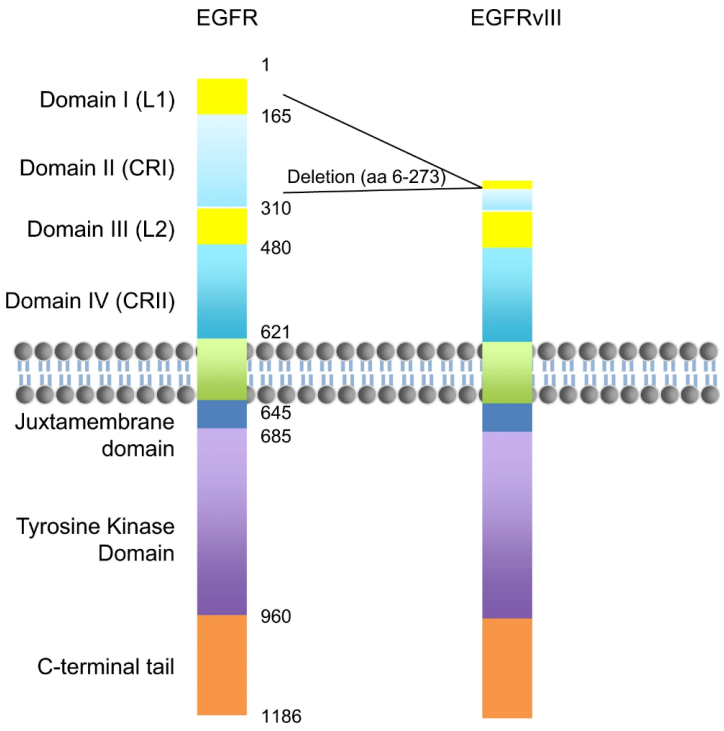

Figure 1.9.2.1. Structure of EGFRvIII compared with EGFRwt. EGFRvIII shows almost complete deletion of Domains I (leucin-rich) and II (cysteine-rich) compared to EGFRwt, resulting in a deficiency in ligand binding. The transmembrane and intracellular regions of EGFR and EGFRvIII are similar. Adapted from Ref. [66].

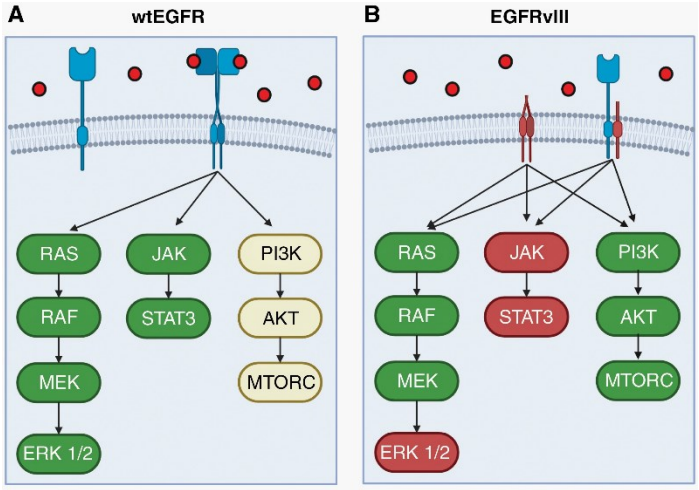

Figure 1.9.2.2. Downstream signaling specific to EGFR variants. (A) EGFRwt is activated upon ligand binding through receptor homo- or heterodimerization. Once activated, EGFRwt strongly signals via the MAPK and STAT3 pathways while also signaling via the PI3K pathway, albeit to a lesser extent. (B) EGFRvIII, due to its truncated extracellular domain (ECD), is unable to bind ligands but can initiate downstream signaling through homodimerization or heterodimerization with EGFRwt. EGFRvIII signals strongly via the PI3K pathway and weakly via the STAT3 pathway. Notably, EGFRvIII strongly activates early MAPK signaling components, but this does not translate to increased ERK signaling. Adapted from Ref. [86].

Whether EGFRvIII expression affects survival of patients with GBM is still controversial; some studies have reported EGFRvIII positivity is a negative prognostic marker [88, 89]. Other authors claim that EGFRvIII is a positive prognostic marker [90] while others reported no differences in outcomes [91, 92]. A recent retrospective analysis that included 336 GBM patients with different MGMT status and EGFRvIII found that the MGMT-/EGFRvIII+ group showed the most favorable survival after standard of care treatment (OS: 26.4 months) compared to MGMT+/EGFRvIII+, MGMT+/EGFRvIII-, and MGMT/EGFRvIII-, with OS: 16.2; 15.2; 20.3 months, respectively [93].

Multiple mutations can occur simultaneously in the same tumor, sometimes as subclonal populations with changes over time, and exhibiting distinct dependencies on various ligands [92]. EGFR missense mutations, while less common than in-frame deletion mutations, have also been observed in IDH wild-type GBM cases. Specifically, mutations such as R108G/K, A289V/T/D, and G598V have been reported in 2.2%, 5.9%, and 1.8% of all cases, respectively [17].

1.9.3. EGFR targeted therapy for cancer treatment

Due to the widespread presence of EGFR mutations and the dependence on EGFR signaling for the development of GBM, EGFR is a promising target for precision oncology in this type of cancer. Significant progress has been made in anti-EGFR therapy, leading to the recognition of EGFR as a critical target in anti-cancer drug development [94]. Currently, clinicians have access to two types of anti-EGFR treatments. The first category consists of EGFR tyrosine kinase inhibitors (TKIs), which inhibit the activation of downstream kinases by binding to the catalytic site of EGFR. The second category includes monoclonal antibodies (mAbs), which block the binding of ligands to the EGFR. Initial clinical trials targeting EGFR in GBM used EGFR TKIs that had been repurposed primarily from non-small cell lung cancer (NSCLC). Clinical trials have tested biological inhibitors, including antibodies, peptide vaccines, and chimeric antigen receptor T (CAR T) cells. The monoclonal antibody (mAb) 806 targets EGFRvIII and EGFRwt. This inhibitor is an antibody-drug conjugated form (ADC) with monomethyl auristatin F (ABT-414 or Depatuxizumab mafodotin) that was tested in the INTELLANCE-2/EORTC phase II trial. However, no difference in overall survival was found between the treatment groups, regardless of the EGFR status. In addition, the treatment induced significant ocular toxicity [95].

EGFR has been targeted in clinical trials for GBM, but none have shown survival benefits [96]. However, post-EGFRvIII targeting CAR T infusion has been successful in penetrating the

tumour and causing a significant loss of EGFRvIII-positive tumour cells. CAR T cells can be detected in the circulation yet three years after infusion [97].

Rindopepimut is a 14 amino acid peptide created to treat GBM through a dendritic cell vaccine approach [98]. Clinical trials, including the ReACT Phase II trial for recurrent GBM and ACTIV Phase III trial for newly diagnosed GBM, failed to show significant statistical results for the primary endpoints [99, 100].

In general, clinical trials using biological inhibitors have not yet resulted in significant improvements in patient outcomes [101-103]. Nonetheless, they have provided valuable insights into the unique biology of EGFR in GBM, which will inform the development of a more effective targeted therapy in the future.

1.9.4. EGFR tyrosine kinase inhibitors (TKIs)

Currently, there are three different generations of EGFR TKIs available, and the most studied in glioma are from the first and second generations. First generation or type I EGFR inhibitors, such as erlotinib and gefitinib, are of low molecular weight, and compete with adenosine triphosphate (ATP) and reversibly bind to the intracellular tyrosine kinase domain of EGFR or EGFRvIII suppressing autophosphorylation of the receptor and further downstream signaling [104, 105]. In preclinical studies, gefitinib and erlotinib have demonstrated anti-glioblastoma activity *in vitro* [106], including the decrease of cell viability, reduced EGF-induced phosphorylation of EGFR, suppression of both Akt and ERK1/2 activation, with eventual inhibition of the MAPK signaling pathway. The second generation of inhibitors, including afatinib, neratinib, vandetanib, and dacomitinib, irreversibly inhibit EGFR and have the added ability to inhibit other RTKs, such as Her2, PDGFR, MET, and VEGFR [107-109]. In a recent

clinical trial, it was found that osimertinib, a third generation inhibitor able to cross the blood-brain barrier, has demonstrated improved overall survival for recurrent GBM patients with EGFR amplification and EGFRVIII mutations [110].

The lack of response to current EGFR TKIs in GBM may be attributed to the different oncogenic variants of EGFR found in GBM compared to those found in NSCLC. In NSCLC, mutations in the EGFR coding sequence are primarily located in the intracellular TK domain [111], while in GBM, EGFR mutations are mainly found in the ECD [112] and include in-frame deletions and/or missense mutations [83]. In GBM cells, the sensitivity to EGFR TKIs that are intended for the TK domain of EGFR-mutant NSCLC can vary among the different EGFR alterations that are specific to GBM [113-115]. Type I EGFR TKIs, such as gefitinib and erlotinib, exhibit affinity for both activated EGFRwt and TK domain mutants [113]. In contrast, Type II TKIs, including lapatinib and neratinib, display a higher affinity for ECD mutants compared to activated EGFRwt [113]. Based on the simultaneous presence of amplified EGFRwt and ECD mutants, these results imply that a TKI capable of blocking both EGFRwt and ECD mutant signaling pathways would be necessary for effective treatment of EGFR-driven GBM.

Studies have shown that in patients with tumors containing the EGFRvIII mutation, there is a consistent overexpression of EGFRwt [116]. EGFRvIII is believed to originate from amplified full-length EGFR due to chromosome 7 rearrangements, as indicated by single nucleotide polymorphism (SNP) analysis [117]. Additionally, approximately 25% of GBM patients have amplified EGFR without mutations, indicating that overexpressed EGFRwt may play a role in the development of some GBM cases [83]. Preclinical studies have demonstrated that suppressing the growth and inducing cell death in GBM models derived from patients with amplified EGFRwt can be achieved through genetic or pharmacological inhibition of EGFR [114, 118, 119]. Previous

research has demonstrated that ectopic expression of EGFRwt has transforming properties, which is consistent with the observed dependence on overexpressed EGFRwt for tumor growth [120]. Moreover, studies have elucidated that cells with EGFRwt and EGFRvIII within the same tumor foster growth and survival through paracrine or direct physical interactions [116, 121, 122].

The current EGFR TKIs have a major limitation that may have influenced their therapeutic failure in patients, which is providing enough exposure to the brain due to the selective permeability of the BBB. Drugs with specific physicochemical properties, such as low molecular weight, low polar surface area, and a low number of rotatable bonds are somewhat more likely to cross, but this physical barrier is highly effective and prevents the passage of more than 98% of small molecule drugs [123]. While some areas of GBM may have disruptions in the BBB, a significant portion of the tumor is still protected by an intact BBB [124]. According to studies on the pharmacokinetics of TKIs, apart from erlotinib and lapatinib, most drugs fail to attain steady state plasma concentrations that are effective in inhibiting cell proliferation *in vitro*. Moreover, the first-generation TKIs were designed for NSCLC and are ineffective in penetrating the brain and targeting the specific variants of EGFR present in GBM [96].

GBM that are driven by EGFR have shown to adapt to EGFR TKIs through various mechanisms. One such mechanism is the de-repression of alternative RTKs like PDGFRβ and MET, which allows for adaptive bypass signaling [125, 126]. It is believed that this adaptive kinome response is controlled by epigenetic changes, which have been linked to kinase inhibitor resistance in other cancer types [127]. Expression of EGFRvIII in U87 GBM cells can trigger a malignant epigenetic state by promoting the activity of transcription factors that collaborate with the chromatin reader BRD4 to reshape the active enhancer landscape and drive the formation of tumors [128]. Inhibiting the oncogenic EGFR signaling pathway therapeutically may help to

reprogram this malignant epigenetic state through enhancer remodeling, which could be a potential mechanism for adapting to EGFR TKI in GBM. These findings imply that targeting epigenetic mechanisms that enable adaptive responses to EGFR TKI may be a promising strategy for developing combination therapies.

Resistance to EGFR-targeted therapies can also be attributed to the heterogeneity of tumors, including presence of EGFR mutant variants. In patient-derived xenografts (PDX) of GBM, it was observed that a single tumor comprises cells with varying levels of EGFRvIII expression, which are regulated by extrachromosomal DNA (ecDNA). This leads to the presence of two distinct cell populations: high EGFRvIII-expressing cells ($EGFRvIII^{high}$) and cells with undetectable levels of EGFRvIII expression ($EGFRvIII^{low}$) [129]. It is noteworthy that $EGFRvIII^{high}$ cells are more responsive to EGFR TKI compared to $EGFRvIII^{low}$ cells [129]. Following erlotinib treatment, studies using fluorescence in situ hybridization (FISH) have revealed the translocation of ecDNA containing EGFRvIII onto cellular chromatin in the form of homogeneous staining regions (HSR) [129]. However, it is noteworthy that the ecDNA population was found to regenerate within a period of 72 hours after discontinuing the drug treatment, **Figure 1.9.4**.

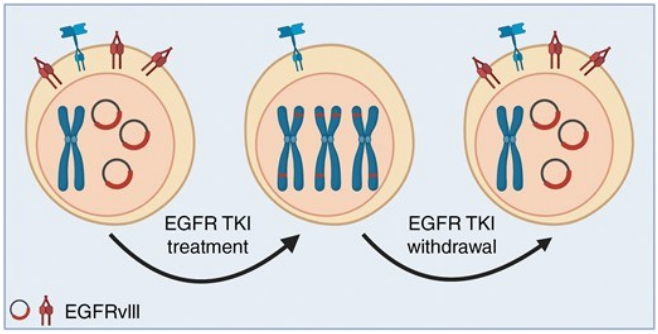

Figure 1.9.4. In GBM, the expression of EGFRvIII in GBM is facilitated by ecDNA. EGFR TKI administration results in the disappearance of EGFRvIII ecDNA and mutant receptor expression.

EGFRvIII translocates onto chromosomes at HSRs. Upon stopping EGFR TKI, the mutant receptor is reinstated [129]. Adapted from Ref. [96].

Another study determined that inter-clonal communication between EGFRvIII and EGFRwt led to the expression of genes that decreased sensitivity to EGFR TKIs: EGFRvIII-expressing U87 cells secreted IL-6, which activated NF-κB in EGFRwt-expressing cells, and NF-κB subsequently by interacting with BRD4 induced the expression of the pro-survival protein survivin [121].

Activation of the EGFR in response to genotoxic stress leads to its translocation into the nucleus, where it has been observed to increase the induction of DNA repair genes such as XRCC1 and ERCC1 [130]. EGFR has also been shown to interact with various DNA repair proteins, including DNA-PKcs, RAD51, ATM, and BRCA1[131]. Therefore, inhibiting the EGFR pathway with TKIs can result in the downregulation of these DNA repair genes.

1.9.4.1 Gefitinib / Iressa

The United States Food and Drug Administration (FDA) approved gefitinib (**Figure 1.9.4.1)** for clinical use as first EGFR inhibitor in patients with NSCLC in 2003 [132]. Unlike erlotinib, gefitinib exhibits anti-tumor activity regardless of EGFR expression levels [133]. *In vitro*, gefitinib inhibits GBM cell migration [134], reduces the proliferation of glioblastoma stem cells [135], and enhances survival in pre-clinical orthotopic models [136]. However, despite obtaining high concentrations in GBM tumor tissue (22-fold higher than in plasma) and significant dephosphorylation of EGFR [137], clinical trials have shown limited effects.

Several Phase I/II studies have demonstrated that adding gefitinib to radiotherapy is well-tolerated but does not improve survival [138, 139]. Investigating the possibility of combining

EGFR-targeting drugs with other agents that work through different mechanisms may result in improved treatment outcomes and provide more effective options for patients.

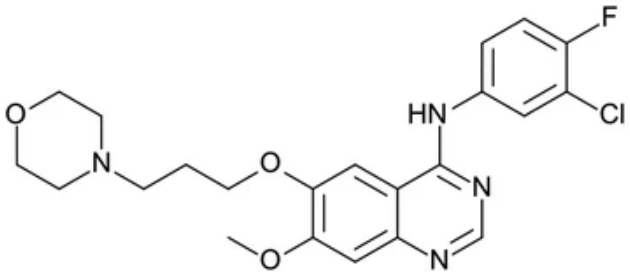

Figure 1.9.4.1. Structure of gefitinib (originally named as ZD1839 and commercialized as Iressa). Adapted from Ref. [140].

1.9.5. Monoclonal antibodies

There are two types of EGFR-targeting antibodies clinically used: blocking antibodies, which hinder the interaction of ligands with their corresponding receptors, and internalized antibodies. Antibodies with both blocking and internalization properties are ideally the most efficient in suppressing receptor function [74]. Many antibodies have been developed to date against EGFR to treat GBM patients. One such antibody is cetuximab, which is an EGFR blocker initially used for colorectal cancer. Cetuximab works by preventing ligand binding without receptor activation [141]. A study demonstrated that cetuximab can effectively bind to both EGFR and its variant EGFRvIII in U87MG cells [142]. This binding leads to internalization of cetuximab–EGFRvIII from the cell surface, resulting in a decrease in the phosphorylated form of the EGFRvIII receptor in transfected cells and a significant reduction in cell proliferation. However, these compounds have been found to be largely ineffective in GBM [143].

1.10. Combi-molecules

In the 2000s, a strategy was devised known as "combi-targeting," which involved the creation of compounds referred to as "combi-molecules" that possessed two bioactive components connected directly or through a linking unit within a single molecule. This design enabled a dual mode of action, enabling the molecule to target multiple cellular targets simultaneously [144, 145]. Combi-molecules can offer a range of benefits including multiple mechanisms of action, improved pharmacokinetic and pharmacodynamic properties, and a reduced likelihood of resistance in comparison to their parent compounds. This class of compounds has been found to have superior anticancer activity and can cause less harm to normal tissues [146-150], making it a highly effective option.

The classification of combi-molecules into three categories was based on their designs. Type I combi-molecules depend on hydrolytic cleavage to activate their dual mechanism of action, whereas Type II combi-molecules do not require metabolic activation to trigger their dual properties (**Figure1.10**) [145]. Type III molecules exhibit features of both Type I and II combi-molecules.

The group of Dr. Bertrand Jean-Claude (Director of the Drug Discovery Platform , McGill University) has synthesized several combi-molecules and also demonstrated *in vitro* and *in vivo* their anticancer effects in different cancer types including breast, lung, prostate cancers, osteosarcoma and GBM [151-154].

Type II Combi-molecules	Targets	Structure
JDD36	DNA-EGFR	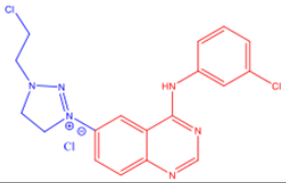
ZR2002	DNA-EGFR	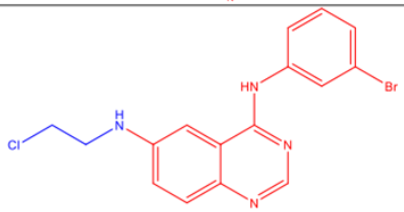
ZR2003	DNA-EGFR	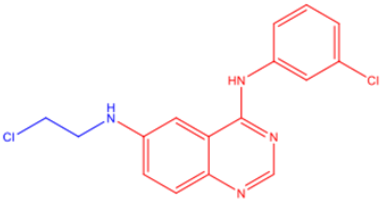
AK04	DNA-BCR/ABL	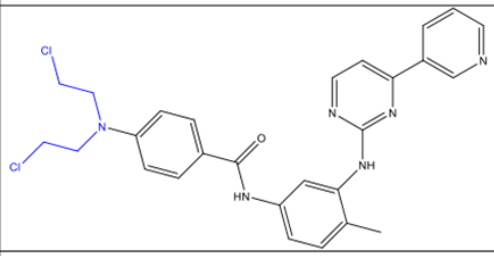
SB163	c-Src-EGFR	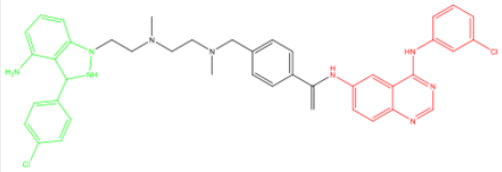
EG40	DNA-PARP	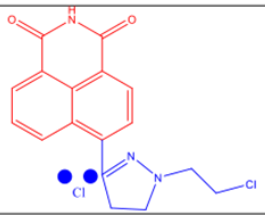

Figure 1.10. Structures of type II combi-molecules. Adapted from Ref [155]

1.10.1 Combi-molecule ZR2002

ZR2002 (6-(2-chloroethylamino)-4-anilinoquinazolines) is a single type II combi-molecule with dual EGFR/DNA targeting property (**Figure 1.10.1**). ZR2002 targets EGFR with its aminoquinazoline moiety which has high affinity for the ATP-binding site of EGFR working as tyrosine kinase inhibitor, while its 2-chloroethyl moiety on the quinazoline ring inflicts strong levels of DNA damage in an irreversible manner by being able to diffuse towards the nucleus and alkylate DNA, to concomitantly overcome the protective effect of EGFR-induced DNA repair [156]. This approach replicates the mechanism of action of classical alkylating agents, such as TMZ, and EGFR TK inhibitors, such as Iressa, by targeting the same molecular pathway.

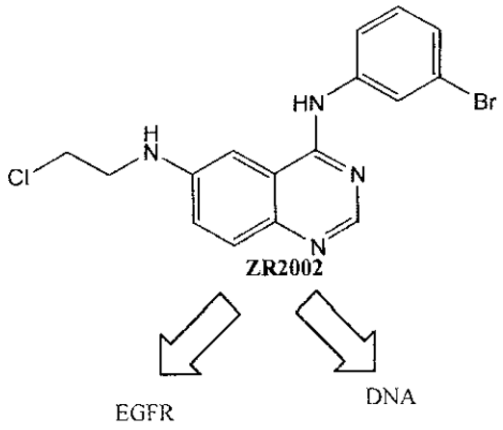

Figure 1.10.1 Structure of ZR2002. ZR2002 is designed to achieve a dual purpose by blocking receptor-mediated DNA repair signaling and inducing DNA damage in cells simultaneously.

Sharifi et al. in recent studies demonstrated the *in vivo* activity of ZR2002 at 150 mg/kg in a TMZ-resistant glioma stem cell model [153, 157]. ZR2002 induced, in a dose-dependent manner, high levels of DNA damage with concomitant blockage of EGFR phosphorylation and inhibition of EGFR-mediated MAPK/ERK and PI3K/AKT signaling pathways [151]. ZR2002 showed

significantly higher cytotoxic activity compared to TMZ or gefitinib, it crossed the BBB, and significantly increased survival in highly aggressive intracranial mouse models of GBM [157].

1.11. Redox balance and cancer

1.11.1. Reactive oxygen species

Reactive oxygen species (ROS) is a collective term for a broad category of oxidants derived from molecular oxygen [158]. These compounds constitute a large class of reactive species, known as reactive nitrogen, sulfur, carbon, selenium, electrophile, and halogen species, which can participate in redox reactions and induce oxidative modifications on biological macromolecules, thereby playing a role in redox signaling and biological function. However, it is firmly established that under supraphysiological conditions, ROS react indiscriminately with proteins, lipids, nucleic acids, and carbohydrates, and also generate other reactive species with potentially harmful effects [159]. The Reactive Species Interactome (RSI) is a comprehensive, multilevel concept introduced in 2017 that describes the intricate network of interactions between reactive species and their downstream biological targets, major cysteine thiols present in proteins, lipids, and DNA [160].

ROS can be classified as free radicals and non-radical species, based on the existence of unpaired electrons in the outer molecular orbitals. Free-radical includes nitric oxide ($NO^{\bullet}$), superoxide radical anion ($O_2^{\bullet-}$), hydroxyl radical ($OH^{\bullet}$), carbonate radical anion ($CO_3^{\bullet-}$), nitrogen dioxide ($NO_2^{\bullet}$), alkoxyl radical ($RO^{\bullet}$), and peroxyl radical ($ROO^{\bullet}$). Non-radicals includes hydrogen peroxide (H_2O_2), peroxynitrite ($ONOO^-$/ONOOH), hypochlorous acid (HOCl), and singlet oxygen ($^1O_2$) [161]. Superoxide, hydrogen peroxide and hydroxyl radicals are the most studied species in cancer [162].

Within cells, ROS are generated at various locations via multiple pathways **(Figure. 1.11.1.1)**. Under normal physiological conditions, the majority of ROS are generated in the mitochondria as a result of aerobic cellular metabolism, accounting for approximately 90% of the total ROS produced in the cell [163]. The mitochondrial ROS are byproducts of metabolic processes and are generated from electron leakage during oxidative phosphorylation in the electron transport chain (ETC) [164]. The ETC comprises complex I (NADH-ubiquinone oxidase) and complex III (ubiquinone-cytochrome c oxidoreductase), which are major sites of superoxide anion generation [165]. During the process of cellular respiration, electrons are transported through a series of complexes and ultimately react with molecular oxygen (O_2) as the final electron acceptor. This reaction produces $O_2^{\bullet -}$ [166], which is dismutated to H_2O_2 by superoxide dismutase, either in the mitochondrial matrix (by SOD2) or in the cytosol (by SOD1) [167]. H_2O_2 is degraded in the matrix by glutathione peroxidase (GPx) [162]. H_2O_2 is also a highly diffusible secondary messenger, and several aquaporins facilitate its movement across membranes, earning them the designation of "peroxiporins" [168]. The rate of H_2O_2 transfer across membranes contributes to the establishment of steady-state gradients. Although H_2O_2 is not a free radical, it is capable of catalyzing free radical reactions and inducing oxidative damage in living cells. For instance, H_2O_2 can accept an electron from free Fe^{2+} through the Fenton reaction to form a short-life highly reactive hydroxyl radical ($OH^{\bullet -}$) that causes DNA damage [169, 170].

The membrane-bound enzymes NADPH oxidases (NOXs) also contribute to the generation of ROS [171-173]; this is critical for immune cells such as macrophages and neutrophils, particularly during the oxidative burst of the immune response [174-176]. Additionally, H_2O_2 can be produced by various other oxidases located in different subcellular compartments, including the endoplasmic reticulum (ER) and peroxisomes, as well as by several superoxide dismutases. Apart

from intracellular sources, oxidants can also be produced as a result of the accumulation of environmental factors known as the "exposome," which encompasses a range of molecular components such as nutrients, pharmaceuticals, toxic substances, and pollutants, as well as physical and psychological stressors like ultraviolet radiation, X-rays, and lifestyle factors [177].

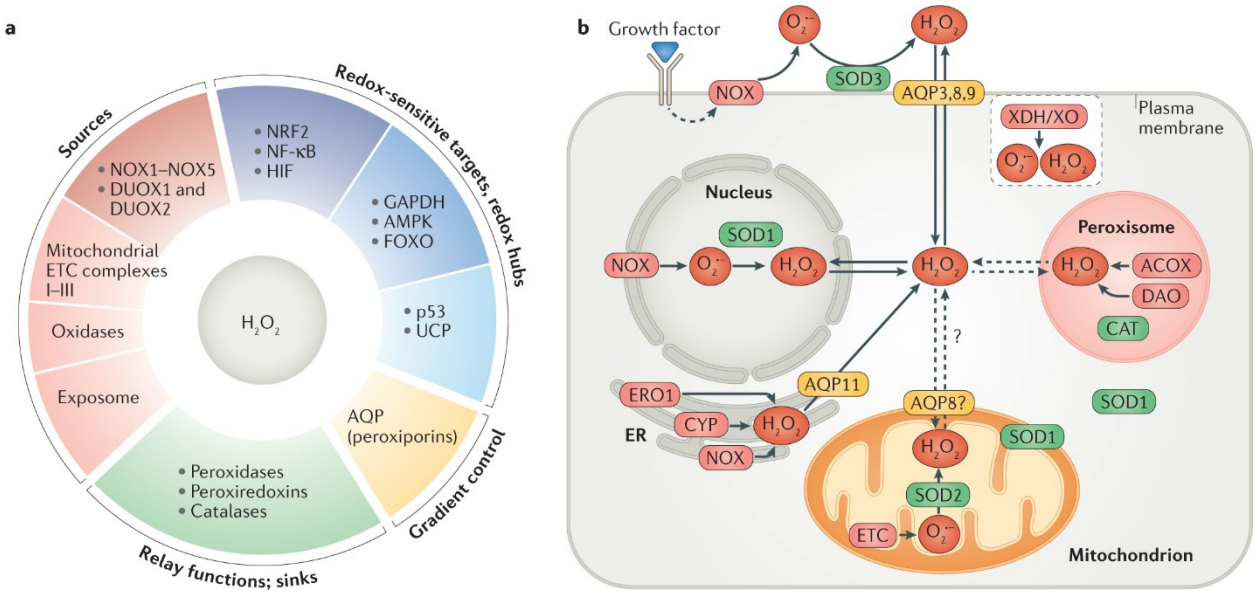

Figure. **1.11.1.1** Important H_2O_2 modulators and targets: a) H_2O_2 sources (red), aquaporins (AQPs) (yellow), sinks (green), and redox-sensitive targets and hubs (blue). Redox-sensitive targets act as biological support hubs. Redox relay (electron transfer) reactions that transfer signalling oxidant are examples of sinks. Additionally, superoxide dismutases (SODs) function as a sink for O_2•$^-$ and a source of H_2O_2. b) The primary reactive oxygen species, $O_2^{\cdot-}$ and H_2O_2, along with the subcellular locations where they are generated. Adapted from Ref. [178].

In the redox regulation of biological activities, H_2O_2 is commonly considered the principal ROS [151]. Within cells, H_2O_2 concentration is strictly regulated, usually staying within the low nanomolar range (roughly 1-100 nM). Growth factors, chemokines, or physical stressors can all act as metabolic cues or stressors to increase the production of H_2O_2, and effective reducing systems can help remove it. "Oxidative eustress" or “good stress” refers to a condition of low-level H_2O_2 maintenance and related physiological redox signalling [179, 180]. However, compared to H_2O_2 (10^{-8} M), the total cellular concentration of $O_2^{\bullet-}$ is maintained at roughly 10^{-11} M (**Figure. 1.11.1.2)** [181].

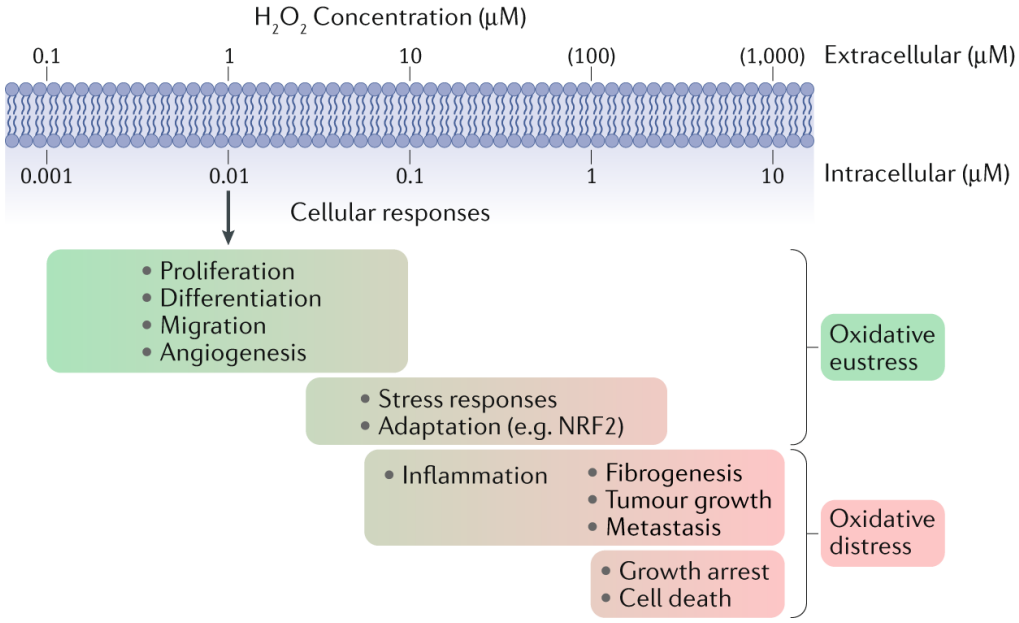

Figure. **1.11.1.2** The concentration of H_2O_2, in relation to cellular responses, can be categorized into two ranges: oxidative eustress and oxidative distress. Oxidative eustress refers to the physiological intracellular range, which is typically up to approximately 100 nM, and is associated with beneficial responses. On the other hand, oxidative distress refers to higher concentrations of H_2O_2, which are associated with stress responses and adaptation. Even higher exposure to H_2O_2 can lead to inflammatory responses, growth arrest, and cell death through various mechanisms,

and is denoted in red, indicating predominantly deleterious effects. Green is used to denote predominantly beneficial effects. Adapted from Ref. [159].

ROS exert their predominant influence on redox regulation through thiol-based modifications of target proteins. $O_2^{\bullet-}$ reacts with Fe–S clusters, while H_2O_2 reacts with the cysteine (Cys) thiolate (S−) of a target protein to form sulfenate (SO−) [159]. This modification of protein function can be caused by this reaction [162].

At low to moderate levels, ROS act as secondary messengers to modulate biological functions by interacting with proteins, transcription factors, and genes involved in cell proliferation, differentiation, and adaptation to metabolic and immune stress [178, 182, 183]. However, an excessive increase in ROS levels can be detrimental to cells due to oxidative damage to key cellular components [184]. Very high ROS levels can ultimately lead to cell senescence or cell death [185].

Whenever the equilibrium between the generation and elimination of ROS is disrupted, an imbalance between oxidant production and antioxidant defense systems arises, leading to a condition known as oxidative stress or distress [186]. Oxidative stress triggers inflammation, mitochondrial dysfunction, and persistent DNA damage that causes replication errors, genomic instability, activation of oncogenes, and inactivation of tumor suppressor genes, ultimately resulting in cell proliferation, angiogenesis, survival, and the development of cancer (see tumorigenic ROS levels, **Figure. 1.11.1.3)** [162, 170, 186-195]. For this work, the mechanisms of ROS as redox signalling or tumor promotion represent an extensive topic that will not be reviewed in depth, however, the regulation of ROS to induce/escape cancer cell death will be highlighted.

Cancer cells sustain their elevated levels of energy through the process of aerobic glycolysis, which is followed by lactic acid fermentation, even in the presence of an abundance of oxygen. This metabolic pathway is also known as the "Warburg effect" [196], and it is essential for the cancer cells to adapt to conditions of low oxygen and minimal mitochondrial defects and ROS production.

Because the generation of ROS is a byproduct of high proliferative rate and metabolic activity, mitochondrial dysfunction [166], and a decrease in ROS-scavenging capacity [197] can result in cancer cells producing a much higher level of ROS compared to non-transformed cells [198]. Consequently, to counteract the detrimental effects of oxidative stress, it is believed that cancer cells must actively upregulate multiple antioxidant systems (**Figure. 1.11.1.3)**. Therefore, targeting the ROS signaling pathways is a promising approach for cancer treatment. By increasing ROS levels selectively in cancer cells [182, 185], pro-oxidant strategies can be employed to reach a cytotoxic threshold, which can lead to irreversible lethal oxidative damage and potentially serve as a viable strategy for cancer therapy [199-203].

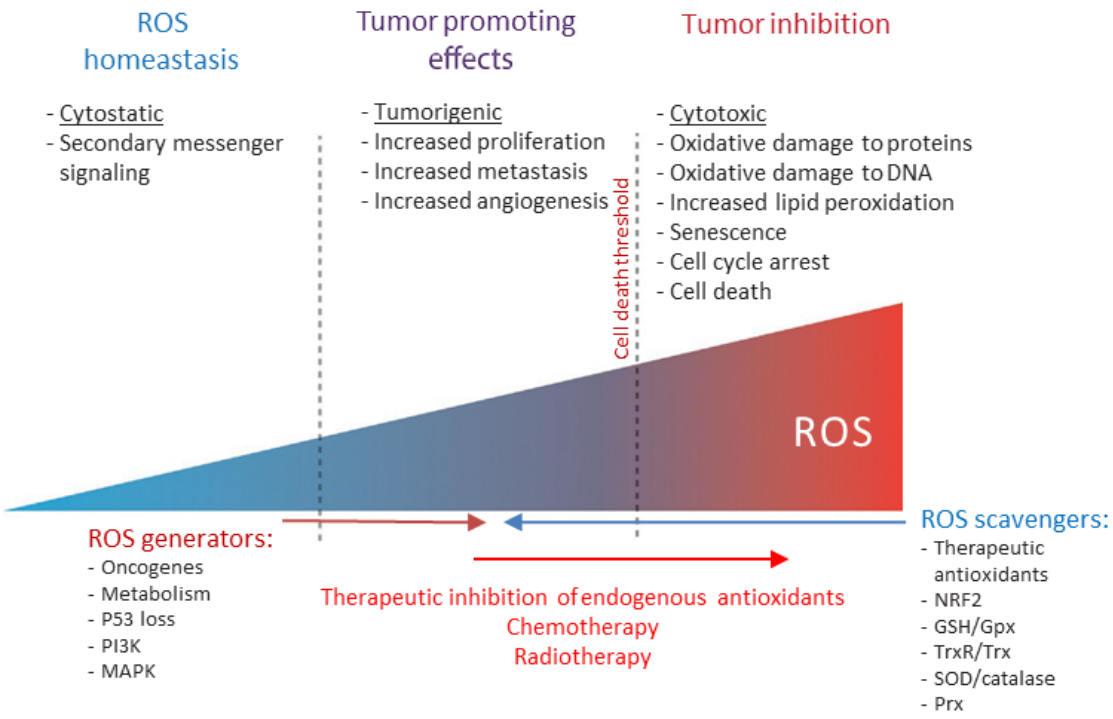

Figure. 1.11.1.3. Cancer cells can adapt to maintain their tumorigenic potential by balancing the generation and the scavenging of ROS. ROS can act as mitogens and initiate cellular adaptations that lead to cell survival, growth, proliferation, and differentiation in a controlled manner. However, an accumulation of ROS can result from characteristics such as oncogene activation, enhanced metabolism, hypoxia, or the loss of the tumor suppressor p53, leading to hyper-active cell signaling and pro-tumorigenic signaling events. This moderate increase in ROS can promote tumor growth through induction of metastasis, angiogenesis, and proliferation. To prevent oxidative stress and damage to proteins, DNA, and lipids, cancer cells up-regulate ROS scavenging systems to maintain ROS levels within a non-toxic range. Cancer cells function with ROS levels that are high enough to support pro-tumorigenic cell signaling without inducing cell death, making them ROS- and antioxidant-addicted. Therapeutic inhibition of endogenous antioxidants, chemotherapy, and radiotherapy increases ROS levels and induce cancer cell death. Adapted from Refs. [204] and [205].

1.11.2. Cell antioxidant system

In mammalian cells, to protect the cells against ROS, sophisticated antioxidant systems have evolved, among them glutathione (GSH), thioredoxin (Trx), superoxide dismutase (SOD), and catalase systems are the most important and well studied. Their components and involved antioxidant pathways are illustrated in **Fig. 1.11.2.**

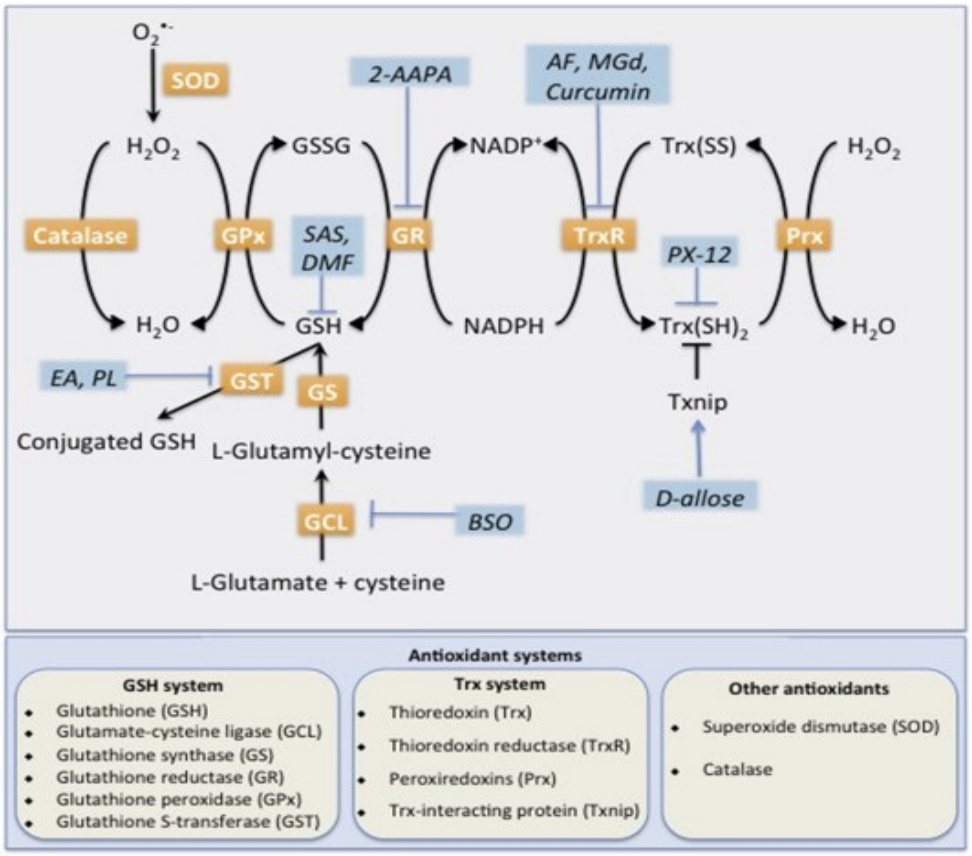

Figure. 1.11.2. The antioxidant pathways. There are four main antioxidant systems that play a vital role in this process: the glutathione (GSH), thioredoxin (Trx), superoxide dismutase (SOD), and catalase systems. GSH directly eliminates ROS through the action of glutathione peroxidase (GPx) and glutathione S-transferase (GST). Trx eliminates ROS through peroxiredoxin (Prx) and can be regenerated by thioredoxin reductase (TrxR) but is inhibited by thioredoxin interacting protein (Txnip). SOD detoxifies ROS by converting $O_2^{\bullet-}$ to H_2O_2, which is further catalyzed to

H_2O by catalase and peroxidases (GPx and Prx). Both GSH and Trx rely heavily on NADPH production for sustaining their activity, while SOD and catalase act independently of NADPH. 2-AAPA= 2-acetylamino-3-[4-(2-acetylamino-2-carboxyethylsulfanylthiocarbonylamino)phenylthiocarbamoylsulfanyl]propionic acid; AF= auranofin; MGd = motexafin gadolinium; SAS = sulfasalazine; DMF = dimethylfumarate; EA = ethacrynic acid; PL = piperlongumine; BSO = L-buthionine sulphoximine. Adapted from Ref. [206].

Superoxide dismutases (SODs) are the initial antioxidant enzymes discovered [207] and catalyze the conversion of the highly reactive $O_2^{\cdot -}$ to oxygen and the less reactive species H_2O_2. Humans possess three forms of SOD, namely cytosolic copper-zinc SOD (CuZn-SOD/SOD1), mitochondrial manganese SOD (Mn-SOD/SOD2), and extracellular SOD (SOD3) [208]. Catalase, primarily located in peroxisomes, decomposes H_2O_2 into water and oxygen, while also detoxifying substances such as phenols and alcohols [209, 210].

1.11.3. Thioredoxin system

The thioredoxin system, which includes nicotinamide adenine dinucleotide phosphate (NADPH), thioredoxin reductase (TrxR), and thioredoxin (Trx), plays a crucial role in maintaining the redox balance within cells and regulating various cellular processes. This system operates through a catalytic cycle in which TrxR reduces oxidized Trx using NADPH, and the resulting reduced Trx then acts as a reducing agent for target proteins [211]. This cycle helps shape the intracellular gradients of hydrogen peroxide (H_2O_2) in cells [212] and regulates processes such as transcription, DNA damage recognition and repair, proliferation, and cellular protection against apoptosis [211, 213-219]. The Trx system can be expanded to incorporate peroxiredoxin (Prx) and Trx-interacting protein (TxNIP). Prx represents a family of six isoenzymes (I to VI) that reduce alkyl hydroperoxides and H_2O_2 to their corresponding alcohols or water by accepting electrons

from Trx [53]. TxNIP impedes Trx activity by directly binding to the catalytic center of Trx [220], preventing the reducing activity of Trx and inhibiting the interaction between Trx and its downstream factors.

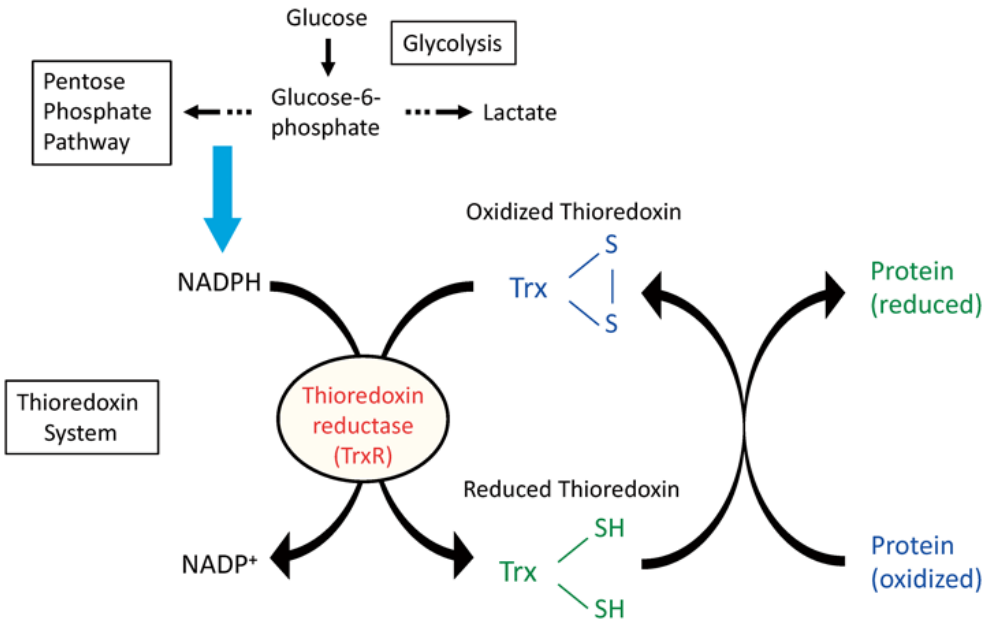

Figure. 1.11.3.1. Trx system. It serves as a primary antioxidant pathway in the body and plays a crucial role in regulating the redox balance in mammalian cells. TrxR employs NADPH as a catalyst to transform the oxidized state of Trx into its reduced state. The pentose phosphate pathway provides NADPH. Adapted from Ref [221].

Mammalian Trx, a small redox protein weighing 12 kDa, features a conserved dithiol-disulfide active site sequence (-Cys-Gly-Pro-Cys-). First identified in the early 1960s, it exhibits reversible oxidation or reduction states. The reduced form of Trx, Trx-$(SH)_2$, reduces target oxidized protein substrates that typically contain a disulfide group, which comprises two cysteine groups. Conversely, the oxidized form of Trx, Trx-[SS], is reduced by TrxR in an NADPH-dependent manner [211, 222]. This regulation of protein function influences a wide range of physiological and biochemical cellular activities including cellular redox environment, inducing

DNA synthesis, growth, apoptosis and cellular defense [197]. Human cells possess two types of Trx: Trx1, encoded by the *TXN* gene, and Trx2, encoded by the *TXN2* gene. Trx1 is present in the cytoplasm and has also been detected in the nucleus of normal endometrial stromal cells, tumor cells, and primary solid tumors [211]. In contrast, Trx2 has a mitochondrial translocation sequence at its N-terminal region and plays a crucial role in maintaining mitochondrial ROS homeostasis [223].

Mammalian TrxRs are dimeric flavoenzymes that contain selenium and have a molecular mass of 58 kDa [224]. These enzymes belong to the TrxR family, which comprises three isoforms: TrxR1, TrxR2, and TrxR3 [225]. Each isoenzyme is encoded by a separate gene: *TXNRD1*, *TXNRD2*, and *TXNRD3*, respectively. Although their overall structures are similar, the expression levels and localization of these proteins differ. TrxR1 is primarily found in the cytoplasm, TrxR2 in the mitochondria, and TrxR3 at low levels in the testis [226]. These proteins possess a conserved catalytic site, comprising -Cys-Val-Asn-Val-Gly-Cys-, which is indispensable for their redox activity, as illustrated in **Figure 1.11.3.2.** [211, 227]. The C-terminal sequence, consisting of -Gly-Cys-SeCys-Gly-, plays a crucial role in communicating with the catalytic site, and is likewise essential for their function. TrxRs catalyze the reduction of oxidized thioredoxin utilizing NADPH as a cofactor [228]. NADPH is generated by glucose-6-phosphate dehydrogenase, which serves as the rate-limiting enzyme of the pentose phosphate pathway. TrxR1 is overexpressed in human cancer cell lines and primary tumors [197].

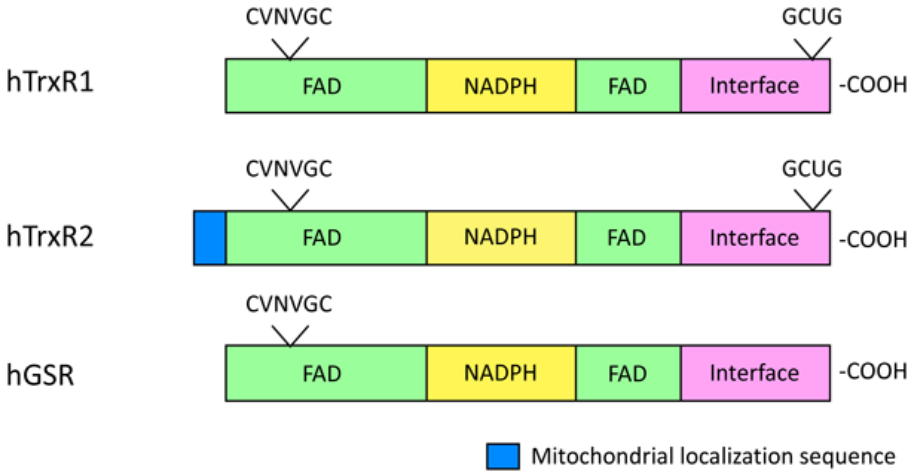

Figure 1.11.3.2. The domain structures of human TrxR1, TrxR2, and glutathione-disulfide reductase/glutathione reductase (GSR). The domain structures of hTrxR and hGSR are similar in nature, however, hGSR does not possess a selenocysteine residue at its C-terminal active site. The active site sequences are indicated in the upper portion of the motifs. Selenocysteine (U) is only present at the penultimate C-terminal amino acid in hTrxR1 and hTrxR2. Adapted from Ref. [221].

The interaction between reduced Trx and apoptosis signal-regulated kinase 1 (ASK1) results in the formation of a Trx-ASK1 complex, which inhibits apoptosis. Conversely, the dissociation of this complex activates ASK1 and promotes apoptosis in cancer cells (**Figure 1.11.3.3**.) [229-232].

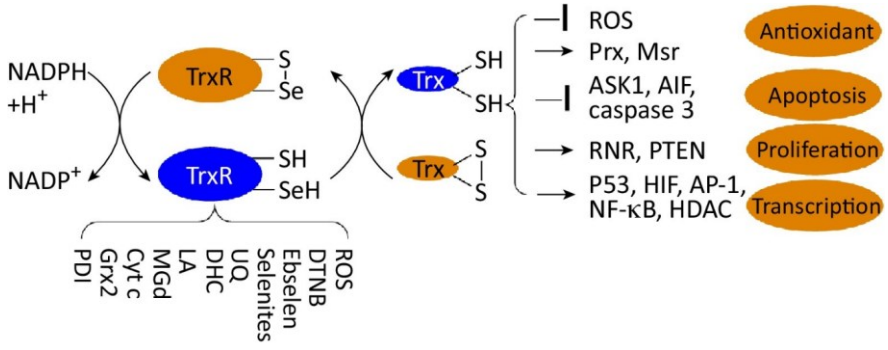

Figure. 1.11.3.3. Functions of the thioredoxin system. Adapted from Ref. [228].

The expression of Trx and TrxR has been demonstrated to exhibit a significant correlation with tumor grade, metastasis, and adverse prognosis in invasive carcinomas, including lung and gastrointestinal malignancies, cervical cancers, oligodendroglial tumours, ovarian cancers, and breast cancers [219, 233, 234].

Prior research has demonstrated that the chemical or genetic suppression of the Trx system leads to the halting of the cell cycle. Tumour growth is significantly suppressed and the spread of cancer cells to other organs is not detected in mice that have been injected with human breast cancer MCF-7 cells and genetically modified with a redox domain mutant of Trx1 [235, 236]. In addition, when human breast cancer MDA-MB-231 cells are genetically modified to have a non-functional redox domain in the Trx1 protein, they show a decrease in the expression of matrix metalloproteinase-9 and a reduction in invasion [237]. These findings indicate that Trx1 plays a crucial role in facilitating the growth and spread of cancer cells.

Disrupting the activity of TrxR leads to a disturbance in redox homeostasis, which results in an increase in oxidative stress triggering apoptosis and necrosis [238, 239]. Yoo et al. revealed that reducing the expression of TrxR1 hinders tumor formation in a mouse xenograft model, confirming the crucial role of TrxR1 in tumor progression [240]. Furthermore, knocking down TrxR1 impedes the growth of cancer cells and the process of DNA replication [241].

Furthermore, the level of TrxR1 expression in tumour cells has been found to be correlated with their sensitivity to cytotoxic drugs in a drug-dependent manner. In particular, the cytotoxicity of cisplatin is increased in cells with high TrxR1 expression compared to those with low expression [242]. Additionally, Yao et al. discovered that high cytoplasmic TrxR expression was significantly linked to worse overall survival (OS) in adult glioblastoma patients [243]. In all cohorts, high TrxR expression was associated with a poorer prognosis. Kemerdere et al. discovered that both serum

and tissue levels of TrxR were elevated in patients with grade 4 astrocytoma, which implies a potential role for TrxR in the progression of this type of cancer [244]. Additionally, Esen et al. [233] found that not only grade 4 astrocytomas but also grade 1-4 gliomas displayed significantly higher TrxR1 expression compared to normal brain tissue. Moreover, TrxR1 expression increased as the tumour grade rose.

Regarding the TrxR1 gene expression and cytoplasmic immunostaining, it was found to be highly correlated with the tumor grade and Ki-67 index [233]. In summary, TrxR may play a significant role in tumor progression and resistance to chemotherapy, potentially due to its anti-apoptotic functions [244]. These findings indicate that targeting the Trx system may be a promising approach for the development of anticancer drugs. By suppressing the antioxidant system, oxidative stress in tumor cells can be increased, leading to inhibition of tumor growth and apoptosis.

1.11.4. Glutathione system

Glutathione (GSH) is a tripeptide thiol and the most prevalent antioxidant in cells, safeguards cell membranes from harmful consequences, and plays a vital function in stabilizing intracellular redox equilibrium, particularly during conditions of hypoxia and elevated levels of ROS and NO [245]. It is available in both reduced (GSH, active) and oxidized states (glutathione disulfide, GSSG, inactive) shown earlier in **Fig. 1.11.2.**

GSH synthesis comprises two consecutive steps. The initial phase involves an interaction between cysteine and glutamate, which is catalyzed by the rate-limiting enzyme γ-glutamylcysteine synthetase (also known as glutamate-cysteine ligase or GCL) [246]. This reaction results in the formation of γ-glutamylcysteine, a crucial step in GSH generation that serves as an active site for oxidizing agents, such as buthionine sulfoximine (L-BSO). Later, glutathione

synthetase (also known as glutathione synthase or GS) adds glycine to the structure and concludes the synthesis of GSH.

GSH plays a crucial role in sequestering ROS and generating GSSG. GSSG can be reconverted to GSH with the help of the glutathione reductase enzyme (GRd or GSR) [162], which utilizes NADPH as its electron source. NADPH is primarily obtained through the pentose phosphate pathway. Under normal physiological conditions, most of the total glutathione (90%) exists in its reduced form (GSH), while the remaining 10% is in the disulfide form (GSSG). Any changes in this ratio can signify oxidative stress [247]. Additionally, to aid in the detoxification of xenobiotics, which may affect cancer therapy [248], glutathione S-transferase (GST) actively catalyzes the conjugation of GSH with its substrates.

GSTs are categorized based on their structure, and among them, GST-θ and GSTp1 have been studied in relation to radiation exposure. The GSH system can be extended further to include glutathione peroxidase (GPx) and glutaredoxin (Grx), which are closely linked to GSH and rely on it for their antioxidant function. Grx is a crucial enzyme involved in processes such as disulphide reduction and deglutathionylation. GPx catalyzes the reduction of free H_2O_2 to water and converts lipid hydroperoxides into their corresponding alcohols, with GSH serving as a cofactor. GPx exists in eight isoforms (GPx1-8), which are present in various tissues and cell fractions throughout the body [206].

The GSH system is one of the defense mechanisms that helps cells adapt to oxidative stress. It is highly expressed in tumor tissues [246]. The Trx and GSH antioxidant pathways synergize to drive cancer initiation and progression, and their upregulation in tumor tissue can confer drug resistance to chemotherapy in cancer cells [249]. Trx and GSH are essential antioxidant systems necessary for cell survival. In the case of tumors deficient in TrxR1, they are highly sensitive to

pharmacological GSH deficiency as the survival and proliferation of these tumors depend on a functional GSH system, both *in vitro* and *in vivo* [235]. Targeting both the Trx and GSH systems simultaneously may have synergistic effects in cancer treatment [249].

1.11.5. Nuclear factor erythroid 2–related factor 2

The transcription factor nuclear factor erythroid 2–related factor 2 (Nrf2) is a crucial regulator of antioxidant pathways. Under normal conditions, Nrf2 is bound and suppressed by Kelch like ECH-associated protein 1 (Keap1), which promotes Nrf2 degradation through the proteasomal pathway.

Keap1 harbours several cysteine residues that can be subject to oxidation. Keap1 respond selectively to various oxidants by multiple cysteine thiol groups [170, 250]. The oxidation process, notably involving the formation of Cys151 disulfide in the Keap1 dimer [251], results in a conformational shift that causes the release of Nrf2 from Keap1, which in turn prevents Nrf2 ubiquitylation, thereby enhancing Nrf2 stability and facilitating its subsequent nuclear translocation.

Once in the nucleus, Nrf2 forms a dimer and binds to antioxidant responsive elements (AREs). The binding of Nrf2-ARE regulates the expression of genes that are involved in the cellular antioxidant and anti-inflammatory defense. These genes include phase 2 detoxification enzymes such as glutathione, superoxide dismutase, glutamate-6-phosphate dehydrogenase, heat shock proteins, and ferritin. Additionally, it regulates the expression of pro- and anti-inflammatory enzymes such as cyclooxygenase-2 (COX-2), inducible nitric oxide synthase (iNOS), and heme oxygenase 1, while also regulating mitochondrial biogenesis [162, 252].

Apart from oxidative stress, Nrf2 activation can also occur in response to cigarette smoking, infections, or inflammation. When the Nrf2/ARE pathway is disrupted, it can lead to oxidative stress, inflammation, and mitochondrial dysfunction [253]. The Nrf2-Keap1 system is regulated by thioredoxin reductase 1 [254] and the sirtuin family of deacetylases [255]. Nrf2 is considered a tumor suppressor due to its cytoprotective function in countering oxidative stress. However, malignant cells can upregulate Nrf2 to protect against oxidative stress caused by chemotherapeutic agents and radiotherapy, increasing their survival and imparting an oncogenic property. As a result, Nrf2 can be a potential therapeutic target in cancer treatment [162].

1.11.6. EGFR and the relationship with reactive oxygen species

Previous studies reported the role of ROS in EGFR activation and the correlation between ROS and EGFR in tumor progression and drug resistance [256-260]. Exposure to mild ROS levels induced an aberrant pattern of phosphorylation and impaired EGFR trafficking and degradation, leading to ROS-mediated tumor progression [261]. Aberrant EGFRvIII expression in GBM has been associated with increased levels of ROS, DNA strand break accumulation, genome instability, and a better sensitivity to DNA repair inhibitors [262]. Furthermore, the crosstalk of EGFR with the GSH system is involved in GBM increased antioxidant capacity and drug resistance.

1.11.7. Redox adaptation/ redox resetting

Redox resetting occurs when cancer cells can modify their metabolism to counteract high levels of ROS by enhancing their antioxidant systems, which allows them to adapt to a new redox balance. This adaptation makes the cancer cells highly dependent on their antioxidant system for survival, making it a potential target for anticancer treatment [162]. There is a mutual relationship between the metabolism and redox balance of cancer cells, with a particular emphasis on the roles of glycolysis, glutaminolysis, fatty acid oxidation, one-carbon metabolism, and the pentose phosphate pathway [263]. The "threshold concept" implies the ability of cancer cells to keep their intrinsic ROS levels at a threshold favourable for tumor growth below the threshold of excessive cytotoxic ROS levels [264]. To this end, cancer cells rely on increasing expression and/or activity of the main endogenous antioxidants, GSH and Trx systems, as key adaptive ROS-scavenging mechanisms via a mechanism called redox resetting [265-269].

1.12. Auranofin, a TrxR inhibitor.

Auranofin is a phosphine complex containing gold (I) that was approved by the United States Food and Drug Administration in 1985 for the primary treatment of rheumatoid arthritis and is marketed under the brand name Ridaura [270, 271]. The drug complex consists of two parts: a water-soluble aurothioglucose entity with a sulfur donor group, and a phosphine ligand that provides lipophilic properties (**Figure 1.12.1**). Auranofin is a prodrug that undergoes irreversible oxidation and hydrolysis and progressive deacetylation to form two active compounds: a triethylphosphinenegold (I) cation, and a gold (I) thioglucose species, with a variable number of acetyl groups [272]. Auranofin exhibits strong affinity towards sulfur and selenium ligand proteins that have free cysteines exposed, owing to its chemical properties [273].

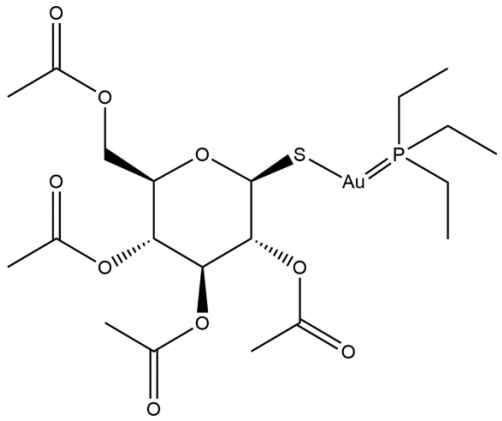

Figure 1.12.1. Chemical structure of Auranofin. This complex comprises a linear molecule of triethylphosphine and thiolate groups attached to a gold (I) center. Adapted from Ref [274].

Auranofin can be taken orally and reaches intestine within 20 minutes [275]. Approximately 25% of the dose is detected in the plasma mostly bound to albumin [276, 277]. Within 1 to 2 hours, the plasma concentration of auranofin can reach 60 to 90 μg/L [278-280] with a half-life ranging from 17 to 25 days. On average, it takes 55 to 80 days for auranofin to be eliminated from the body [223, 281, 282], with the majority (85%) being excreted through the feces and the remaining 15% through the kidneys [280].

The main function of auranofin is to act as a pro-oxidant by interfering with the redox system of the cell. This is achieved by strongly inhibiting the two isoforms of thioredoxin reductases, TrxR1 and TrxR2 (**Figure 1.12.2**) [283-285]. TrxRs serve as antioxidants by controlling the ROS levels, thereby protecting cells from the detrimental effects of oxidative stress. TrxRs isoforms are selenoproteins containing a redox-active site that includes a selenocysteine residue that is readily accessible and highly nucleophilic. This characteristic makes them highly vulnerable to irreversible inhibition by auranofin [286, 287], thereby hindering electron transfer [197]. Classic proteomic strategies and mass spectrometry-based redox proteomics analysis reveals that TrxRs exhibit interaction with approximately four triethylphosphine gold (I) molecules

[285] while auranofin oxidizes over five hundred cysteine-containing peptides [288, 289]. TrxRs act in a nicotinamide adenine dinucleotide phosphate (NADPH)-dependent manner, by transferring electrons from NADPH to the active disulfide site on the oxidized thioredoxin (Trx) protein. The reduced form of Trx functions as an electron donor for both peroxiredoxin and ribonucleotide reductase [269]. By increasing the reduced form of Trx, cell growth is promoted, transcription factors that regulate gene expression are activated, and programmed cell death is inhibited, leading to cell survival. However, when TrxR is inhibited by auranofin, the levels of the oxidized form of Trx rise, causing an increase in intracellular oxidized substances and ROS, ultimately leading to apoptosis [221].

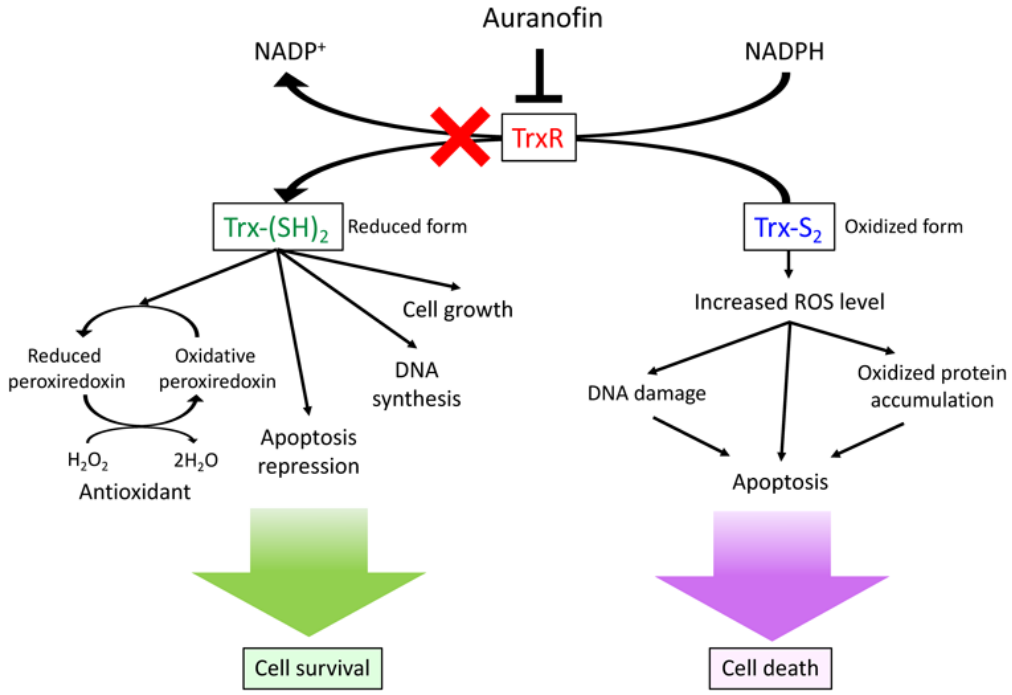

Figure 1.12.2. The impact of auranofin-induced inhibition of TrxR within the cell. Adapted from Ref. [221].

Studies have shown that the TrxR1/Trx1 system is upregulated in different types of cancer such as breast, ovarian, colorectal, lung, pancreatic, and gastric cancers [216, 221, 290-292] as

well it has been implicated in the resistance of several human tumour cells to chemotherapeutics [284, 293, 294]. As a result, auranofin is a promising repurposing therapeutic option against cancer by targeting this system.

Auranofin has demonstrated significant anticancer effects in various types of cancer types, either alone [289, 295-322] or in combination with other drugs [323-325]. Anticancer effects of auranofin include high levels of oxidative stress and hampered reductive pathways in both the cytoplasm and mitochondria [284, 326, 327]. As an example, research has shown that the ability of auranofin to kill human chronic leukemia and gastric cancer cells was linked to mitochondrial dysfunction and accumulation of ROS [296, 328].

A study showed that auranofin alone effectively inhibited multiple key nodes in the PI3K/AKT/mTOR signaling pathways and elicited cytotoxic effects in NSCLC cells [303]. The combination of auranofin with the AKT inhibitor MK2206 causes simultaneous inhibition of the TrxR1 and AKT pathways, inducing robust ROS production, and apoptosis [329]. Interestingly, synthetic lethality occurred while targeting AKT and TrxR1 through the Keap1/Nrf2 antioxidant system [329]. Tumour Suppressor Candidate 2 (TUSC2) negatively regulates cancer growth and progression in multiple cancer types [330]. The same previous research group discovered that the addition of auranofin-TrxR inhibition sensitized NSCLC cells to TUSC2 overexpression/erlotinib treatment combination and resulted in increased cell apoptosis and colony formation inhibition [197].

Guo-Xin Hou et al. reported that auranofin decreased cell viability and sphere formation of GBM stem cells in a concentration-dependent manner. Interestingly, besides ROS increase, auranofin caused ATP depletion by inhibition of glycolysis. Also the combination of auranofin

with adriamycin decreased tumor growth in mice bearing xenografts of A549 human lung cancer cells [331].

In GBM a study showed that auranofin induced cell death in different brain cancer cell models, including neuroblastoma SK-N-AS cells, glioblastoma U251 cells, and patient-derived GBM neurospheres [325]. Activating the Small-conductance Ca2+-activated K+ channels (SK channel) in healthy brain cells with CyPPA results in a minor reduction in mitochondrial respiration and a moderate rise in ROS within the mitochondria [332]. The application of auranofin with CyPPA resulted in the promotion of apoptosis in U251 gliomas cells, as well as an increase in the loss of mitochondrial transmembrane potential (MMP), lipid peroxidation, and mitochondrial and cytosolic ROS in neuroblastoma cells. Additionally, this treatment combination had a mild effect on non-cancerous brain cells [325].

A recent study found auranofin and cold atmospheric plasma synergized to trigger distinct cell death mechanisms and immunogenic responses in GBM [323]. Auranofin monotherapy caused a significant accumulation of intracellular ROS, yet this increase was more pronounced in the combination treatment. In an *in vivo* setting, auranofin-induced inhibition of the antioxidant system was able to sensitize GBM tumours to plasma treatment, decreasing tumour size and increasing mice survival [323].

The inhibitory activity of auranofin against TrxR may lead to further pharmacologic effects For example, auranofin was found to inhibit mitochondrial activity and to induce oxidative stress in human cancer HepG2 and MCF-7 cells, it also inhibited the proteasome triggering the endoplasmic reticulum stress by targeting proteasome-associated deubiquitinases (DUBs) UCHL5 and USP14 [301, 333].

The anti-inflammatory properties of auranofin are associated with a blockade of the Janus kinase 1 (JAK1)/ signal transducer and activator of transcription 3 (STAT3) signalling. Auranofin inhibits IL-6-induced phosphorylation of JAK1 and STAT3 and the STAT3 translocation into the nucleus [312, 334]. In cancer cells auranofin reduced the production of acute-phase proteins such as haptoglobin, fibrinogen, C3 complement, and α1-acid glycoprotein, as well as the gene expression of vascular endothelial growth factor, all of which are regulated by STAT3 [312].

1.12.1. Clinical trials using auranofin

The CUSP9 (Coordinated Undermining of Survival Paths with 9 repurposed drugs) treatment protocol started as a concept using several re-purposed drugs that had demonstrated evidence of inhibiting one or more of the identified GBM growth and cell survival pathways, eventually selecting a combination of nine drugs with specific rationale including auranofin [335]. This cocktail was further tested in patient-derived Glioblastoma Stem Cells (GSCs) demonstrating high sensitivity to the combination treatment compared to each drug alone [336]. The 9 drugs of the CUSP9v3 protocol included: aprepitant, auranofin, celecoxib, captopril, disulfiram itraconazole minocycline, ritonavir, and sertraline, which their primary non-oncology use is for nausea, rheumatoid arthritis, pain, hypertension, alcohol abuse, fungal infection, bacterial infection, viral infection, and depression, respectively. The CUSP9v3 protocol was tested in a clinical trial (NCT02770378) using the combination of the 9 drugs, in addition to the standard-of-care, and temozolomide added metronomic (low-dose, repetitive, for long period) for recurrent GBM. Results did not show significant safety concerns and after 3 years of daily, uninterrupted use of CUSP9v3 regime three of ten originally enrolled patients were still alive [337].

In addition, auranofin has also been included in other phase I/II clinical trials to treat patients with chronic lymphocytic leukemia, non-small cell lung cancer or small cell lung cancer,

and ovarian, peritoneal, and fallopian tube cancers due to its promising evidence as an anti-cancer agent (NCT01419691, NCT01737502, NCT01747798, and NCT03456700; www.clinicaltrials.gov).

1.13. L-buthionine sulfoximine: a GSH inhibitor

L-Buthionine-sulfoximine (L-BSO) is a synthetic amino acid widely used in pharmacological and biomedical studies that strongly blocks the biosynthesis of GSH because of inhibition of γGCS. GSH is often up-regulated in chemotherapy–resistant tumors. Consequently, by depleting GSH, L-BSO enhances the cytotoxicity of chemotherapeutic agents in drug-resistant tumors [248]. L-BSO is less toxic than its predecessor methionine sulfoximine (MSO) and may be safely administered intravenously in humans [248, 338].

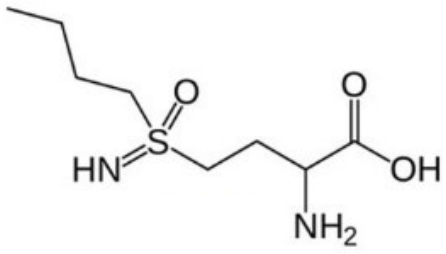

Figure 1.13. The molecular structure of L-BSO. Adapted from Ref. [248].

A systematic review has revealed the cytotoxic potential of L-BSO against cancer cells. The collected data indicate that, depending on the concentration and cell line, the exposure to L-BSO alone can exhibit cytotoxic activity. However, L-BSO is more effective when combined with other well-established drugs to enhance cytotoxicity by depleting the antioxidant capacity of GSH [248]. When utilized as a pretreatment or concurrently with anticancer therapy, L-BSO demonstrates enhanced tumor growth suppression, however, more pronounced effects are observed when L-BSO is administered simultaneously with other chemotherapeutics [248].

Among the chemotherapeutic agents used in co-treatment with L-BSO, alkylating agents and platinum analogues were found to be particularly effective in exhibiting antitumor effects. It

was observed that these agents induced programmed cell death via both apoptotic and non-apoptotic pathways [248].

L-BSO has shown anticancer effects *in vitro* in different cancer cells, including breast, colon, myeloma, and leukemia in a time-dependent cytotoxicity (24 h IC_{50} of 100 μM, 850 μM, 450 μM, and 2 μM, respectively). In an *in vivo* mice model it was well tolerated despite high doses; however, it did not decrease tumour growth or improve survival in tumour-harboring mice unless used in combination with melphalan (L-PAM) [339]. In ovarian cancer cells, the concentration of L-BSO needed to reach 50% of the maximum cytotoxic effect (EC50) was 56.23 mM for ES2 cells and 38.49 mM for OVCAR-3 cells [340].

L-BSO was found to induce apoptosis in esophageal cancer cells when treated with 1 mM [341]. Furthermore, L-BSO was demonstrated to increase apoptosis and cleaved PARP expression in hepatocellular carcinoma cell lines when treated with 200 μM, and when combined with the structural analog of pyruvic acid, 3-BP, it resulted in a decrease in tumour growth and an increase in apoptotic index in a mouse model of disease [342].

L-BSO elicited cytotoxic effects for most 18 human neuroblastomas (IC_{90} = 2.1–>1000 μM) below equivalent steady state plasma levels of L-BSO reported in adult human trials; the same study reported that L-BSO (500 μM for 72 h) induced apoptosis as detected by DNA laddering, nuclear morphology, and TUNEL staining of DNA fragments using flow cytometry [343].

The selective toxicity of L-BSO towards melanoma cells was evident both *in vitro* and *in vivo*. *In vitro* studies revealed that L-BSO caused a decline in the GSH levels of melanoma cells, which led to impaired clonogenic survival. *In vivo* studies showed that L-BSO treatment in mice

injected with melanoma cells resulted in extended animal survival and reduced metastatic spread of tumor cells [344].

According to the systematic review no obvious toxicity was observed in animals, rat or mouse species, both genders, when L-BSO was administered in different dosage regimens, such as a single dose of 32 mmol/kg, multiple doses totaling 72 mmol/kg, or daily water consumption containing 20 mM L-BSO for 45 days [345, 346]. While there was no direct toxicity associated with continuous L-BSO administration, most tissues experienced a subsequent GSH depletion that rendered them more vulnerable to the harmful effects of other substances, including heavy metals [347] and medications [348]. According to another report, oral administration of L-BSO (20 mM) in mice for 14 days did not result in any toxic signs [348]; however, the combination with paracetamol caused hepatocyte and renal tubule epithelium necrosis, which in turn led to the death of 9 out of 10 mice [349].

Phase I or pilot clinical trials have demonstrated that L-BSO has minimal toxicity in patients with neuroblastoma [350], myeloblastic leukemia [351], and a cohort of individuals carrying ovarian, lung, melanoma, colorectal, breast, pancreas and renal cancers [352]. Human subjects received a 30-min infusion of 3 g/m^2 L-BSO, followed by a continuous infusion for 24 to 72 hours, with minimal adverse reactions, including nausea and vomiting [352]. Notably, L-BSO was used at subtoxic concentrations to potentiate cytotoxic effects in most studies; toxic doses, may require high plasma concentrations (roughly 500 μM) [353].

1.14. Role of P53 in GBM

The p53 gene, often referred to as the "guardian of the genome," plays a significant role in the development of cancer [354]. It is the most frequently mutated gene in human cancer overall. Somatic mutations lead to the loss of wild-type p53 (wt-p53) activity and the gain of oncogenic functions such as resistance to apoptosis and increased genome instability [355]. These mutations also result in the deregulation of cell cycle control, senescence, apoptosis, and DNA repair (**Figure 1.14**). Consequently, cancer cells acquire new properties, such as increased invasion, migration, angiogenesis, proliferation, genomic instability, and drug resistance [356]. Mutant-p53 is linked to aggressive tumor phenotypes and poor patient survival [357].

The p53 tumor suppressor protein activates multiple target genes, including p21Waf1/Cip1, GADD45A, Bax, Noxa, PUMA, KILLER/DR5, and Fas among others. The TP53 gene has been found to have alterations in approximately 25-30% of primary GBM cases [358], with a higher incidence of TP53 mutations in the "proneural" subtype. Many of these mutations, which are mainly missense mutations, occur within the DNA-binding domain of p53 and disrupt its ability to bind to DNA and regulate target genes. This leads to impaired transactivation of the p53 antagonist MDM2. Inhibition of MDM2-mediated degradation of mutant (mut)p53 contributes to the stabilization and increased expression of mutp53 protein [359].

Mutations in the TP53 gene result in the inactivation of wt-p53 or the formation of cotetramers with co-expressed wt-p53 that act as dominant negative inhibitors. Additionally, some TP53 missense mutations can give rise to oncogenic properties known as "gain-of-function" (GOF) [360], which promote tumor cell invasion, prevent apoptosis, and increase resistance to anticancer treatments. Previous studies have suggested that wt-p53 plays a role in regulating MGMT levels in various human cancer cell lines, including GBM [361]. Therefore, strategies

aimed at restoring wt-p53 function may also lead to decreased MGMT levels in GBM tumours, potentially overcoming resistance to alkylating agents that are commonly used in GBM treatment. [362]. Moreover, p53 activity is dependent on the TrxR1–Trx antioxidant system [363]. Interestingly, p53 overexpression enhanced p53-induced ROS-accumulation leading to apoptosis and necrosis in glioma cells [364]. Consequently, approaches that aim to restore the functionality of wt-p53 may also result in an increase in ROS in GBM tumors. This increase in ROS could potentially bypass resistance to ROS compensatory mechanisms [364].

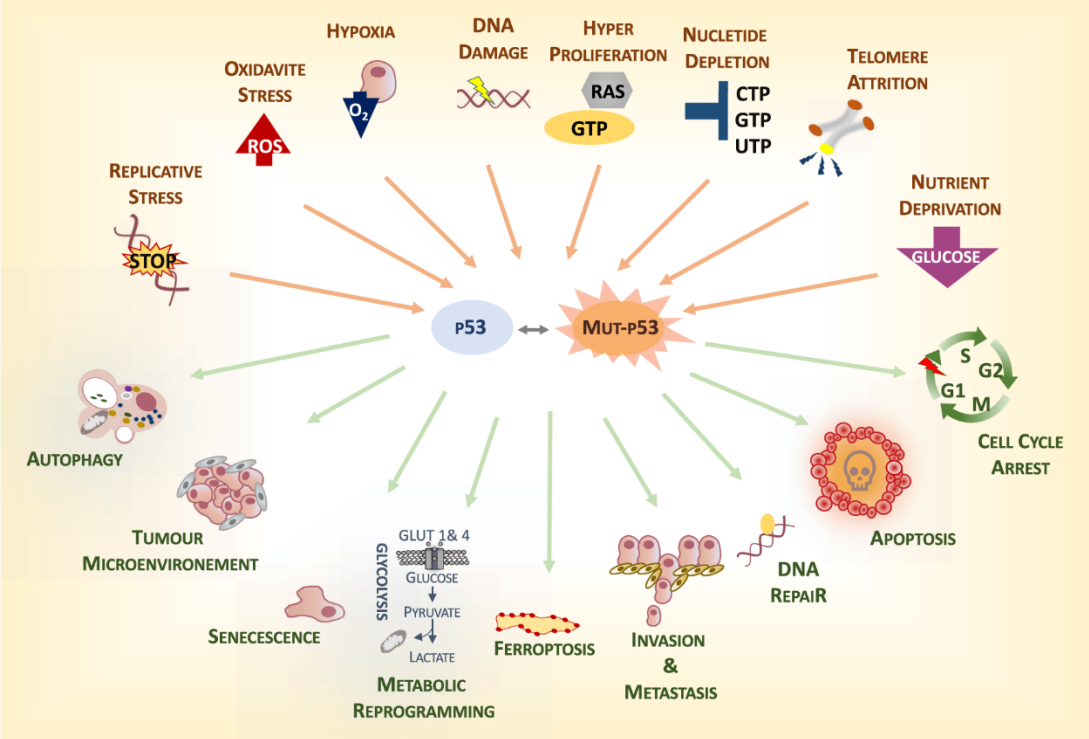

Figure 1.14. p53 is a stress response protein. p53 serves as a critical molecular connection between external stimuli and the cellular biological response that have tumor suppressor properties. In response to stress, functional p53 activates protective mechanisms such as apoptosis, DNA repair, senescence, and metabolic rewiring, as well as autophagy. However, when p53 is mutated, these physiological responses can be disrupted, leading to abnormal cellular processes that contribute to tumour development. Adapted from Ref. [363].

1.15. APR-246 (Prima-1^{Met}): a p53 stabilizer

As mentioned previously, primary GBM can be categorized into various subtypes based on molecular characteristics, among these subtypes, the proneural and mesenchymal subtypes exhibit the highest prevalence of p53 mutations, with rates of 54% and 32% respectively [15]. Other malignancies such as High-Grade Serous Ovarian Cancer (HGSOC) are also frequently associated with p53 mutations, with more than 96% of patients that can either result in gain-of-function (oncogenic) and loss-of-function (loss of p53 activity) mutations [365-368].

The prevalence of TP53 mutations in human tumors has spurred the development of therapeutic approaches aimed at targeting mutant p53 in cancer. Pharmacologically reactivating mutant p53 is believed to lead to significant cell death. This concept is supported by research that demonstrates the prompt eradication of tumours through apoptosis and/or senescence when functional p53 is reintroduced in mouse tumours *in vivo* [369-371].

A quarter-century ago, a collection of small molecules was discovered through chemical library screening or rational drug design that had the ability to restore the wild-type tumor suppressor activity of mutant p53 [372-375]. This finding increased optimism for the development of innovative and efficient cancer treatments that could overcome the proliferative and anti-apoptotic advantages gained through the loss of p53 function in various types of cancer, including gliomas [376-380].

A library screening led to the identification by Bykov and colleagues of the molecule PRIMA-1. PRIMA-1 and its methylated analog form PRIMA-1^{MET} (also named as APR-246 or Eprenetapopt) have been studied in several models, alone or associated with other cancer treatments [356].

Studies have demonstrated that PRIMA-1 and PRIMA-1^{MET} can effectively hinder the growth and trigger apoptosis in ovarian, osteosarcoma, and lung cancer cells that harbor mutp53, both *in vitro* and *in vivo* [372, 381, 382]. PRIMA-1 and PRIMA-1^{MET} have shown anticancer effects such as inhibition of cell proliferation and vitality, inhibition of colony formation and cancer cell migration, induction of apoptosis by the activation of caspases in varied mutp53 cells [356]. The sensitivity to the cytotoxic effects of PRIMA-1 and PRIMA-1^{MET} varied with IC_{50s} ranging from 0.75 μM to 200 μM [356]. However, PRIMA-1^{MET} is more active than PRIMA-1 [383], exhibiting superior permeability properties [384], and demonstrating cytotoxicity towards prostate and melanoma cell lines, regardless of TP53 mutational status [385, 386]. No significant cytotoxic impact has been reported when PRIMA-1^{MET} was used in human normal cells (hematological and fibroblasts); similarly, it is well tolerated in *in vivo* studies using doses ranging from 20 mg/kg/day to 400mg/kg/day [356]. From a clinical perspective, PRIMA-1^{MET} was among the p53 rescuing small molecules with favorable safety and pharmacokinetic profiles, having already undergone clinical trials [387-389].

PRIMA-1 and PRIMA-1^{MET} are prodrugs that are converted into methylene quinuclidinone (MQ), a Michael acceptor (α,β-unsaturated carbonyl that creates a carbon-carbon bond) that reacts covalently with thiol groups of mutp53, as well as wt p53 **(Figure 1.15.1)** [390]. The specific molecular mechanisms responsible for the reactivation of mutp53 by PRIMA-1 and PRIMA-1^{MET} are not yet fully understood. Nevertheless, it is established that these compounds induce proper folding of the mutated protein [372, 383, 391]. Specifically Cys124 of the p53 core domain, has been identified as a possible target of PRIMA-1 [392].

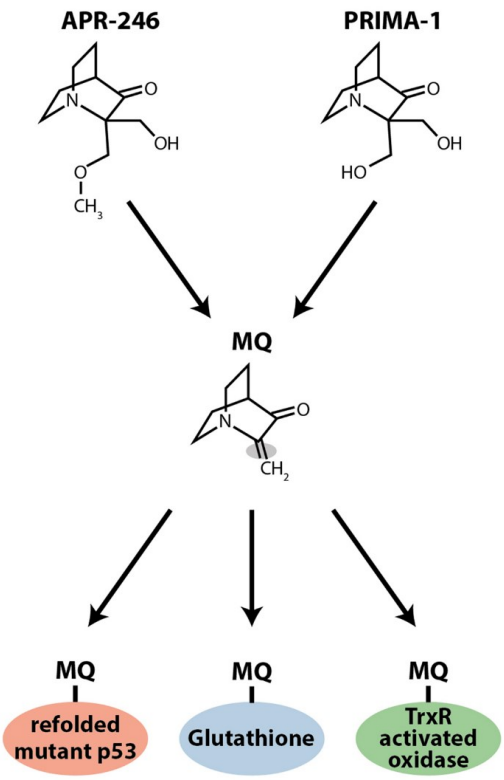

Figure 1.15.1 Chemical structures of PRIMA-1^{MET} (APR-246) and PRIMA-1. Both compounds undergo metabolism to produce the active moiety, methylene quinuclidinone (MQ). MQ forms a covalent bond with thiol groups in mutp53, and it also binds to TrxR, transforming the enzyme into an active oxidase. Moreover, MQ binds to GSH, reducing the amount of free GSH in the cell. Both later processes result in an increase in ROS. Adapted from Ref. [384].

In GBM, GSCs represent a disease reservoir leading to resistance and recurrence, and MGMT expression, is also an important predictor of response. Previous studies have shown that wtp53 down-regulates MGMT [361, 393, 394]. With this notion, reactivating p53 could serve as a strategy to sensitize MGMT positive cells to standard treatment. Patyka et al. showed that PRIMA-1^{MET} produced cytotoxic effects on various patient-derived GSCs with varying levels of MGMT regardless of p53 status. However, low MGMT and mutp53 levels were linked to increased cell sensitivity to PRIMA-1^{MET} [362]. PRIMA-1^{MET} induced activation of wtp53, and

downregulated MGMT in MGMT positive GSCs cells [362]. Despite PRIMA-1^{MET} did not induce PARP-1 or caspase-3 cleavage in GSCs, it disrupted neutrospheres evoking necrotic cell death. These effects were observed at lower concentrations compared to established GBM cell lines [362].

Studies have shown PRIMA-1 and PRIMA-1^{MET} produce massive ROS induction which presumably contributes to the anti-tumor activity, and can trigger a p53-dependent [390] or independent cell death [395, 396]. ROS induction results from a combination of decrease of antioxidant capacity and the increase of pro-oxidant activity.

PRIMA-1^{MET} inhibits anti-oxidant enzymes—such as TrxR1 [397] Prx3, or GPx-1 [398] and also converts TrxR1 to an active NADPH oxidase increasing the oxidant activity [397]. The decrease of cellular GSH occurs due to the fact that PRIMA-1^{MET} /MQ binds to and depletes cellular GSH [395, 399, 400]. Additionally, mutp53 sensitizes tumour cells to PRIMA-1^{MET} induced oxidative stress, by inhibiting the synthesis of GSH because mutp53 binds to and inhibits the antioxidant transcription factor Nrf2 [401], leading to decreased expression of *SLC7A11* and consequent inhibition of system xc− [395]. *SLC7A11* encodes the functional subunit of the cystine-glutamate antiporter, system xc− [402]. The import of cystine through system xc− provides the predominant source of intracellular cysteine *for de novo* synthesis of GSH. The decreased expression of *SLC7A11*, sensitizes cells to TrxR1 inhibition and GSH depletion by PRIMA-1^{MET} [395], providing an explanation for the selectivity of PRIMA-1^{MET} against mutp53 cancer cells. Consequently, *SLC7A11* expression is a marker for sensitivity of mutp53-carrying tumors to PRIMA-1^{MET}. Interestingly PRIMA-1^{MET} shows synergy in ROS production with inhibitors of GSH synthesis or cysteine transporter (for example with L-BSO) inducing cell death irrespective of p53 status [356].

Recently, another mechanism of action found of PRIMA-1 and PRIMA-1^{MET} entails the activation of XBP1, GRP78, and CHOP, which are important components of the endoplasmic reticulum stress response, commonly referred to as the unfolded protein response (UPR) [356]. The UPR response is activated when there is an accumulation of unfolded or misfolded proteins in the endoplasmic reticulum and aims to restore normal cell function by degrading misfolded proteins and increasing the production of molecular chaperones. When the UPR becomes overwhelmed, it may lead to apoptosis [356].

More than 10 clinical trials have been completed or are ongoing using PRIMA-1^{MET} in combination with chemotherapy, including ovarian cancer, prostate cancer, esophageal cancer myelodysplastic syndromes, acute myeloid leukemia, and non-Hodgkin lymphomas. To mention, one of these a Phase II clinical trial (NCT03268382) assessed the efficacy and safety of combined treatment with PRIMA-1^{MET} and pegylated liposomal doxorubicin in platinum-resistant recurrent HGSOC with mutated TP53 where it showed a disease control rate of 70% [403]. Another Phase Ib/II clinical trial (NCT02098343) was assessed similarly in patients with platinum sensitive recurrent HGSOC with mutated TP53 using carboplatin with or without PRIMA-1^{MET} and a disease control rate of 75% was reported [403].

1.16. Combi-molecule JS440

JS440 is an experimental combi-molecule that was designed to have components of PRIMA-1^{MET} and gefitinib with the purpose to have dual action: p53 stabilizer and EGFR TKI; it was synthesized by the postdoctoral fellow Dr. Julie Schmitt (Cancer Drug Research laboratory, McGill University, CA) in Dr. Bertrand Jean-Claude's research group (Director of the Drug Discovery Platform, and Professor in the Division of Experimental Medicine, McGill University). Currently there is no information publicly available about its cytotoxic effectiveness in preclinical studies.

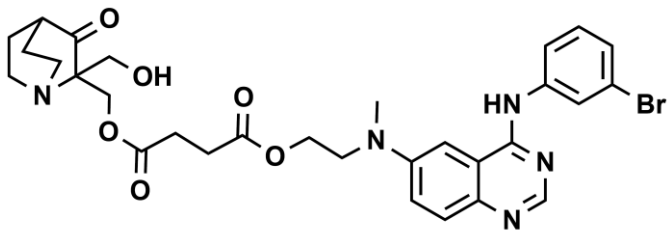

JS440

Chemical Formula: $C_{30}H_{34}BrN_5O_6$
Molecular Weight: 640,54

Figure 1.14.2. Structure of JS440

1.17. Targeting DNA damage response pathways

The most effective non-surgical treatment options for glioma include DNA-damaging agents, such as radiation therapy (RT) and cytotoxic chemotherapy. It is a promising strategy to increase the effectiveness of these therapies while minimizing harm to normal tissue, especially in tumours like GBM. One innovative approach is to target the unique DNA repair vulnerabilities in GBM, which contains a significant stem cell compartment where DNA repair is heightened and contributes to treatment resistance [404].

The DNA damage response (DDR) is a series of signaling and effector events that occur after DNA damage. This response is summarized in **Figure 1.17**. DNA double-strand breaks (DSBs) are the most common toxic lesions caused by DNA-damaging agents, but single-strand breaks (SSBs) are also important for lethality [405]. Unrepaired SSBs can slow down replication forks, which can indirectly increase the number of DSBs, especially under conditions of replication stress. Using DDR inhibitors with DNA-damaging agents can increase the number of unrepaired DSBs and SSBs in cells, potentially enhancing chemo- and radio sensitivity [20].

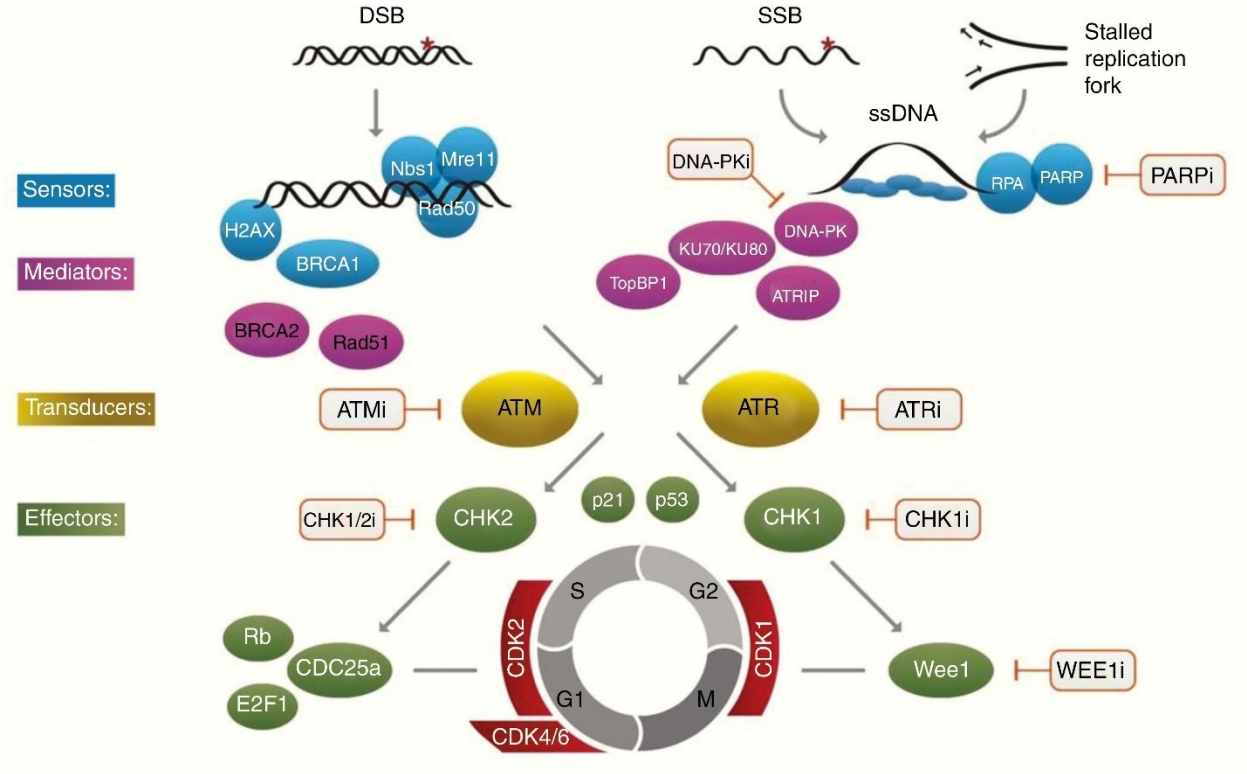

Figure 1.17. Overview of types of DNA damage and DDR. Proteins like histone γH2AX initially detect damage, which is rapidly phosphorylated by ATM at a specific serine residue in response to chromatin structure alteration at DSB sites. This activation leads to the recruitment of repair proteins, including BRCA1 and the MRN complex (MRE11, Rad51, NBS1). The repair of DSBs is carried out by the end-joining pathway, which involves the kinase DNA-PK and Ku protein binding partners, as well as the homologous recombination pathway, which involves Rad51 and associated proteins. Single-strand breaks (SSB) and replication stress cause stalled replication forks, which activate PARP and recruit repair factors, including XRCC1, to promote chromatin remodeling at the break site and base excision repair. ATR and ATM function in the initial signaling cascade and as transducers to downstream activation of the cell cycle checkpoint inhibitors Chk1 and Chk2, which produce cell cycle delay to facilitate repair. Points in the pathway at which specific inhibitors are available are indicated. As predicted from their roles in the DDR

pathway, ATM and ATR inhibitors sensitize cells to a broad range of DNA damaging agents that cause single or double strand breaks. PARP inhibitors (PARPi) and cell cycle checkpoint inhibitors, including Wee1 inhibitors, are specifically effective in cells undergoing rapid replication. Adapted from Ref. [20].

Poly (ADP-Ribose) polymerase (PARP) represents a group of enzymes that catalyze the formation of linear or branched polymers of ADP-ribose (PAR) using NAD+ as a substrate, functioning as a radiosensitizer [406]. When PARP detects single-strand DNA breaks, it attaches to DNA through its DNA-binding domain to cause structural changes and initiates the synthesis of a linear chain of adenosine diphosphate ribose. The auto-PARylation of PARP on its auto-modification domain is a signal that recruits DNA ligase III (LigIII), DNA polymerase beta (polβ), and scaffolding proteins such as X-ray cross-complementing gene 1 (XRCC1) to repair the damaged DNA, a process known as base excision repair (BER) [407]. Poly (ADP-ribose) glycohydrolase (PARG) degrades the PAR chain to recycle PARP. Currently, there are 18 members in the PARP family, but PARP1 and PARP2 play major roles in repairing DNA, especially the first one. Additionally, the other members perform different functions, and the PARylation of proteins, including histones and various transcription factors, can also regulate multiple cellular processes such as caspase-independent apoptosis by transporting apoptosis-inducing factors into the nucleus [408-410].

The expression of PARP-1 was found to be high in various types of cancers [409]. Initial studies showed that PARP inhibitors suppressed the activity of PARP and impeded the base excision repair (BER) system by competing with the substrate NAD+ [411]. This led to the accumulation of N-methylpurine DNA damage (N7-methylguanine and N3-methyladenine) caused by TMZ, and ultimately increased sensitivity to TMZ and other alkylating agents. Higuchi

et al. discovered that the role of PARP inhibitor as a TMZ sensitizer was independent of base excision repair [412]. There may be other pathways that PARP inhibitors target to enhance the effectiveness of chemoradiotherapy. For instance, continuous inhibition of PARP-1 activity delays the recurrence of GBM by promoting radiation-induced senescence [412]. PARP inhibitors can increase the sensitivity of cells, including glioma stem cells, to ionizing radiation. This is because the radiation produces single-stranded DNA damage, which is necessary for its therapeutic effect [413]. Although overexpressing PARP can promote resistance to radiation [414, 415], the PARP inhibitors can still sensitize cells to radiation even in glioma stem cells, which overexpress PARP, because the radiation generates single-stranded DNA damage to exert clinical effect.

The mechanism by which PARP inhibitors suppress tumor growth is known as "synthetic lethality." In certain cases of breast and ovarian cancer with BRCA mutations, which indicate a lack of the homologous recombination repair (HR) system, PARP-mediated BER serves as a compensatory mechanism. Therefore, the inhibition of PARP can enhance the anti-tumour effect [416, 417]. In gliomas, the frequent deletion of PTEN, which occurs in primary GBM, can impact genomic stability by decreasing the expression of RAD51, an essential component of the homologous recombination repair process [418]. *In vitro* studies have shown that cell lines with PTEN deficiency are more sensitive to PARP inhibitors than PTEN wild-type cell lines [406]. Recent studies have also demonstrated that IDH1/2 mutations not only impair the HR system but also compromise the BER associated with PARP by decreasing NAD+ availability. This may explain why patients with IDH1/2 mutations have a better prognosis than those with wild-type IDH when receiving chemoradiotherapy, and it also makes tumour cells sensitive to PARP inhibitors [419-421].

1.17.1. Olaparib: a PARP inhibitor

Olaparib, also known as AZD2281 and marketed as Lynparza, is an orally administered inhibitor of PARP. Olaparib (**Figure 1.17.1.1**) is specifically designed to competitively inhibit NAD+ at the catalytic site of PARP1 and PARP2 [422]. The function of these enzymes is of paramount importance in detecting and mending DNA SSBs through the BER pathway.

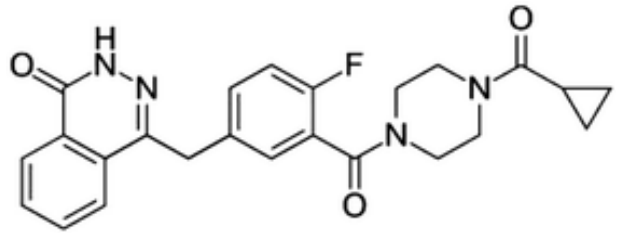

Figure 1.17.1.1 Molecular structure Olaparib; $C_{24}H_{23}FN_4O_3$; the molecular weight is 435.08 g/mol. Adapted from Ref. [423]

Inhibition of BER pathway by olaparib results in the accumulation of unrepaired SSBs, which subsequently leads to the formation of deleterious DSBs. In normal cells, DSBs can be effectively repaired with high fidelity through the homologous recombination (HR) pathway or non-homologous end-joining (NHEJ), although the latter is an error-prone repair process that may lead to genetic instability [422].

In tumours with HR repair deficiencies, such as those lacking functional BRCA1/2 genes, olaparib induces synthetic lethality [421]. This phenomenon arises from the interaction of two molecular events that ultimately result in cell or organismal death (**Figure 1.17.1.2**) [417]. In contrast, PARP inhibition has no significant impact on normal cells with intact HR repair pathways, as these cells are capable of accurately repairing DSBs through HR [424].

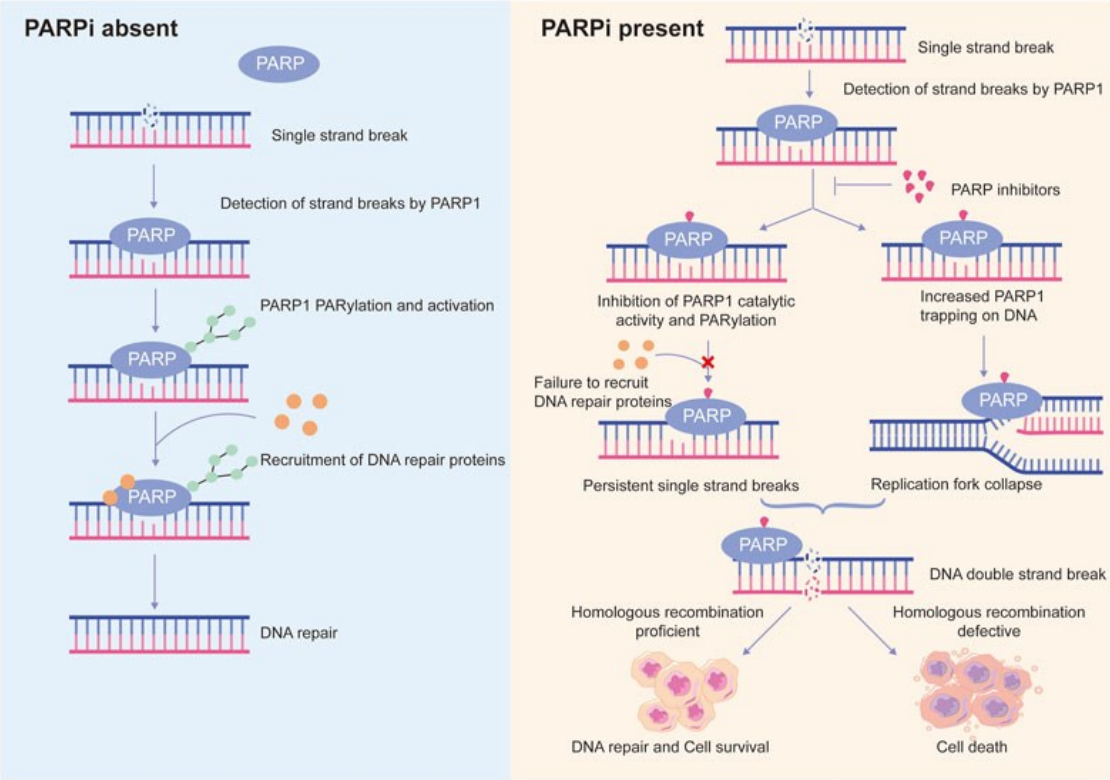

Figure 1.17.1.2 Proposed PARP inhibitors mechanisms of action. Left: PARP1 typically recognizes DNA single strand breaks (SSBs) and becomes activated in response, resulting in PARP1 auto-PARylation and the assembly of DNA repair proteins to initiate the repair process. Right: The presence of PARP inhibitors (PARPi) has two consequences. Initially, PARPi diminishes the activity of PARP1, hindering the recruitment of DNA repair proteins to the damaged locations. This results in the persistence of SSBs. Additionally, PARPi captures PARP1 at DNA lesions, forming harmful complexes that cause the replication fork to collapse, ultimately leading to cell death. Continuous SSBs and collapsing of replication forks will ultimately result in DNA double strand breaks (DSBs). In cells that are proficient in HR, DSBs can be efficiently repaired. However, cells that are defective in HR are unable to repair DSBs accurately, leading to cell death, phenomenon known as synthetic lethality. Adapted from Ref. [425].

Olaparib has been authorized for the treatment of patients with recurrent ovarian cancer and a BRCA mutation, and it has been demonstrated to provide significant clinical benefits to these patients. Although only about 25% of patients with serous ovarian cancer have germline or somatic BRCA mutations, research indicates that approximately half of them have HR deficient tumors [368, 426-428]. This suggests that the population that may benefit from olaparib may extend beyond those with BRCA mutations.

Currently, the FDA has approved three PARP inhibitors for use in women with ovarian cancer: olaparib, rucaparib, and niraparib [424]. Among these, olaparib is the only one that has been granted FDA approval for front-line maintenance therapy in patients with BRCA mutations.

In 2018 the FDA granted approval for olaparib as a monotherapy and then in 2020 also in combination with bevacizumab for the first-line maintenance treatment of BRCA-mutated advanced ovarian cancer [429], a substantial modification to the standard of care for adult patients receiving initial therapy for ovarian cancer. The approval for olaparib monotherapy was based on the results of the SOLO-1 trial [430, 431], while the approval in combination with bevacizumab was based on the PAOLA-1 trial [432]. In patients with BRCA-mutated tumours, olaparib monotherapy was shown to reduce the risk of disease progression or death by 70% compared to placebo. Meanwhile, olaparib in combination with bevacizumab demonstrated a 67% reduction in the risk of disease progression or death compared to bevacizumab alone in HR deficient-positive tumours [429].

Olaparib has demonstrated encouraging results in patients with metastatic breast or prostate cancer who possess a germline BRCA mutation [423]. In the context of gliomas, there may be potential benefits from utilizing PARP inhibitors in combination with other therapies, such as radiotherapy, chemotherapy (serving as a chemo- and/or radiosensitizer), and immunotherapy,

particularly in specific subgroups like IDH-mutant gliomas [423, 433]. IDH mutations can lead to a phenotype similar to that caused by mutations in the BRCA1/2 genes [419]; this mutation results in a neomorphic (new function) activity that converts α-ketoglutarate into the oncometabolite 2-hydroxyglutarate [434] which disrupts the HR pathway, making the tumour cells sensitive to PARP inhibitors.

The combination of PARP inhibitors and radiotherapy, which is part of the GBM standard of care, may exhibit synergistic effects through multiple mechanisms:

1. The BER pathway is a critical process for repairing ionizing radiation-damaged bases. However, the use of PARP inhibitors can impede this pathway, resulting in increased sensitivity to radiation in glioma cells, with sensitizer enhancement ratios ranging from 1.2 to 1.7 [413]. Notably, this effect appears to be dependent on replication, as higher levels of replication lead to greater DNA turnover and damage.
2. The ability of cancer stem cells to persist is a factor that contributes to radioresistance. One mechanism that enables cancer stem cells to survive is the enhancement of DNA damage repair pathways [435]. It has been suggested that PARP inhibitors may play a role in mitigating this response [436].
3. Tumour hypoxia is a well-known contributor to radioresistance, and PARP inhibitors have demonstrated the potential to mitigate this effect. By exerting a vasodilatory effect, PARP inhibitors can reduce tumor hypoxia, thus enhancing radiosensitivity [437]. Furthermore, PARP inhibitors may possess separate anti-angiogenic effects, which can further increase radiation sensitivity [438, 439].
4. Radiotherapy has proven to be effective in disrupting the BBB, assisted by contemporary localization methods, including focused ultrasound, electric field modulation, and laser

therapy [440]. These strategies may facilitate the delivery of PARP inhibitors into tumor tissues [424].

Pharmacokinetics of olaparib in GBM has been investigated in the OPARATIC trial [441]. Patients diagnosed with recurrent GBM were administered olaparib prior to undergoing neurosurgical resection. Subsequently, olaparib concentrations in tumour core and tumour margin samples were measured using mass spectrometry. Olaparib was detected in all tumour core samples obtained from the 27 patients and in all tumour margin samples obtained from the 9 patients at radiosensitizing concentrations, indicating reliable penetration.

The use of olaparib in the treatment of recurrent GBM warrants further investigation due to the drug's successful penetration into both the core and margin regions of the tumor at concentrations similar to those observed in breast cancer patients; this may be due to the disruption of the BBB caused by tumor invasion [441]. Despite its inability to cross the intact BBB in preclinical models [442], these findings suggest that clinical testing of olaparib in GBM, particularly in combination with radiation therapy, is justified. Furthermore, these observations highlight the limitations of traditional preclinical models in predicting clinical pharmacokinetics of drugs at the BBB.

In a recent pharmacokinetic investigation involving mouse intracranial *BRCA2*mut capan-1-luc tumour xenograft models, the efficacy of niraparib was evaluated in comparison to olaparib [443]. The results indicated that niraparib demonstrated superior tumour exposure, consistent distribution within the brain, and more potent inhibition of tumor growth when compared to olaparib [433].

The ongoing clinical trial (ISRCTN51253312), PARADIGM-2 consists of two parallel phase I studies of olaparib and radiotherapy or olaparib and radiotherapy plus TMZ in patients with newly diagnosed GBM, with treatment stratified by MGMT status [444]; it showed some encouraging results with no significant safety concerns.

1.18. Combi-molecule JS470

JS470 is an experimental combi-molecule that was designed to include components of PRIMA-1^{MET} and Olaparib, **Figure 1.18**, with the purpose to have dual actions: as p53 stabilizer and as DNA repair inhibitor; it was synthesized by postdoctoral fellow Dr. Julie Schmitt (Cancer Drug Research laboratory, McGill University, CA) in Dr. Bertrand Jean-Claude's research group (Director of the Drug Discovery Platform, and Professor in the Division of Experimental Medicine, McGill University). Currently there is no information publicly available about its cytotoxic effectiveness in preclinical studies.

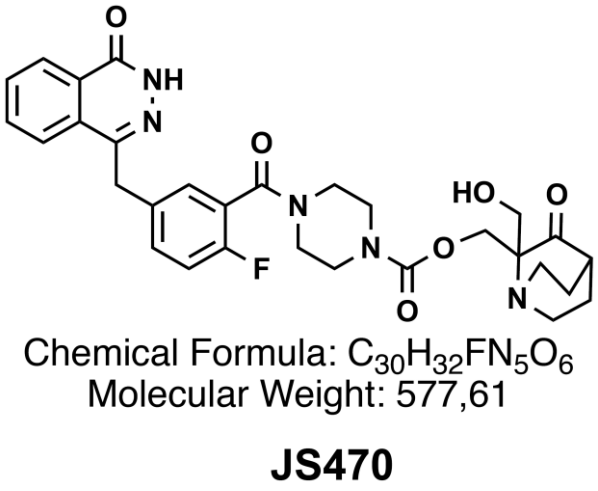

Figure 1.18. Structure of JS470

1.19. Challenges in GBM

The progress of creating more effective treatments for GBM is hindered by the slow and inefficient clinical trial process. The challenge is that many agents' ability to cross the BBB and achieve therapeutic concentrations in the tumour while inhibiting the appropriate molecular pathways is either unknown or insufficient. To address this, there is a need for more "window-of-opportunity" phase 0 surgical trials early in the drug development process. In these trials, patients receive the therapeutic agent for 1-2 weeks before surgery, and the tumor samples from both enhancing and non-enhancing areas are analyzed for drug concentrations and pharmacodynamic effects. Developing more efficient clinical trial networks focused on these studies is essential to identify agents that deserve further development [20]. Most treatments for GBM have been initially evaluated through uncontrolled single-arm studies, where progression-free survival (PFS) or overall survival (OS) were compared to contemporary or historical controls as the main outcome measures. Despite evidence indicating that only around one-third of patients with GBM benefited from TMZ, no single therapeutic biomarker, including MGMT promoter methylation, has been consistently utilized.

The BBB is a vital consideration when it comes to treating GBM. These tumours are located within and intertwined with the brain, and they exploit the brain's natural defense mechanism against toxins via the BBB. The BBB is composed of endothelial cells linked by tight junctions against a basement membrane, surrounded by pericytes and astrocyte foot processes. This barrier restricts the diffusion of compounds to small, uncharged, lipid-soluble molecules, which is why most drugs do not cross the BBB to a significant degree. Additionally, the BBB is reinforced with ATP-binding cassette transporter family proteins, which are drug efflux transporters on the luminal side of the BBB that remove toxic metabolites, xenobiotics, and drugs

from the brain. Together, these components prevent 98% of all small molecules from crossing the BBB. Although some parts of GBM tumors can have a leaky, compromised BBB, significant regions of the tumor, particularly the infiltrative tumor edge left behind in patients after resection, still have an intact BBB, which impedes effective drug delivery [124].

Glioblastoma also presents a significant therapeutic challenge due to its pronounced inter- and intratumoral heterogeneity. GBM, the first cancer to be characterized by The Cancer Genome Atlas, has been found to possess numerous distinct genetic drivers [14]. The variations among GBM are additionally intricate due to the presence of intratumoural heterogeneity at both molecular and functional levels. For instance, various areas within a tumour may consist of cells with different genetic compositions, transcriptional subtypes, and/or rates of proliferation. Although the effect of intratumour heterogeneity on therapeutic outcome is not well understood, preclinical studies indicate that functionally distinct glioma cells within a tumour (such as putative glioma stemlike cells compared to more differentiated cells) can respond differently to TMZ or ionizing radiation [435, 445, 446]. This differential response may explain the resistance to these conventional treatments.

Glioblastoma has been shown to adapt and survive in response to targeted tyrosine kinase inhibitors through various mechanisms, such as dynamic regulation of extrachromosomal DNA, chromatin remodeling to a slow-cycling/drug-tolerant persistent state, suppression of PTEN tumor suppressor, and reactivation of oncogenic signaling pathways (e.g. phosphatidylinositol-3 kinase, Ras-mitogen-activated protein kinase signaling) [129, 447, 448]. This redundancy in restoring oncogenic signaling flux can occur through RTK switching or the coactivation of multiple RTKs, both of which can maintain persistent oncogenic signaling to promote tumour viability. Although some targeted molecular therapies have shown benefit, most have failed due to low BBB

penetration of the drugs used, redundant signaling pathways, molecular heterogeneity, and increased toxicity of drug combinations, requiring suboptimal dosing. Alternative combination approaches, such as those that target orthogonal signaling/functional networks to induce synthetic lethality in GBM, have been proposed as a potential solution [20].

Precision oncology for GBM has failed not only for lack of molecular stratification in clinical trials, but due to fundamental differences in its EGFR biology relative to other EGFR-driven neoplasms. Decades of work has shown that EGFR-mutant GBM (e.g., EGFRvIII) rely on sustained signaling to drive tumor initiation and maintenance (proliferation, growth, survival, and metabolism) [449, 450]. Mutational distribution in EGFR in GBM is distinct from NSCLC [83, 113]. NSCLC harbor TK domain mutations and their molecular detection by random biopsy sampling is sufficient to establish the diagnosis of EGFR-mutant NSCLC and guide therapy with TKI. In contrast, multiple different oncogenic EGFR variants, both deletions and mis-sense mutations, typically co-exist with EGFR amplification in GBM [83].

GSCs subpopulations of GBM are characterized by stem cell-like properties with the ability to self-renew and differentiate, constituting the diverse hierarchy of cells composing the tumour; they are considered to be at the top of the hierarchy of cellular differentiation, characterized by the highest entropy and capacity for adaptation, they escape chemo-RT and proliferate residual tumor cells following treatment with capacity for multipotent differentiation [451]. One of the states characterizing GSCs is the entrance into quiescence. The quiescent state protects these cells, particularly from antiproliferative agents, and is thus an important factor of therapy resistance. Other mechanisms, including the ones mentioned in the previous paragraphs, epigenetic modifications, increased drug efflux, epithelial-to-mesenchymal transition, lncRNA, and exosome-mediated cell–cell communications, were suggested to be characteristic of the

tumour stem cell-like population in lung and thyroid cancers resistant to kinase inhibitors [452]. Therefore, similar aspects could be employed by GSC to circumvent the toxic effects of small kinase inhibitors.

1.20. Thesis rationale and objectives

Glioblastoma (GBM), the most prevalent primary brain malignancy characterized by a dismal prognosis, has been the focus of extensive research in recent years, with the development of novel therapies such as tumour-treating fields. Despite these efforts, substantial improvements in patient outcomes have yet to be achieved, emphasizing the need for new strategies aimed at enhancing the treatment options available for individuals diagnosed with GBM. A recent update to the WHO classification of central nervous system tumours utilized EGFR amplification/overexpression as a diagnostic criterion for GBM. Given the significant prevalence of EGFR alterations in GBM, which affects approximately 50% of patients, and the prominent role of the EGFRvIII mutated version associated with high proliferation and genomic instability, it is crucial to identify therapeutic options for this patient population.

This study aimed to evaluate various drugs using a combinatorial approach owing to the high heterogeneity that characterizes GBM. Employing drugs that target multiple mechanisms of action to kill cancer cells is the most effective strategy to circumvent compensatory pathways and can include both experimental and repurposed drugs.

Aberrant EGFRvIII expression in GBM has been associated with increased ROS levels, DNA strand break accumulation, genome instability, and better sensitivity to DNA repair inhibitors [262]. The impact of EGFRwt or EGFRvIII overexpression in response to a pro-oxidant Trx/GSH co-targeting strategy to reach the lethal ROS threshold is currently unknown in GBM. Hence, increased intrinsic ROS levels in EGFRvIII-positive GBM and the role of EGFR overexpression in potentially distinct antioxidant capacity underlies the rationale for investigating a pro-oxidant Trx/GSH co-targeting strategy in EGFR-positive GBM cells.

We hypothesized that combining auranofin, a pro-oxidant drug, with a second oxidant agent, L-BSO, would overcome redox adaptation and subsequent drug resistance in GBM cell lines stably expressing EGFRwt and EGFRvIII.

Auranofin may also sensitize GBM cells to TKIs such as gefitinib or the combi-molecule ZR2002 in GBM cell lines stably expressing EGFRwt and EGFRvIII. ZR2002 has shown promising preclinical *in vitro* and *in vivo* results in GBM owing to its dual targeting of DNA and EGFR properties.

Finally, following the multi-target approach, we aimed to investigate the efficiency of new combi-molecules targeting mutp53, using the rescuing-p53 PRIMA-1^{MET} moiety with the tyrosine kinase inhibitor gefitinib (JS440) in a GBM model, or with olaparib (JS470) in an HGSOC model.

Objective 1: To evaluate cytotoxic effects and molecular changes induced by auranofin in GBM.

Objective 2: To assess the efficacy of auranofin in combination with ZR2002 or gefitinib.

Objective 3: To evaluate combi-molecule strategy compared to single drugs regarding toxicity in GBM and HGSOC models.

Objective 4: To assess the efficacy and molecular changes induced by auranofin in combination with L-BSO.

Chapter 2 - MATERIALS AND METHODS

2.1. Cell culture and reagents

U87MG and its isogenic counterparts stably transfected to overexpress EGFR (U87/EGFRwt) or EGFRvIII (U87/EGFRvIII) GBM cell lines (kindly provided by Dr. Bertrand Jean-Claude [154]) and T98G (glioma cells positive for EGFR and MGMT [362, 453]) were obtained from American Type Culture Collection. Cells were maintained either in 1X DMEM (Cat. No. 11885092, Gibco, Life Technologies Corporation, Carlsbad, CA, USA), low glucose (1g/mL), L-glutamine (4 mM), sodium pyruvate (1mM), phenol red; or 1X DMEM, (Cat No 319-010-CL, Wisent Inc, St-Jean-Baptiste, QC, Canada) low glucose (1g/mL), L -glutamine (4 mM), sodium pyruvate (1mM), and phenol red. All 1X DMEM was supplemented with 10% premium fetal bovine serum (FBS) (Cat. No. 080-150, Wisent Inc.), 1X penicillin-streptomycin 50 U/mL (Cat. No. 15070063, Gibco), and incubated in 5% CO_2 atmosphere at 37°C.

PEO1 cells are high-grade serous ovarian cancer (HGSOC) epithelial cells obtained from a patient 22 months after the initial relapse following treatment with cisplatin, 5-fluorouracil, and chlorambucil while the patient was still sensitive to platinum-based chemotherapy [454]. Subsequently, PEO4 cells were isolated from the same patient following a second relapse after the patient became resistant to platinum-based chemotherapy. These cells were cultured in RPMI 1640 medium (Mediatech, Manassas, VA, USA) supplemented with 5% fetal bovine serum (FBS) (Atlanta Biologicals, Lawrenceville, GA, USA), 5% bovine serum (Life Technologies, Auckland, New Zealand), 0.01 mg/mL of human insulin (Roche, Indianapolis, IN, USA), 10 mM HEPES (Corning, Corning, NY, USA), 100 IU penicillin (Mediatech), 100 μg/mL streptomycin (Mediatech), 2 mM L-Alanyl-L-Glutamine (Glutagro, Corning), and 1 mM sodium pyruvate (Corning).

Cells were treated with dimethyl sulfoxide (DMSO, Cat. No BPBP231, Fisher Scientific Company, Fair Lawn, NJ, USA) as a vehicle control, auranofin (AU; Cat. No 15316-25, Cayman Chemical Co. Ann Arbor, MI, USA), N-Acetyl cysteine (NAC; Cat. No A9165, Sigma, Saint Louis, MO, USA), L-buthionine sulfoximide (L-BSO; Cat. No B2515, Sigma), gefitinib (Cat. No, SML1657, Sigma), PRIMA-1^{MET} (APR-246, Cat. No. 3710, Tocris Bioscience, Bristol, UK), and olaparib (AZD2281, Cat. No SML3705, Sigma). ZR2002 (McGill University, CA, patent #US7879861B2, USA [455]), a quinazolin combi-molecule EGFR and DNA damaging irreversible inhibitor [151, 156, 157], was kindly provided by Dr. Bertrand Jean-Claude. JS440 (combi-molecule having PRIMA-1^{MET}/gefitinib) and JS470 (combi-molecule having PRIMA-1^{MET}/olaparib) were both synthesized and provided by Dr. Julie Schmitt (McGill University, CA).

2.2. Cell vitality assay

Glioblastoma cells growing at 70% confluency were harvested and seeded in triplicate in 96-well plates at a density of $2.5x10^3$ cells/well and were allowed to adhere overnight at 37°C under 5% CO_2. The cells were then treated with AU, NAC, L-BSO, or a combination of the drugs at varying concentrations for 72 h. Similar conditions were used to treat cells with ZR2002, gefitinib, PRIMA-1^{MET}, and JS440; a similar procedure was done in PEO1 and PEO4 treated with JS470, PRIMA-1^{MET}, and olaparib. Cell vitality (a measure of cellular well-being via assessing the activity of the mitochondria [456]) was measured by adding 10 µl/well of 5 mg/ml MTT [3-(4,5-dimethylthiazol-2-yl)-2,5-diphenyltetrazolium bromide (Cat. No M6494, Invitrogen, Life Technologies Corporation, Carlsbad, CA, USA) in 1X Phosphate Buffered Saline (PBS, Cat. No 311-012, Wisent Inc) solution. Cells were incubated for 4 h at 37°C in 5% CO_2 where tetrazolium dye is reduced to insoluble formazan, then 100 µl/well of 10% sodium dodecyl sulfate (SDS)/0.01M HCl was added to stop the assay [457]. The absorbance was recorded at 570 nm on

a Bio-Tek Cytation 3 Multi-Mode Reader (Serial No. 131106B, Agilent, Santa Clara, CA, USA) following overnight incubation. Blank controls were subtracted and % cell vitality relative to control was calculated.

2.3. Total cell count and viability

To determine the count and viability of GBM cellular samples, triplicate cultures were trypsinized, separated by centrifugation at 1000 × g for 3 min, and washed with 1X PBS. The cells were resuspended in the ViaCount reagent (Cat. No. MCH600103, EMD Millipore, Hayward, CA, USA), incubated at room temperature for 5 min, and analyzed by flow cytometry using a Muse cell analyzer (EMD Millipore Cat. No 0500-3115, Serial No. 72001504335, Burlington, MA, USA). The ViaCount reagent distinguishes viable and non-viable cells based on the differential permeability of two DNA-binding dyes, providing the exact cell count of suspended cells and the percentage of viable cells. The Muse® 1.4.0 Analysis Software (EMD Millipore) was used to collect and examine the data. Cells treated with DMSO were used as controls. The percentage of viable (live) cells was represented in relation to the total cell number under each experimental condition. The cell number was represented as a percentage relative to the cell number in the control (100%) [458].

2.4. Clonogenic survival assays

During the exponential growth phase, the GBM cells were trypsinized, and 3 x 10^2 single-cell suspensions were seeded in triplicate in complete medium in 6-well plates and incubated to adhere overnight at 37°C, 5% CO_2. The next day, the medium was replaced with DMSO control or drug-containing medium, and the cells were kept in an incubator at 37°C for 9–11 days. After fixing with 10% formalin and staining with 0.05% crystal violet, colonies containing more than 50 cells were counted. The surviving fraction was normalized to the plating efficiency of the

corresponding DMSO controls using the following formula: (number of colonies/ number of cells plated) / (plating efficiency of DMSO-treated control cells × 100). Plating efficiency of DMSO-treated control cells = number of colonies formed in DMSO control/number of cells plated x 100 [459].

To evaluate the residual toxicity of AU (chronic long-term effects) on GBM cells, 300 viable cells exposed to AU for 72 h were seeded in a 6-well plate containing drug-free medium and allowed to grow for 9–11 days until DMSO-treated control cells exhibited positive colonies (50 or more cells).

2.5. Western blot analysis

Cells were grown overnight in standard medium, treated for the times and drug concentration shown in the result's section. The cells were cooled down at 4 °C for 5 min, followed by scraping, collection, and centrifugation at 1000 × *g* for 3 min; the supernatant was removed, and the cell pellet was resuspended in 1 mL of ice-cold 1X PBS. The samples were centrifuged at 2000 × *g* for 5 min, the supernatant was discarded, and the cell pellets were quickly frozen in liquid nitrogen and stored at -80 °C. Total proteins were isolated by adding lysis buffer to the cell pellets. Lysis buffer was prepared by mixing 0.5% NP-40, 1 mM dithiothreitol (DTT), 1 mM phenylmethylsulphonyl fluoride (PMSF), 2 µg/mL aprotinin, 2 µg/mL pepstatin, 2 g/mL leupeptin, 50 mM sodium fluoride, and 1 mM sodium orthovanadate. The cell pellets were resuspended in lysis buffer by gentle vortexing, and then were placed on ice in a shaker at 4 °C for 30 min. At 4 °C, the samples were centrifuged for 15 min at 12000 × *g*. The protein in the residue was then removed and placed in a different tube. Protein concentrations in the samples were determined using the Pierce BCA Protein Assay (Thermo Fisher Scientific Inc, Waltham, MA, USA). The Cytation 3 Multi-Mode Reader from BioTek (Agilent) was used to quantify the absorbance at 562

nm. Twenty-five µg of proteins per sample were subjected to electrophoretic separation using 10 or 12% SDS-PAGE (TGX Stain-Free FastCast Acrylamide kit, Cat. No. 161-0185; 1610185, BioRad Laboratories Inc, Hercules, CA, USA), and subsequently transferred onto Immuno-Blot® PVDF membranes (Cat. No.10026934, BioRad Laboratories Inc) using a Trans-Blot® Turbo™ transfer system (Serial No. 690BR014594, BioRad Laboratories Inc). Membranes were blocked with 5% milk at room temperature for 1 h followed by 5 washes of 5 min with 1X TBS-Tween and incubated at 4°C overnight with primary antibodies. Corresponding anti-mouse or anti-rabbit horseradish peroxidase–conjugated secondary antibodies were used for 1 h incubation followed by 5 washes of 5 min with 1X TBS-Tween. Protein detection was performed via a ChemiDoc Imaging System (Serial No. 732BR1945, BioRad Laboratories Inc) using chemiluminescence Clarity Western ECL Imaging System (Cat. No. 170-5060, BioRad Laboratories Inc).

Table 2.1: Primary and secondary antibodies used in this research project.

Antibody	Catalogue No.	Company	Concentration
Akt	2920S	Cell Signaling Technology, Danvers, MA, USA	1:1000
Akt	sc-81434	Santa Cruz, Dallas, TX, USA	1:500
ERK	9102L	Cell Signaling Technology	1:1000
Goat anti-mouse IgG (H+L)-HRP conjugate	170-6516	BioRad Laboratories Inc.	1:5000
Goat anti-rabbit IgG (H+L) conjugate	170-6515	BioRad Laboratories Inc.	1:5000
NRF2 (D1Z9C)	12721S	Cell Signaling Technology	1:1000
p53 (DO-1)	sc-126	Santa Cruz	1:1000
p-Akt/Ser473 (193H12)	4058S	Cell Signaling Technology	1:1000
PARP	9542L	Cell Signaling Technology	1:1000
p-EGFR/Y1068 (D7A5)	3777S	Cell Signaling Technology	1:1000
p-ERK	9106L	Cell Signaling Technology	1:1000
EGFR (1005)	sc-03	Santa Cruz	1:1000
TrxR1 (B-2)	sc-28321	Santa Cruz	1:1000

ubiquitin P37	58395	Cell Signaling Technology	1:1000
β-actin	A5441	Sigma Lifesciences	1:10000
γH2A.X (Ser139)	05-636	EMD Millipore Corp.	1:1000

2.6. Microscopic fluorescence imaging

To visualize ROS using microscopy, GBM cells were seeded in an 8-chamber cell culture slide (Cat. No. 229168, Ultident Scientific, Montreal, QC, Canada), and incubated overnight, then treated with 3 μM AU for 24 h. Then the media was replaced by red phenol-free media containing 5 μM of the general stress oxidative indicator CM-H2DCFDA (Cat. No. C6827, Invitrogen) for 20 min followed by 2 μM Hoechst 33342 dye (Cat. No. 62249, Thermo Scientific, Waltham, MA, USA) or 0.1 μg/mL DAPI (Cat. No. D9542, Sigma) to stain nuclei for 10 min at 37 °C under 5% CO_2. Wells were washed once and left in 1X PBS. AxioVert.A1 microscope (Cat. No. 491206-0002-000, Zeiss, Oberkochen, BW, Germany) and EVOS M5000 Imaging System microscope (Cat. No. 12563631, Invitrogen) were used to capture the images.

2.7. Detection of DNA damage

To evaluate the potential of AU to cause DNA damage in U87MG cells, cells were exposed to 1, 3, or 5 μM AU for 48 h. Thereafter, cell samples were collected and centrifuged at 300 × *g* for 5 min, and the supernatant was discarded. A cell suspension was prepared by adding 50 μL of 1X assay buffer (Multicolor DNA Damage, Cat. No. MCH200107; EMD Millipore Corp) to 1×10^5 cells. An equivalent volume of fixation buffer was added to the cell suspension, which was then incubated at 4°C for 10 min. The samples were then centrifuged at 300 × *g* for 5 min, and the supernatant was removed. The cell suspension was reconstituted in 90 μL of 1X assay buffer per 100,000 cells and stained using 10 μL of antibody solution. This solution was prepared by mixing 5 μL of anti-phospho-ATM (Ser1981) with Phycoerythrin (PE), and 5 μL of anti-phospho-histone

H2A.X (Ser139) labeled with PE-Cyanine®5 (PeCy5). The samples were incubated in the dark for 30 min at room temperature. Next, 100 µL of 1X assay buffer were added, and the samples were centrifuged at 300 x *g* for 5 min. The liquid above the sedimented material was removed, and the cells were resuspended in 200 µL assay buffer. Cells were analyzed on the multicolor DNA damage protocol using the Guava Muse® Cell Analyzer (EMD Millipore Corp).

2.8. Measurement of annexin-V translocation to the outside of the plasma membrane

The U87MG cells were treated with 1, 3, or 5 µM AU for 72 h. The cells were then collected and resuspended as 1×10^6 cells in 100 µL of cell suspension. The suspension was placed in a tube and stained with 100 µL of Annexin V & Dead Cell Reagent (Cat. No. MCH100105, EMD Millipore Corp) for 20 minutes at room temperature in the dark. Annexin V, a calcium-dependent phospholipid-binding protein, binds to phosphatidylserine (PS), which translocates to the extracellular surface during apoptosis. The Dead Cell Reagent integrates into late apoptotic and dead cells to detect live and dead cells. The cells were analyzed using the Guava Muse Cell Analyzer and Annexin V and Dead Cell Protocol.

2.9. Detection of mitochondrial membrane depolarization

U87MG cells were harvested 24 h after treatment with 2 or 4 µM AU. Five $\times 10^5$ cells were resuspended in 500 µL of 1X assay buffer. One hundred microliters of the cell suspension were placed in a 1.5 mL microcentrifuge tube and incubated for 20 min at 37 °C in 5% CO2 with 95 µL of MitoPotential working solution prepared by diluting Muse MitoPotential Dye at 1:1000 in 1X assay buffer. Each tube received five microliters of Muse MitoPotential 7-AAD reagent and was incubated for five minutes at room temperature. Guava Muse Cell Analyzer was used following the MitoPotential Protocol analysis (Cat. No. MCH100110).

2.10. Measurement of caspase-3/7 activation

The Luminex Muse Caspase-3/7 assay (Cat. No. MCH100108) was utilized in this study. U87MG cells were treated with 1, 3, or 5 μM AU for 48 hours. A tube containing a suspension of 5×10^5 cells was incubated in the dark for 30 minutes at 37°C in a 5% CO2 incubator with five microliters of the Caspase-3/7 reagent working solution, which was prepared by diluting the stock solution 1:8 with 1X PBS. This reagent includes a DNA-binding DEVD peptide substrate, which once caspase-3/7 is activated, undergoes cleavage followed by translocation to the nucleus where it binds DNA and emit fluorescence. The cells were stained for 5 minutes at room temperature in the dark with 150 μL of the Muse Caspase 3/7-AAD substrate working solution, which was diluted 1:75 in 1X assay buffer. 7-AAD is a cell-permeable DNA-binding dye that integrates through cells that have lost their membrane structural integrity. The analysis was performed using the caspase-3/7 protocol on the Muse cell analyzer (Millipore).

2.11. Treatment with caspase inhibitor (z-DEVD-fmk)

For 2 h, U87MG and U87EGFRvIII cells were pretreated with 50 μM z-DEVD-fmk (Catalog No.S7312, Selleck Chemicals, Houston, TX, USA), a selective irreversible caspase-3 inhibitor that also inhibits caspase-6, caspase-7, caspase-8, and caspase-10. Cell viability was measured using cytometry and a Guava Muse Cell Analyzer after 24 h of treatment with five μM AU.

2.12. Measurement of intracellular ROS and superoxide anions

To determine whether AU increased intracellular ROS generation in GBM cells, the cells were seeded in 96 well plates, incubated overnight, and then treated with 3 or 6 μM AU alone or in combination with 5 μM L-BSO for 2.5 or 24 h; thereafter, media was replaced by phenol red-free media containing 5 μM of the general stress oxidative indicator CM-H2DCFDA (Cat. No.

C6827, Invitrogen) for 20 min. Then, 2 μM Hoechst 33342 dye (Cat. No. 62249, Thermo Scientific, Waltham, MA, USA) was added to stain the nuclei for 10 min at 37 °C in 5% CO2. CM-H2DCFDA was measured at ex/em 493/528 nm. Wells were washed once and left in 1X PBS. For Hoechst 33342 staining, wells were measured in a plate reader at ex/em 350/450 nm and values were used to normalize ROS levels. Similar procedure was applied to analyse ROS levels for cells treated with ZR2002 and gefitinib at different concentrations.

The intracellular superoxide levels were measured using the Luminex Oxidative Stress Kit (Cat. No. MCH100111, EMD Millipore Corp), which involved adding dihydroethidium (DHE), a cell-permeable reagent that binds to DNA and produces red fluorescence when superoxide interacts with it. Studies have suggested however, that DHE can be oxidized also by hydroxyl radical, nitrogen dioxide, trioxidocarbonate radical anion, glutathione and cysteine thiyl radical [460]. After treatment, the cells were collected and processed in 1X assay buffer at a concentration of 1 x 10^6 to 1 x 10^7 cells per mL. The 1:100 dilution of Muse Oxidative Stress reagent in 1X assay buffer resulted in an intermediate solution. This intermediate solution was further diluted 1:80 to create the Muse Oxidative Stress working solution. The working solution was then pipetted into 10 μL of cells and incubated at 37 °C for 30 minutes. Following incubation, the Muse Cell Analyzer (EMD Millipore Corp) assessed the stained samples using the Oxidative Stress protocol.

2.13. Determining drug interaction

At a cell confluency of 70%, cells were seeded in triplicate in 96-well plates with 2.5x10^3 cells/well in DMEM supplemented and incubated at 37°C in 5% CO2. The cells were then treated with varying concentrations of AU (1-3 μM), either alone or in combination with L-BSO (5 μM), and allowed to grow for 72 h. After the MTT assay was performed to determine vitality, we used the CompuSyn software to calculate drug interaction utilizing the combination index (CI)

following the Chou-Talalay method [461]. Similar method was applied to analyse drug interactions of AU-ZR2002 and AU-gefitinib. The fraction affected (fa)-value represents the fraction of cell vitality affected by treatment.

2.14. Determination of TrxR activity

TrxR activity was measured with a thioredoxin reductase colorimetric assay (Cat. No. ab83463; Abcam, Cambridge, MA, USA). The principle of the assay consists in reducing 5,5'-dithiobis (2-nitrobenzoic) acid (DTNB) with NADPH to form TNB^{2-}, and the absorbance is read at 412 nm. Briefly, drug-treated cells were scraped and rinsed twice with 1X PBS on ice, and centrifugated at 1000 × *g* for 3 min. The supernatant was decanted, and the cell pellets were snap-frozen in liquid nitrogen and stored at -80°C until further studied. The cells were homogenized on ice with 100 µL of cold 1X assay buffer containing 1X protease inhibitor cocktail (Cat. No. ab65621, Abcam) and centrifuged at 2000 × *g* for 15 min at 4°C. Protein content of the supernatant was determined using the Pierce BCA Protein Assay Kit (Thermo Fisher Scientific); 50 µg of protein was used for each analysis. The TrxR assays were carried out in 96-well microplate in duplicates. The positive control and each sample received a reaction mix containing TrxR assay buffer, DTNB solution, and NADPH. Samples and TrxR positive control were incubated 20 min at 25°C with assay buffer or TrxR inhibitor to measure the background enzyme activity; total DTNB reduction was measured by optical density (OD) at 0 min (A1AB and A1INH).) and at 20 min (A2AB and A2INH). Where AB is the assay buffer and INH is the inhibitor. A standard curve was generated with 0, 10, 20, 30, 40, and 50 nmol/well of TNB standard. The following equation was used to determine the OD of TNB^{2-} generated by TrxR: ΔA412 nm = (A2AB − A2INH) − (A1AB − A1INH). TrxR activity was determined using the following formula: TrxR activity = (ΔB × Sample Dilution Factor = nmol/min/ml = mU/ml) / ((T2 − T1) × V). Where ΔB nmol is

calculated by applying ΔA412nm to the TNB standard curve. T1 is the time of the first reading (min), T2 is the time of the second reading (min), and V is the pretreated sample volume (mL). One unit of TrxR is the amount of enzyme that generates 1.0 μmol of TNB per minute at 25 °C.

2.15. Glutathione (GSH) assay

GSH levels were measured using a GSH colorimetric assay (Cat. No ab239727, Abcam). The assay consists of the use of a chromophore, which enzymatic reduction can be determined kinetically by measuring the absorbance at 450 nanometers. The absorbance is directly proportional to the reduced GSH that is present in each sample. The assays were carried out in 96-well microplates in duplicates. Drug treated cells were placed on ice, collected by scraping, and washed twice with 1 X PBS. Cells were centrifuged at 1,000 x *g* for 3 min, and the supernatants were removed. Cells were resuspended in 1X PBS, and split into two tubes, centrifuged at 2,000 x *g* for 5 minutes, supernatants were discarded, and cell pellets were snap-frozen in liquid nitrogen and stored at -80°C until analyzed. One set of samples was used to determine the protein concentration (mg/mL) using the Pierce BCA protein assay kit (Thermo Fisher Scientific), as previously described. The other set of pelleted cells were vortexed, and homogenized with 100 μL 5% sulfosalicylic acid (SSA) solution and incubated on ice for 10 min. The samples were then centrifuged at 12,000 x *g* at 4°C for 20 minutes, and the supernatant was collected and kept on ice. The samples were diluted 5-fold using the GSH assay buffer, 10 μL of the diluted samples were added per well in a 96-well plate for the sample well and the sample background control well. A standard curve was produced with 0, 0.4, 0.8, 1.2, 1.6, and 2 nmol/well of the GSH standard. The reaction mix was applied to the standard and sample wells, and absorbance was measured at 450 nm for 60 minutes at room temperature using a microplate reader. The absorbances corresponding to two time-points were selected for each sample. Then, the rate of each standard and sample

reading was calculated; rate = $[(OD_2 - OD_1)/t_2 - t_1)]$ where OD_2 = optical density at the second time point, OD_1 = optical density for the first time point; t_1 = initial time (min), t_2 = second time. The GSH amount in sample was calculated as (B/ [VxP]) x D = nmol/mg, where B is the amount of GSH obtained from the standard curve (nmol), B = rate background corrected samples /slope of the standard curve, V is the volume of sample added in each well (mL), P is the protein concentration in mg/mL, and D is the sample dilution factor. The rate of the background corrected samples was calculated by $[\text{rate}_{\text{sample}} - \text{rate}_{\text{background control}}]$.

2.16. TCGA data analysis

We performed comparative retrospective analyses to identify EGFR and γ-GCL mRNA expression correlated genes in GBM. For this, we examined available patient datasets from The Cancer Genome Atlas Network (TCGA) projects GBM U133 microarray (Firehose Legacy). The criteria for significant expression correlation were Pearson correlation coefficient $r \geq 0.3$ or ≤ -0.3, Spearman correlation coefficient $r \geq 0.4$ or ≤ -0.4, and P values < 0.05. The results shown here are in whole or part based upon data generated by the TCGA Research Network: https://www.cancer.gov/tcga.

2.17. Statistical analysis

We used GraphPad Prism (GraphPad Software Inc., La Jolla, CA, USA) for all statistical analysis. Data are reported as mean ± SEM and are representative of at least 3 independent experiments unless otherwise stated. Statistics were performed using two-way ANOVA followed by Tukey's multiple-comparison test unless otherwise stated and *p* values < 0.05 were considered statistically significant.

Chapter 3 – RESULTS (Part 1)

3.1. ZR2002 decreases vitality of GBM cells in a dose-dependent manner.

Shariff et al. demonstrated the efficacy and anticancer effects of ZR2002 in GBM cells isogenic for EGFR [156, 157]. In an MTT assay using different concentrations of ZR2002 for 72 h and 120 h treatment, we showed that this drug decreased the vitality of U87MG, U87EGFRwt and U87EGFRvIII cells. IC_{50s} of ZR2002 for U87MG and U87EGFRvIII cells were significantly lower than for U87EGFRwt at 72 h and 120 h (**Figure 3.1A and B).**

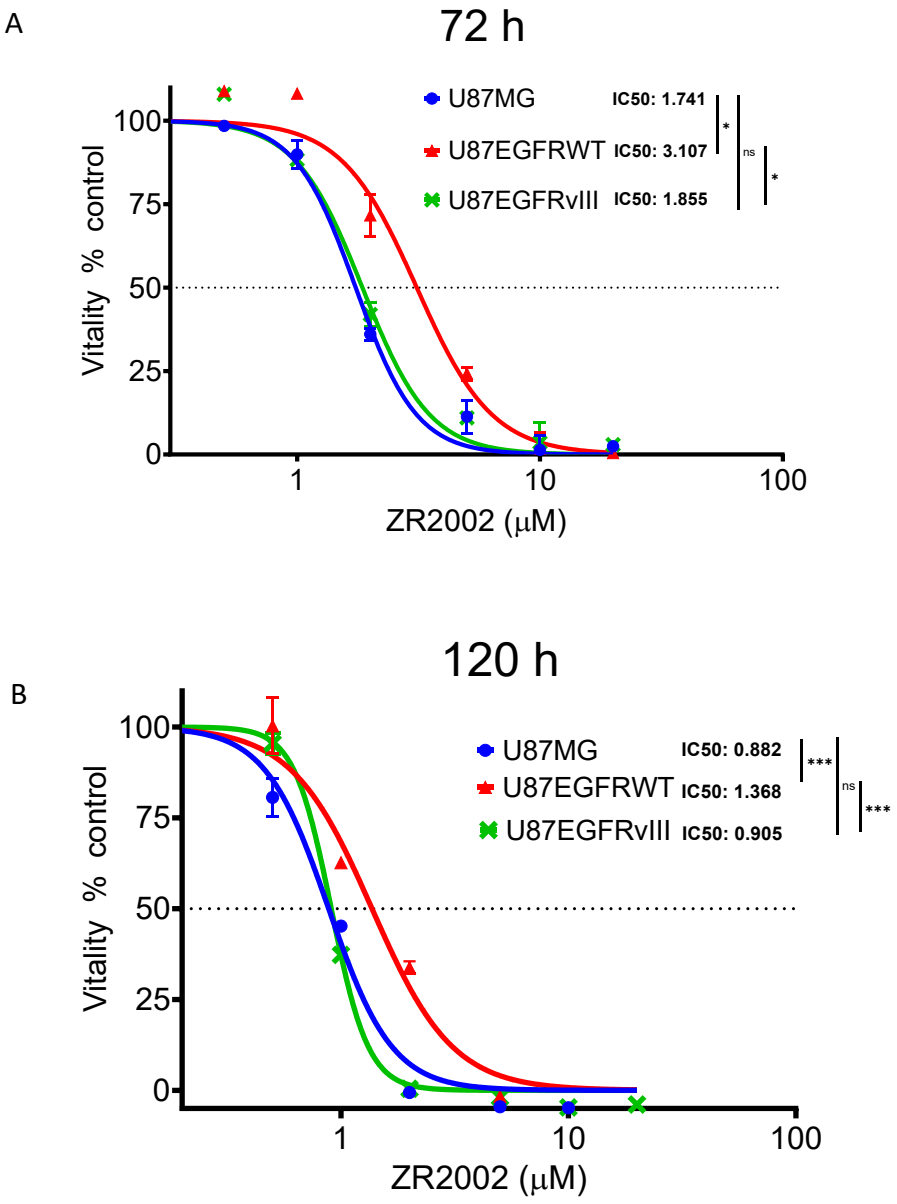

Figure 3.1. ZR2002 short-term toxicity in EGFR isogenic cell lines. Vitality of U87MG cells, U87/EGFRwt, U87/EGFRvIII cells treated with ZR2002 at 72 h (A) and 120 h (B). Bars show the mean ± SEM (*$p < 0.05$ * $p < 0.001$, two-way ANOVA followed by Tukey's multiple comparison test).

3.2. ZR2002 increases ROS in U87/EGFRvIII cells only at high concentrations

Whether ZR2002 induces an increase in general intracellular ROS is not known; consequently, we determined the effect of ZR2002 at increasing concentrations after 2 h treatment in U87MG and U87/EGFRvIII. Although we observed an increase in ROS in a dose dependent manner, only the effects at high concentrations (16 and 32 μM) were statistically significant. There were no significant differences when comparing U87MG and U87/EGFRvIII responses at the same concentration of ZR2002 (**Figure 3.2A**). Furthermore, we measured the general intracellular ROS in U87MG cells, U87/EGFRwt, and U87/EGFRvIII following 2.3 and 4.6 μM ZR2002 at 24 h of treatment. The concentration of 2.3 μM represents the average of IC50s among U87MG, U87/EGFRwt, and U87/EGFRvIII. No statistically significant differences were found in ROS levels using 2.3 or 4.6 μM ZR2002 in U87MG and U87/EGFRwt when comparing to vehicle control; however, U87EGFRvIII showed statistically significant higher ROS levels at 2.3 μM ZR2002 and no difference at 4.6 μM concentration compared to its vehicle control; ROS levels at 2.3 μM ZR2002 were also significantly higher in U87/EGFRvIII compared to U87MG and no difference compared to U87/EGFRwt as shown in **Figure 3.2B.**

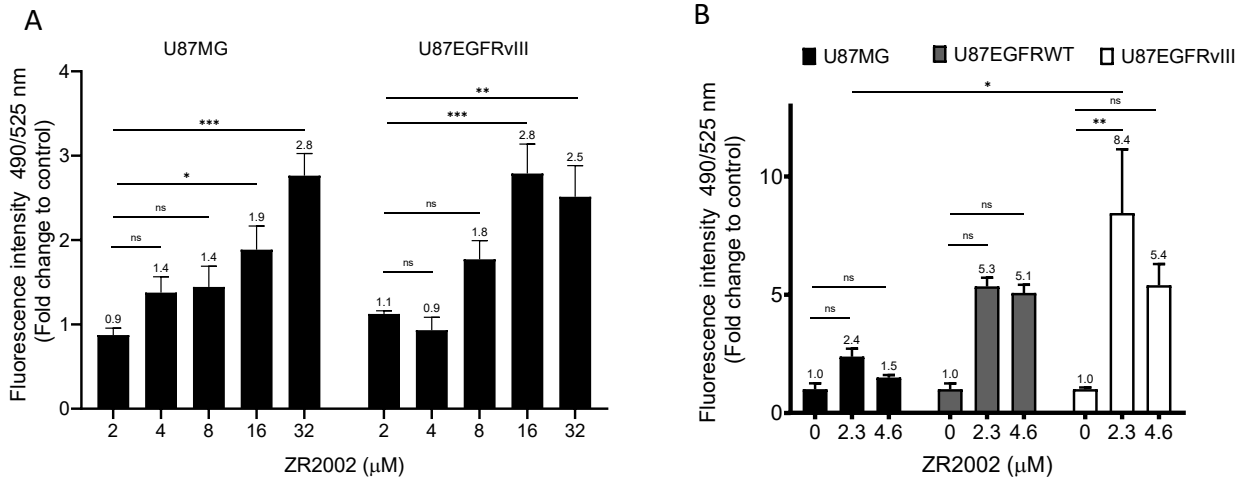

Figure 3.2. Effects of ZR2002 on intracellular levels of ROS in GBM cells. (A) ROS levels in U87MG and U87EGFRvIII after 2 h treatment with different concentrations of ZR2002, (B) ROS levels in U87MG, U87EGFRwt, and U87EGFRvIII after 24 h treatment with 2.3 and 4.6 μM ZR2002. CM-H2DCFDA was used as the general ROS-sensitive probe; bars represent the mean ± SEM (*$p < 0.05$ **$p < 0.01$ ***$p < 0.001$, two-way ANOVA followed by Tukey's multiple comparison test).

3.3. NAC does not protect GBM cells against ZR2002 toxicity

To investigate whether the toxicity of ZR2002 was related to ROS generation, we used 1.8 μM or 3.6 μM of ZR2002 for 72 h followed by the presence or absence of 2 mM of the ROS scavenger NAC in U87MG, U87EGFRwt, and U87EGFRvIII cells. The outcome of the treatment was assessed by measuring vitality. No statistical differences were found in vitality when NAC was added to ZR2002 in the 3 GBM cell types (**Figure 3.3**).

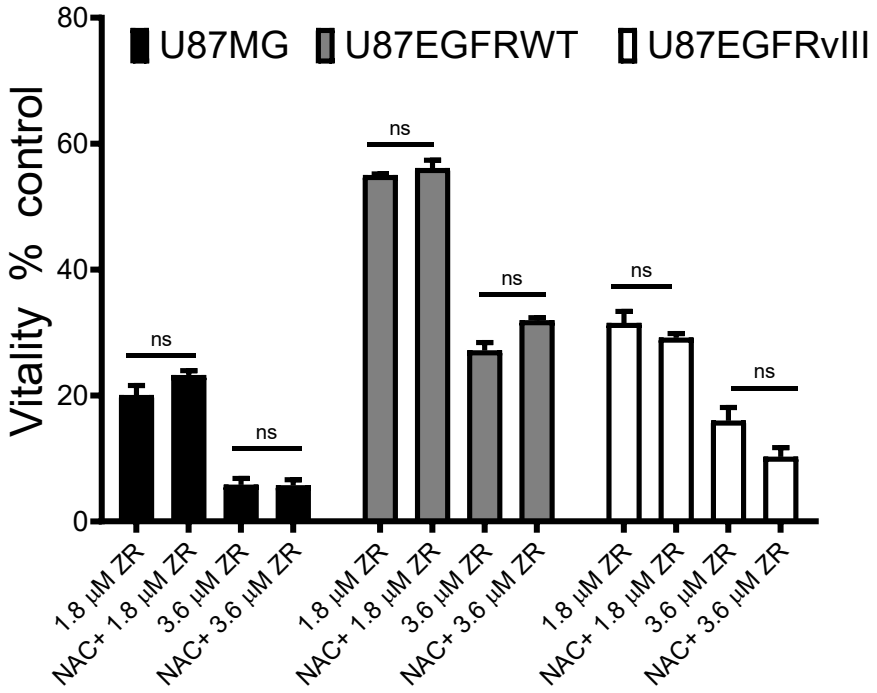

Figure 3.3. ZR2002 (ZR) effects on cell vitality with and without NAC in EGFR isogenic cell lines. Bar graphs show the mean ± SEM (ns = not significant $p > 0.05$, two-way ANOVA followed by Tukey's multiple comparison test).

3.4. Auranofin in combination with ZR2002 decreases clonogenicity in U87EGFRWT cells

We tested 0.5 and 1 µM ZR2002 for colony formation capacity alone or in combination with 0.5 or 1 µM auranofin in U87EGFRwt cells, which previously showed to be the least sensitive to ZR2002 in the vitality assay. Cells were incubated for 10 days. Concentrations of 0.5, 1 µM ZR2002 and 0.5, 1 µM auranofin as single agents significantly decreased the % of positive colonies compared to DMSO control; however, 1 µM ZR2002 produced no visible abortive colonies in comparison to 1 µM auranofin in which some residual abortive colonies were present (**Figure 3.4A**)**.** The combination of 0.5 µM ZR2002 with 0.5 µM auranofin decreased significantly the % of positive colonies compared to single drugs alone and the DMSO control (**Figure 3.4B**).

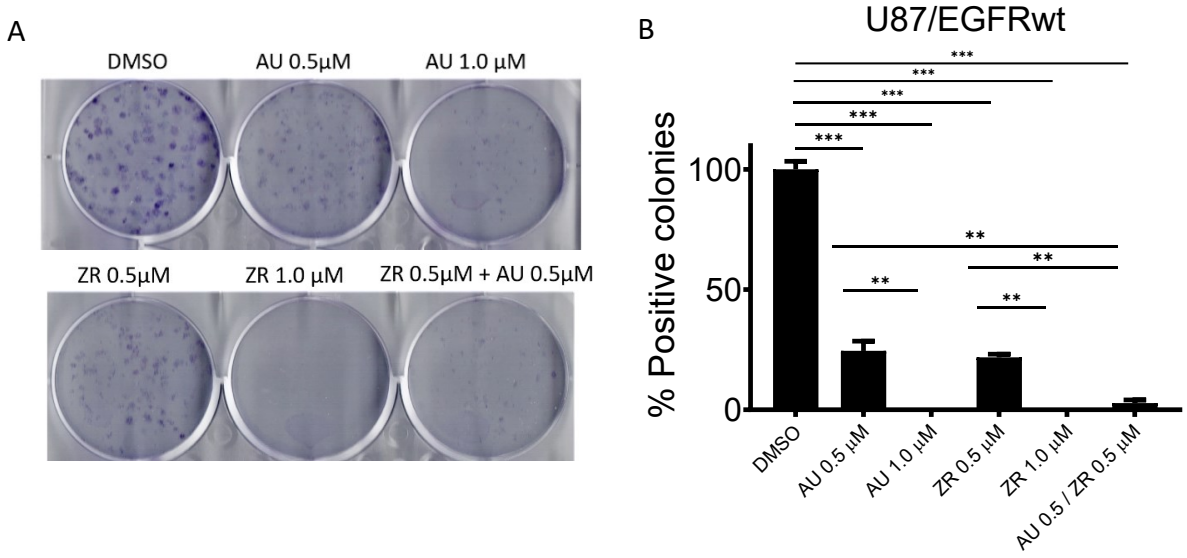

Figure 3.4. Clonogenicity of U87EGFRwt after treatment with ZR2002 alone or in combination with auranofin. (A) Representative clonogenic assay (B) U87EGFRwt treated with 0.5, 1 µM

ZR2002 (ZR), or 0.5, 1 µM auranofin (AU) alone or in combinations of 0.5/0.5 µM. Bars show the mean ± SEM (**$p < 0.01$ ***$p < 0.001$, one-way ANOVA followed by Tukey's multiple comparison test).

3.5. Auranofin/ZR2002 combination is largely antagonistic in EGFR-positive GBM cells.

We assessed the combination index of ZR2002 together with auranofin at 72 h in U87MG cells, U87/EGFRwt, and U87/EGFRvIII cells, using ratios of the average IC_{50s} for these drugs in the three cell types. Drug interaction analysis showed that most combinations produced an index equal to or higher than 1, which means the combination was antagonistic; with the exception of U87EGFRwt cells, where corresponding IC_{50s} or double IC_{50s} for ZR2002/auranofin combination produced some synergistic effects (**Figure 3.5**).

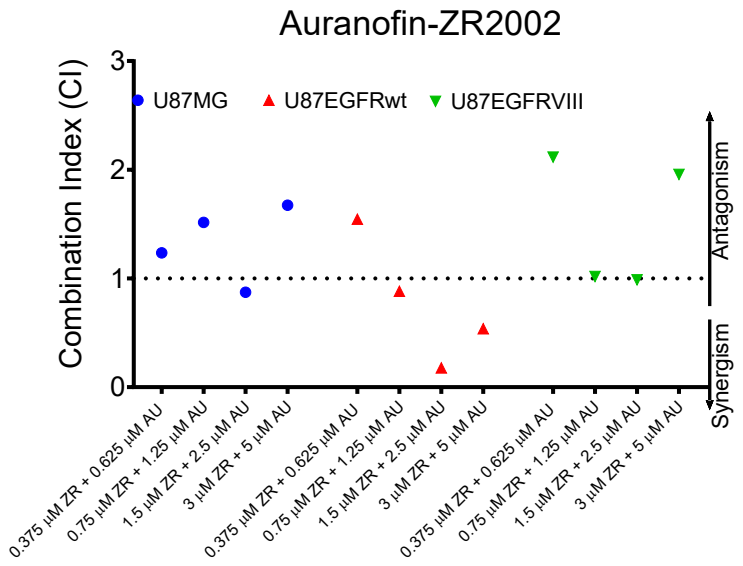

Figure 3.5. Combination index of ZR2002 (ZR) – auranofin (AU) toxicity in EGFR isogenic cell lines. U87MG cells, U87/EGFRwt, and U87/EGFRvIII cells treated with different ratios of their corresponding drug IC_{50s} were analysed using the Chou-Talalay method for drug combination analysis. Synergism was determined when CI was <1, antagonism, CI >1, additive effect with CI =1.

3.6. One µM Auranofin and ZR2002 combination < 2 µM is synergistic in U87MG and U87/EGFRvIII but not in U87/EGFRwt cells

To explore a different combination strategy, we decided to test the effects of 1 µM auranofin together with different concentrations of ZR2002 for 72 h in the three cell lines. Effects on vitality and the combination index showed that 1 µM auranofin combined with concentrations lower than 2 µM ZR2002 were synergistic for U87MG and U87EGFRvIII cells; however, combinations higher than 2 µM ZR2002 displayed antagonistic effects. For U87EGFRwt cells, no relevant synergistic effects were observed using this combination strategy (**Figure 3.6.**).

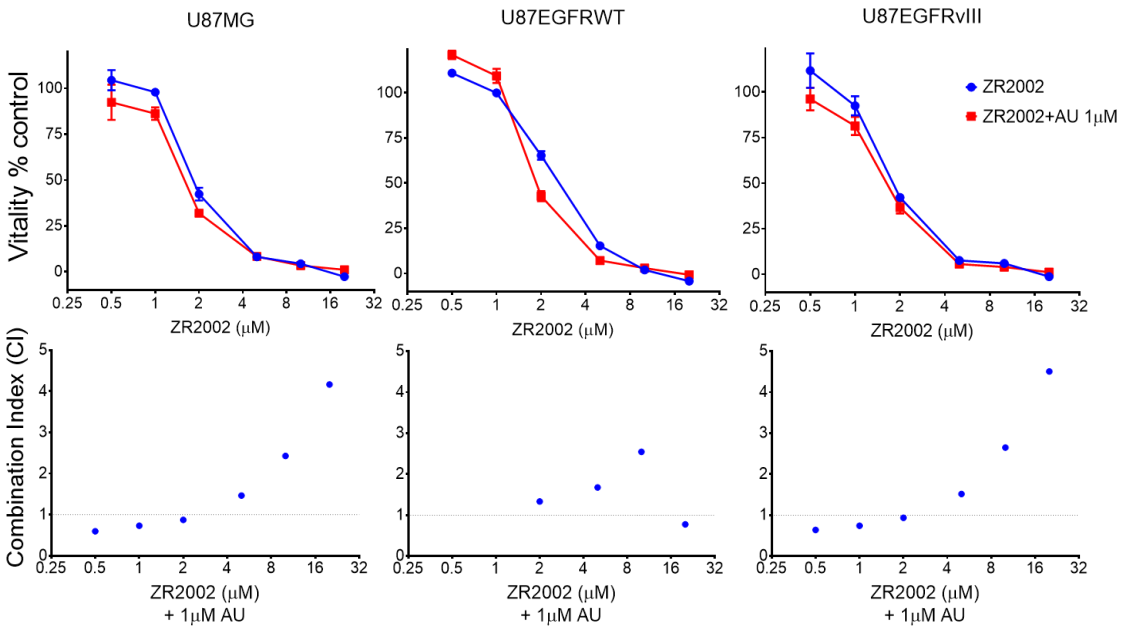

Figure 3.6. (A) Vitality and (B) the combination index using different concentrations of ZR2002 and a fixed concentration of 1 µM auranofin (AU) for 72 h treatment in U87MG, U87/EGFRwt, and U87/EGFRvIII cells. The combination indexes were calculated using the method of Chou & Talalay. Synergism was determined when CI was <1, antagonism, CI >1 or additive effect with CI =1.

3.7. Auranofin/ZR2002 combination is antagonistic in EGFR-positive cells

Ratio combinations (double, half, and quarter) of 1.5 µM ZR2002 and 2.5 µM auranofin which correspond to ratios of the average IC_{50s} for these drugs in the three cell types, were administered for 72 h and cell survival and combination index were assessed for in U87MG, U87/EGFRwt, and U87/EGFRvIII cells. No synergistic effects were observed at any drug combinations in any of the GBM cell lines (**Figure 3.7A).** In contrast the combination was antagonistic in all concentrations tested.

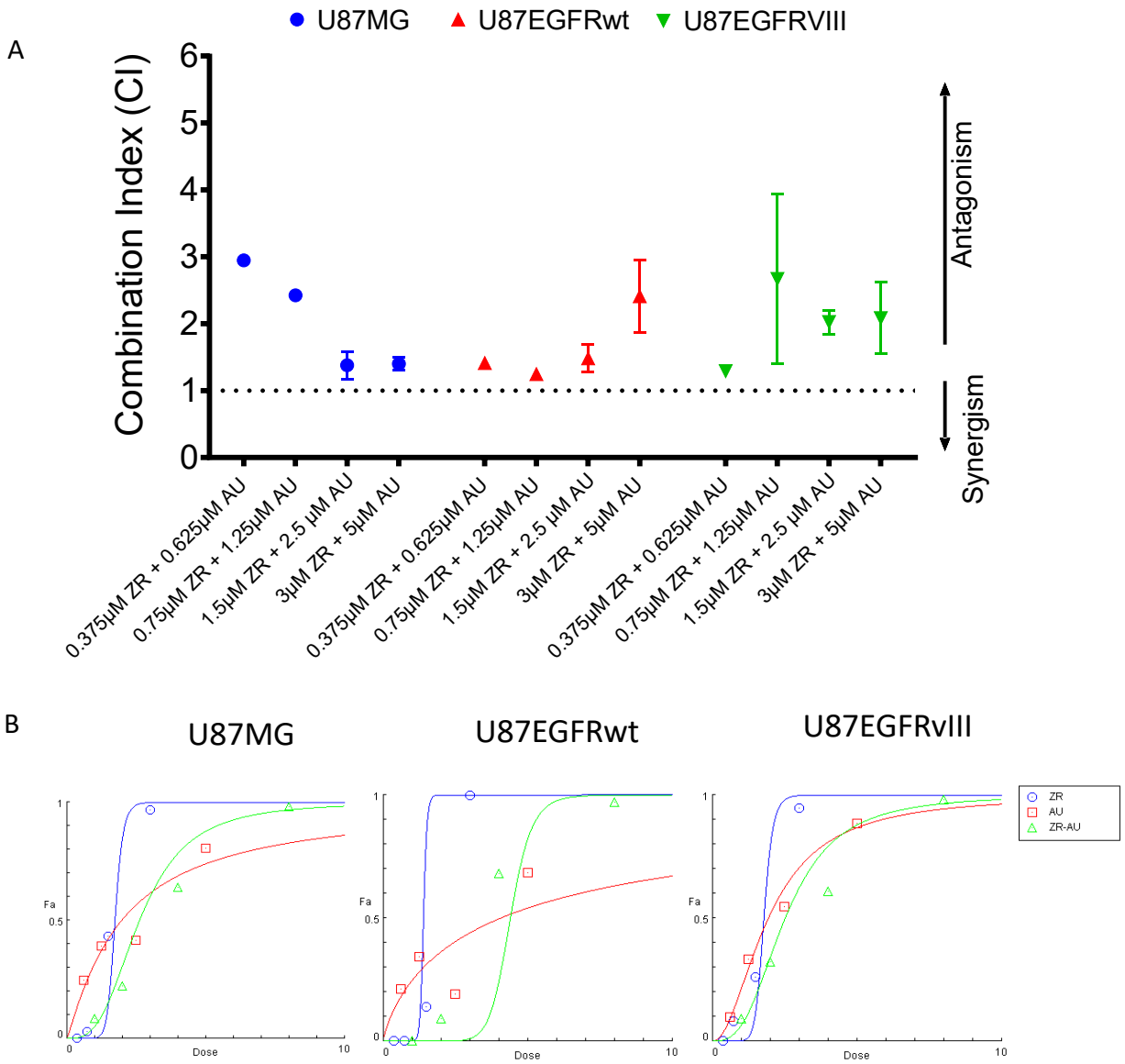

Figure 3.7. Drug interaction analysis of ZR2002 (ZR) / auranofin (AU) combination. (A) Combination index resulting from ratios of a standard mixture of 1.5 μM ZR2002 and 2.5 μM auranofin for 72 h treatment in U87MG, U87/EGFRwt, and U87/EGFRvIII cells. Synergism produces a CI <1, antagonism, CI >1 and additive effect CI =1. (B) Representative graphs of the fraction affected (Fa) for the corresponding drug combinations in figure A.

3.8. Auranofin combined with a fixed 0.5 µM ZR2002 is mostly antagonistic in EGFR-positive cells

To explore another combination strategy, we decided to use a fixed concentration of 0.5 µM ZR2002 combined with varying concentrations of auranofin (0.5, 1, 3, and 6 µM) for 72 h in U87MG, U87/EGFRwt, and U87/EGFRvIII cells. No relevant synergistic effects were observed using this combination strategy (**Figure 3.8.A).** As previously shown, ZR2002 was very effective as single drug in comparison to combination with auranofin as shown in the fraction affected (**Figure 3.8.B).**

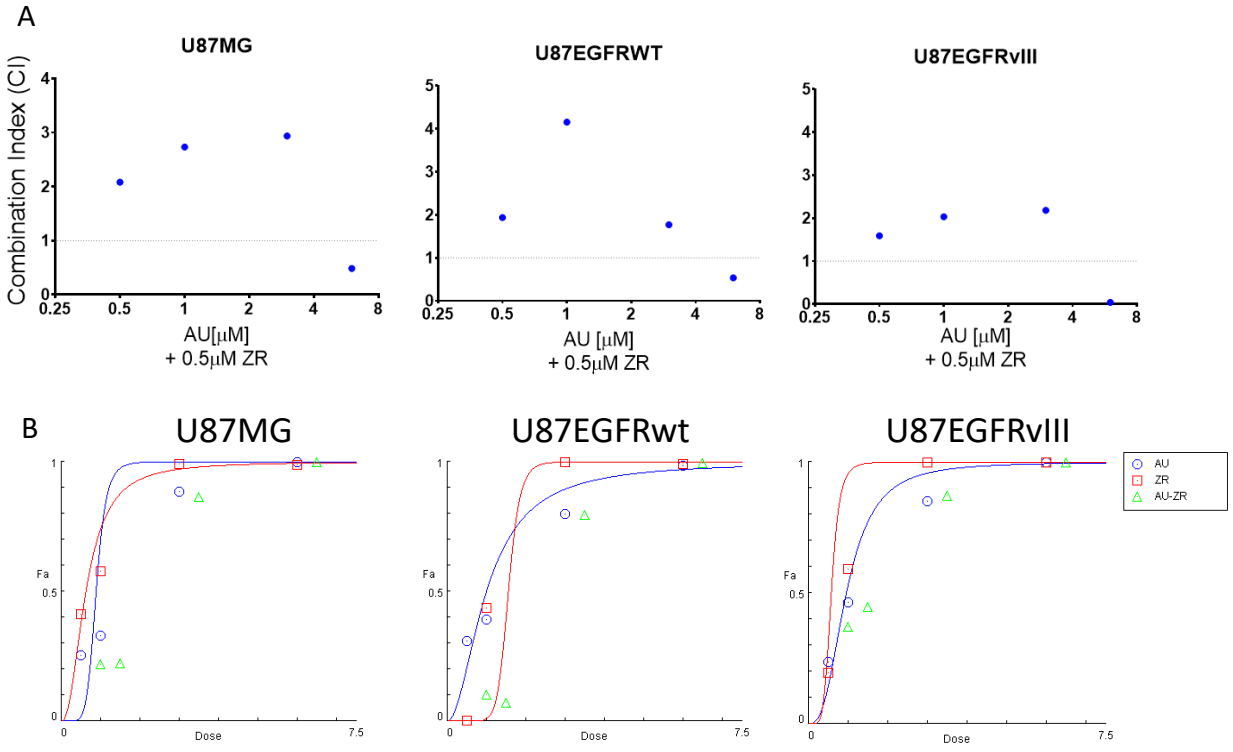

Figure 3.8. Drug interaction study using a fixed concentration of 0.5 µM ZR2002 (ZR) with varying concentrations of auranofin. (A) Combination index of ratio concentrations of 0.5 µM ZR2002 with 0.5, 1, 3, or 6 µM auranofin for 72 h treatment in U87MG, U87/EGFRwt, and U87/EGFRvIII cells using the Chou & Talalay method. Synergism was determined when CI was

<1, antagonism, CI >1 or additive effects with CI =1. (B) Representative graphs of the fraction affected (Fa) for the corresponding drug combinations in panel A.

3.9. Sequential treatment with auranofin followed by ZR2002 is mostly antagonistic in EGFR-positive cells

The sequential order of drug combination is another factor that can influence drug interaction and potentiation effects. We evaluated synergistic, antagonistic, or additive effects using pretreatment with 1 µM auranofin followed by varying concentrations of ZR2002 (0.5, 1, 3, 6 µM) for 72 h in U87MG, U87/EGFRwt, and U87/EGFRvIII cells. In general, no relevant synergistic effects were observed using this combination strategy; at higher doses 3 µM ZR2002 produced some synergism in U87/EGFRwt, and 6 µM ZR2002 had a small effect with auranofin in U87MG and U87/EGFRvIII cells (**Figure 3.9**).

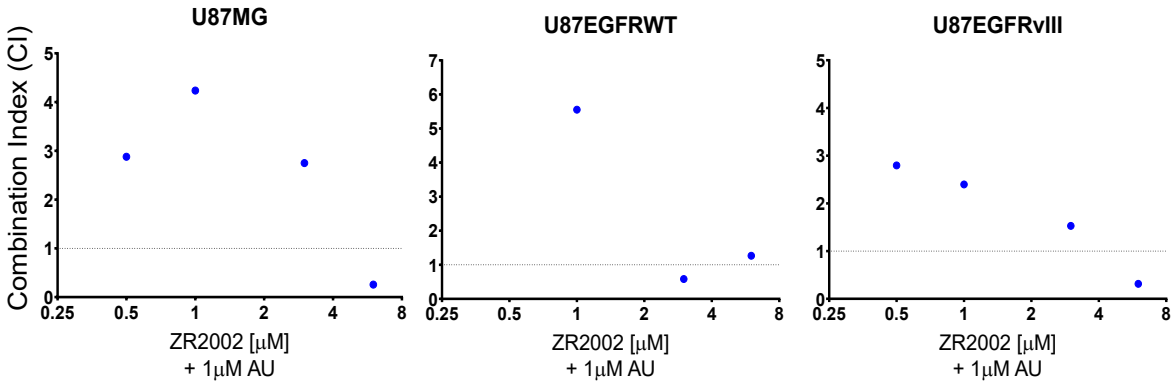

Figure 3.9. Drug interaction study using auranofin pre-treatment followed by increasing doses of ZR2002**.** The combination index was calculated using of 1 µM auranofin (AU) followed by 0.5, 1, 3, 6 µM ZR2002 (ZR) for 72 h treatment in U87MG, U87/EGFRwt, and U87/EGFRvIII cells using the Chou & Talalay method of drug interaction analysis. Synergism was determined when CI was <1, antagonism when CI was >1 or additive effect when CI was =1.

3.10. Sequential treatment with ZR2002 and auranofin is lethal in EGFR positive cells

To find the most effective drug combination for ZR2002 and auranofin, we used an MTT assay to evaluate the effects of treatment with ZR2002 (1.3 µM) and auranofin (1.6 µM) alone in comparison to preincubation (2 h and 4 h) with 1 µM ZR2002 or 1 µM auranofin followed by ZR2002 (1.3 µM) or auranofin (1.6 µM) for 24 h, 48 h or 72h in U87MG, U87EGFRwt, and U87EGFRvIII cells. The most effective combination to decrease cell vitality were preincubation of 2 h or 4 h with 1 µM ZR2002 followed by 1.6 µM auranofin in all GBM cells (**Figure 3.10.**).

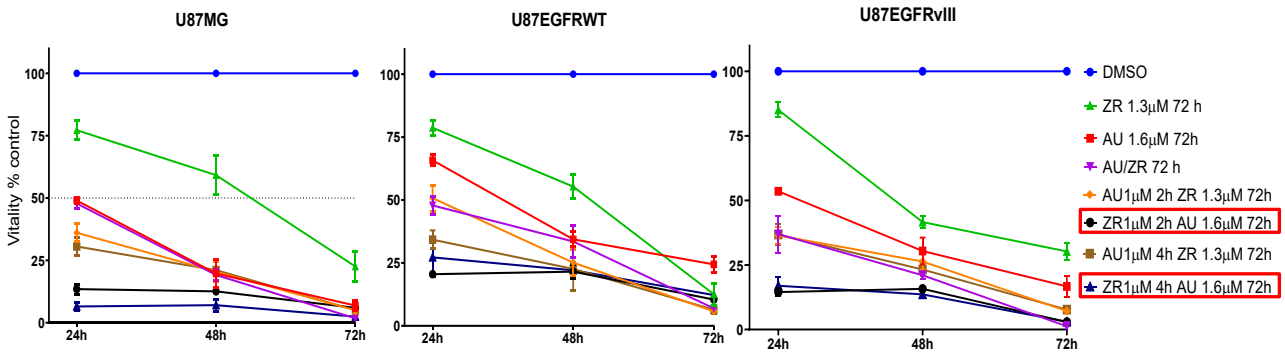

Figure 3.10. Drug interaction study using ZR2002 or auranofin for 72 h following pre-treatment with the opposite drug for 2 or 4 h in EGFR positive cell lines. MTT assay documenting vitality obtained after single and combined incubation with 1 or 1.3 µM ZR2002 (ZR) and 1 or 1.6 µM auranofin (AU), in the sequences and time indicated. Synergy was noted in all drug combinations, with the greatest effect produced by 1 µM ZR2002 followed by 1.6 µM auranofin for 24 h, 48 h and 72 h in U87MG, U87EGFRwt, and U87EGFRvIII cells. Bars show the mean ± SEM.

3.11. Gefitinib is cytotoxic in EGFR-positive GBM cells and increases ROS only in U87EGFRwt cells

To investigate potential synergistic combinations using Gefitinib we first assessed the effects of the drug alone in EGFR GBM isogenic cells. In an MTT assay using different

concentrations of gefitinib for 72 h, we showed that this drug decreased the vitality of U87MG, U87EGFRwt, and U87EGFRvIII cells. No significant difference was found in IC_{50s} for gefitinib among the cell lines (**Figure 3.11A**). Additionally, we measured intracellular ROS levels after 30 µM gefitinib. Although a notable ROS increase was observed in all cell lines, the only statistically significant increase occurred in U87EGFRwt compared to vehicle-treated controls (**Figure 3.11B.**).

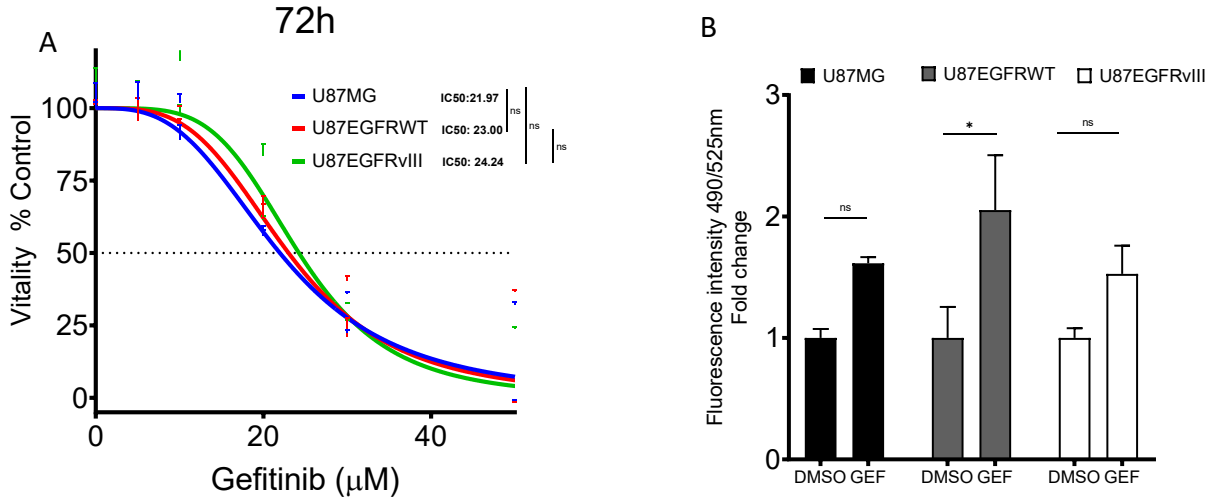

Figure 3.11. Gefitinib short-term toxicity and intracellular ROS levels in EGFR isogenic cell lines. (A) MTT assay showing vitality after different concentrations of gefitinib for 72 h in the three GBM cell lines. (B) Intracellular ROS levels after 30 µM gefitinib (GEF) for 24 h in U87MG, U87/EGFRwt, and U87/EGFRvIII cells. CM-H2DCFDA was used as a general ROS-sensitive probe. Bars show the mean ± SEM (ns= not significant $p > 0.05$, *$p < 0.05$, two-way ANOVA followed by Tukey's multiple comparison test).

3.12. Gefitinib and auranofin in combination are synergistic in EGFR-positive GBM cells

Next, we evaluated the interaction between gefitinib (30 μM) and auranofin (3 μM) in ratio combinations, (double, half, and quarter) on cell vitality. Results showed that all combinations were synergistic or additive as illustrated in **Figure 3.12**.

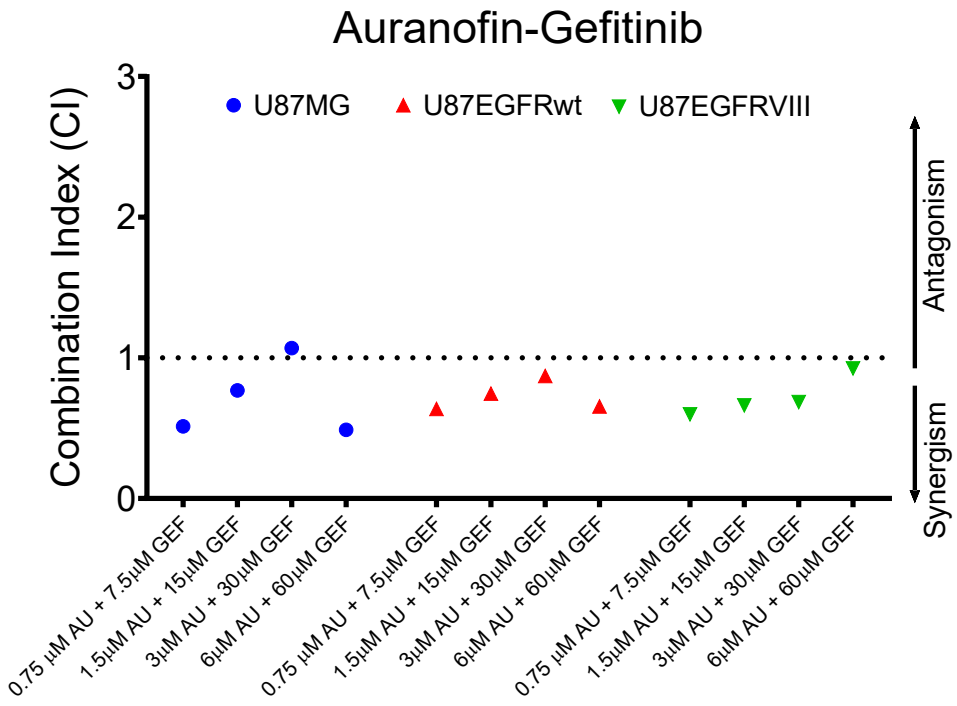

Figure 3.12. Combination index of gefitinib/auranofin toxicity in EGFR isogenic cell lines. U87MG, U87/EGFRwt, and U87/EGFRvIII cells were treated with different concentration ratios of gefitinib (GEF) and auranofin (AU) and cell vitality was used to quantify the drug interaction using the Chou & Talalay method to calculate the combination index. Synergism was determined when CI was <1, antagonism with CI >1, and additive effect with CI =1.

3.13. Gefitinib/auranofin synergistically decrease viability in EGFR-positive GBM cells

To further confirm synergistic effects of gefitinib and auranofin in GBM EGFR cells we performed MTT assays after 72 h of treatment with combinations of 1, 2, or 3 μM auranofin with 5, 10, or 20 μM of gefitinib in U87MG, U87EGFRwt and U87EGFRvIII cells. We observed that concentrations of 5, 10, or 20 μM gefitinib sensitised the cells in terms of toxicity when combined with auranofin 1, 2, or 3 μM as shown in **Figure 3.13A.** Representative images of cell morphology after combination treatment are shown in **Figure 3.13B.** The drug combination index showed that in U87MG cells most combinations were synergistic or additive; for U87EGFRwt cells only the combinations of 20 μM gefitinib with auranofin were synergistic, whereas for U87EGFRvIII cells, most combinations of 10 and 20 μM gefitinib with auranofin were synergistic (**Figure 3.13C**).

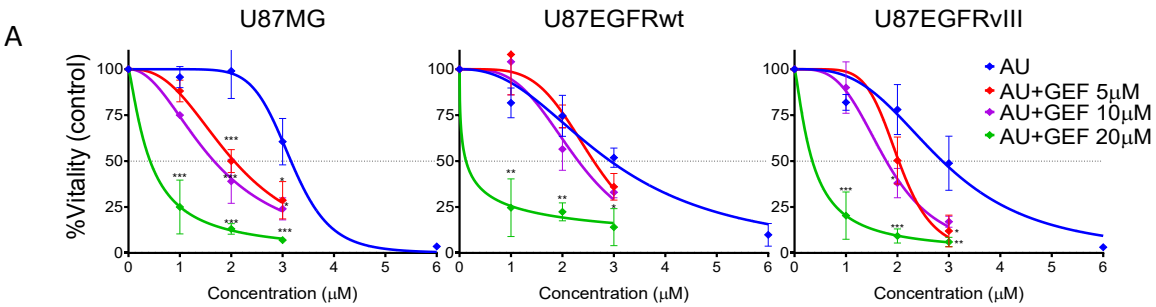
A
U87MG
U87EGFRwt
U87EGFRvIII
%Vitality (control)
Concentration (μM)
AU
AU+GEF 5μM
AU+GEF 10μM
AU+GEF 20μM

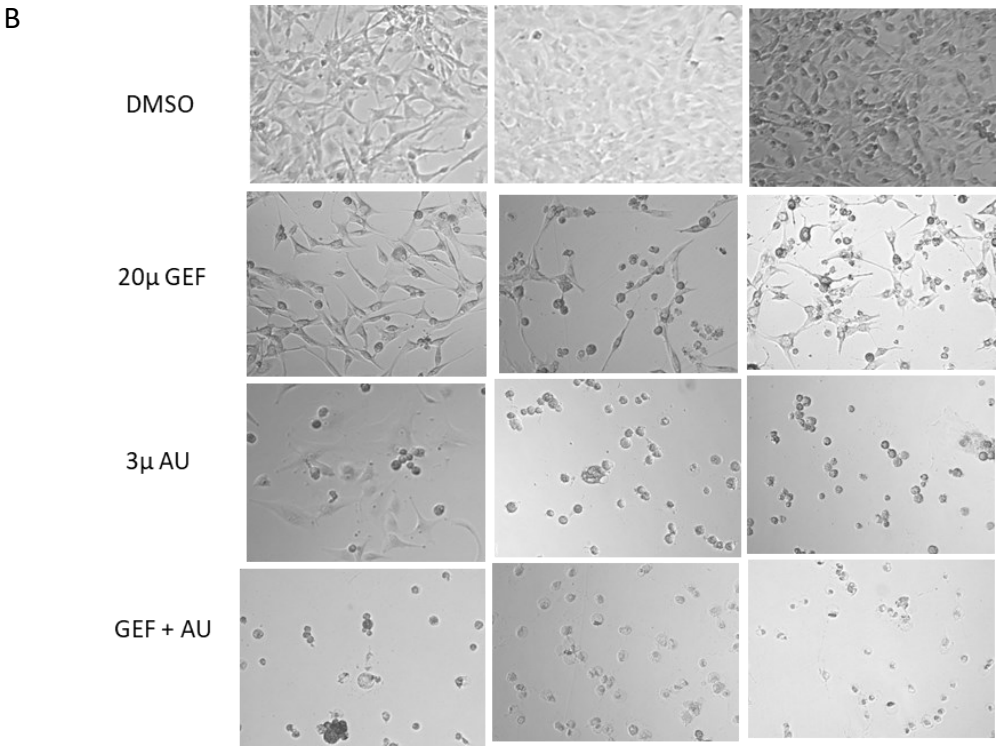
B
DMSO
20μ GEF
3μ AU
GEF + AU

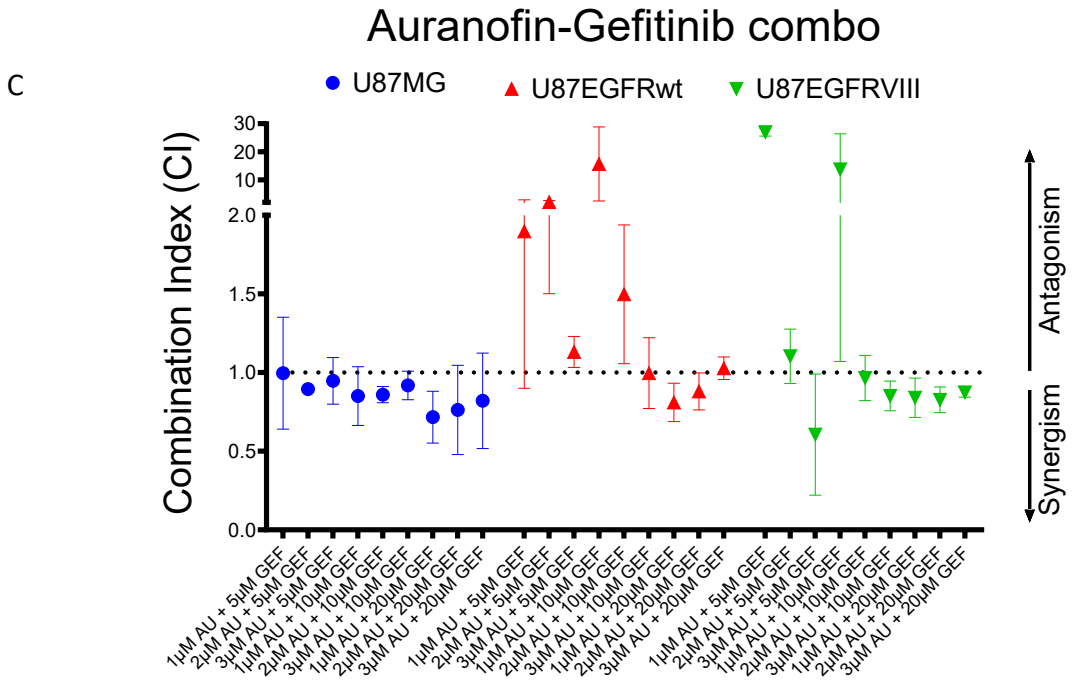
Auranofin-Gefitinib combo
C
U87MG
U87EGFRwt
U87EGFRVIII
Combination Index (CI)
Antagonism
Synergism
1μM AU + 5μM GEF
2μM AU + 5μM GEF
3μM AU + 5μM GEF
1μM AU + 10μM GEF
2μM AU + 10μM GEF
3μM AU + 10μM GEF
1μM AU + 20μM GEF
2μM AU + 20μM GEF
3μM AU + 20μM GEF

Figure 3.13. The toxicity of gefitinib in EGFR isogenic cell lines. (**A**) MTT assays for cell vitality after 72 h of treatment combinations using 1- 3 μM auranofin (AU) with 5 - 20 μM gefitinib (GEF) in U87MG, U87EGFRwt, and U87EGFRvIII cells. Bars show the mean ± SEM (*$p < 0.05$, **$p < 0.01$, ***$p < 0.001$ two-way ANOVA followed by Dunnett's multiple comparison test). (B) Cell morphology of U87MG, U87EGFRwt and U87EGFRvIII cells treated with 20 μM gefitinib and 3 μM auranofin as single drugs or in combination. (C) Combination index analysis of drug treatments from panel A in EGFR isogenic cell lines. Bars show the mean ± SEM.

3.14. GBM cells are sensitive to PRIMA-1^{MET} regardless of EGFR status

PRIMA-1^{MET} offers a promising effect by reverting the abnormal function of mutant p53 [356]. To test the efficacy of this drug to induce toxicity in GBM isogenic cells for EGFR we conducted an MTT assay using different concentrations of PRIMA-1^{MET} for 72 h in U87MG, U87EGFRwt and U87EGFRvIII cells. PRIMA-1^{MET} caused cytotoxicity in a dose dependent manner in the 3 GBM cell lines; no statistical difference was found in the IC_{50s} among the cell lines (**Figure 3.14**).

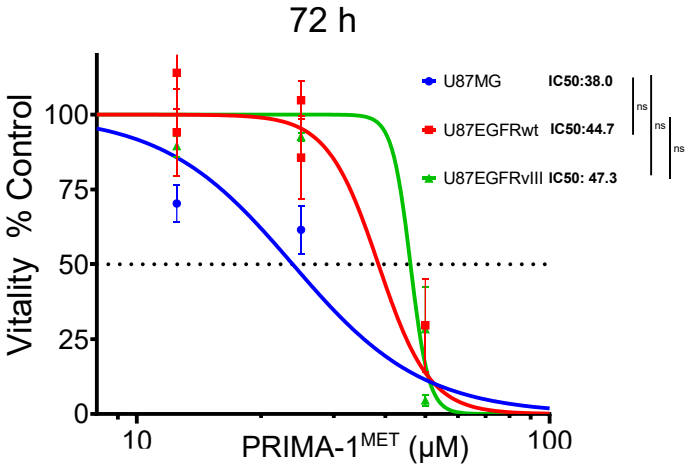

Figure 3.14. Short-term impact of PRIMA-1^{MET} on GBM cells isogenic for EGFR. The vitality of U87MG, U87EGFRwt and U87EGFRvIII cells following different concentrations of PRIMA-1^{MET} for 72 h treatment was assessed by the MTT assay; bars show the mean ± SEM (one-way ANOVA; ns= not significant $p > 0.05$).

3.15. JS440 does not provide lower IC_{50} compared to combined PRIMA-1^{MET} /Gefitinib to GBM EGFR isogenic cells

JS440 is a combi-molecule that shares components of gefitinib and PRIMA-1^{MET}. We assessed the effect of JS440 in U87MG and T98G (positive for EGFR and MGMT), after 72 h of treatment; we then compared the IC_{50s} of the individual drugs gefitinib and PRIMA-1^{MET}, alone or together at equimolar concentrations with JS440, and also with auranofin. Although there was a decrease in the IC50 with JS440 compared to individual gefitinib and PRIMA-1^{MET}, both drugs combined had still lower IC_{50s} than JS440. Auranofin-treated cells showed the lowest IC_{50} in U87MG and T98G **(Figure 3.15).**

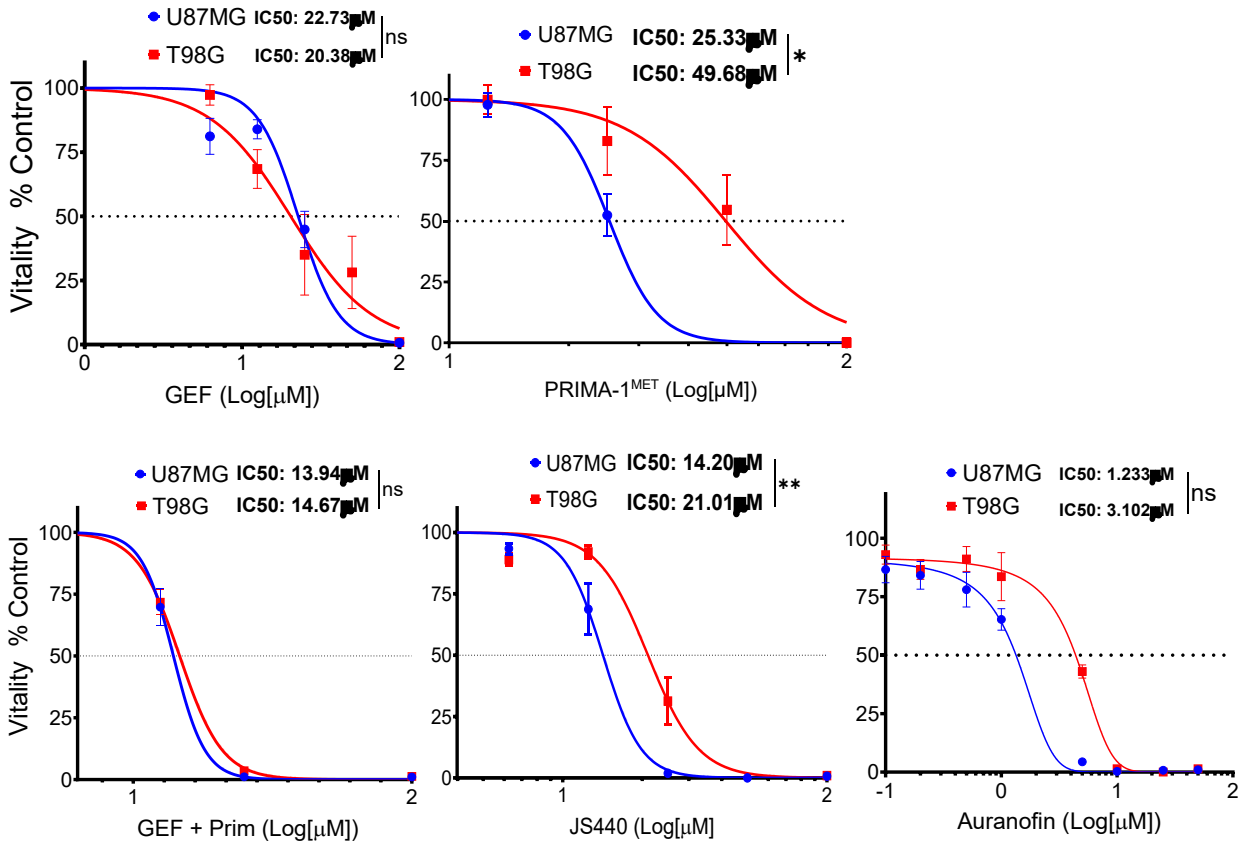

Figure 3.15. Impact of JS440 compared to single gefitinib and PRIMA-1^{MET} or their combination, and auranofin, on the vitality of U87MG and T98G cells. The MTT assay was performed after

treatment for 72h with the indicated concentrations of gefitinib (GEF) and PRIMA-1^{MET} (Prim) alone or in combination, as well as JS440 and auranofin; the IC_{50} of each drug or combination is included above the corresponding illustration; bars show the mean ± SEM, (ns= not significant $p > 0.05$ *$p < 0.05$ **$p < 0.01$ unpaired, two tailed t-test) when comparing the IC_{50s} obtained.

3.16. Auranofin shows sub-micromolar cytotoxicity for cisplatin sensitive and resistant HGSOC cells

To confirm the strong short-term toxicity of auranofin, we tested auranofin in a different cancer: ovarian cancer represented by cisplatin-sensitive PEO1 and cisplatin-resistant PEO4 cells [462]. Auranofin decreased the vitality of PEO1 and PEO4 cells in a dose dependent manner but without difference in the IC_{50s} between the cell lines (**Figure 2.16.).**

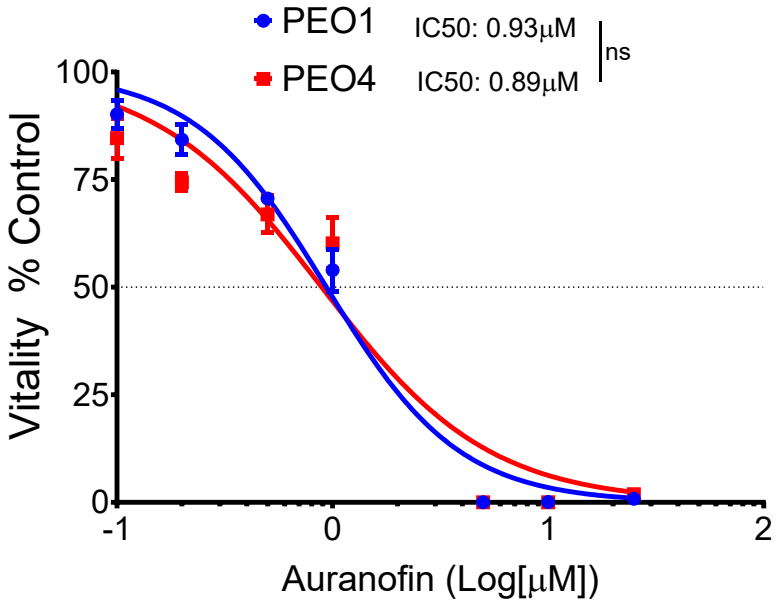

Figure 3.16. Impact of Auranofin on vitality of PEO1 and PEO4 cells. MTT assay in PEO1 and PEO4 cells treated with auranofin at different concentrations; bars show the mean ± SEM (ns= not significant $p > 0.05$ unpaired, two tailed t-test) when comparing the IC50s obtained.

3.17. Auranofin decreases viability in PEO1 cells

Next, we validated that PEO1 cells treated with increasing concentrations of auranofin were unhealthy (i.e., they had reduced vitality). We confirmed the toxic effect as we observed a decrease in viability of PEO1 cells treated with auranofin, with an IC_{50} of 1.23 μM, which is slightly higher than the IC_{50} obtained with the vitality (i.e., MTT) assay (**Figure 3.17**).

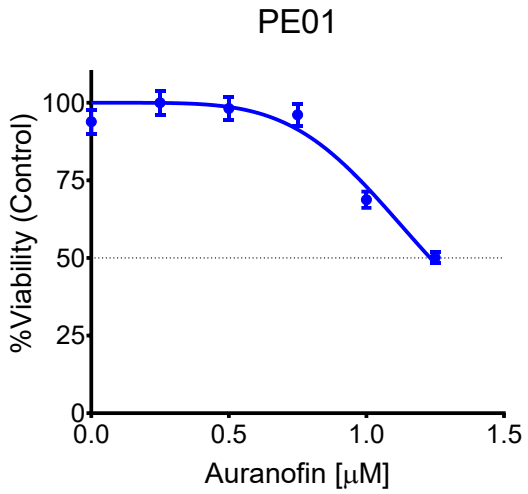

Figure 3.17. Impact of auranofin on the viability of PEO1 cells. Cells were treated with increasing concentrations of auranofin, and viability was assessed by flow cytometry; bars show the mean ± SEM.

3.18. Combi-molecule JS470 did not provide an advantage over PRIMA-1^{MET} and Olaparib together in PEO1 and PEO4 cells

We explored the efficacy of the JS470 combi-molecule, which shares the components of PRIMA-1^{MET} and olaparib, in comparison to the individual drugs alone and together in equimolar concentrations on the survival of PEO1 and PEO4 cells. JS470 did not produce a lower IC_{50s} than PRIMA-1^{MET} -olaparib in combination or in PEO1 and PEO4 cells.

Table 3.18.1. IC_{50s} using JS470, Olaparib, PRIMA-1^{MET} and Olaparib/ PRIMA-1^{MET} (O+P) in PEO1 cells.

Drug in PEO1	**IC_{50} (µM)**	**SEM (µM)**
JS470	16.11	0.95
O+P	4.70	0.86
PRIMA-1^{MET}	5.98	0.85
Olaparib	5.12	0.78

Table 3.18.2. IC_{50s} using JS470, Olaparib, PRIMA-1^{MET} and Olaparib/ PRIMA-1^{MET} (O+P) in PEO4 cells.

Drug in PEO4	**IC_{50} (µM)**	**SEM (µM)**
JS470	26.377	2,50
O+P	8.738	1.3
PRIMA-1^{MET}	8.787	1.5
Olaparib	154176.133	14237.8

Chapter 3 – RESULTS (Part 2)

3.1. Auranofin induces mitochondrial membrane depolarization, DNA damage, late apoptosis, and caspase 3/7 activation in U87MG GBM cells

Recent research has shown that auranofin has anti-cancer effects on various cancers [463], including GBM [323-325, 464]. To investigate the cytotoxicity of auranofin in U87MG GBM cells, we treated them with DMSO (vehicle control) or auranofin (0-5 μM for 24 h, 48 h, or 72 h). Our results revealed that auranofin caused a significant dose-dependent mitochondrial membrane depolarization at 3 and 5 μM for 24 h (**Figure 3.1A),** it increased phosphorylation of the DNA double-strand break (DSB) marker γH2AX (Ser139) at 5 μM for 48 h (**Figure 3.1B**), it increased the number of late-stage apoptotic Annexin V/7AAD-positive cells (**Figure 3.1C**) at 3 and 5 μM for 72 h and also increased caspase activation (**Figure 3.1D**) as determined by flow cytometry in U87MG cells.

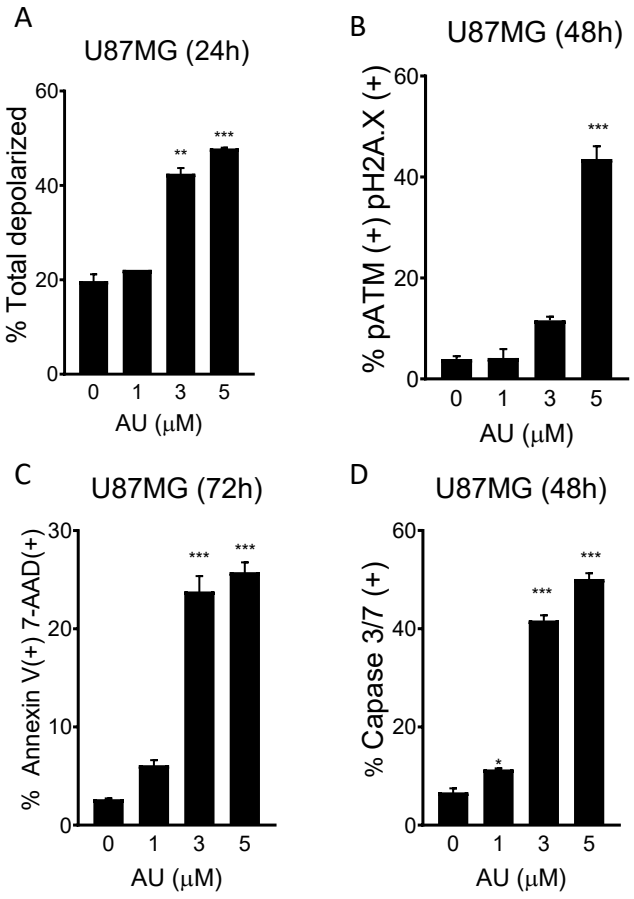

Figure 3.1. Effects of increasing doses of auranofin (AU) on U87MG cells. (A) Mitochondrial depolarization after 24 h treatment. (B) DNA damage after 48 h treatment. (C) Annexin V/ 7-AAD staining after 72 h treatment. (D) Caspase 3/7 activation after 48 h. Bars show mean ± SEM (** $p < 0.01$, *** $p < 0.001$, one-way ANOVA followed by Dunnett's multiple comparison test).

3.2. Auranofin anticancer effects are caspase 3/7 independent

Studies on lung and cervical cancer cell lines showed that the anticancer effects of auranofin were dependent on caspase activation [306, 322]. To investigate whether our previous findings were also dependent on caspase activation, we treated U87MG cells with auranofin (5 μM) for 18 hours with or without a 1-hour preincubation with 50 μM of the pan-caspase inhibitor, z-vad-fmk. We then used a flow cytometer to assess caspase-3/7 activation and viability. Our results showed that exposure to 5 μM of auranofin caused a significant increase in caspase-3/7 activation, but when we added the pan-caspase inhibitor, z-vad-fmk, we observed an even higher increase in caspase-3/7 activation (**Figure 3.2A)**. This was consistent with a significantly greater decrease in viability compared to treatment with auranofin or a vehicle solution (**Figure 3.2B)**. We also assessed the viability and quantified the total number of cells in U87MG and U87EGFRvIII cultures following exposure to auranofin (5 μM) with or without a 2-hour preincubation with 50 μM of the caspase-3 inhibitor, z-devd-fmk. We did not observe any significant recovery in viability or in the number of cells in either U87MG or U87EGFRvIII cells using z-devd-fmk prior to auranofin exposure (**Figure 3.2C and D**).

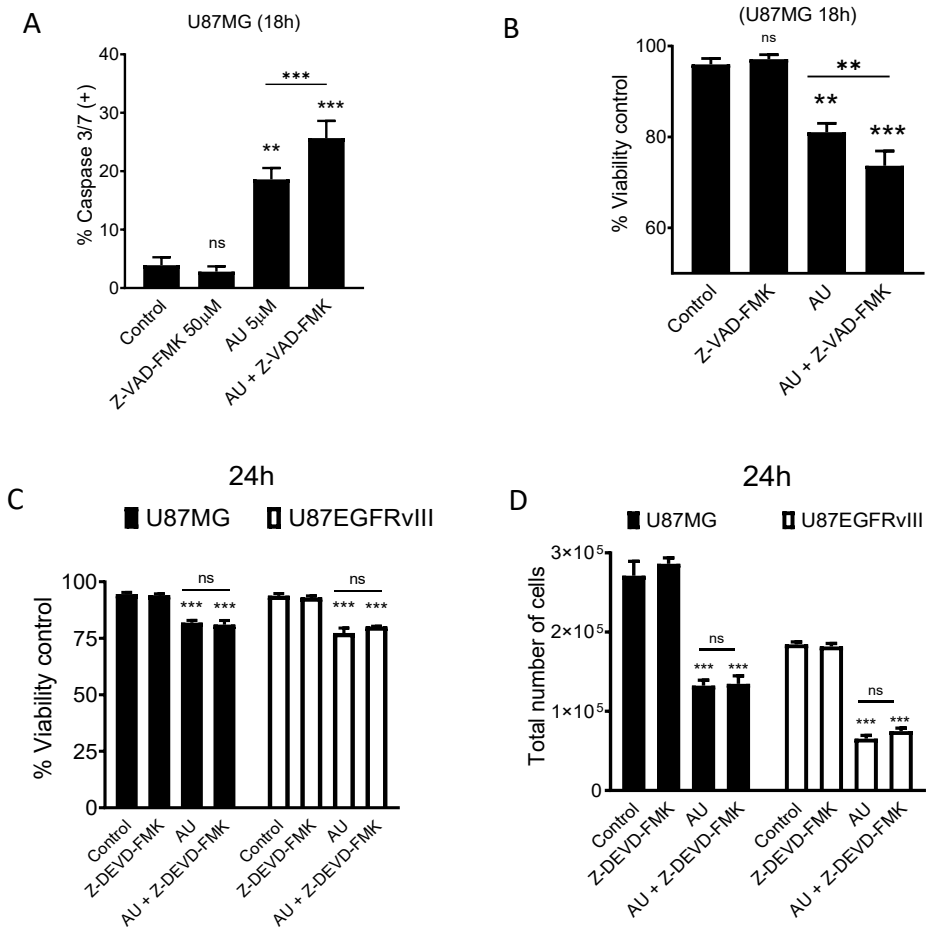

Figure 3.2. Auranofin (AU) effects were caspase-3/7 independent in U87MG cells. (A) Caspase -3/7 activation and (B) viability of U87MG cells treated with 5 μM auranofin during 18 h with or without 1 h preincubation with 50 μM the pan-caspase inhibitor z-vad-fmk. Bars show mean ± SEM (** $p < 0.01$, *** $p < 0.001$, one-way ANOVA and Dunnett's post-test). (C) Viability of U87MG and U87EGFRvIII cells and (D) total number of these cells after 24 h exposure to 5 μM auranofin with or without 2 h preincubation with 50 μM of caspase-3 inhibitor z-devd-fmk. Bars show mean ± SEM (** $p < 0.01$, *** $p < 0.001$, two-way ANOVA and Tukey's multiple comparison test).

3.3. Auranofin induced short term cytotoxicity in both parental and isogenic EGFRwt or EGFRvIII GBM cells

Abnormal EGFR expression is associated with increased oxidative stress due to EGFR hyperactivation [256, 262]. To investigate the hypothesis that auranofin affects the viability of GBM cells with abnormal EGFR expression, we used parental U87MG cells and their isogenic GBM cell lines that were stably transfected with EGFRwt (U87/EGFRwt) or EGFRvIII (U87/EGFRvIII) [157]. First, we performed immunoblotting to assess Tyr1068 phosphorylation (p-EGFR), expression in EGFRwt and EGFRvIII, and expression of TrxR1, the main target of auranofin [331, 333, 465]. As expected, U87MG cells did not express EGFR or p-EGFR. U87/EGFRvIII cells displayed higher p-EGFR expression than U87EGFRwt cells (**Figure 3.3A**). Auranofin at a concentration of only 0.5 μM for 24 h, significantly decreased TrxR activity in U87MG cells ($p=0.003$), U87/EGFRwt ($p=0.004$), and U87/EGFRvIII cells ($p=0.025$) compared to the DMSO control (**Figure 3.3B**). No significant differences were observed among the three isogenic cell lines tested.

We evaluated the cytotoxicity of auranofin on U87/EGFR isogenic cell lines by conducting an MTT assay for 72 hours. The half-maximal inhibitory concentrations (IC50s) were 3.07±0.11 μM, 3.21±0.50 μM, and 3.13±0.45 μM for U87MG, U87/EGFRwt, and U87/EGFRvIII cell lines, respectively. These values showed no statistical difference among the cell lines (**Figure 3.3C**). However, the MTT assay measures metabolic activity, which may not directly correspond to the actual viability of the cells. Therefore, we also measured viability and total cell number by flow cytometry. Our results revealed that auranofin significantly decreased the viability and total number of cells in a dose-dependent manner (**Figure 3.3D-F**). Auranofin, at an IC_{50} of 3 μM, decreased the total number of U87MG, U87/EGFRwt, and U87/EGFRvIII cells by 15%, 41%, and

20%, respectively. Additionally, the viability was reduced to 11%, 39%, and 15% in each of these cell lines. Notably, U87/EGFRvIII displayed a similar sensitivity to auranofin as did U87MG, but it had a more significant decrease in both total cell number ($p<0.001$) and cell viability ($p<0.001$) compared to U87EGFRwt. These findings are shown in **Figure 3D-F** and **Table 3.1**.

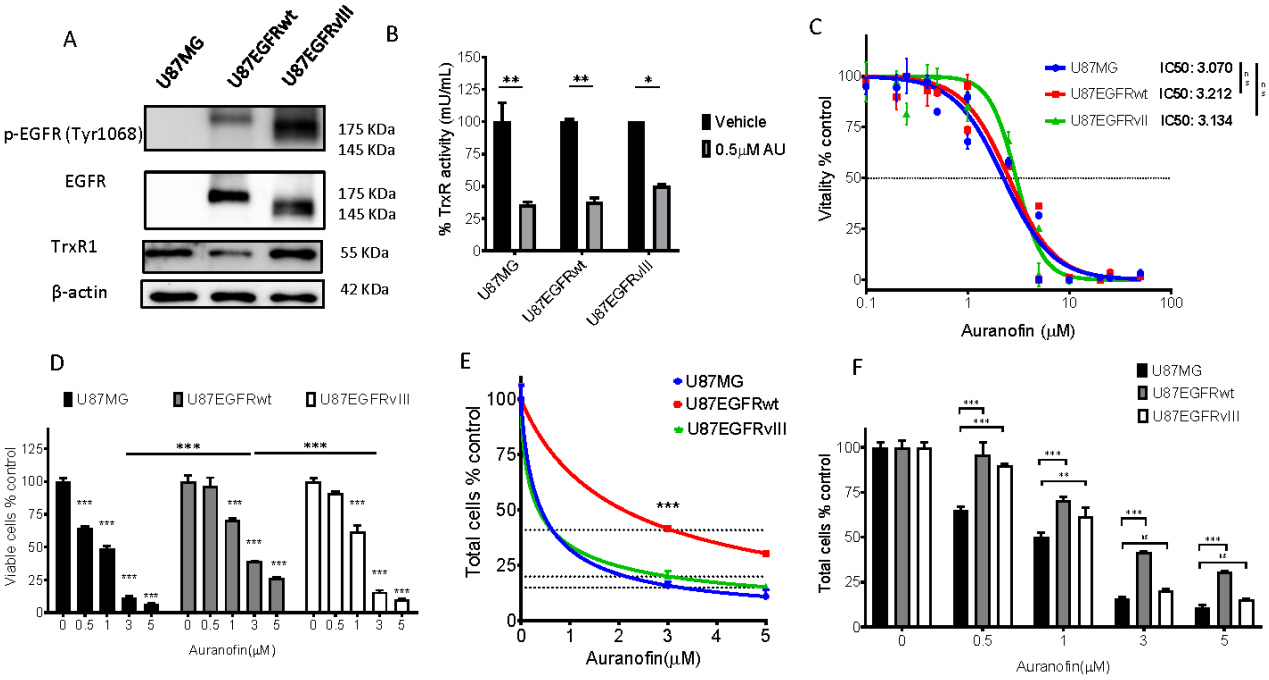

Figure 3.3. Short-term impact of auranofin on EGFR isogenic cell lines. (A) Phosphorylated EGFR (Tyr1068), total EGFR, TrxR1 and β-actin expression levels in three GBM cell lines, U87MG, U87/EGFRwt, and U87/EGFRvIII. (B) TrxR activity after treatment for 24 h with 0.5 μM auranofin compared to DMSO control. Bars show the mean ± standard error of the mean (SEM) (* $p < 0.05$, ** $p < 0.01$, two-way ANOVA and Sidak's post-test). (C) MTT assay showing the IC_{50} in the EGFR isogenic cell lines treated with auranofin for 72 h (D-F) Viability and total cell count in the cultures after 72 h of exposure to increasing concentrations of auranofin. All bars show the mean ± SEM (*$p < 0.05$, **$p < 0.01$, ***$p < 0.001$, two-way ANOVA followed by Tukey's post-test).

3.4. Auranofin induced long-term cytotoxicity in both parental and isogenic EGFRwt or EGFRvIII GBM cells

To investigate the long-term cytotoxicity of auranofin in U87/EGFR isogenic cells, we carried out a clonogenic survival assay. The aim of this assay was to determine the drug's ability to inhibit colony formation in these cells. Our results showed that auranofin caused long-lasting cytotoxic effects (9-10 days) at concentrations lower than the IC_{50} calculated using MTT **(Figure 3.4A)**. Exposure to 0.25 μM, 0.5 μM, and 1.0 μM of auranofin significantly decreased the survival fraction of U87MG, U87/EGFRwt, and U87/EGFRvIII cells compared to their respective controls ($p<0.001$ for the 3 cell lines) as shown in **Figure 3.4B.** In particular, the survival fraction of U87MG, U87/EGFRwt, and U87/EGFRvIII cells at 0.5 μM auranofin was 0.19±0.08, 0.30±0.22, 0.130±0.13, respectively. Additionally, while there was no statistically significant difference between U87/EGFRvIII and U87MG ($p>0.05$), auranofin at 0.5 μM significantly decreased U87/EGFRvIII clonogenic potential compared to U87/EGFRwt ($p=0.036$) (**Figure 3.4B**). Furthermore, at a concentration of 1.0 μM, the drug significantly impeded colony formation, and caused spindle-shaped cell morphology and scattered cells in abortive colonies compared to dense colonies in the DMSO control (**Figure 3.4C**).

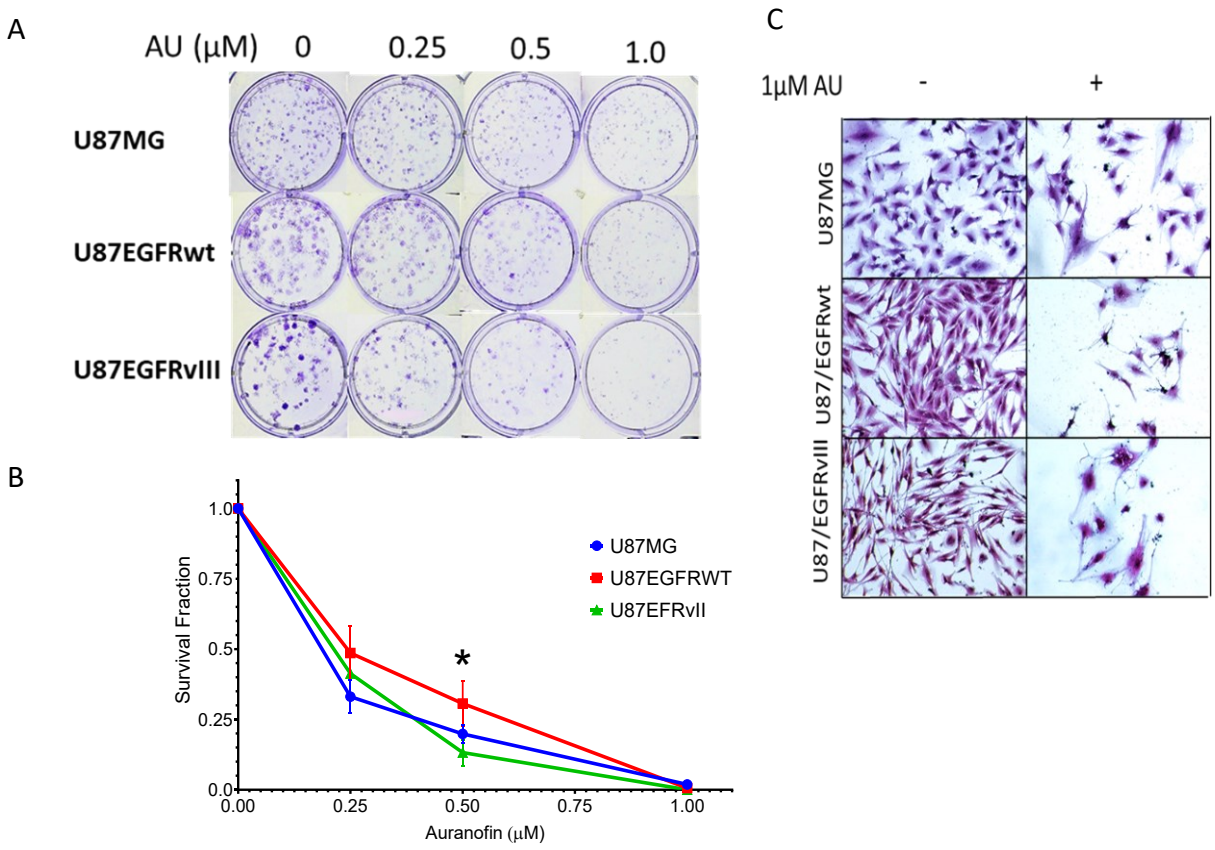

Figure 3.4. Auranofin (AU) long-term impact on EGFR isogenic cell lines. (A) Colony formation assay showing colony formation capacity at different concentrations of auranofin after 9-10 days incubation. (B) The survival fraction of U87MG, U87/EGFRwt, and U87/EGFRvIII cells decreased in a dose dependent manner with no significant difference among cell lines, except between U87/EGFRwt and U87/EGFRvIII at 0.5 μM AU; bars show the mean ±SEM (*$p < 0.05$, two-way ANOVA and Tukey's post-test). (C) Microscopic images showing individual colony disruption of GBM cells exposed to vehicle (-) or 1 μM of auranofin (+).

3.5. Auranofin induced residual cytotoxicity in both parental and isogenic EGFRwt or EGFRvIII GBM cell lines

To assess the residual/extended/chronic long-term cytotoxicity of auranofin, we exposed cells to different concentrations of auranofin or a DMSO control for 72 hours, and then seeded the surviving cells in drug-free medium for a colony formation assay. Over the course of 9-10 days, the percentage of colonies that were formed decreased in a dose-dependent manner. Both U87/EGFRvIII and U87MG cells exhibited similar sensitivity to auranofin's residual long-term cytotoxicity at a concentration of 3 μM, although their sensitivity was significantly higher than that of U87EGFRwt cells (p=0.002) (**Figure 3.5A-B**).

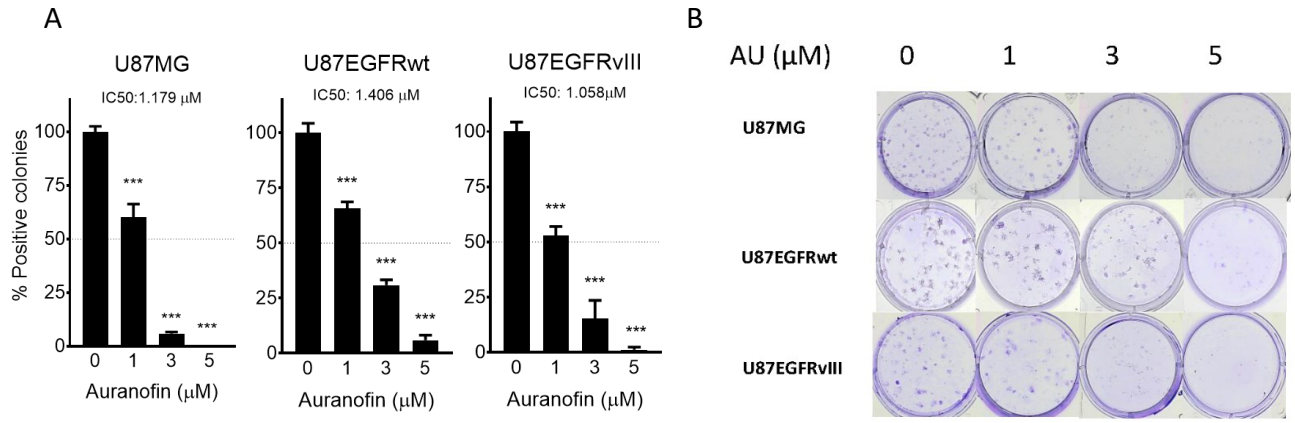

Figure 3.5. Long-term effects (chronic) in a colony formation on U87MG, U87/EGFRwt, and U87/EGFRvIII cells treated with auranofin (AU). (A) Colony formation capacity after GBM cells were exposed for 72 h to different concentrations of AU followed by plating in drug-free media and then incubation for 9-10 days. The bars show the mean ± SEM (** $p < 0.01$, *** $p < 0.001$, one-way ANOVA and Dunnett's multiple comparison test). (B) Representative colony formation assay plates stained with crystal violet.

Overall, these results reveal that overexpression of EGFRwt or EGFRvIII did not substantially affect the short- or long-term cytotoxicity of auranofin, while U87/EGFRvIII showed heightened sensitivity to auranofin compared to U87/EGFRwt *in vitro*.

3.6. Auranofin leads to an increase in intracellular reactive oxygen species in EGFR isogenic glioblastoma cells

Auranofin has been found to increase the production of ROS and to disrupt intracellular redox homeostasis in several cancer cell lines [296, 305, 322, 323, 466, 467]. Using the fluorescent ROS-sensitive probe CM-H2DCFDA, we measured auranofin-induced ROS levels in U87/EGFR isogenic cell lines by quantifying fluorescence with a microplate reader. We observed that auranofin at 6 μM for 2.5 h significantly increased ROS levels in all GBM cells (**Figure 3.6A**). There was no significant difference in ROS levels among the cell lines.

Auranofin, at a concentration of 3 μM for 24 hours, significantly increased the levels of reactive oxygen species (ROS) in the three isogenic cell lines compared to their respective controls (U87MG, $p<0.001$; U87EGFRwt, $p<0.05$; U87EGFRvIII, $p<0.001$) (**Figure 3.6B**). In particular, the ROS increase was more pronounced in U87/EGFRvIII cells compared to U87/EGFRwt cells ($p<0.05$), as demonstrated by both **Figure 3.6B** and fluorescence microscopy in **Figure 3.6C**.

The overproduction of ROS involves an increase in multiple types of ROS, including superoxide anions. Flow cytometry analysis using the superoxide anion-specific probe dihydroetidium (DHE) showed that auranofin significantly increased superoxide anions at a dose of 5 μM, for 24 hours. At this concentration, U87EGFRvIII exhibited significantly less superoxide anions compared to U87EGFRwt and U87MG cells ($P <0.001$ and $P <0.01$, respectively) **Figure 3.6D**.

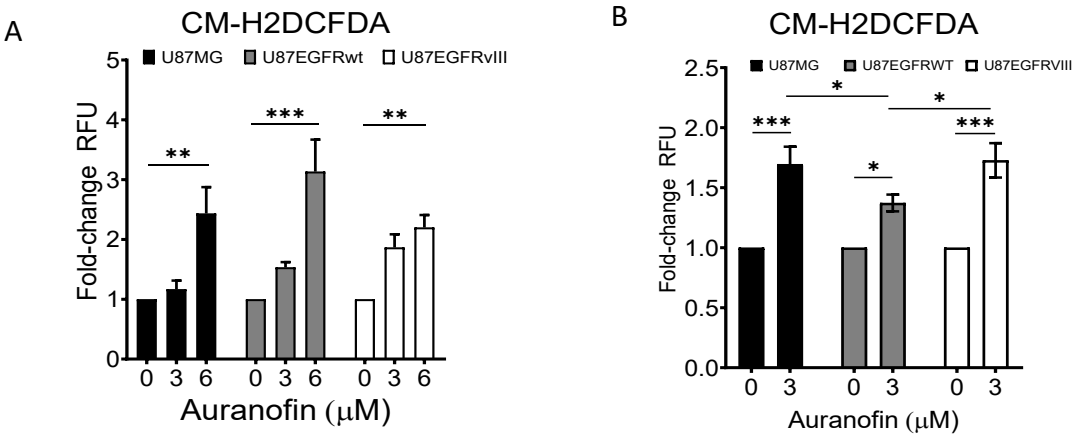
A
CM-H2DCFDA
U87MG
U87EGFRwt
U87EGFRvIII
Fold-change RFU
Auranofin (μM)
B
CM-H2DCFDA
U87MG
U87EGFRWT
U87EGFRVIII
Fold-change RFU
Auranofin (μM)

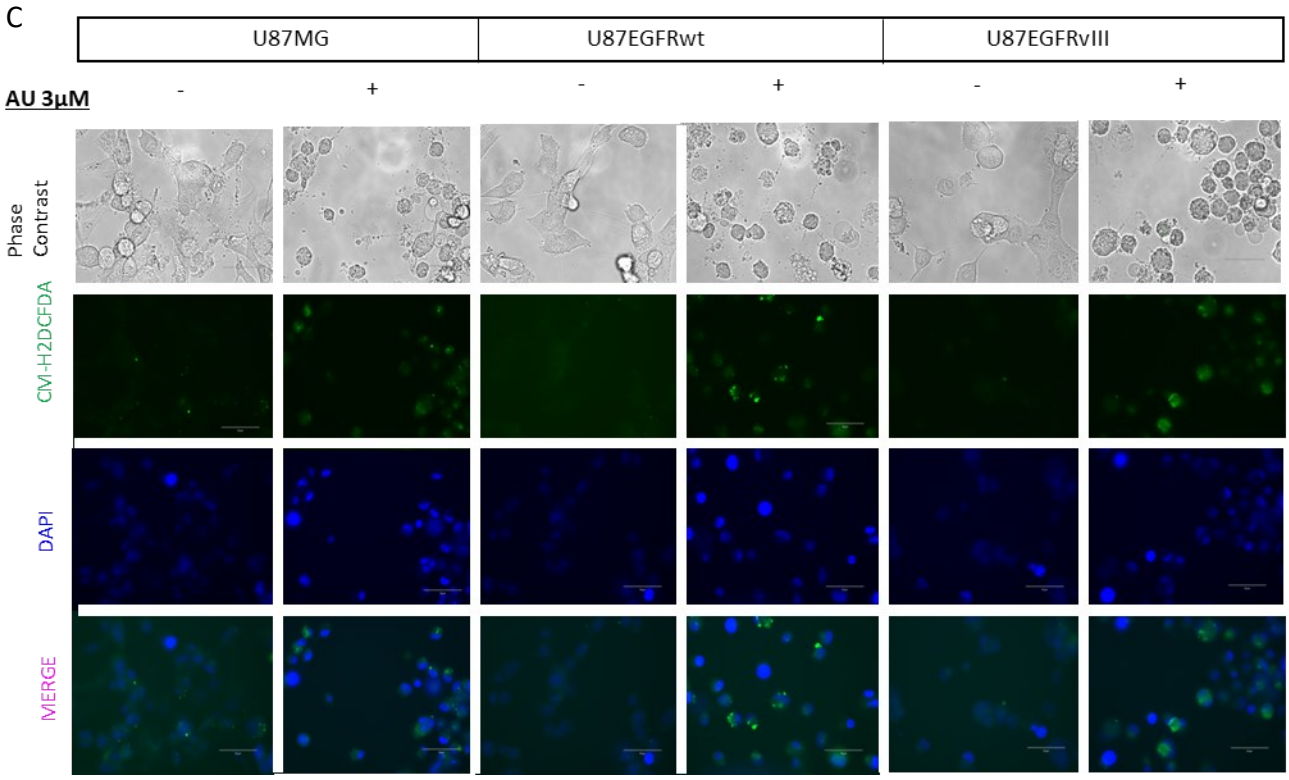
C
U87MG
U87EGFRwt
U87EGFRvIII
AU 3μM
Phase Contrast
CM-H2DCFDA
DAPI
MERGE

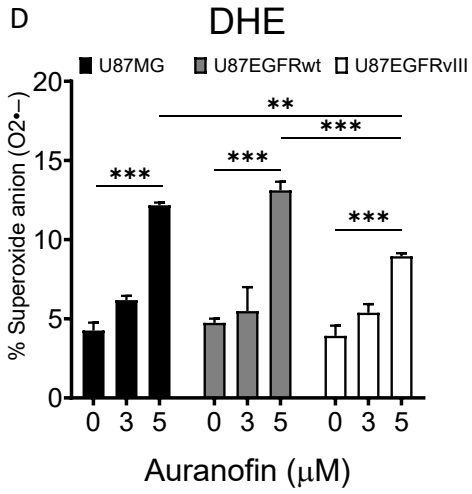
D
DHE
U87MG
U87EGFRwt
U87EGFRvIII
% Superoxide anion (O2•–)
Auranofin (μM)

Figure 3.6. Auranofin induced oxidative stress. (A) Relative fluorescence units (fold change) of ROS intracellular levels detected using a plate reader after GBM cells were treated with 3 and 6 μM AU for 2.5 h. (B) Relative fluorescence units (fold change) of ROS intracellular levels detected using a plate reader after GBM cells were treated with 3 μM auranofin for 24 h. (C) Microscopic images after treatment with 3 μM auranofin (AU) for 24 h. U87MG, U87/EGFRwt, and U87/EGFRvIII cells exhibited increased intracellular ROS levels following 30 min incubation with the general ROS indicator, CM-H2DCFDA, whereas nuclei were stained with DAPI. (D) U87MG, U87/EGFRwt, and U87/EGFRvIII cells treated with 3 or 5 μM AU for 24 h followed by staining with dihydroethidium (DHE) to detect superoxide radical anion that was quantified by flow cytometry. For all graphs bars show the mean ± SEM (** $p < 0.01$, *** $p < 0.001$, two-way ANOVA followed by Dunnett's multiple comparison test).

3.7. N-acetyl-cysteine (NAC) prevents intracellular ROS generation by auranofin in GBM EGFR isogenic cells

Next, we used N-acetylcysteine (NAC), a conventional ROS scavenger [324, 468], to determine whether ROS play a role in the cytotoxic effects of auranofin in U87/EGFR isogenic cell lines. We treated the cells with 1- or 2-mM NAC for 72 hours and observed that the drug did not significantly affect cellular metabolic activity, which we will refer to as vitality (**Figure 3.7A**). We also used a general ROS-sensitive probe, CM-H2DCFDA, to visualize the intracellular ROS levels following auranofin treatment at 3 μM for 24 hours. We found that the addition of 2 mM NAC prevented the increase in ROS levels induced by auranofin in all cell lines (**Figure 3.7B**).

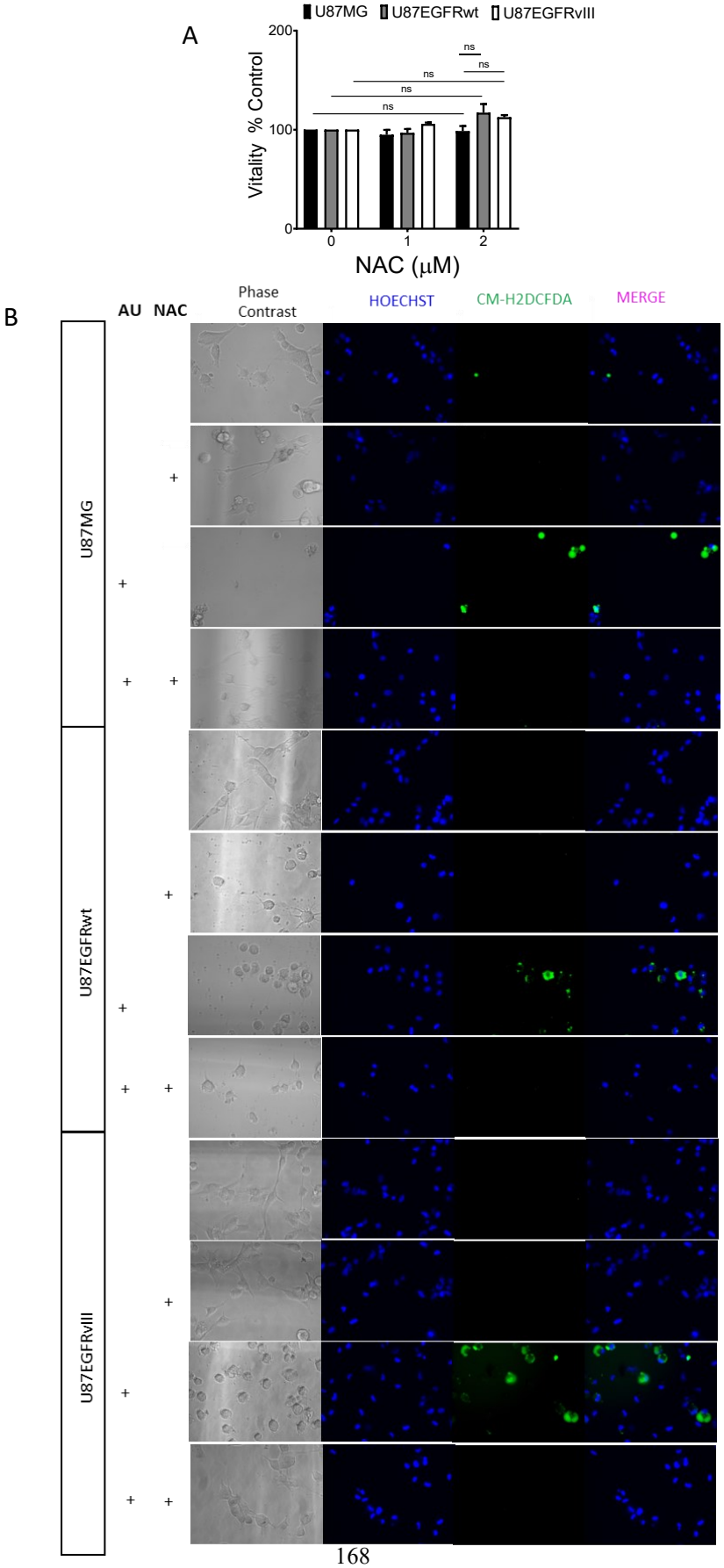
A
U87MG
U87EGFRwt
U87EGFRvIII
Vitality % Control
200
100
0
ns
ns
ns
ns
ns
0
1
2
NAC (μM)
B
AU
NAC
Phase Contrast
HOECHST
CM-H2DCFDA
MERGE
U87MG
U87EGFRwt
U87EGFRvIII

Figure 3.7. Effects of NAC in auranofin (AU)-induced ROS in GBM EGFR isogenic cells. (A) U87MG, U87/EGFRwt, and U87/EGFRvIII cellular vitality when cells were treated with 1- and 2-mM NAC for 72 h in an MTT assay; bars show the mean ± SEM ($p > 0.05$, two-way ANOVA and Dunnett's multiple comparison test). (B) Fluorescence microscopy images showing intracellular ROS generation using AU in U87MG, U87/EGFRwt, and U87/EGFRvIII treated with 3 μM AU for 24 h, with and without NAC. Cells were probed with the general ROS indicator, CM-H2DCFDA, whereas nuclei were stained with Hoechst 33342.

3.8. NAC protects GBM EGFR isogenic cell lines from acute auranofin-induced toxicity

The MTT assay, conducted using auranofin at 3 μM alone or in combination with 2 mM NAC for 72 hours, revealed that NAC significantly prevented the cytotoxic effects of auranofin on the metabolic activity of the three cell lines (**Figure 3.8A**). The results showed that NAC significantly decreased the cytotoxicity of auranofin by 34% in U87MG, 22% in U87/EGFRwt, and 50% in U87EGFRvIII (all $p < 0.001$); the protective effect of NAC was more evident in U87EGFRvIII cells than in U87MG and U87EGFRwt cells, with statistically significant differences ($p = 0.003$ and $p < 0.001$, respectively) (**Figure 3.8B**). Additionally, NAC rescued the auranofin-induced cell rounding observed by phase contrast microscopy (**Figure 3.8C**). The efficacy of NAC in blocking auranofin-induced lethality was validated in U87MG cells by flow cytometry (**Figure 3.8D**).

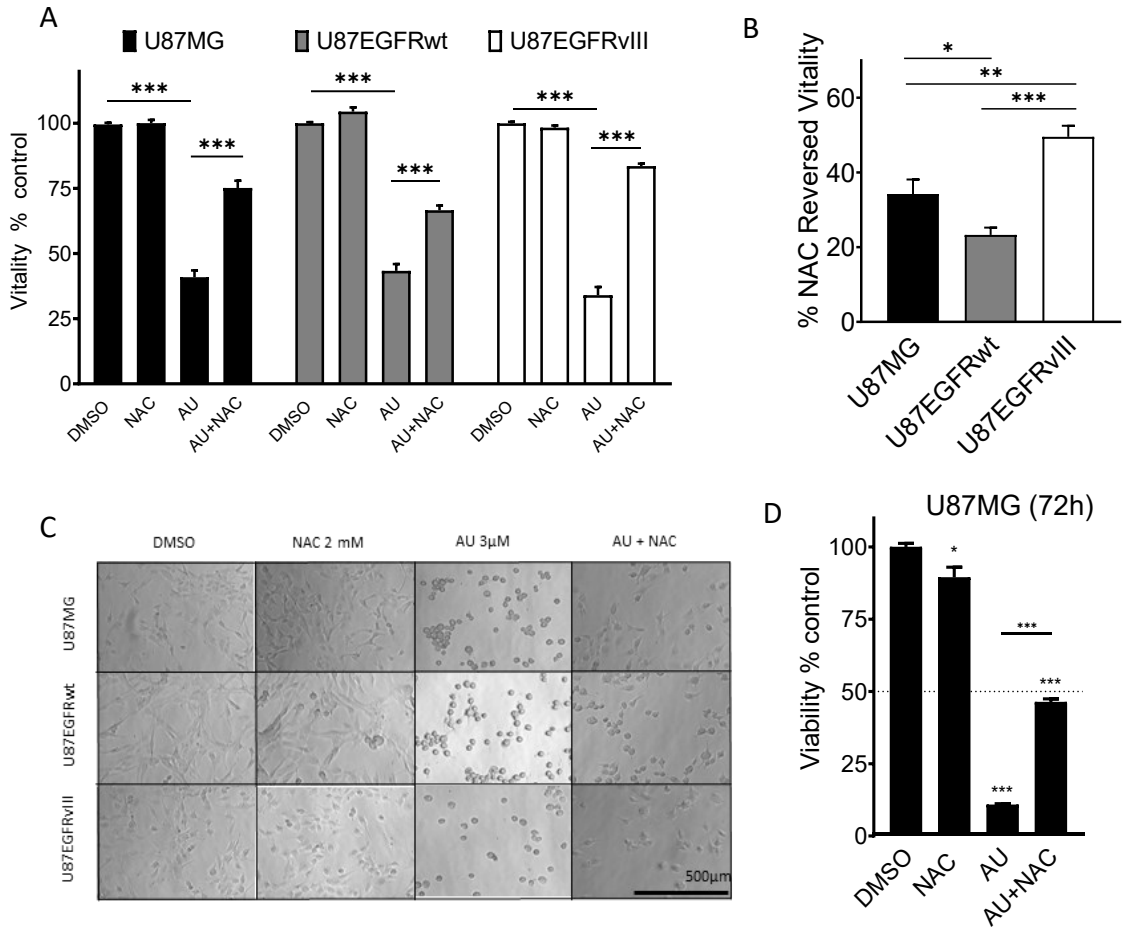

Figure 3.8. NAC prevents acute auranofin (AU)-induced toxicity. (A) MTT assay showing decreased in vitality caused by AU (3 µM for 72 h) alone or in combination with 2 mM NAC; bars show the mean ± SEM (***p < 0.001, two-way ANOVA, Tukey's multiple comparison test). (B) NAC protective effects on vitality relative to control in AU treated cells, bar graphs show the mean ± SEM (*p < 0.05 **p < 0.01 ***p < 0.001, one-way ANOVA, Tukey's post-test). (C) Morphology of GBM cells treated with AU (3 µM for 72 h) with or without NAC. DMSO was used as control. (D) Flow cytometry assay measuring viability in U87MG cells treated with AU (3 µM for 72 h) in the presence or absence of NAC. Bars show the mean ± SEM (*p < 0.05 ***p < 0.001, one-way ANOVA followed by Tukey's multiple comparison test).

3.9. NAC protects GBM EGFR isogenic cells from chronic auranofin-induced toxicity

The addition of 2 mM NAC to the colony formation assay significantly attenuated the cytotoxicity of 0.5 μM auranofin on the colony formation capacity of the three cell lines ($p<0.001$) compared to auranofin treatment alone (**Figure 3.9A and B**). Notably, NAC reversed the survival fractions to 0.48 in U87MG, 0.71 in U87EGFRwt, and 0.9 in U87EGFRvIII. This protective effect was more prominent in U87EGFRvIII cells than in U87MG cells ($p=0.018$); however, the difference between U87EGFRvIII and U87EGFRwt cells was not statistically significant ($p>0.05$) (**Figure 3.9C**).

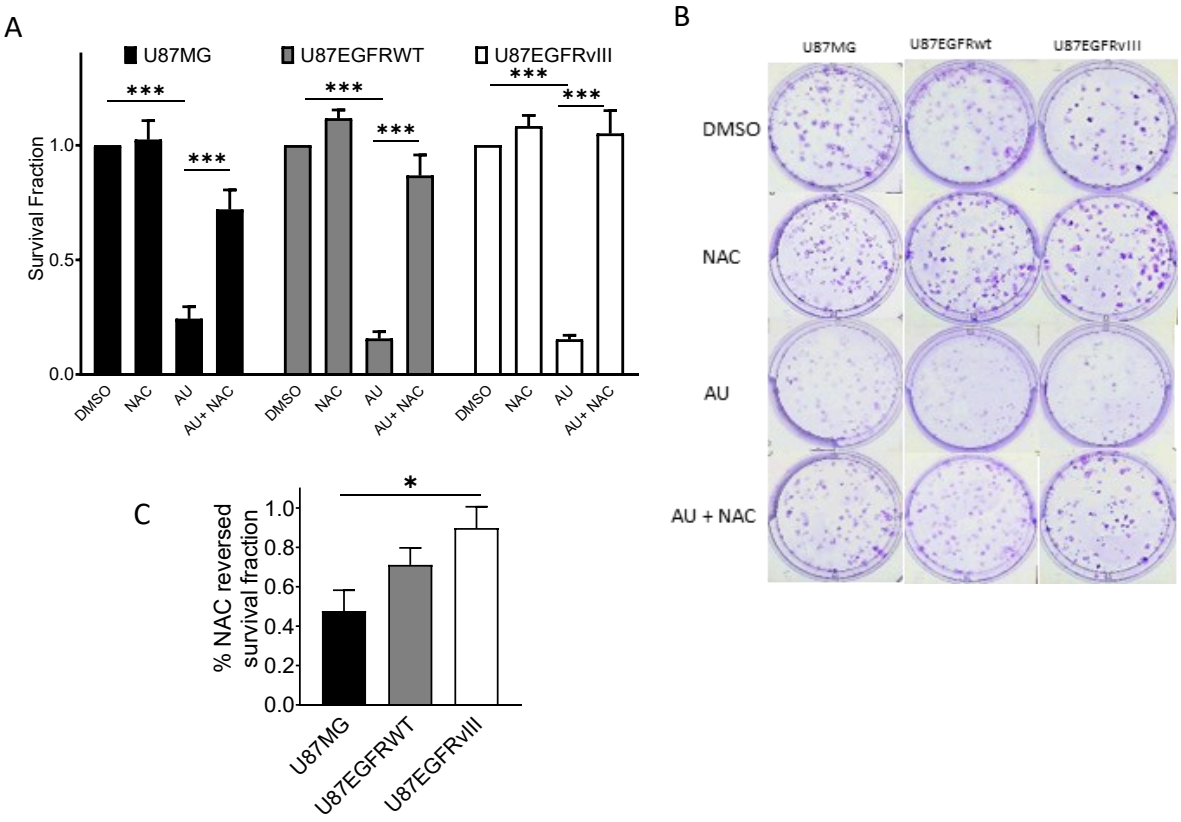

Figure 3.9. The toxicity of auranofin (AU) is mediated by ROS in GBM cells. (A) Survival fraction calculated from colony formation capacity in cells treated with AU or AU in combination with NAC; bars show the mean ± SEM (***$p < 0.001$, two-way ANOVA followed by the Tukey's multiple comparison test). (B) Colony formation assay plates representative of Figure 2a. (C) Protective effects provided by NAC on survival fraction when GMB cells were treated with 0.5 μM AU in the colony formation assay in Figure 2a; bars show the mean ± SEM (*$p < 0.05$ one-way ANOVA, followed by Tukey's multiple comparison test)

3.10. NAC prevents auranofin induced EGFR downregulation in U87EGFRvIII cells

Previous research has indicated that there is a relationship between ROS and EGFRwt or EGFRvIII and their downstream signaling pathways [256]. In this work, we examined the impact of EGFR overexpression in EGFRwt or EGFRvIII on auranofin-induced toxicity and the role of ROS in these effects using western blotting in U87/EGFR isogenic cell lines.

Auranofin treatment (IC_{50} 3 μM for 24 h) led to an increase in the level of phospho-EGFR (Tyr1068), a major autophosphorylation site of EGFR [469], in both U87/EGFRwt and U87/EGFRvIII cells compared to the DMSO-treated control. However, owing to the high basal phosphorylation level and subsequent oversaturation of the chemiluminescence signal in U87/EGFRvIII, we selected a low exposure time that produced a marked increase in p-EGFR (Tyr1068) in U87EGFRvIII cells compared to the U87/EGFRwt cells. Exposure to 2 mM NAC prevented p-EGFR(Tyr1068) upregulation in U87EGFRwt and U87EGFRvIII cells and prevented auranofin-induced downregulation of total EGFR in U87EGFRvIII cells (**Figure 3.10A**). Densitometric analysis confirmed the differential effects of auranofin in U87/EGFRvIII versus U87/EGFRwt cells. The ratio of p-EGFR (Tyr1068)/total EGFR increased by 4-fold in U87EGFRvIII cells compared to DMSO controls, and treatment with 2 mM NAC completely reversed the ratio to basal levels (**Figure 3.10B**).

Auranofin treatment induced cleavage of poly (ADP-ribose) polymerase (PARP-1), a hallmark of apoptosis only in U87EGFRvIII cells, which displayed the cleaved fragment (89kDa); however, this effect was prevented with 2 mM NAC. The anticancer activities of auranofin have been linked to its ability to inhibit deubiquitinases that are involved in the proteasome-mediated degradation of proteins [301, 315, 470, 471]. Anti-ubiquitin immunoblotting analysis revealed that

treatment with 3 μM auranofin led to an increase in polyubiquitinated proteins in the three GBM cell lines, an effect that was prevented by NAC (**Figure 3.10C**).

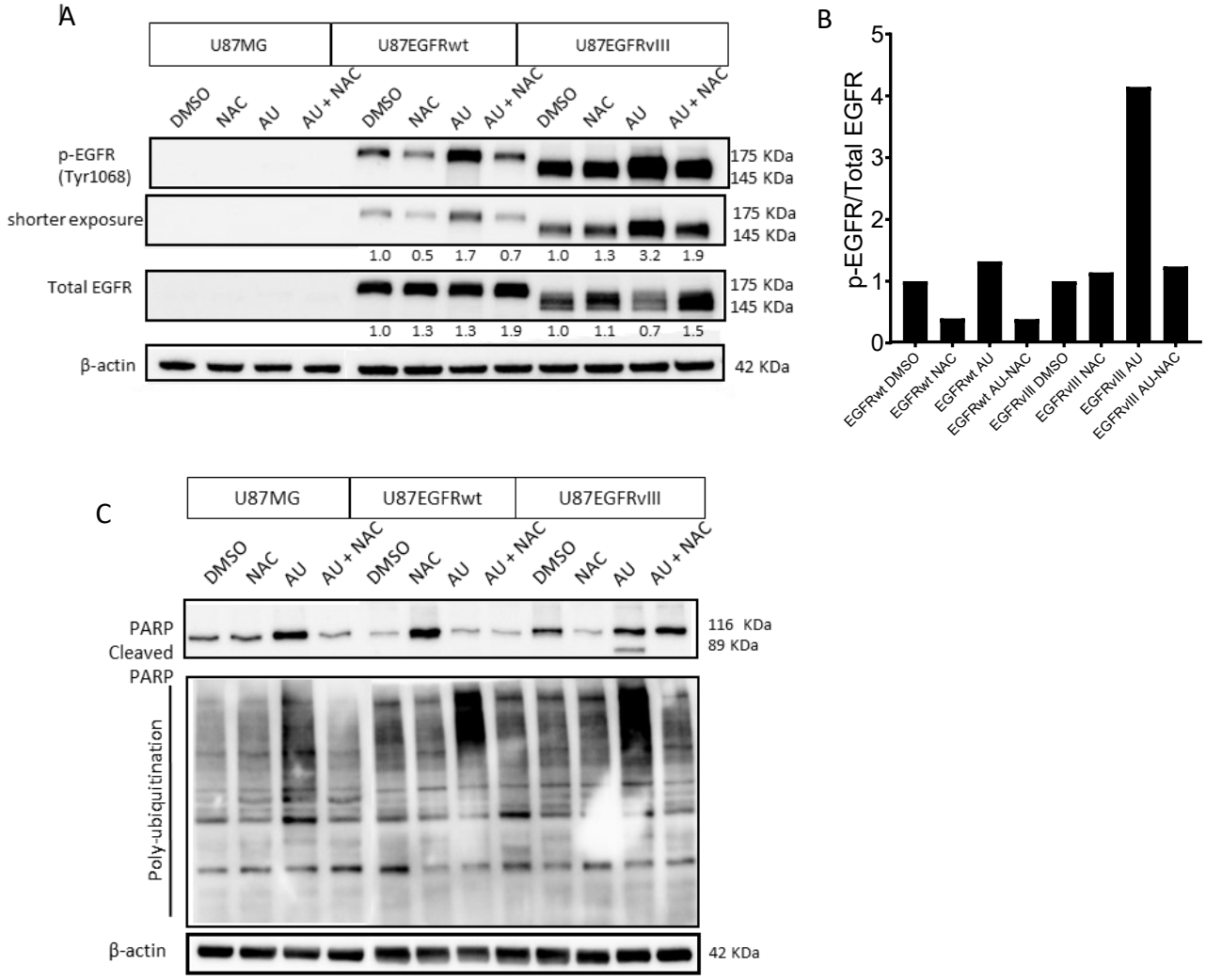

Figure 3.10. Effect of auranofin on ROS-associated signaling in GBM cells. (A) The effects of auranofin (IC_{50} 3 μM, 24 h) in the presence or absence of 2 mM NAC on phosphorylated (Tyr1068) EGFR and total EGFR in the three GBM cell lines. (B) Ratio of p-EGFR (Tyr1068)/total EGFR of immunoblot in A. (C) PARP cleavage and protein polyubiquitination in cells treated with 3 μM auranofin for 24 h in the presence or absence of 2 mM NAC.

3.11. Targeting gamma-glutamylcysteine synthetase overcomes auranofin-induced antioxidant response of U87EGFRwt cells

Although auranofin displays anticancer properties against various types of cancer cells, its therapeutic efficacy as a monotherapy is quite limited in clinical settings [472]. Previous studies reported GSH-induced compensation mechanisms in response to TrxR1 inhibition [235, 249, 267, 473-477]. Drug-induced redox resetting has recently been shown to result in drug resistance [301]. We analyzed the potential significance of co-targeting the TrxR1 and GSH antioxidant systems in GBM. Nuclear factor erythroid 2–related factor 2 (Nrf2), a master transcription factor, controls cellular Trx and GSH antioxidant response [478, 479]. Auranofin at 3 μM for 24 h increased Nrf2 expression in U87MG, U87EGFRwt, and U87EGFRvIII cell lines. This upregulation was blocked by 2 mM NAC (**Figure 3.11A**). Under similar conditions, TrxR1 expression remained unchanged.

Next, we measured intracellular basal GSH levels [480, 481]; U87/EGFRwt and U87EGFRvIII both had significantly lower basal levels compared to parental U87MG ($p<0.001$) and the level in U87/EGFRwt cells was less than in U87EGFRvIII ($p=0.004$). **Figure 3.11B**.

L-buthionine-sulfoximine (L-BSO) inhibits the enzyme gamma-glutamylcysteine synthetase (γ-GCL) [482], which is responsible for the synthesis of the main intracellular non-enzymatic antioxidant GSH, resulting in a decrease of GSH levels. To examine the role of L-BSO first, we demonstrated in an MTT assay that L-BSO at 2 or 10 μM for 72 h did not affect the vitality of U87MG, U87EGFRwt, and U87EGFRvIII cells (**Figure 3.11C**). We documented that auranofin at 2 μM for 24 h, significantly increased GSH levels in U87EGFRwt cells ($p=0.045$), compared to the DMSO control group, while U87MG and U87EGFRvIII cells were unaffected ($p>0.05$). Auranofin decreased GSH levels significantly in U87EGFRvIII compared to U87MG cells ($p=0.046$), while U87EGFRwt cells had higher GSH levels than in U87EGFRvIII cells

(p=0.002). L-BSO at 5 μM significantly decreased GSH levels (p<0.001) in the three cell lines, compared to their respective DMSO control group. While there was no significant difference (p=0.210) between U87MG and U87EGFRvIII cells, U87EGFRwt cells were significantly less sensitive to L-BSO treatment compared to U87MG (p=0.046) and U87EGFRvIII (p=0.002) cells. Auranofin and L-BSO combined treatment depleted significantly GSH levels compared to their corresponding control group (p<0.001) in the three cell lines as shown in **Figure 3.11D.**

To investigate the significance of γ-GCL expression in the context of EGFR alterations in GBM, we analyzed EGFR and γ-GCL mRNA expression in a cohort of 528 GBM patients from the TCGA GBM patient dataset. There was no correlation between EGFR and γ-GCL mRNA expression in GBM patient samples (n = 528). Interestingly, a subgroup of GBM patients based on EGFR status (altered or wildtype) did have a low positive correlation between EGFR wildtype and γ-GCL mRNA levels (n = 284). Conversely, there was a very weak negative correlation between altered-EGFR and γ-GCL mRNA expression, (n = 244), as shown in **Figure 3.11E.**

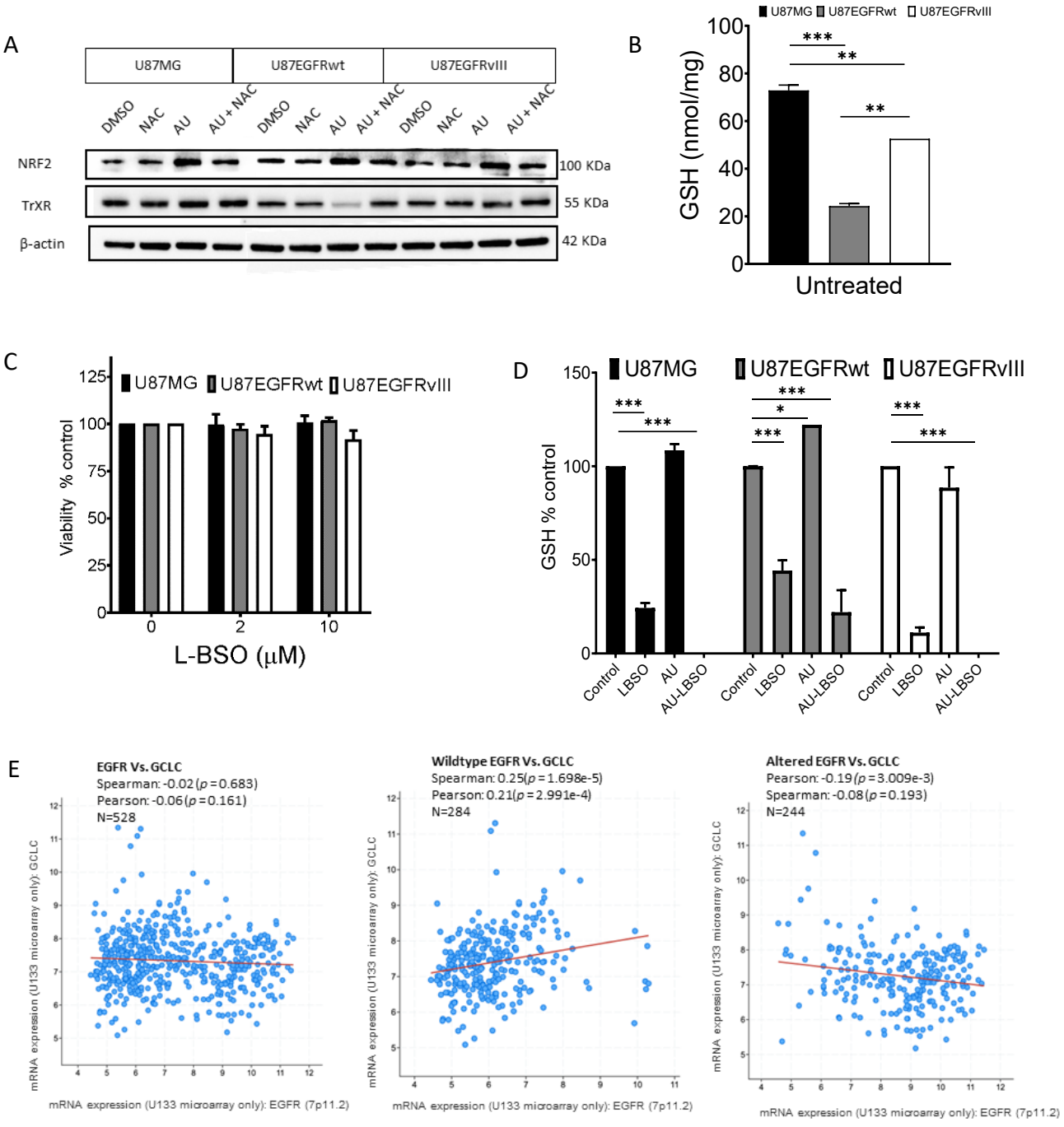
A
U87MG
U87EGFRwt
U87EGFRvIII
DMSO
NAC
AU
AU + NAC
NRF2
TrXR
β-actin
100 KDa
55 KDa
42 KDa
B
U87MG U87EGFRwt U87EGFRvIII
GSH (nmol/mg)
Untreated
C
U87MG U87EGFRwt U87EGFRvIII
Viability % control
L-BSO (μM)
D
U87MG U87EGFRwt U87EGFRvIII
GSH % control
Control
LBSO
AU
AU-LBSO
E
EGFR Vs. GCLC
Spearman: -0.02 (p = 0.683)
Pearson: -0.06 (p = 0.161)
N=528
Wildtype EGFR Vs. GCLC
Spearman: 0.25(p = 1.698e-5)
Pearson: 0.21(p = 2.991e-4)
N=284
Altered EGFR Vs. GCLC
Pearson: -0.19 (p = 3.009e-3)
Spearman: -0.08 (p = 0.193)
N=244
mRNA expression (U133 microarray only): GCLC
mRNA expression (U133 microarray only): EGFR (7p11.2)

Figure 3.11. Targeting compensatory adaptive mechanisms in auranofin-treated GBM cells. (A) GBM cells were treated with 3 μM AU with and without 2 mM NAC 24 h; Nrf2 antioxidant response expression levels were assessed by western blotting. DMSO was used as vehicle control. (B) MTT assay in in U87MG, U87/EGFRwt, and U87/EGFRvIII cells showing the effects on vitality of 2 and 10 μM of L-BSO treatment for 72 h. (C) Basal GSH levels in U87MG, U87EGFRwt, and U87EGFRvIII cells; bars show the mean ± SEM (**$p < 0.01$ ***$p < 0.001$, one-way ANOVA followed by Tukey's multiple comparison test). (D) GSH levels quantified in GBM cells treated with 2 μM AU alone or combined with 5 μM L-BSO for 24 h; bars show the mean ± SEM (*$p < 0.05$ ***$p < 0.001$, two-way ANOVA followed by Dunnett's multiple comparison test). (E) RNA expression correlation between EGFR status and γ-GCL (L-BSO target) using The Cancer Genome Atlas Network (TCGA) GBM patient dataset.

3.12. Co-targeting TrxR and gamma-glutamylcysteine synthetase in EGFR isogenic cell lines resulted in synergistic cytotoxicity

L-BSO inhibits γ-GCL, leading to an intracellular decrease in GSH levels and an increase in ROS, resulting in cytotoxic anticancer effects [482-484]. At a concentration of 5 μM for 72 hours, L-BSO did not significantly impact the vitality of U87MG, U87EGFRwt, and U87EGFRvIII cells. However, when combined with 1, 2, or 3 μM auranofin, L-BSO significantly decreased vitality in the three GBM cell lines compared with auranofin treatment alone ($p<0.001$) **Figure 3.12A.**

Figure 3.12B displays the ability of a non-toxic concentration of L-BSO (5 μM) to potentiate the toxicity of auranofin (1, 2, or 3 μM) leading to drastic morphological changes, such as increased cell rounding, detachment, and decreased cell density. Drug interaction analysis showed that the combination of 5 μM L-BSO with auranofin at 1, 2, or 3 μM was synergistic (combination index; CI<1) in all GBM cell lines. This is depicted in **Figure 3.12C**. Interestingly, the addition of 2 mM NAC to the combination of auranofin 3 μM and L-BSO 5 μM partially restored the vitality by 58% in U87MG, 54% in U87/EGFRwt, and 51% in U87EGFRvIII, as shown in **Figure 3.12D**.

A colony formation assay confirmed that auranofin at 0.25 μM combined with L-BSO at 1 μM significantly decreased the clonogenicity of the three GBM cell lines, compared to auranofin alone; this effect was more pronounced for U87/EGFVIII cells (**Figure 3.12E and F**).

A

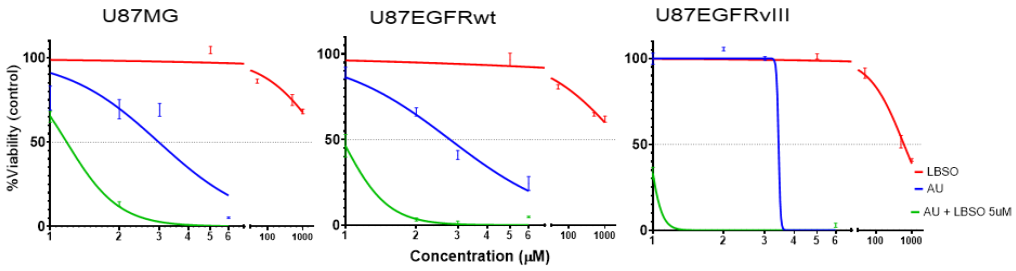
U87MG
U87EGFRwt
U87EGFRvIII
%Viability (control)
Concentration (μM)
LBSO
AU
AU + LBSO 5uM

B

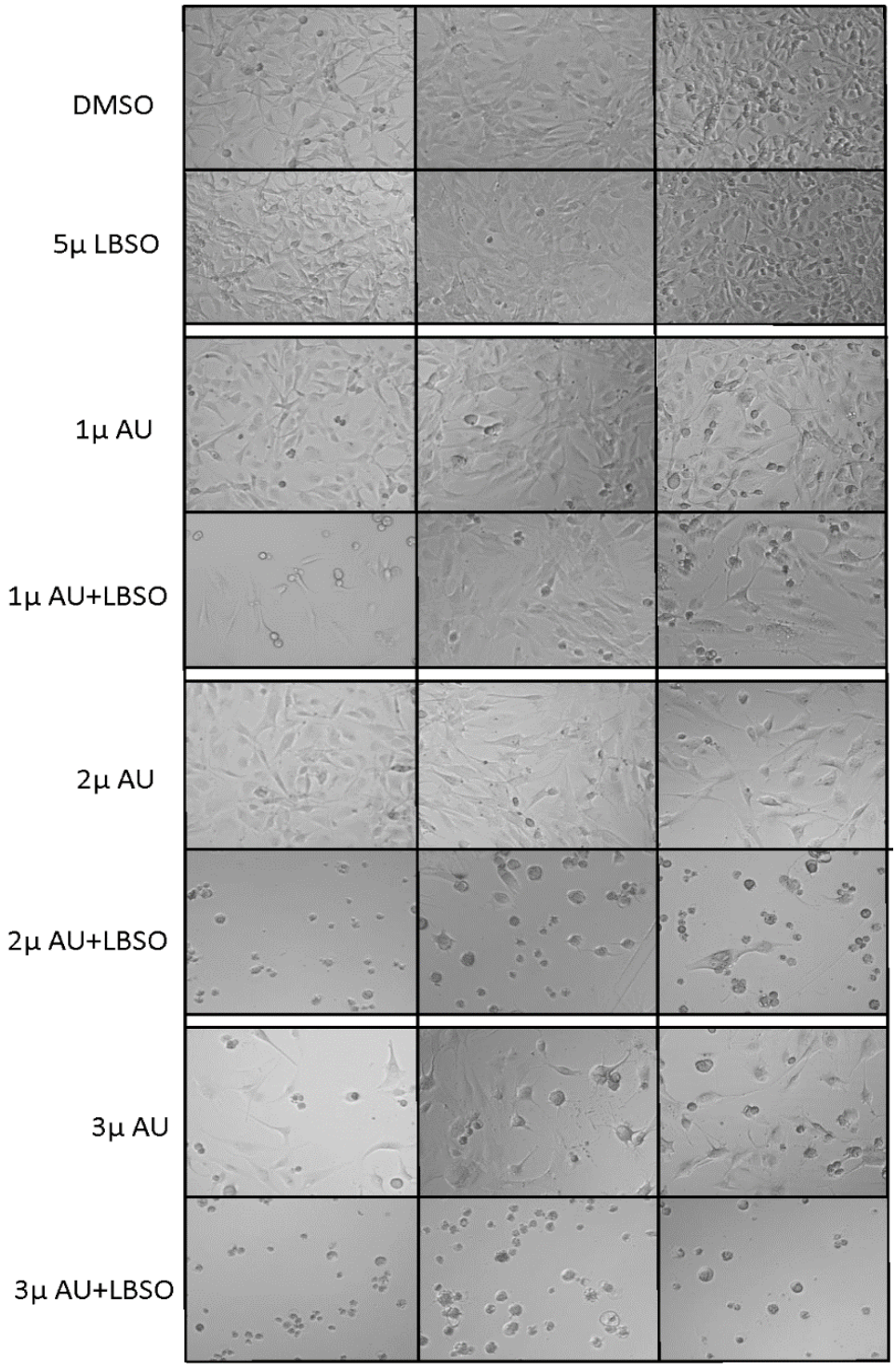
DMSO
5μ LBSO
1μ AU
1μ AU+LBSO
2μ AU
2μ AU+LBSO
3μ AU
3μ AU+LBSO

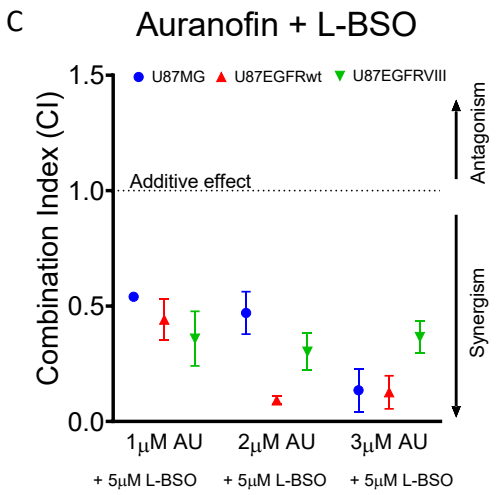
C
Auranofin + L-BSO
U87MG
U87EGFRwt
U87EGFRVIII
Combination Index (CI)
1.5
1.0
0.5
0.0
Additive effect
Antagonism
Synergism
1μM AU
2μM AU
3μM AU
+ 5μM L-BSO
+ 5μM L-BSO
+ 5μM L-BSO

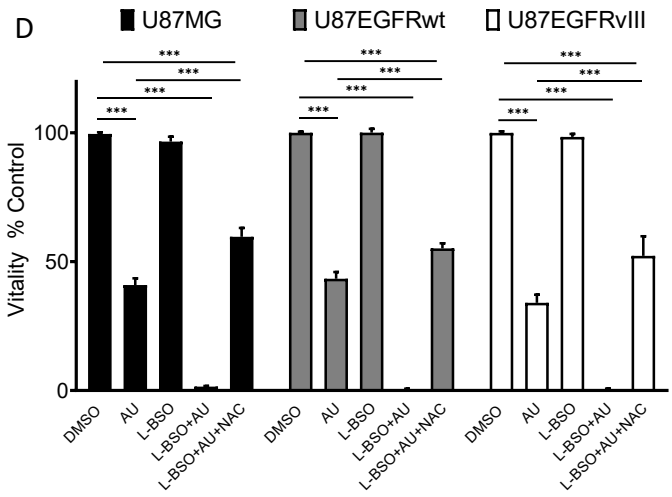
D
U87MG
U87EGFRwt
U87EGFRvIII
Vitality % Control
100
50
0
***
DMSO
AU
L-BSO
L-BSO+AU
L-BSO+AU+NAC

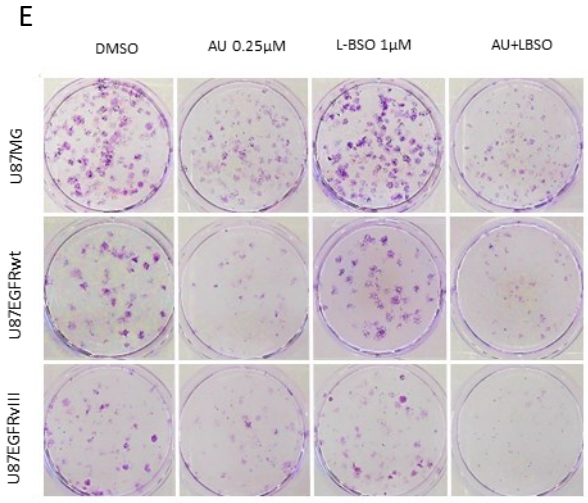
E
DMSO
AU 0.25μM
L-BSO 1μM
AU+LBSO
U87MG
U87EGFRwt
U87EGFRvIII

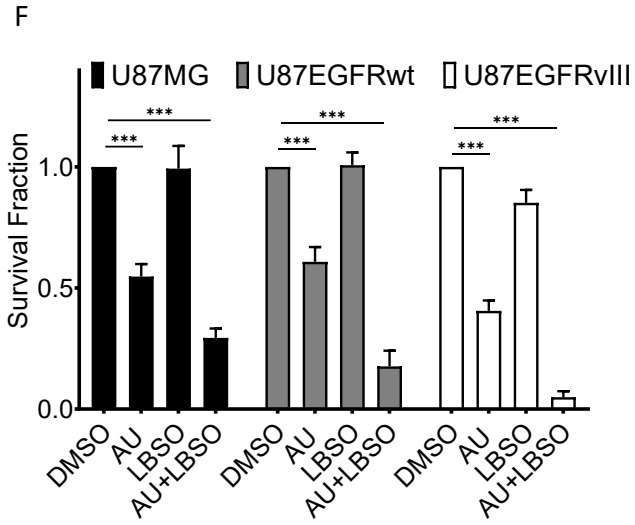
F
U87MG
U87EGFRwt
U87EGFRvIII
Survival Fraction
1.0
0.5
0.0
***
DMSO
AU
LBSO
AU+LBSO

Figure 3.12 The effect of auranofin in combination with L-BSO on EGFR isogenic cell lines. (A) U87MG, U87/EGFRwt, and U87/EGFRvIII cells were incubated with various concentrations of auranofin (1-3 μM) in combination with 5 μM L-BSO and assessed for vitality using the MTT assay. (B) Changes in cell morphology at drug combinations in the three cell lines documented in panel A. (C) Combination index [CI] of auranofin and L-BSO analysed by the Chou & Talalay method for drug combination analysis. Synergism was determined when CI was <1, antagonism when CI was >1, and additive effect when CI was =1. The values are shown for each drug concentration. (D) Effect of 2 mM NAC in mitigating the toxicity of 5 μM L-BSO and 3 μM auranofin in combination for 72 h in the three cell lines, as determined by the MTT assay. (E) Representative colony formation in the three cell lines exposed to 0.25 μM auranofin, 1 μM L-BSO or their combination. (F) The survival fraction of GBM cells treated with auranofin ± L-BSO in the colony formation assay. For all graphs, bars show the mean ± SEM (*** $p < 0.001$, two-way ANOVA Tukey's multiple comparison test).

3.13. The combination of auranofin and L-BSO increased oxidative stress

We assessed the effect of auranofin and/or L-BSO on intracellular levels of ROS. U87MG, U87/EGFRwt, and U87/EGFRvIII cells were treated with auranofin at 3 μM, 5 μM L-BSO, or in combination of both drugs for 24 h. The combination produced significantly higher levels of intracellular ROS in comparison to the DMSO control in the three cell lines (U87MG, $p<0.001$, U87/EGFRwt $p<0.01$; U87/EGFRvIII, $p<0.001$), and significantly higher levels than auranofin alone in U87MG ($p<0.001$) and U87/EGFRvIII ($p<0.001$) cells, but not in U87/EGFRwt. Of note, the auranofin/L-BSO combined treatment induced the highest ROS increase in U87/EGFRvIII (15.7-fold) compared to U87MG (5.6-fold) or U87/EGFRwt (2.5-fold) as shown in **Figure 3.13A**. The duration of exposure was an important factor, since treatment for 2 h produced smaller changes, and a significantly greater level of intracellular ROS in comparison to DMSO controls only occurred in U87EGFRwt cells exposed to auranofin (1.6-fold), auranofin/L-BSO (1.7-fold) (both $p<0.001$), and L-BSO (1.4-fold) ($p<0.05$), as shown in **Figure 3.13B**.

We also evaluated the effect of the auranofin/L-BSO combined treatment on superoxide anion generation in the three cell lines. Auranofin at 3 μM combined with L-BSO at 5 μM for 24 h significantly increased superoxide generation compared to the DMSO controls (in U87MG $p<0.001$, U87EGFRwt, $p<0.01$, U87EGFRvIII, $p<0.001$), or L-BSO alone (all GBM cells $p<0.001$). Auranofin/L-BSO induced higher superoxide levels in U87MG cells than in U87EGFRwt ($p<0.001$) and U87/EGFRvIII ($p<0.01$) cells (**Figure 3.13C**). At a shorter exposure time of 12 h, the auranofin/L-BSO combination produced consistent effects, generating greater superoxide levels in each cell line compared to their DMSO control group (U87MG $p<0.01$ and U87/EGFRwt, $p<0.05$, U87/EGFRvIII, $p<0.001$). At this time point, superoxide levels were

significantly higher in U87/EGFRvIII cells than in U87MG ($p<0.01$) and U87/EGFRwt ($p<0.05$) cells (**Figure 3.13 D**).

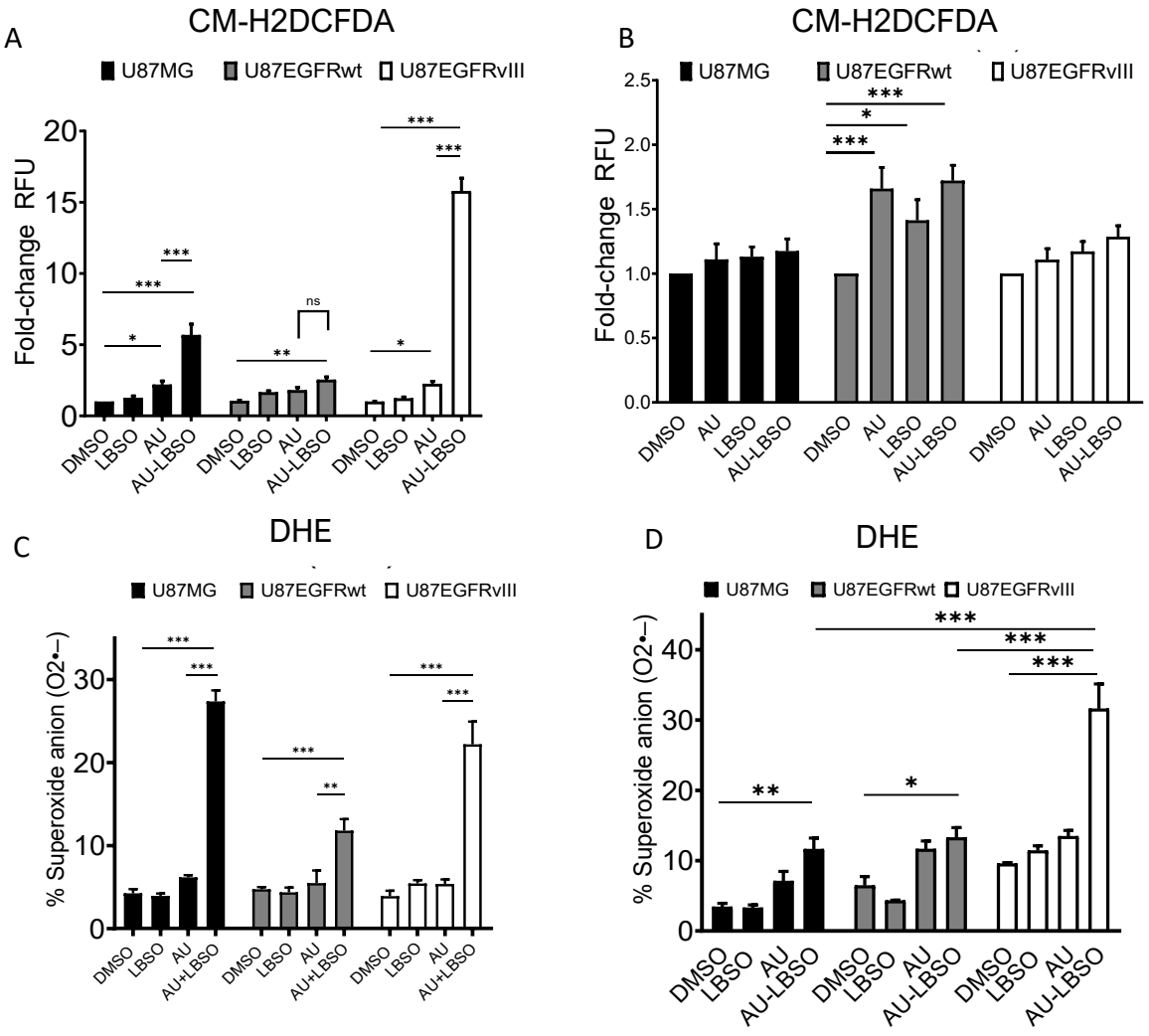

Figure 3.13. Effect of the auranofin (AU)/L-BSO combination on ROS levels in U87MG, U87/EGFRwt, and U87/EGFRvIII GBM cells. (A) Cells were treated with 3 µM AU and 5 µM L-BSO for 24 h and ROS levels were quantified using general ROS indicator, CM-H2DCFDA, (B) Relative Fluorescence Units (Fold Change) of intracellular ROS levels after 2 h exposure to 3 µM AU/5 µM L-BSO combination or single drugs using CM-H2DCFDA measured in a plate reader. (C) Dihydroethidium (DHE) was used to detect superoxide radical anion using a plate reader or

cytometer. (D) Superoxide generation after 12 h exposure to 3 μM AU/5 μM L-BSO combination and single drugs using dihydroethidium (DHE) and quantified by flow cytometry. Bars indicate the mean ± SEM (*$p < 0.05$ **$p < 0.01$ ***$p < 0.001$, two-way ANOVA followed by the Tukey's multiple comparison test)

3.14. Auranofin/L-BSO in combination led to downregulation of total EGFR and AKT in U87EGFRvIII cells compared to U87EGFRwt cells

Next, we used western blotting to analyze the molecular effects of auranofin/L-BSO combined treatment in U87/EGFR isogenic cell lines treated with 3 μM auranofin alone, 5 μM L-BSO alone or their combination for 6 h. There was no effect on p-EGFR (Tyr1068) or total EGFR expression in the U87/EGFRwt cell line. In sharp contrast, auranofin increased the phosphorylation of p-EGFR (Tyr1068), which was further increased following treatment with the auranofin/L-BSO combination in U87EGFRvIII. Remarkably, these effects were associated with decreased total EGFR expression.

The Ras/PI3K/AKT pathway is one of the major pathways that regulate cell proliferation, survival, and differentiation downstream of EGFR signaling [485, 486]. Auranofin led to a decrease in the phosphorylation of p-AKT (Ser473) in all three cell lines. Decreased p-AKT (Ser473) accompanied by decreased total AKT was more pronounced following treatment with the auranofin/L-BSO combination in U87/EGFRwt cells and to a greater extent in the U87EGFRvIII cell line (**Figure 3.14A**).

Cells treated with a sub-lethal dose of auranofin at 2 μM and auranofin plus 5 μM L-BSO in combination for 24 h, exhibited high phosphorylation levels of the DNA damage marker γH2AX (Ser139) in U87/EGFRwt and U87EGFRvIII cells, but not in the U7MG cell line, while 2 mM NAC treatment inhibited the effect in U87/EGFRwt and U87EGFRvIII. There was no effect of either drug alone in any of the 3 cell lines (**Figure 3.14B and C**).

A

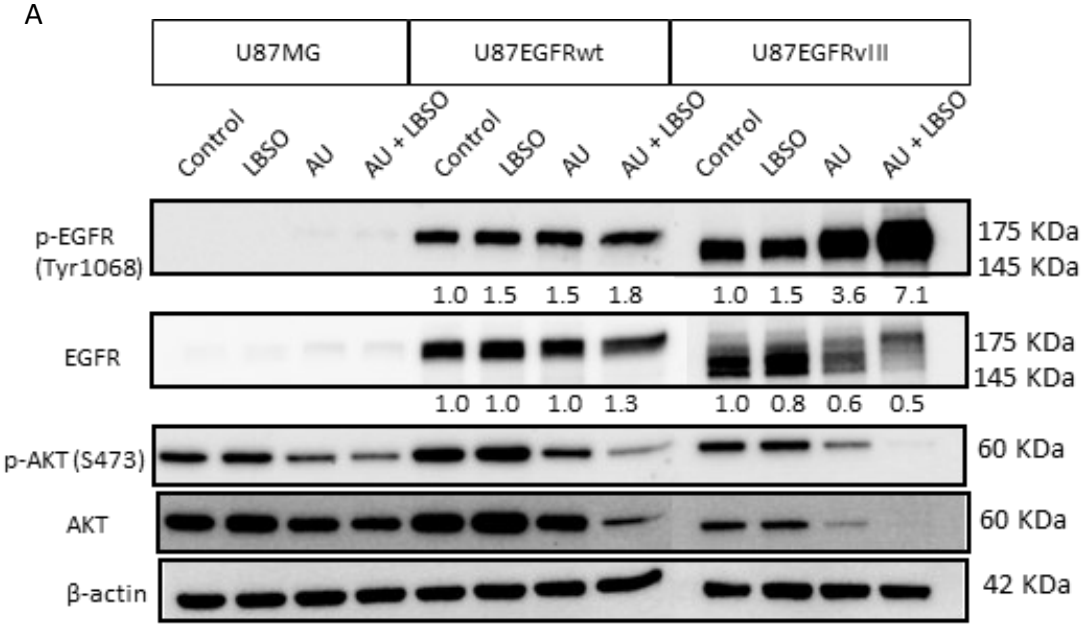
U87MG
U87EGFRwt
U87EGFRvIII
Control
LBSO
AU
AU + LBSO
p-EGFR (Tyr1068)
175 KDa
145 KDa
1.0 1.5 1.5 1.8 1.0 1.5 3.6 7.1
EGFR
175 KDa
145 KDa
1.0 1.0 1.0 1.3 1.0 0.8 0.6 0.5
p-AKT (S473)
60 KDa
AKT
60 KDa
β-actin
42 KDa

B

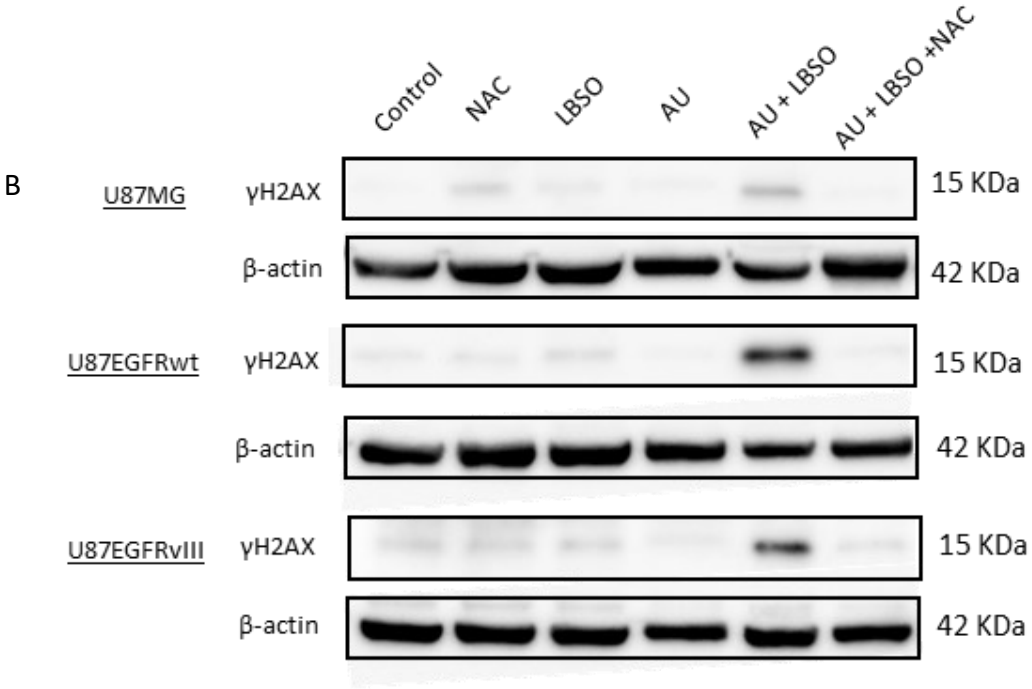
Control
NAC
LBSO
AU
AU + LBSO
AU + LBSO +NAC
U87MG
γH2AX
15 KDa
β-actin
42 KDa
U87EGFRwt
γH2AX
15 KDa
β-actin
42 KDa
U87EGFRvIII
γH2AX
15 KDa
β-actin
42 KDa

Figure 3.14. Effects of auranofin (AU) and L-BSO alone and in combination on GBM EGFR isogenic cell lines. (A) U87MG, U87/EGFRwt, and U87/EGFRvIII cells were treated with 3 μM AU, either alone or in combination with 5 μM L-BSO for 6 hours, and the expression levels of EGFR, AKT, and their respective phosphorylation were assessed by western blotting. (B) GBM cells were treated with 2 μM AU, either alone or in combination with 5 μM L-BSO for 24 hours, and the DNA damage marker γH2AX was analyzed.

Chapter 4 – GENERAL DISCUSSION

Glioblastoma IDH-wildtype CNS WHO grade 4 (GBM; previously known as Glioblastoma multiforme) is the most aggressive and the most common primary tumor of the central nervous system in adults (with a median age at diagnosis of 65 years). GBM is characterized by rapid progression and a dismal prognosis, with a median survival of less than 15-18 months from the initial diagnosis. Given the substantial prevalence of EGFR alterations in GBM, found in roughly 50% of patients, and the prominent role of the EGFRvIII mutated version, which is associated with high proliferation and genomic instability, it is essential to identify therapeutic options for this patient population. The development of more effective treatment is of paramount importance and cannot be overstated. In this study, we investigated potential strategies for future therapy by including the targeting of EGFR and antioxidant pathways, using both experimental and repurposed drugs in the GBM cell lines U87MG and isogenic counterparts stably transfected to overexpress EGFR: U87/EGFRwt and EGFRvIII.

The initial set of experiments involving the combi-molecule ZR2002 corroborated the findings of Shariff [157] that this drug has potent short-term cytotoxic effects against EGFR-positive GBM cells, at concentrations in the sub-micromolar range for 72 or 120 h in all cell lines, although U87EGFRwt displayed a slight but significantly lower sensitivity to ZR2002 compared to U87MG and U87EGFRvIII. These results were consistent with independent experiments conducted at the 72-h time point, which suggested a differential sensitivity based on EGFR expression. Our study also found that ZR2002 was able to elevate ROS only at very high concentrations, and the antioxidant NAC did not protect the U87MG, U87EGFRwt, and U87EGFRvIII cells against ZR2002 toxicity. These results suggest that ROS generation is not the primary mechanism of action of the drug.

Although we observed that ZR2002 plus auranofin decreased clonogenicity in U87EGFRwt cells to a greater extent than either drug alone, most of our results indicated that the actions of ZR2002 and auranofin were largely antagonistic. For instance, various ratios of the IC_{50} of each drug when applied together only produced synergistic effects in U87EGFRwt and not in the other cell lines. However, when a fixed 1 micromolar concentration of auranofin was combined with different concentrations of ZR2002, we observed dose-related effects, with slight synergy in U87MG and U87EGFRvIII at low concentrations and pronounced antagonism in all cell lines as the concentration increased. Similar results were obtained with other fixed or ratio combinations. These findings suggest that an interaction between the two drugs hinders their actions when both are present, resulting in antagonism.

Considering these findings, we pursued a sequential treatment strategy, beginning with auranofin and followed by ZR2002. This approach aimed to sensitize cells by first inhibiting TrxR activity and inducing ROS. However, this strategy ultimately proved unsuccessful in demonstrating synergistic effects. One explanation for this outcome may involve the presence of compensatory mechanisms, whereby the inhibition of TrxR by auranofin leads to negative regulation of Nrf2. Consequently, upregulation of Nrf2 could enhance antioxidant capacity and downstream signaling of growth factor receptors. Notably, when the treatment order was reversed, with ZR2002 administered first and auranofin second, we observed toxic effects in U87MG, U87EGFRwt, and U87EGFRvIII cells after 24 hours, but a comprehensive analysis of the combination index was not conducted. Based on our observations, ZR2002 proved to be a highly potent drug, but its combination with auranofin as cotreatment failed to produce synergistic effects.

Gefitinib produced equal levels of short-term toxicity in all three cell lines, and 30 μM significantly elevated intracellular ROS levels in all cell types, being most effective in

U87EGFRwt. The combination of auranofin with gefitinib produced synergistic effects when using the ratios of their corresponding IC_{50} in the three cell lines. Additionally, when using fixed drug concentrations, consistent results were obtained. It is noteworthy that in the EGFR-expressing cells additive or antagonistic effects were seen at low concentrations of each drug, but combinations equal to or less than IC_{50} were still synergistic in the three types of GBM cells. This finding is important as both drugs are FDA-approved, and it could be easier to assess their potential efficacy in clinical trials. A limitation in therapy for GBM is the blood-brain barrier (BBB) that prevents access to most chemotherapeutic drugs, but studies have shown that although gefitinib poorly crosses the BBB (about 1-1.3%), radiotherapy [487], which is part of standard care for GBM, can significantly increase the penetration of the drug [488] and may allow a lower concentration of gefitinib to achieve a significant therapeutic response.

Prima-1^{Met} exhibits various mechanisms of action, one of which is to rescue mutp53 in cancer cells. However, other mechanisms contributing to its toxicity, such as the increase in ROS due to targeting TrxR and the induction of endoplasmic reticulum (ER) stress, have also been described [384, 489]. The short-term toxicity of PRIMA-1^{Met} was assessed in EGFR isogenic cells, and the results demonstrated similar sensitivity in all three cell lines. Building on this observation and in collaboration with the lab of Dr. Bertrand Jean-Claude (Division of Experimental Medicine, McGill University), new anticancer molecules were created. JS440 was synthesized using components of Prima-1^{Met} and gefitinib. The short-term toxicity of JS440 was compared to that of gefitinib combined with Prima-1^{Met} in equimolar concentrations in glioma cells with wildtype and mutant p53 status (U87MG and T98G, respectively). While the IC_{50} of JS440 was like that of the combined single drugs in U87MG (wildtype p53), it was not the case for T98G (mutant p53). The IC_{50} values of the single drugs combined in equimolar concentrations were lower than that of

JS440. One possible explanation may be that the structural changes required to covalently bind both drugs into one might sacrifice the active relevant site of each drug, thereby losing some of their cytotoxic activity.

Notably, the IC_{50} values for auranofin in U87MG and T98G cells were remarkably low (1.2 and 3.1 micromolar, respectively), compared to the other drugs tested, except for ZR2002. We then proceeded to evaluate auranofin's effectiveness in a model of platinum-sensitive and platinum-resistant high-grade serous ovarian cancer (HGSOC) cells - PEO1 and PEO4, respectively. The short-term toxicity of auranofin was assessed in an MTT assay, revealing IC_{50} values in the submicromolar range for both cell lines. These findings were further validated by flow cytometry in PEO1 cells, which had an IC_{50} value for auranofin of 1.23 micromolar, consistent with the potency of targeting TrxR and providing additional support for the continued use of auranofin in GBM cells expressing EGFR.

The compound JS470 comprises both PRIMA-1^{MET} and olaparib (a PARP inhibitor), and we sought to determine whether its cytotoxicity surpassed that of the individual drugs when administered in equal concentrations to HGSOC PEO1 and PEO4 cells. Our findings indicated that JS470 was not more toxic than the single drugs used in combination, which may be attributed to significant structural changes that occur when the drug molecules are covalently bound, potentially impeding their anticancer effects.

The second part of this work elucidated the complex relationship between auranofin and GBM cells exhibiting aberrant epidermal growth factor receptor (EGFR) expression, including EGFR wild-type (EGFRwt) and EGFR variant III (EGFRvIII), suggesting the potential value of auranofin as a therapeutic agent in EGFR-driven GBM. Furthermore, this study emphasized the synergistic lethality between auranofin and L-BSO in the eradication of GBM cells. It is proposed

that co-targeting antioxidant systems in EGFR-overexpressing GBM cells would result in a lethal level of oxidative stress. The combination of auranofin and L-BSO led to enhanced cytotoxicity, likely due to the depletion of intracellular GSH levels and subsequent increase in ROS. This drug combination represents a promising strategy for enhancing the efficacy of auranofin-based treatments.

Auranofin is an FDA-approved drug, known for its clinical safety, and ability to successfully penetrate the BBB at doses ranging from 0.2 to 5 μmol/L [490]. Recent studies have highlighted the promising anticancer effects of auranofin in various cancer types [289, 295-322] alone or as part of a drug combination [323-325]. In glioblastoma, auranofin has also been used as monotherapy or in drug combination [274] but studies to date have not provided information on the effects of auranofin in the context of EGFR overexpression. EGFR alterations are present in around 50% of GBMs cases [70] and, previous investigations have associated EGFR hyperactivation with increased oxidative stress [262], which could provide a vulnerability to target antioxidant systems.

Our research investigated the underlying mechanisms of auranofin-induced cytotoxicity, yielding several important discoveries. Our findings indicated that auranofin caused DNA damage and elevated levels of Annexin V, suggesting that it triggers apoptosis in U87MG GBM cells. These findings are consistent with previous results in other cancer cell lines [301, 305, 466, 467, 491]. Auranofin's primary target, thioredoxin reductase 1 (TrxR1), was significantly inhibited in both parental and EGFR-transfected cells. It is worth noting that the inhibition of TrxR alone may not be sufficient to kill GMB cells, as evidenced by the fact that auranofin did not lead to cell death when used at the low concentrations that inhibit TrxR. These results are consistent with those of Van Loenhout et al. [323] and Abdalbari et al. [462], who tested auranofin in U87MG, and in

ovarian cancer cells, respectively, and detected TrxR inhibition with subtoxic concentrations, suggesting other mechanisms might be involved in its induced toxicity.

Our study also determined the concentrations of auranofin required for 50% inhibition of metabolic activity (IC_{50s}) in the EGFR-transfected cells, revealing that all three cell lines had similar IC_{50} values, suggesting that the presence of EGFRwt or EGFRvIII did not substantially alter the sensitivity to auranofin. However, using flow cytometry and assessing total number and viability of cells, and monitoring their morphological changes, we showed that U87EGFRwt was slightly less sensitive to auranofin. These discrepancies have been previously reported by Jakstys, B. et al. [492] and they concluded that colony formation assay was the most reliable indicator of cellular health, pointing out the limitations of the methods used when assessing drug toxicity in cell cultures.

Long-term cytotoxic effects of auranofin were assessed through clonogenic assays, and it was found that auranofin inhibited colony formation at concentrations lower than the IC_{50}, underscoring its potential to inhibit the clonogenic capacity of GBM cells. Notably, U87EGFRvIII cells were statistically significant less sensitive to auranofin toxicity in comparison to U87EGFRwt cells, suggesting that EGFRvIII expression may modulate auranofin-induced cytotoxicity. However, this difference was not observed in the extended long-term toxicity assay, indicating that EGFRwt and EGFRvIII do not substantially differ their long-term response to auranofin.

Compounds that inhibit TrxR enzymatic activity result in increased oxidative stress [493, 494]. Oxidative stress plays a central role in auranofin-induced cytotoxicity, as evidenced by increased ROS levels in GBM cells upon auranofin treatment [324]. In our study, we employed N-acetyl cysteine (NAC) to mitigate oxidative stress. NAC is widely recognized for its ability to reduce ROS by providing cysteines necessary for GSH synthesis, an antioxidant that effectively

scavenges ROS molecules [468]. The addition of NAC, as ROS scavenger, effectively protected GBM cells from auranofin-induced oxidative stress significantly improving cell viability. This effect was particularly pronounced in U87EGFRvIII cells, further highlighting the role of EGFR variants in modulating auranofin-induced oxidative stress.

Our study also examined the impact of auranofin on EGFR signaling pathways. Our findings indicated that auranofin treatment led to degradation of EGFR and AKT, which are critical signaling molecules in cell proliferation and survival [485, 486]. Importantly, the addition of NAC prevented these effects, underscoring the role of ROS in mediating the EGFR and AKT degradation induced by auranofin. EGFRvIII-expressing cells showed greater vulnerability to EGFR degradation. Interestingly, auranofin increased the phosphorylation of EGFR at Tyr1068, an effect in which phosphorylation is dependent on ROS modulation. This increase in EGFR phosphorylation has been explained by studies showing that ROS transiently inactivates protein tyrosine phosphatases (PTPs) to enhance or prolong EGFR activation [495-497]. H_2O_2 inactivates protein-tyrosine phosphatase 1B (PTP1B) by oxidizing its catalytic site cysteine, most likely to sulfenic acid [495]. Dagnell et al. discovered that TrxR1/NADPH directly protects PTP1B from inactivation when present during the H_2O_2 exposure. This protection was dependent on the concentration of TrxR1 and independent of Trx1 and Prx2. The protection was blocked by auranofin and required an intact selenocysteine residue in TrxR1 [498].

Casitas B-lineage lymphoma (Cbl or c-Cbl) is a RING ubiquitin ligase that negatively regulates protein tyrosine kinase (PTK) signalling [499, 500]. It has been demonstrated that ROS including H_2O_2 activates and aberrantly phosphorylates the EGFR, leading to the loss of c-Cbl-mediated ubiquitination of the receptor [501-503]. As a result, the receptor is not targeted for clathrin-mediated internalization and degradation, thus prolonging receptor signaling. In our study

despite high p-EGFR (Tyr1068)-induced expression, auranofin alone and in combination with L-BSO, led to very high downregulation of EGFRvIII and AKT and resulted in higher cell death.

Nrf2 upregulation after auranofin exposure indicated activation of the cellular antioxidant response, an effect that was reversed by NAC. Additionally, auranofin-induced protein polyubiquitination was mitigated by NAC treatment, suggesting that auranofin-induced poly-ubiquitination is related to auranofin-mediated ROS increase. Some studies have shown that auranofin inhibits proteasome-associated deubiquitinases to induce the accumulation of polyubiquitinated proteins [333, 465, 470]. At present, it is not clear which of these mechanisms may be involved in the polyubiquitination produced by auranofin in GBM.

Intriguingly, combining auranofin with L-buthionine-sulfoximine (L-BSO), the inhibitor of gamma-glutamylcysteine synthetase (γ-GCL) and GSH synthesis, yielded synergistic cytotoxic effects in GBM cells, likely due to the depletion of GSH levels and the consequent increase in ROS beyond levels generated by auranofin alone. This synergy emphasizes the significance of targeting antioxidant pathways in combination with existing therapies. The observed increase in GSH levels in U87EGFRwt cells following auranofin treatment indicates a compensation mechanism in response to the oxidative stress induced by the inhibition of TrxR. Nevertheless, the inclusion of L-BSO with auranofin effectively eliminated this phenomenon, leading to increased lethality in cells treated with auranofin-L-BSO compared to those receiving auranofin alone. These findings align with the growing interest in developing combination therapies that exploit the vulnerabilities of cancer cells related to redox balance [200].

Numerous studies have assessed auranofin and L-BSO in treating various types of cancer, including mesothelioma, human lung cancer, rhabdomyosarcoma, and pancreatic cancer, yielding promising results [305, 462, 467, 471, 504]. However, the current study is the first to investigate

the impact of these drugs in a context of EGFR overexpression in GBM cell lines. The only clinical trial in glioblastoma using auranofin involved a limited cohort of 10 patients with recurrent GBM and no genetic mutation profile stratification; auranofin treatment was included in a combination strategy involving 9 repurposing drugs in the CUSP9v3 Treatment Protocol (NCT02770378). For L-BSO, there have only been two clinical trials conducted in patients with neuroblastoma (NCT00002730, NCT00005835), and they demonstrated that L-BSO is a tolerable drug. Interestingly, The Cancer Genome Atlas Program (TCGA) analysis supports the potential clinical relevance of the current findings, indicating potential modulation of redox pathways by EGFR alterations in the initiation and progression of various cancers. *In silico* analysis of TCGA data revealed significant positive correlations between EGFR wildtype expression and the expression of γ-GCL, involved in GSH biosynthesis, potentially rendering EGFR wildtype tumors more vulnerable to γ-GCL inhibitors like L-BSO, providing potential benefit to this subgroup of patients.

In conclusion, AU/LBSO combined treatment is highly synergistic against GBM cell lines with aberrant EGFR expression in vitro through a ROS-dependent mechanism. This study is a strong foundation for investigating this drug combination in vivo. The following illustration (**Figure 4.1**) summarizes this proposal's basic concepts and potential value.

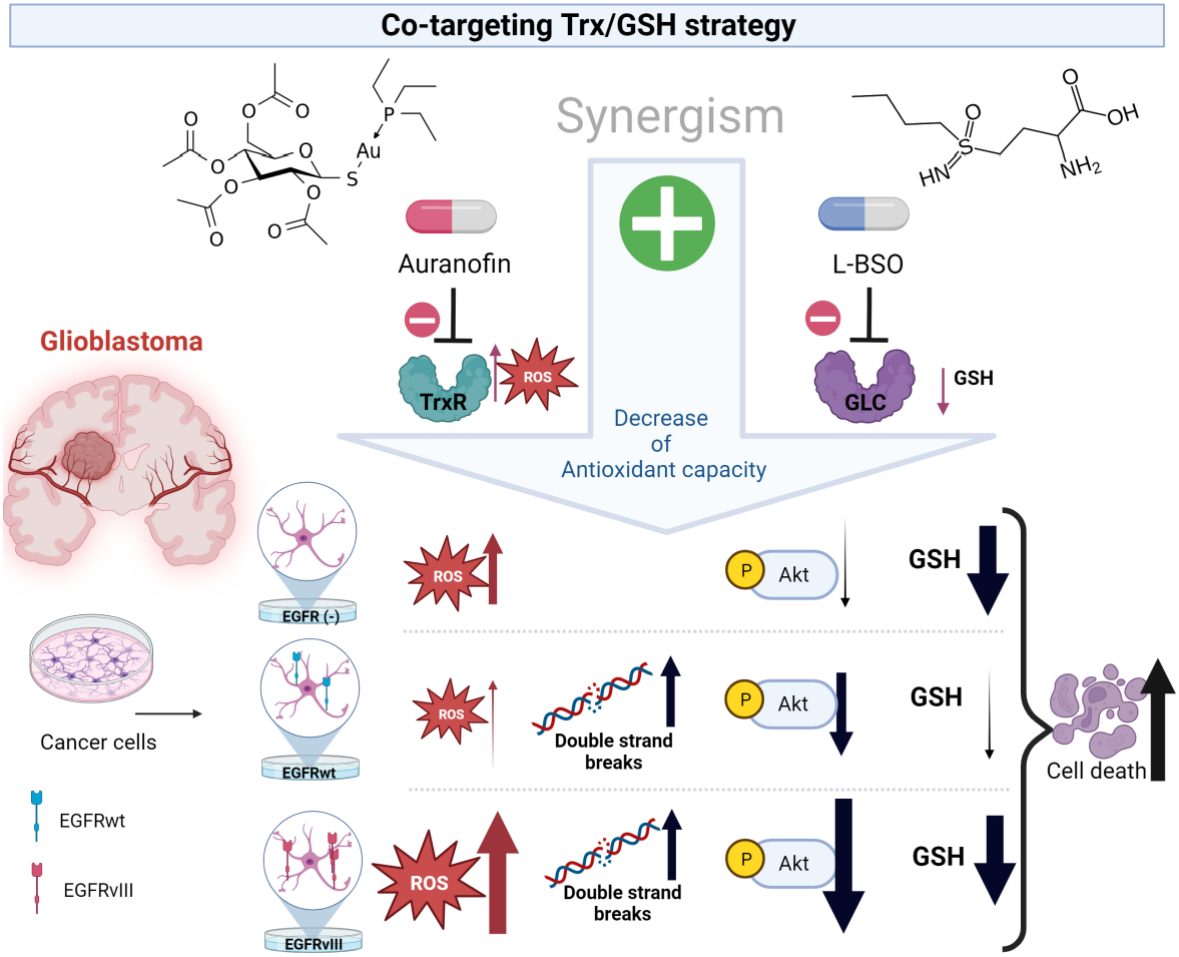

Figure 4.1 Model for combining auranofin and L-buthionine-sulfoximine (L-BSO) to kill malignant cells in glioblastoma, derived from studies on U87MG, U87/EGFRwt, and U87/EGFRvIII glioblastoma cell lines. Auranofin targets thioredoxin reductase 1 (TrxR1) to increase cellular levels of damaging reactive oxygen species (ROS) while L-BSO targets gamma-glutamylcysteine synthetase (γ-GCL) to block glutathione (GSH) biosynthesis and decrease antioxidant capacity. Each drug induces a different level of cytotoxicity in each of the three cell lines, and the combination of both drugs creates synergistic effects, including an increase in ROS, DNA damage, the downregulation of phospho-AKT, and the depletion of GSH, all of which contribute to death of the cancer cells. The combination of auranofin and L-BSO is extremely potent regardless of the cellular variant of EGFR and is a promising strategy for patient therapy.

BIBLIOGRAPHY

BIBLIOGRAPHY

1. Miller CR, Perry A. Glioblastoma. Arch Pathol Lab Med. 2007;131(3):397-406.
2. Louis DN, Perry A, Wesseling P, Brat DJ, Cree IA, Figarella-Branger D, et al. The 2021 WHO Classification of Tumors of the Central Nervous System: a summary. Neuro Oncol. 2021;23(8):1231-51.
3. Rodriguez-Camacho A, Flores-Vazquez JG, Moscardini-Martelli J, Torres-Rios JA, Olmos-Guzman A, Ortiz-Arce CS, et al. Glioblastoma Treatment: State-of-the-Art and Future Perspectives. Int J Mol Sci. 2022;23(13).
4. Rong L, Li N, Zhang Z. Emerging therapies for glioblastoma: current state and future directions. J Exp Clin Cancer Res. 2022;41(1):142.
5. Stupp R, Mason WP, van den Bent MJ, Weller M, Fisher B, Taphoorn MJ, et al. Radiotherapy plus concomitant and adjuvant temozolomide for glioblastoma. N Engl J Med. 2005;352(10):987-96.
6. Paolillo M, Boselli C, Schinelli S. Glioblastoma under Siege: An Overview of Current Therapeutic Strategies. Brain Sci. 2018;8(1).
7. Armento A, Ehlers J, Schotterl S, Naumann U. Glioblastoma (de Vleeschouwer S., ed.). Codon Publications, Australia. DOI; 2017.
8. Fernandes C, Costa A, Osorio L, Lago RC, Linhares P, Carvalho B, et al. Current Standards of Care in Glioblastoma Therapy. In: De Vleeschouwer S, editor. Glioblastoma. Brisbane (AU)2017.
9. Nam JY, de Groot JF. Treatment of Glioblastoma. J Oncol Pract. 2017;13(10):629-38.
10. Poon MTC, Sudlow CLM, Figueroa JD, Brennan PM. Longer-term (>/= 2 years) survival in patients with glioblastoma in population-based studies pre- and post-2005: a systematic review and meta-analysis. Sci Rep. 2020;10(1):11622.
11. Zhao Z, Zhang KN, Wang Q, Li G, Zeng F, Zhang Y, et al. Chinese Glioma Genome Atlas (CGGA): A Comprehensive Resource with Functional Genomic Data from Chinese Glioma Patients. Genomics Proteomics Bioinformatics. 2021;19(1):1-12.
12. Sottoriva A, Spiteri I, Piccirillo SG, Touloumis A, Collins VP, Marioni JC, et al. Intratumor heterogeneity in human glioblastoma reflects cancer evolutionary dynamics. Proc Natl Acad Sci U S A. 2013;110(10):4009-14.
13. Patel AP, Tirosh I, Trombetta JJ, Shalek AK, Gillespie SM, Wakimoto H, et al. Single-cell RNA-seq highlights intratumoral heterogeneity in primary glioblastoma. Science. 2014;344(6190):1396-401.
14. Cancer Genome Atlas Research N. Comprehensive genomic characterization defines human glioblastoma genes and core pathways. Nature. 2008;455(7216):1061-8.
15. Verhaak RG, Hoadley KA, Purdom E, Wang V, Qi Y, Wilkerson MD, et al. Integrated genomic analysis identifies clinically relevant subtypes of glioblastoma characterized by abnormalities in PDGFRA, IDH1, EGFR, and NF1. Cancer Cell. 2010;17(1):98-110.
16. Barthel FP, Johnson KC, Varn FS, Moskalik AD, Tanner G, Kocakavuk E, et al. Longitudinal molecular trajectories of diffuse glioma in adults. Nature. 2019;576(7785):112-20.
17. Binder ZA, O'Rourke DM. Glioblastoma: The Current State of Biology and Therapeutic Strategies. Cancer Res. 2022;82(5):769-72.
18. Ostrom QT, Price M, Neff C, Cioffi G, Waite KA, Kruchko C, et al. CBTRUS Statistical Report: Primary Brain and Other Central Nervous System Tumors Diagnosed in the United States in 2016-2020. Neuro Oncol. 2023;25(Supplement_4):iv1-iv99.

19. Walker EV, Zhou Y, Wu Y, Liu J, Climans SA, Davis FG, et al. The Incidence and Prevalence of Primary Central Nervous System (CNS) Tumours in Canada (2010-2017), and the Survival of Patients Diagnosed with CNS Tumours (2008-2017). Curr Oncol. 2023;30(4):4311-28.
20. Wen PY, Weller M, Lee EQ, Alexander BM, Barnholtz-Sloan JS, Barthel FP, et al. Glioblastoma in adults: a Society for Neuro-Oncology (SNO) and European Society of Neuro-Oncology (EANO) consensus review on current management and future directions. Neuro Oncol. 2020;22(8):1073-113.
21. Sofroniew MV, Vinters HV. Astrocytes: biology and pathology. Acta Neuropathol. 2010;119(1):7-35.
22. Bradl M, Lassmann H. Oligodendrocytes: biology and pathology. Acta Neuropathol. 2010;119(1):37-53.
23. Kang X, Zheng Y, Hong W, Chen X, Li H, Huang B, et al. Recent Advances in Immune Cell Therapy for Glioblastoma. Front Immunol. 2020;11:544563.
24. Semwal S, Boukherroub R, Savvides SN, Bouckaert J. Natural Antibodies: Protecting Role of IgM in Glioblastoma and Brain Tumours. Curr Pharm Des. 2021;27(45):4515-29.
25. Wirsching HG, Galanis E, Weller M. Glioblastoma. Handb Clin Neurol. 2016;134:381-97.
26. Perry A, Wesseling P. Histologic classification of gliomas. Handb Clin Neurol. 2016;134:71-95.
27. Chen J, Han P, Dahiya S. Glioblastoma: Changing concepts in the WHO CNS5 classification. Indian Journal of Pathology and Microbiology. 2022;65(5):24-32.
28. II FJW, Lämmle M, Anatelli F, Lennerz J, Perry A. Neuropathology for the Neuroradiologist: Palisades and Pseudopalisades. American Journal of Neuroradiology. 2006;27(10):2037-41.
29. Ferris SP, Hofmann JW, Solomon DA, Perry A. Characterization of gliomas: from morphology to molecules. Virchows Arch. 2017;471(2):257-69.
30. Torp SH, Solheim O, Skjulsvik AJ. The WHO 2021 Classification of Central Nervous System tumours: a practical update on what neurosurgeons need to know-a minireview. Acta Neurochir (Wien). 2022;164(9):2453-64.
31. Gritsch S, Batchelor TT, Gonzalez Castro LN. Diagnostic, therapeutic, and prognostic implications of the 2021 World Health Organization classification of tumors of the central nervous system. Cancer. 2022;128(1):47-58.
32. McNamara C, Mankad K, Thust S, Dixon L, Limback-Stanic C, D'Arco F, et al. 2021 WHO classification of tumours of the central nervous system: a review for the neuroradiologist. Neuroradiology. 2022;64(10):1919-50.
33. Motomura K, Kibe Y, Ohka F, Aoki K, Yamaguchi J, Saito R. Clinical characteristics and radiological features of glioblastoma, IDH-wildtype, grade 4 with histologically lower-grade gliomas. Brain Tumor Pathol. 2023;40(2):48-55.
34. Antonelli M, Poliani PL. Adult type diffuse gliomas in the new 2021 WHO Classification. Pathologica. 2022;114(6):397-409.
35. Mendonça ML, Coletti R, Gonçalves CS, Martins EP, Costa BM, Vinga S, et al. Updating TCGA glioma classification through integration of molecular profiling data following the 2016 and 2021 WHO guidelines. bioRxiv. 2023:2023.02.19.529134.
36. Louis DN, Aldape K, Brat DJ, Capper D, Ellison DW, Hawkins C, et al. Announcing cIMPACT-NOW: the Consortium to Inform Molecular and Practical Approaches to CNS Tumor Taxonomy. Acta Neuropathol. 2017;133(1):1-3.

37. Wang Q, Hu B, Hu X, Kim H, Squatrito M, Scarpace L, et al. Tumor Evolution of Glioma-Intrinsic Gene Expression Subtypes Associates with Immunological Changes in the Microenvironment. Cancer Cell. 2017;32(1):42-56 e6.
38. Noroxe DS, Poulsen HS, Lassen U. Hallmarks of glioblastoma: a systematic review. ESMO Open. 2016;1(6):e000144.
39. Stommel JM, Kimmelman AC, Ying H, Nabioullin R, Ponugoti AH, Wiedemeyer R, et al. Coactivation of receptor tyrosine kinases affects the response of tumor cells to targeted therapies. Science. 2007;318(5848):287-90.
40. Snuderl M, Fazlollahi L, Le LP, Nitta M, Zhelyazkova BH, Davidson CJ, et al. Mosaic amplification of multiple receptor tyrosine kinase genes in glioblastoma. Cancer Cell. 2011;20(6):810-7.
41. Gilbert MR, Wang M, Aldape KD, Stupp R, Hegi ME, Jaeckle KA, et al. Dose-dense temozolomide for newly diagnosed glioblastoma: a randomized phase III clinical trial. J Clin Oncol. 2013;31(32):4085-91.
42. Stupp R, Taillibert S, Kanner A, Read W, Steinberg D, Lhermitte B, et al. Effect of Tumor-Treating Fields Plus Maintenance Temozolomide vs Maintenance Temozolomide Alone on Survival in Patients With Glioblastoma: A Randomized Clinical Trial. JAMA. 2017;318(23):2306-16.
43. Lee SY. Temozolomide resistance in glioblastoma multiforme. Genes Dis. 2016;3(3):198-210.
44. Arora A, Somasundaram K. Glioblastoma vs temozolomide: can the red queen race be won? Cancer Biol Ther. 2019;20(8):1083-90.
45. Li GM. Mechanisms and functions of DNA mismatch repair. Cell Res. 2008;18(1):85-98.
46. Hirose Y, Katayama M, Stokoe D, Haas-Kogan DA, Berger MS, Pieper RO. The p38 mitogen-activated protein kinase pathway links the DNA mismatch repair system to the G2 checkpoint and to resistance to chemotherapeutic DNA-methylating agents. Mol Cell Biol. 2003;23(22):8306-15.
47. Nayak L, DeAngelis LM, Brandes AA, Peereboom DM, Galanis E, Lin NU, et al. The Neurologic Assessment in Neuro-Oncology (NANO) scale: a tool to assess neurologic function for integration into the Response Assessment in Neuro-Oncology (RANO) criteria. Neuro Oncol. 2017;19(5):625-35.
48. Singh S, Sadhukhan S, Sonawane A. 20 years since the approval of first EGFR-TKI, gefitinib: Insight and foresight. Biochim Biophys Acta Rev Cancer. 2023;1878(6):188967.
49. Appert-Collin A, Hubert P, Cremel G, Bennasroune A. Role of ErbB Receptors in Cancer Cell Migration and Invasion. Front Pharmacol. 2015;6:283.
50. Huang W, Hao Z, Mao F, Guo D. Small Molecule Inhibitors in Adult High-Grade Glioma: From the Past to the Future. Front Oncol. 2022;12:911876.
51. Kapoor GS, O'Rourke DM. Receptor tyrosine kinase signaling in gliomagenesis: pathobiology and therapeutic approaches. Cancer Biol Ther. 2003;2(4):330-42.
52. Runkle KB, Kharbanda A, Stypulkowski E, Cao XJ, Wang W, Garcia BA, et al. Inhibition of DHHC20-Mediated EGFR Palmitoylation Creates a Dependence on EGFR Signaling. Mol Cell. 2016;62(3):385-96.
53. Tilak M, Holborn J, New LA, Lalonde J, Jones N. Receptor Tyrosine Kinase Signaling and Targeting in Glioblastoma Multiforme. Int J Mol Sci. 2021;22(4).
54. Orpana A, Salven P. Angiogenic and lymphangiogenic molecules in hematological malignancies. Leuk Lymphoma. 2002;43(2):219-24.

55. Cheng F, Guo D. MET in glioma: signaling pathways and targeted therapies. J Exp Clin Cancer Res. 2019;38(1):270.
56. Campos B, Olsen LR, Urup T, Poulsen HS. A comprehensive profile of recurrent glioblastoma. Oncogene. 2016;35(45):5819-25.
57. Jimenez-Pascual A, Hale JS, Kordowski A, Pugh J, Silver DJ, Bayik D, et al. ADAMDEC1 Maintains a Growth Factor Signaling Loop in Cancer Stem Cells. Cancer Discov. 2019;9(11):1574-89.
58. Jackson EL, Garcia-Verdugo JM, Gil-Perotin S, Roy M, Quinones-Hinojosa A, VandenBerg S, et al. PDGFR alpha-positive B cells are neural stem cells in the adult SVZ that form glioma-like growths in response to increased PDGF signaling. Neuron. 2006;51(2):187-99.
59. Wee P, Wang Z. Epidermal Growth Factor Receptor Cell Proliferation Signaling Pathways. Cancers (Basel). 2017;9(5).
60. Tomas A, Futter CE, Eden ER. EGF receptor trafficking: consequences for signaling and cancer. Trends Cell Biol. 2014;24(1):26-34.
61. Zeng F, Harris RC. Epidermal growth factor, from gene organization to bedside. Semin Cell Dev Biol. 2014;28:2-11.
62. Salomon DS, Brandt R, Ciardiello F, Normanno N. Epidermal growth factor-related peptides and their receptors in human malignancies. Crit Rev Oncol Hematol. 1995;19(3):183-232.
63. Normanno N, Bianco C, De Luca A, Salomon DS. The role of EGF-related peptides in tumor growth. Front Biosci. 2001;6:D685-707.
64. Normanno N, De Luca A, Bianco C, Strizzi L, Mancino M, Maiello MR, et al. Epidermal growth factor receptor (EGFR) signaling in cancer. Gene. 2006;366(1):2-16.
65. Zandi R, Larsen AB, Andersen P, Stockhausen MT, Poulsen HS. Mechanisms for oncogenic activation of the epidermal growth factor receptor. Cell Signal. 2007;19(10):2013-23.
66. An Z, Aksoy O, Zheng T, Fan QW, Weiss WA. Epidermal growth factor receptor and EGFRvIII in glioblastoma: signaling pathways and targeted therapies. Oncogene. 2018;37(12):1561-75.
67. Hatanpaa KJ, Burma S, Zhao D, Habib AA. Epidermal growth factor receptor in glioma: signal transduction, neuropathology, imaging, and radioresistance. Neoplasia. 2010;12(9):675-84.
68. Ekstrand AJ, James CD, Cavenee WK, Seliger B, Pettersson RF, Collins VP. Genes for epidermal growth factor receptor, transforming growth factor alpha, and epidermal growth factor and their expression in human gliomas in vivo. Cancer Res. 1991;51(8):2164-72.
69. Wong AJ, Ruppert JM, Bigner SH, Grzeschik CH, Humphrey PA, Bigner DS, et al. Structural alterations of the epidermal growth factor receptor gene in human gliomas. Proc Natl Acad Sci U S A. 1992;89(7):2965-9.
70. Xu H, Zong H, Ma C, Ming X, Shang M, Li K, et al. Epidermal growth factor receptor in glioblastoma. Oncol Lett. 2017;14(1):512-6.
71. Sigismund S, Avanzato D, Lanzetti L. Emerging functions of the EGFR in cancer. Mol Oncol. 2018;12(1):3-20.
72. Hynes NE, Lane HA. ERBB receptors and cancer: the complexity of targeted inhibitors. Nat Rev Cancer. 2005;5(5):341-54.
73. Hu C, Leche CA, 2nd, Kiyatkin A, Yu Z, Stayrook SE, Ferguson KM, et al. Glioblastoma mutations alter EGFR dimer structure to prevent ligand bias. Nature. 2022;602(7897):518-22.
74. Nadeem Abbas M, Kausar S, Wang F, Zhao Y, Cui H. Advances in Targeting the Epidermal Growth Factor Receptor Pathway by Synthetic Products and Its Regulation by Epigenetic Modulators As a Therapy for Glioblastoma. Cells. 2019;8(4).

75. Schlessinger J. Ligand-induced, receptor-mediated dimerization and activation of EGF receptor. Cell. 2002;110(6):669-72.
76. Nagane M, Coufal F, Lin H, Bögler O, Cavenee WK, Huang HJ. A common mutant epidermal growth factor receptor confers enhanced tumorigenicity on human glioblastoma cells by increasing proliferation and reducing apoptosis. Cancer Res. 1996;56(21):5079-86.
77. Huang L, Fu L. Mechanisms of resistance to EGFR tyrosine kinase inhibitors. Acta Pharm Sin B. 2015;5(5):390-401.
78. Orellana L, Thorne AH, Lema R, Gustavsson J, Parisian AD, Hospital A, et al. Oncogenic mutations at the EGFR ectodomain structurally converge to remove a steric hindrance on a kinase-coupled cryptic epitope. Proc Natl Acad Sci U S A. 2019;116(20):10009-18.
79. Furnari FB, Cloughesy TF, Cavenee WK, Mischel PS. Heterogeneity of epidermal growth factor receptor signalling networks in glioblastoma. Nat Rev Cancer. 2015;15(5):302-10.
80. Humphrey PA, Gangarosa LM, Wong AJ, Archer GE, Lund-Johansen M, Bjerkvig R, et al. Deletion-mutant epidermal growth factor receptor in human gliomas: effects of type II mutation on receptor function. Biochem Biophys Res Commun. 1991;178(3):1413-20.
81. Francis JM, Zhang CZ, Maire CL, Jung J, Manzo VE, Adalsteinsson VA, et al. EGFR variant heterogeneity in glioblastoma resolved through single-nucleus sequencing. Cancer Discov. 2014;4(8):956-71.
82. Kim HM, Lee SH, Lim J, Yoo J, Hwang DY. The epidermal growth factor receptor variant type III mutation frequently found in gliomas induces astrogenesis in human cerebral organoids. Cell Prolif. 2021;54(2):e12965.
83. Brennan CW, Verhaak RG, McKenna A, Campos B, Noushmehr H, Salama SR, et al. The somatic genomic landscape of glioblastoma. Cell. 2013;155(2):462-77.
84. Yamoutpour F, Bodempudi V, Park SE, Pan W, Mauzy MJ, Kratzke RA, et al. Gene silencing for epidermal growth factor receptor variant III induces cell-specific cytotoxicity. Mol Cancer Ther. 2008;7(11):3586-97.
85. Stec W, Rosiak K, Treda C, Smolarz M, Peciak J, Pacholczyk M, et al. Cyclic trans-phosphorylation in a homodimer as the predominant mechanism of EGFRvIII action and regulation. Oncotarget. 2018;9(9):8560-72.
86. Huang PH, Xu AM, White FM. Oncogenic EGFR signaling networks in glioma. Sci Signal. 2009;2(87):re6.
87. Huang K, Liu X, Li Y, Wang Q, Zhou J, Wang Y, et al. Genome-Wide CRISPR-Cas9 Screening Identifies NF-kappaB/E2F6 Responsible for EGFRvIII-Associated Temozolomide Resistance in Glioblastoma. Adv Sci (Weinh). 2019;6(17):1900782.
88. Feldkamp MM, Lala P, Lau N, Roncari L, Guha A. Expression of Activated Epidermal Growth Factor Receptors, Ras-Guanosine Triphosphate, and Mitogen-activated Protein Kinase in Human Glioblastoma Multiforme Specimens. Neurosurgery. 1999;45(6):1442.
89. Shinojima N, Tada K, Shiraishi S, Kamiryo T, Kochi M, Nakamura H, et al. Prognostic Value of Epidermal Growth Factor Receptor in Patients with Glioblastoma Multiforme1. Cancer Research. 2003;63(20):6962-70.
90. Montano N, Cenci T, Martini M, D'Alessandris QG, Pelacchi F, Ricci-Vitiani L, et al. Expression of EGFRvIII in glioblastoma: prognostic significance revisited. Neoplasia. 2011;13(12):1113-21.
91. Heimberger AB, Hlatky R, Suki D, Yang D, Weinberg J, Gilbert M, et al. Prognostic effect of epidermal growth factor receptor and EGFRvIII in glioblastoma multiforme patients. Clin Cancer Res. 2005;11(4):1462-6.

92. Hoogstrate Y, Ghisai SA, de Wit M, de Heer I, Draaisma K, van Riet J, et al. The EGFRvIII transcriptome in glioblastoma: A meta-omics analysis. Neuro Oncol. 2022;24(3):429-41.
93. Struve N, Binder ZA, Stead LF, Brend T, Bagley SJ, Faulkner C, et al. EGFRvIII upregulates DNA mismatch repair resulting in increased temozolomide sensitivity of MGMT promoter methylated glioblastoma. Oncogene. 2020;39(15):3041-55.
94. Seshacharyulu P, Ponnusamy MP, Haridas D, Jain M, Ganti AK, Batra SK. Targeting the EGFR signaling pathway in cancer therapy. Expert Opin Ther Targets. 2012;16(1):15-31.
95. Clement PMJ, Dirven L, Eoli M, Sepulveda-Sanchez JM, Walenkamp AME, Frenel JS, et al. Impact of depatuxizumab mafodotin on health-related quality of life and neurological functioning in the phase II EORTC 1410/INTELLANCE 2 trial for EGFR-amplified recurrent glioblastoma. Eur J Cancer. 2021;147:1-12.
96. Lin B, Ziebro J, Smithberger E, Skinner KR, Zhao E, Cloughesy TF, et al. EGFR, the Lazarus target for precision oncology in glioblastoma. Neuro Oncol. 2022;24(12):2035-62.
97. O'Rourke DM, Nasrallah MP, Desai A, Melenhorst JJ, Mansfield K, Morrissette JJD, et al. A single dose of peripherally infused EGFRvIII-directed CAR T cells mediates antigen loss and induces adaptive resistance in patients with recurrent glioblastoma. Sci Transl Med. 2017;9(399).
98. Sampson JH, Archer GE, Mitchell DA, Heimberger AB, Herndon JE, 2nd, Lally-Goss D, et al. An epidermal growth factor receptor variant III-targeted vaccine is safe and immunogenic in patients with glioblastoma multiforme. Mol Cancer Ther. 2009;8(10):2773-9.
99. Weller M, Butowski N, Tran DD, Recht LD, Lim M, Hirte H, et al. Rindopepimut with temozolomide for patients with newly diagnosed, EGFRvIII-expressing glioblastoma (ACT IV): a randomised, double-blind, international phase 3 trial. Lancet Oncol. 2017;18(10):1373-85.
100. Reardon DA, Desjardins A, Vredenburgh JJ, O'Rourke DM, Tran DD, Fink KL, et al. Rindopepimut with Bevacizumab for Patients with Relapsed EGFRvIII-Expressing Glioblastoma (ReACT): Results of a Double-Blind Randomized Phase II Trial. Clin Cancer Res. 2020;26(7):1586-94.
101. Aldaz P, Arozarena I. Tyrosine Kinase Inhibitors in Adult Glioblastoma: An (Un)Closed Chapter? Cancers (Basel). 2021;13(22).
102. Kim G, Ko YT. Small molecule tyrosine kinase inhibitors in glioblastoma. Arch Pharm Res. 2020;43(4):385-94.
103. Liu H, Qiu W, Sun T, Wang L, Du C, Hu Y, et al. Therapeutic strategies of glioblastoma (GBM): The current advances in the molecular targets and bioactive small molecule compounds. Acta Pharm Sin B. 2022;12(4):1781-804.
104. Raymond E, Faivre S, Armand JP. Epidermal growth factor receptor tyrosine kinase as a target for anticancer therapy. Drugs. 2000;60 Suppl 1:15-23; discussion 41-2.
105. Lynch TJ, Bell DW, Sordella R, Gurubhagavatula S, Okimoto RA, Brannigan BW, et al. Activating mutations in the epidermal growth factor receptor underlying responsiveness of non-small-cell lung cancer to gefitinib. N Engl J Med. 2004;350(21):2129-39.
106. Lal A, Glazer CA, Martinson HM, Friedman HS, Archer GE, Sampson JH, et al. Mutant epidermal growth factor receptor up-regulates molecular effectors of tumor invasion. Cancer Res. 2002;62(12):3335-9.
107. Fallahi P, Ferrari SM, Galdiero MR, Varricchi G, Elia G, Ragusa F, et al. Molecular targets of tyrosine kinase inhibitors in thyroid cancer. Semin Cancer Biol. 2022;79:180-96.

108. Maarof NNN, Alsalahi A, Abdulmalek E, Fakurazi S, Tejo BA, Abdul Rahman MB. Efficacy of Afatinib in the Treatment of Patients with Non-Small Cell Lung Cancer and Head and Neck Squamous Cell Carcinoma: A Systematic Review and Meta-Analysis. Cancers (Basel). 2021;13(4).
109. Galanti D, Inno A, La Vecchia M, Borsellino N, Incorvaia L, Russo A, et al. Current treatment options for HER2-positive breast cancer patients with brain metastases. Crit Rev Oncol Hematol. 2021;161:103329.
110. Nahm J, Schumann EH, Vu M, Sinha M, Ware C, Hsu S, et al. Biom-44. Improved Overall Survival Of Recurrent Glioblastoma (GBM) Patients With EGFR Amplification And EGFR VIII Mutations Treated With Osimertinib: A Retrospective Review. Neuro-Oncology. 2023;25(Supplement_5):v14-v.
111. Sharma SV, Bell DW, Settleman J, Haber DA. Epidermal growth factor receptor mutations in lung cancer. Nat Rev Cancer. 2007;7(3):169-81.
112. Lee JC, Vivanco I, Beroukhim R, Huang JH, Feng WL, DeBiasi RM, et al. Epidermal growth factor receptor activation in glioblastoma through novel missense mutations in the extracellular domain. PLoS Med. 2006;3(12):e485.
113. Vivanco I, Robins HI, Rohle D, Campos C, Grommes C, Nghiemphu PL, et al. Differential sensitivity of glioma- versus lung cancer-specific EGFR mutations to EGFR kinase inhibitors. Cancer Discov. 2012;2(5):458-71.
114. Mai WX, Gosa L, Daniels VW, Ta L, Tsang JE, Higgins B, et al. Cytoplasmic p53 couples oncogene-driven glucose metabolism to apoptosis and is a therapeutic target in glioblastoma. Nat Med. 2017;23(11):1342-51.
115. Lee JK, Liu Z, Sa JK, Shin S, Wang J, Bordyuh M, et al. Pharmacogenomic landscape of patient-derived tumor cells informs precision oncology therapy. Nat Genet. 2018;50(10):1399-411.
116. Fan QW, Cheng CK, Gustafson WC, Charron E, Zipper P, Wong RA, et al. EGFR phosphorylates tumor-derived EGFRvIII driving STAT3/5 and progression in glioblastoma. Cancer Cell. 2013;24(4):438-49.
117. Koga T, Li B, Figueroa JM, Ren B, Chen CC, Carter BS, et al. Mapping of genomic EGFRvIII deletions in glioblastoma: insight into rearrangement mechanisms and biomarker development. Neuro Oncol. 2018;20(10):1310-20.
118. Talasila KM, Soentgerath A, Euskirchen P, Rosland GV, Wang J, Huszthy PC, et al. EGFR wild-type amplification and activation promote invasion and development of glioblastoma independent of angiogenesis. Acta Neuropathol. 2013;125(5):683-98.
119. Sarkaria JN, Yang L, Grogan PT, Kitange GJ, Carlson BL, Schroeder MA, et al. Identification of molecular characteristics correlated with glioblastoma sensitivity to EGFR kinase inhibition through use of an intracranial xenograft test panel. Mol Cancer Ther. 2007;6(3):1167-74.
120. Velu TJ, Beguinot L, Vass WC, Willingham MC, Merlino GT, Pastan I, et al. Epidermal-growth-factor-dependent transformation by a human EGF receptor proto-oncogene. Science. 1987;238(4832):1408-10.
121. Zanca C, Villa GR, Benitez JA, Thorne AH, Koga T, D'Antonio M, et al. Glioblastoma cellular cross-talk converges on NF-kappaB to attenuate EGFR inhibitor sensitivity. Genes Dev. 2017;31(12):1212-27.
122. Inda MM, Bonavia R, Mukasa A, Narita Y, Sah DW, Vandenberg S, et al. Tumor heterogeneity is an active process maintained by a mutant EGFR-induced cytokine circuit in glioblastoma. Genes Dev. 2010;24(16):1731-45.

123. Pardridge WM. The blood-brain barrier: bottleneck in brain drug development. NeuroRx. 2005;2(1):3-14.
124. Sarkaria JN, Hu LS, Parney IF, Pafundi DH, Brinkmann DH, Laack NN, et al. Is the blood-brain barrier really disrupted in all glioblastomas? A critical assessment of existing clinical data. Neuro Oncol. 2018;20(2):184-91.
125. Jun HJ, Acquaviva J, Chi D, Lessard J, Zhu H, Woolfenden S, et al. Acquired MET expression confers resistance to EGFR inhibition in a mouse model of glioblastoma multiforme. Oncogene. 2012;31(25):3039-50.
126. Akhavan D, Pourzia AL, Nourian AA, Williams KJ, Nathanson D, Babic I, et al. De-repression of PDGFRbeta transcription promotes acquired resistance to EGFR tyrosine kinase inhibitors in glioblastoma patients. Cancer Discov. 2013;3(5):534-47.
127. Zawistowski JS, Bevill SM, Goulet DR, Stuhlmiller TJ, Beltran AS, Olivares-Quintero JF, et al. Enhancer Remodeling during Adaptive Bypass to MEK Inhibition Is Attenuated by Pharmacologic Targeting of the P-TEFb Complex. Cancer Discov. 2017;7(3):302-21.
128. Liu F, Hon GC, Villa GR, Turner KM, Ikegami S, Yang H, et al. EGFR Mutation Promotes Glioblastoma through Epigenome and Transcription Factor Network Remodeling. Mol Cell. 2015;60(2):307-18.
129. Nathanson DA, Gini B, Mottahedeh J, Visnyei K, Koga T, Gomez G, et al. Targeted therapy resistance mediated by dynamic regulation of extrachromosomal mutant EGFR DNA. Science. 2014;343(6166):72-6.
130. Rupp M, Mouhri ZS, Williams C, Jean-Claude BJ. Molecular analysis of the dual targeting of the epidermal growth factor receptor and the O(6)-methylguanine-DNA methyltransferase with a double arm hybrid molecule. Oncotarget. 2018;9(80):35041-55.
131. Meyn RE, Munshi A, Haymach JV, Milas L, Ang KK. Receptor signaling as a regulatory mechanism of DNA repair. Radiother Oncol. 2009;92(3):316-22.
132. Cohen MH, Williams GA, Sridhara R, Chen G, McGuinn WD, Jr., Morse D, et al. United States Food and Drug Administration Drug Approval summary: Gefitinib (ZD1839; Iressa) tablets. Clin Cancer Res. 2004;10(4):1212-8.
133. Mellinghoff IK, Wang MY, Vivanco I, Haas-Kogan DA, Zhu S, Dia EQ, et al. Molecular determinants of the response of glioblastomas to EGFR kinase inhibitors. N Engl J Med. 2005;353(19):2012-24.
134. Parker JJ, Dionne KR, Massarwa R, Klaassen M, Foreman NK, Niswander L, et al. Gefitinib selectively inhibits tumor cell migration in EGFR-amplified human glioblastoma. Neuro Oncol. 2013;15(8):1048-57.
135. Griffero F, Daga A, Marubbi D, Capra MC, Melotti A, Pattarozzi A, et al. Different response of human glioma tumor-initiating cells to epidermal growth factor receptor kinase inhibitors. J Biol Chem. 2009;284(11):7138-48.
136. Joshi AD, Loilome W, Siu IM, Tyler B, Gallia GL, Riggins GJ. Evaluation of tyrosine kinase inhibitor combinations for glioblastoma therapy. PLoS One. 2012;7(10):e44372.
137. Hegi ME, Diserens AC, Bady P, Kamoshima Y, Kouwenhoven MC, Delorenzi M, et al. Pathway analysis of glioblastoma tissue after preoperative treatment with the EGFR tyrosine kinase inhibitor gefitinib--a phase II trial. Mol Cancer Ther. 2011;10(6):1102-12.
138. Uhm JH, Ballman KV, Wu W, Giannini C, Krauss JC, Buckner JC, et al. Phase II evaluation of gefitinib in patients with newly diagnosed Grade 4 astrocytoma: Mayo/North Central Cancer Treatment Group Study N0074. Int J Radiat Oncol Biol Phys. 2011;80(2):347-53.

139. Chakravarti A, Wang M, Robins HI, Lautenschlaeger T, Curran WJ, Brachman DG, et al. RTOG 0211: a phase 1/2 study of radiation therapy with concurrent gefitinib for newly diagnosed glioblastoma patients. Int J Radiat Oncol Biol Phys. 2013;85(5):1206-11.
140. Rawluk J, Waller CF. Gefitinib. Recent Results Cancer Res. 2018;211:235-46.
141. Sampson JH, Akabani G, Archer GE, Berger MS, Coleman RE, Friedman AH, et al. Intracerebral infusion of an EGFR-targeted toxin in recurrent malignant brain tumors. Neuro Oncol. 2008;10(3):320-9.
142. Patel D, Lahiji A, Patel S, Franklin M, Jimenez X, Hicklin DJ, et al. Monoclonal Antibody Cetuximab Binds to and Down-regulates Constitutively Activated Epidermal Growth Factor Receptor vIII on the Cell Surface. Anticancer Research. 2007;27(5A):3355-66.
143. Hasselbalch B, Lassen U, Hansen S, Holmberg M, Sorensen M, Kosteljanetz M, et al. Cetuximab, bevacizumab, and irinotecan for patients with primary glioblastoma and progression after radiation therapy and temozolomide: a phase II trial. Neuro Oncol. 2010;12(5):508-16.
144. Rachid Z, Brahimi F, Katsoulas A, Teoh N, Jean-Claude BJ. The combi-targeting concept: chemical dissection of the dual targeting properties of a series of "combi-triazenes". J Med Chem. 2003;46(20):4313-21.
145. Qiu Q, Domarkas J, Banerjee R, Katsoulas A, McNamee JP, Jean-Claude BJ. Type II combi-molecules: design and binary targeting properties of the novel triazolinium-containing molecules JDD36 and JDE05. Anticancer Drugs. 2007;18(2):171-7.
146. Saha P, Debnath C, Berube G. Steroid-linked nitrogen mustards as potential anticancer therapeutics: a review. J Steroid Biochem Mol Biol. 2013;137:271-300.
147. Musso L, Dallavalle S, Zunino F. Perspectives in the development of hybrid bifunctional antitumour agents. Biochem Pharmacol. 2015;96(4):297-305.
148. Levine PM, Garabedian MJ, Kirshenbaum K. Targeting the androgen receptor with steroid conjugates. J Med Chem. 2014;57(20):8224-37.
149. Gediya LK, Njar VC. Promise and challenges in drug discovery and development of hybrid anticancer drugs. Expert Opin Drug Discov. 2009;4(11):1099-111.
150. Bansal R, Acharya PC. Man-made cytotoxic steroids: exemplary agents for cancer therapy. Chem Rev. 2014;114(14):6986-7005.
151. Brahimi F, Rachid Z, Qiu Q, McNamee JP, Li YJ, Tari AM, et al. Multiple mechanisms of action of ZR2002 in human breast cancer cells: a novel combi-molecule designed to block signaling mediated by the ERB family of oncogenes and to damage genomic DNA. Int J Cancer. 2004;112(3):484-91.
152. Senhaji Mouhri Z, Goodfellow E, Jean-Claude B. A type I combi-targeting approach for the design of molecules with enhanced potency against BRCA1/2 mutant- and O6-methylguanine-DNA methyltransferase (mgmt)- expressing tumour cells. BMC Cancer. 2017;17(1):540.
153. Facchin C, Fraga-Timiraos AB, Schmitt J, Babaa N, Pannu N, Aliaga A, et al. Molecular Analysis of the Superior Efficacy of a Dual Epidermal Growth Factor Receptor (EGFR)-DNA-Targeting Combi-Molecule in Comparison with Its Putative Prodrugs 6-Mono-Alkylamino- and 6,6-Dialkylaminoquinazoline in a Human Osteosarcoma Xenograft Model. Cells. 2023;12(6).
154. Watt HL, Rachid Z, Jean-Claude BJ. The Concept of Divergent Targeting through the Activation and Inhibition of Receptors as a Novel Chemotherapeutic Strategy: Signaling Responses to Strong DNA-Reactive Combinatorial Mimicries. J Signal Transduct. 2012;2012:282050.

155. Sharifi Z. Preclinical development of dual EGFR/DNA targeting agent in glioblastoma: McGill University (Canada); 2019.
156. Sharifi Z, Meehan B, Daniel P, Eppert K, Jean-Claude B, Rak J, et al. Pharmacokinetics of ZR2002, a combi-molecule with EGFR and DNA-damaging properties and its efficacy in an orthotopic glioblastoma mouse model. Annals of Oncology. 2018;29:iii12.
157. Sharifi Z, Abdulkarim B, Meehan B, Rak J, Daniel P, Schmitt J, et al. Mechanisms and Antitumor Activity of a Binary EGFR/DNA-Targeting Strategy Overcomes Resistance of Glioblastoma Stem Cells to Temozolomide. Clin Cancer Res. 2019;25(24):7594-608.
158. Cairns RA, Harris IS, Mak TW. Regulation of cancer cell metabolism. Nat Rev Cancer. 2011;11(2):85-95.
159. Sies H, Jones DP. Reactive oxygen species (ROS) as pleiotropic physiological signalling agents. Nat Rev Mol Cell Biol. 2020;21(7):363-83.
160. Cortese-Krott MM, Koning A, Kuhnle GGC, Nagy P, Bianco CL, Pasch A, et al. The Reactive Species Interactome: Evolutionary Emergence, Biological Significance, and Opportunities for Redox Metabolomics and Personalized Medicine. Antioxid Redox Signal. 2017;27(10):684-712.
161. Zhang L, Wang X, Cueto R, Effi C, Zhang Y, Tan H, et al. Biochemical basis and metabolic interplay of redox regulation. Redox Biol. 2019;26:101284.
162. Kumari S, Badana AK, G MM, G S, Malla R. Reactive Oxygen Species: A Key Constituent in Cancer Survival. Biomark Insights. 2018;13:1177271918755391.
163. Gao L, Laude K, Cai H. Mitochondrial pathophysiology, reactive oxygen species, and cardiovascular diseases. Vet Clin North Am Small Anim Pract. 2008;38(1):137-55, vi.
164. Murphy MP. How mitochondria produce reactive oxygen species. Biochem J. 2009;417(1):1-13.
165. Glasauer A, Chandel NS. Targeting antioxidants for cancer therapy. Biochem Pharmacol. 2014;92(1):90-101.
166. Wallace DC. Mitochondria and cancer. Nat Rev Cancer. 2012;12(10):685-98.
167. Crompton M. The mitochondrial permeability transition pore and its role in cell death. Biochemical Journal. 1999;341(2):233-49.
168. Henzler T, Steudle E. Transport and metabolic degradation of hydrogen peroxide in Chara corallina: model calculations and measurements with the pressure probe suggest transport of H(2)O(2) across water channels. J Exp Bot. 2000;51(353):2053-66.
169. Fukai T, Ushio-Fukai M. Superoxide dismutases: role in redox signaling, vascular function, and diseases. Antioxid Redox Signal. 2011;15(6):1583-606.
170. Jones DP. Radical-free biology of oxidative stress. Am J Physiol Cell Physiol. 2008;295(4):C849-68.
171. Parascandolo A, Laukkanen MO. Carcinogenesis and Reactive Oxygen Species Signaling: Interaction of the NADPH Oxidase NOX1-5 and Superoxide Dismutase 1-3 Signal Transduction Pathways. Antioxid Redox Signal. 2019;30(3):443-86.
172. Knock GA. NADPH oxidase in the vasculature: Expression, regulation and signalling pathways; role in normal cardiovascular physiology and its dysregulation in hypertension. Free Radic Biol Med. 2019;145:385-427.
173. Bedard K, Krause KH. The NOX family of ROS-generating NADPH oxidases: physiology and pathophysiology. Physiol Rev. 2007;87(1):245-313.
174. Panday A, Sahoo MK, Osorio D, Batra S. NADPH oxidases: an overview from structure to innate immunity-associated pathologies. Cell Mol Immunol. 2015;12(1):5-23.

175. Wright DT, Cohn LA, Li H, Fischer B, Li CM, Adler KB. Interactions of oxygen radicals with airway epithelium. Environ Health Perspect. 1994;102 Suppl 10(Suppl 10):85-90.
176. Dansen TB, Wirtz KW. The peroxisome in oxidative stress. IUBMB Life. 2001;51(4):223-30.
177. Niedzwiecki MM, Walker DI, Vermeulen R, Chadeau-Hyam M, Jones DP, Miller GW. The Exposome: Molecules to Populations. Annu Rev Pharmacol Toxicol. 2019;59:107-27.
178. Zeida A, Trujillo M, Ferrer-Sueta G, Denicola A, Estrin DA, Radi R. Catalysis of Peroxide Reduction by Fast Reacting Protein Thiols. Chem Rev. 2019;119(19):10829-55.
179. Sies H, Berndt C, Jones DP. Oxidative Stress. Annu Rev Biochem. 2017;86:715-48.
180. Sies H. Hydrogen peroxide as a central redox signaling molecule in physiological oxidative stress: Oxidative eustress. Redox Biol. 2017;11:613-9.
181. Chance B, Sies H, Boveris A. Hydroperoxide metabolism in mammalian organs. Physiol Rev. 1979;59(3):527-605.
182. Gorrini C, Harris IS, Mak TW. Modulation of oxidative stress as an anticancer strategy. Nat Rev Drug Discov. 2013;12(12):931-47.
183. Sena LA, Chandel NS. Physiological roles of mitochondrial reactive oxygen species. Mol Cell. 2012;48(2):158-67.
184. Wiseman H, Halliwell B. Damage to DNA by reactive oxygen and nitrogen species: role in inflammatory disease and progression to cancer. Biochem J. 1996;313 (Pt 1)(Pt 1):17-29.
185. Trachootham D, Alexandre J, Huang P. Targeting cancer cells by ROS-mediated mechanisms: a radical therapeutic approach? Nat Rev Drug Discov. 2009;8(7):579-91.
186. Gius D, Spitz DR. Redox signaling in cancer biology. Antioxid Redox Signal. 2006;8(7-8):1249-52.
187. del Rio LA, Sandalio LM, Palma JM, Bueno P, Corpas FJ. Metabolism of oxygen radicals in peroxisomes and cellular implications. Free Radic Biol Med. 1992;13(5):557-80.
188. Liou GY, Storz P. Reactive oxygen species in cancer. Free Radic Res. 2010;44(5):479-96.
189. Kehrer JP, Klotz LO. Free radicals and related reactive species as mediators of tissue injury and disease: implications for Health. Crit Rev Toxicol. 2015;45(9):765-98.
190. Halliwell B, Gutteridge JM. Role of free radicals and catalytic metal ions in human disease: an overview. Methods Enzymol. 1990;186:1-85.
191. Quinlan CL, Perevoshchikova IV, Hey-Mogensen M, Orr AL, Brand MD. Sites of reactive oxygen species generation by mitochondria oxidizing different substrates. Redox Biol. 2013;1(1):304-12.
192. Negrini S, Gorgoulis VG, Halazonetis TD. Genomic instability--an evolving hallmark of cancer. Nat Rev Mol Cell Biol. 2010;11(3):220-8.
193. Okon IS, Zou MH. Mitochondrial ROS and cancer drug resistance: Implications for therapy. Pharmacol Res. 2015;100:170-4.
194. Kang SW, Lee S, Lee EK. ROS and energy metabolism in cancer cells: alliance for fast growth. Arch Pharm Res. 2015;38(3):338-45.
195. Laurent A, Nicco C, Chéreau C, Goulvestre C, Alexandre J, Alves A, et al. Controlling tumor growth by modulating endogenous production of reactive oxygen species. Cancer Res. 2005;65(3):948-56.
196. Lewis A, Du J, Liu J, Ritchie JM, Oberley LW, Cullen JJ. Metastatic progression of pancreatic cancer: changes in antioxidant enzymes and cell growth. Clin Exp Metastasis. 2005;22(7):523-32.

197. Xiaobo C, Majidi M, Feng M, Shao R, Wang J, Zhao Y, et al. TUSC2(FUS1)-erlotinib Induced Vulnerabilities in Epidermal Growth Factor Receptor(EGFR) Wildtype Non-small Cell Lung Cancer(NSCLC) Targeted by the Repurposed Drug Auranofin. Sci Rep. 2016;6:35741.
198. Trachootham D, Zhou Y, Zhang H, Demizu Y, Chen Z, Pelicano H, et al. Selective killing of oncogenically transformed cells through a ROS-mediated mechanism by beta-phenylethyl isothiocyanate. Cancer Cell. 2006;10(3):241-52.
199. Van Loenhout J, Peeters M, Bogaerts A, Smits E, Deben C. Oxidative Stress-Inducing Anticancer Therapies: Taking a Closer Look at Their Immunomodulating Effects. Antioxidants (Basel). 2020;9(12).
200. Jiang H, Zuo J, Li B, Chen R, Luo K, Xiang X, et al. Drug-induced oxidative stress in cancer treatments: Angel or devil? Redox Biol. 2023;63:102754.
201. Perillo B, Di Donato M, Pezone A, Di Zazzo E, Giovannelli P, Galasso G, et al. ROS in cancer therapy: the bright side of the moon. Exp Mol Med. 2020;52(2):192-203.
202. Nizami ZN, Aburawi HE, Semlali A, Muhammad K, Iratni R. Oxidative Stress Inducers in Cancer Therapy: Preclinical and Clinical Evidence. Antioxidants (Basel). 2023;12(6).
203. Hayes JD, Dinkova-Kostova AT, Tew KD. Oxidative Stress in Cancer. Cancer Cell. 2020;38(2):167-97.
204. Freire Boullosa L, Van Loenhout J, Deben C. Chapter 4 - Endogenous antioxidants in the prognosis and treatment of lung cancer. In: Preedy VR, Patel VB, editors. Cancer (Second Edition). San Diego: Academic Press; 2021. p. 39-48.
205. Sullivan LB, Chandel NS. Mitochondrial reactive oxygen species and cancer. Cancer Metab. 2014;2:17.
206. Jiang H, Wang H, De Ridder M. Targeting antioxidant enzymes as a radiosensitizing strategy. Cancer Lett. 2018;438:154-64.
207. Perry JJ, Shin DS, Getzoff ED, Tainer JA. The structural biochemistry of the superoxide dismutases. Biochim Biophys Acta. 2010;1804(2):245-62.
208. Zheng M, Liu Y, Zhang G, Yang Z, Xu W, Chen Q. The Applications and Mechanisms of Superoxide Dismutase in Medicine, Food, and Cosmetics. Antioxidants (Basel). 2023;12(9).
209. Glorieux C, Calderon PB. Catalase, a remarkable enzyme: targeting the oldest antioxidant enzyme to find a new cancer treatment approach. Biol Chem. 2017;398(10):1095-108.
210. Wilson JX. Antioxidant defense of the brain: a role for astrocytes. Canadian Journal of Physiology and Pharmacology. 1997;75(10-11):1149-63.
211. Powis G, Montfort WR. Properties and biological activities of thioredoxins. Annu Rev Pharmacol Toxicol. 2001;41:261-95.
212. Mishina NM, Bogdanova YA, Ermakova YG, Panova AS, Kotova DA, Bilan DS, et al. Which Antioxidant System Shapes Intracellular H(2)O(2) Gradients? Antioxid Redox Signal. 2019;31(9):664-70.
213. Naranjo-Suarez S, Carlson BA, Tobe R, Yoo MH, Tsuji PA, Gladyshev VN, et al. Regulation of HIF-1alpha activity by overexpression of thioredoxin is independent of thioredoxin reductase status. Mol Cells. 2013;36(2):151-7.
214. Woolston CM, Zhang L, Storr SJ, Al-Attar A, Shehata M, Ellis IO, et al. The prognostic and predictive power of redox protein expression for anthracycline-based chemotherapy response in locally advanced breast cancer. Mod Pathol. 2012;25(8):1106-16.
215. Selenius M, Hedman M, Brodin D, Gandin V, Rigobello MP, Flygare J, et al. Effects of redox modulation by inhibition of thioredoxin reductase on radiosensitivity and gene expression. J Cell Mol Med. 2012;16(7):1593-605.

216. Raffel J, Bhattacharyya AK, Gallegos A, Cui H, Einspahr JG, Alberts DS, et al. Increased expression of thioredoxin-1 in human colorectal cancer is associated with decreased patient survival. J Lab Clin Med. 2003;142(1):46-51.
217. Bhatia M, McGrath KL, Di Trapani G, Charoentong P, Shah F, King MM, et al. The thioredoxin system in breast cancer cell invasion and migration. Redox Biol. 2016;8:68-78.
218. Soini Y, Kahlos K, Näpänkangas U, Kaarteenaho-Wiik R, Säily M, Koistinen P, et al. Widespread expression of thioredoxin and thioredoxin reductase in non-small cell lung carcinoma. Clin Cancer Res. 2001;7(6):1750-7.
219. Lincoln DT, Ali Emadi EM, Tonissen KF, Clarke FM. The thioredoxin-thioredoxin reductase system: over-expression in human cancer. Anticancer Res. 2003;23(3b):2425-33.
220. Nishiyama A, Matsui M, Iwata S, Hirota K, Masutani H, Nakamura H, et al. Identification of thioredoxin-binding protein-2/vitamin D(3) up-regulated protein 1 as a negative regulator of thioredoxin function and expression. J Biol Chem. 1999;274(31):21645-50.
221. Onodera T, Momose I, Kawada M. Potential Anticancer Activity of Auranofin. Chem Pharm Bull (Tokyo). 2019;67(3):186-91.
222. Nishinaka Y, Nakamura H, Masutani H, Yodoi J. Redox control of cellular function by thioredoxin; a new therapeutic direction in host defence. Archivum Immunologiae Et Therapiae Experimentalis-English Edition-. 2001;49(4):285-92.
223. Engman L, Al-Maharik N, McNaughton M, Birmingham A, Powis G. Thioredoxin reductase and cancer cell growth inhibition by organotellurium antioxidants. Anticancer Drugs. 2003;14(2):153-61.
224. Luthman M, Holmgren A. Rat liver thioredoxin and thioredoxin reductase: purification and characterization. Biochemistry. 1982;21(26):6628-33.
225. Sun QA, Wu Y, Zappacosta F, Jeang KT, Lee BJ, Hatfield DL, et al. Redox regulation of cell signaling by selenocysteine in mammalian thioredoxin reductases. J Biol Chem. 1999;274(35):24522-30.
226. Söderberg A, Sahaf B, Rosén A. Thioredoxin reductase, a redox-active selenoprotein, is secreted by normal and neoplastic cells: presence in human plasma. Cancer Res. 2000;60(8):2281-9.
227. Mustacich D, Powis G. Thioredoxin reductase. Biochemical Journal. 2000;346(1):1-8.
228. Zhang J, Li X, Han X, Liu R, Fang J. Targeting the Thioredoxin System for Cancer Therapy. Trends Pharmacol Sci. 2017;38(9):794-808.
229. Matsuzawa A, Ichijo H. Redox control of cell fate by MAP kinase: physiological roles of ASK1-MAP kinase pathway in stress signaling. Biochim Biophys Acta. 2008;1780(11):1325-36.
230. Saitoh M, Nishitoh H, Fujii M, Takeda K, Tobiume K, Sawada Y, et al. Mammalian thioredoxin is a direct inhibitor of apoptosis signal-regulating kinase (ASK) 1. EMBO J. 1998;17(9):2596-606.
231. Lu J, Holmgren A. Thioredoxin system in cell death progression. Antioxid Redox Signal. 2012;17(12):1738-47.
232. Hanschmann EM, Godoy JR, Berndt C, Hudemann C, Lillig CH. Thioredoxins, glutaredoxins, and peroxiredoxins--molecular mechanisms and health significance: from cofactors to antioxidants to redox signaling. Antioxid Redox Signal. 2013;19(13):1539-605.
233. Esen H, Erdi F, Kaya B, Feyzioglu B, Keskin F, Demir LS. Tissue thioredoxin reductase-1 expression in astrocytomas of different grades. J Neurooncol. 2015;121(3):451-8.

234. Kahlos K, Soini Y, Saily M, Koistinen P, Kakko S, Paakko P, et al. Up-regulation of thioredoxin and thioredoxin reductase in human malignant pleural mesothelioma. Int J Cancer. 2001;95(3):198-204.
235. Mandal PK, Schneider M, Kolle P, Kuhlencordt P, Forster H, Beck H, et al. Loss of thioredoxin reductase 1 renders tumors highly susceptible to pharmacologic glutathione deprivation. Cancer Res. 2010;70(22):9505-14.
236. Gallegos A, Gasdaska JR, Taylor CW, Paine-Murrieta GD, Goodman D, Gasdaska PY, et al. Transfection with human thioredoxin increases cell proliferation and a dominant-negative mutant thioredoxin reverses the transformed phenotype of human breast cancer cells. Cancer Res. 1996;56(24):5765-70.
237. Farina AR, Cappabianca L, DeSantis G, Di Ianni N, Ruggeri P, Ragone M, et al. Thioredoxin stimulates MMP-9 expression, de-regulates the MMP-9/TIMP-1 equilibrium and promotes MMP-9 dependent invasion in human MDA-MB-231 breast cancer cells. FEBS Lett. 2011;585(20):3328-36.
238. Barnard PJ, Berners-Price SJ. Targeting the mitochondrial cell death pathway with gold compounds. Coordination Chemistry Reviews. 2007;251(13):1889-902.
239. Benhar M, Forrester MT, Hess DT, Stamler JS. Regulated protein denitrosylation by cytosolic and mitochondrial thioredoxins. Science. 2008;320(5879):1050-4.
240. Yoo MH, Xu XM, Carlson BA, Gladyshev VN, Hatfield DL. Thioredoxin reductase 1 deficiency reverses tumor phenotype and tumorigenicity of lung carcinoma cells. J Biol Chem. 2006;281(19):13005-8.
241. Yoo MH, Xu XM, Carlson BA, Patterson AD, Gladyshev VN, Hatfield DL. Targeting thioredoxin reductase 1 reduction in cancer cells inhibits self-sufficient growth and DNA replication. PLoS One. 2007;2(10):e1112.
242. Eriksson SE, Prast-Nielsen S, Flaberg E, Szekely L, Arner ES. High levels of thioredoxin reductase 1 modulate drug-specific cytotoxic efficacy. Free Radic Biol Med. 2009;47(11):1661-71.
243. Yao A, Storr SJ, Al-Hadyan K, Rahman R, Smith S, Grundy R, et al. Thioredoxin System Protein Expression Is Associated with Poor Clinical Outcome in Adult and Paediatric Gliomas and Medulloblastomas. Mol Neurobiol. 2020;57(7):2889-901.
244. Kemerdere R, Kacira T, Hanimoglu H, Kucur M, Tanriverdi T, Canbaz B. Tissue and plasma thioredoxin reductase expressions in patients with glioblastoma multiforme. J Neurol Surg A Cent Eur Neurosurg. 2013;74(4):234-8.
245. Meister A. Selective modification of glutathione metabolism. Science. 1983;220(4596):472-7.
246. Estrela JM, Ortega A, Obrador E. Glutathione in cancer biology and therapy. Crit Rev Clin Lab Sci. 2006;43(2):143-81.
247. Griffith OW. Biologic and pharmacologic regulation of mammalian glutathione synthesis. Free Radic Biol Med. 1999;27(9-10):922-35.
248. Dos Reis Oliveira C, Pereira JC, Barros Ibiapina A, Roseno Martins IR, de Castro ESJM, Ferreira PMP, et al. Buthionine sulfoximine and chemoresistance in cancer treatments: a systematic review with meta-analysis of preclinical studies. J Toxicol Environ Health B Crit Rev. 2023;26(8):417-41.
249. Harris IS, Treloar AE, Inoue S, Sasaki M, Gorrini C, Lee KC, et al. Glutathione and thioredoxin antioxidant pathways synergize to drive cancer initiation and progression. Cancer Cell. 2015;27(2):211-22.

250. Marinho HS, Real C, Cyrne L, Soares H, Antunes F. Hydrogen peroxide sensing, signaling and regulation of transcription factors. Redox Biol. 2014;2:535-62.
251. Fourquet S, Guerois R, Biard D, Toledano MB. Activation of NRF2 by nitrosative agents and H2O2 involves KEAP1 disulfide formation. J Biol Chem. 2010;285(11):8463-71.
252. Zhang H, Liu H, Davies KJ, Sioutas C, Finch CE, Morgan TE, et al. Nrf2-regulated phase II enzymes are induced by chronic ambient nanoparticle exposure in young mice with age-related impairments. Free Radic Biol Med. 2012;52(9):2038-46.
253. Sun Z, Wu T, Zhao F, Lau A, Birch CM, Zhang DD. KPNA6 (Importin alpha7)-mediated nuclear import of Keap1 represses the Nrf2-dependent antioxidant response. Mol Cell Biol. 2011;31(9):1800-11.
254. Cebula M, Schmidt EE, Arner ES. TrxR1 as a potent regulator of the Nrf2-Keap1 response system. Antioxid Redox Signal. 2015;23(10):823-53.
255. Singh CK, Chhabra G, Ndiaye MA, Garcia-Peterson LM, Mack NJ, Ahmad N. The Role of Sirtuins in Antioxidant and Redox Signaling. Antioxid Redox Signal. 2018;28(8):643-61.
256. Weng MS, Chang JH, Hung WY, Yang YC, Chien MH. The interplay of reactive oxygen species and the epidermal growth factor receptor in tumor progression and drug resistance. J Exp Clin Cancer Res. 2018;37(1):61.
257. Gamou S, Shimizu N. Hydrogen peroxide preferentially enhances the tyrosine phosphorylation of epidermal growth factor receptor. FEBS Lett. 1995;357(2):161-4.
258. Bae YS, Kang SW, Seo MS, Baines IC, Tekle E, Chock PB, et al. Epidermal Growth Factor (EGF)-induced Generation of Hydrogen Peroxide: Role In EGF Receptor-Mediated Tyrosine Phosphorylation *. Journal of Biological Chemistry. 1997;272(1):217-21.
259. Paulsen CE, Truong TH, Garcia FJ, Homann A, Gupta V, Leonard SE, et al. Peroxide-dependent sulfenylation of the EGFR catalytic site enhances kinase activity. Nat Chem Biol. 2011;8(1):57-64.
260. Truong TH, Carroll KS. Redox regulation of epidermal growth factor receptor signaling through cysteine oxidation. Biochemistry. 2012;51(50):9954-65.
261. Ravid T, Sweeney C, Gee P, Carraway KL, III, Goldkorn T. Epidermal Growth Factor Receptor Activation under Oxidative Stress Fails to Promote c-Cbl Mediated Down-regulation *. Journal of Biological Chemistry. 2002;277(34):31214-9.
262. Nitta M, Kozono D, Kennedy R, Stommel J, Ng K, Zinn PO, et al. Targeting EGFR induced oxidative stress by PARP1 inhibition in glioblastoma therapy. PLoS One. 2010;5(5):e10767.
263. Du W, Jiang P, Mancuso A, Stonestrom A, Brewer MD, Minn AJ, et al. TAp73 enhances the pentose phosphate pathway and supports cell proliferation. Nat Cell Biol. 2013;15(8):991-1000.
264. Kong Q, Beel JA, Lillehei KO. A threshold concept for cancer therapy. Med Hypotheses. 2000;55(1):29-35.
265. Liu Y, Li Q, Zhou L, Xie N, Nice EC, Zhang H, et al. Cancer drug resistance: redox resetting renders a way. Oncotarget. 2016;7(27):42740-61.
266. Yu Y, Di Trapani G, Tonissen KF. Thioredoxin and Glutathione Systems. In: Chakraborti S, Ray BK, Roychoudhury S, editors. Handbook of Oxidative Stress in Cancer: Mechanistic Aspects. Singapore: Springer Nature Singapore; 2022. p. 2407-20.
267. Ren X, Zou L, Zhang X, Branco V, Wang J, Carvalho C, et al. Redox Signaling Mediated by Thioredoxin and Glutathione Systems in the Central Nervous System. Antioxid Redox Signal. 2017;27(13):989-1010.
268. Jaganjac M, Milkovic L, Sunjic SB, Zarkovic N. The NRF2, Thioredoxin, and Glutathione System in Tumorigenesis and Anticancer Therapies. Antioxidants (Basel). 2020;9(11).

269. Lee S, Kim SM, Lee RT. Thioredoxin and thioredoxin target proteins: from molecular mechanisms to functional significance. Antioxid Redox Signal. 2013;18(10):1165-207.
270. Sutton BM, McGusty E, Walz DT, DiMartino MJ. Oral gold. Antiarthritic properties of alkylphosphinegold coordination complexes. J Med Chem. 1972;15(11):1095-8.
271. Madeira JM, Gibson DL, Kean WF, Klegeris A. The biological activity of auranofin: implications for novel treatment of diseases. Inflammopharmacology. 2012;20(6):297-306.
272. Kupiec M, Ziolkowski R, Massai L, Messori L, Pawlak K. The electrochemical profiles of Auranofin and Aubipy(c), two representative medicinal gold compounds: A comparative study. J Inorg Biochem. 2019;198:110714.
273. Zoppi C, Messori L, Pratesi A. ESI MS studies highlight the selective interaction of Auranofin with protein free thiols. Dalton Trans. 2020;49(18):5906-13.
274. Abdalbari FH, Telleria CM. The gold complex auranofin: new perspectives for cancer therapy. Discov Oncol. 2021;12(1):42.
275. Madeira JM, Renschler CJ, Mueller B, Hashioka S, Gibson DL, Klegeris A. Novel protective properties of auranofin: inhibition of human astrocyte cytotoxic secretions and direct neuroprotection. Life Sci. 2013;92(22):1072-80.
276. Shaw CF, 3rd, Schmitz G, Thompson HO, Witkiewicz P. Bis(L-cysteinato)gold(I): chemical characterization and identification in renal cortical cytoplasm. J Inorg Biochem. 1979;10(4):317-30.
277. Kean WF, Kean IR. Clinical pharmacology of gold. Inflammopharmacology. 2008;16(3):112-25.
278. Walz DT, DiMartino MJ, Griswold DE. The pharmacological profile of auranofin, an orally active gold compound. Scand J Rheumatol Suppl. 1983;51:16-25.
279. Giannini EH, Brewer EJ, Person DA. Blood gold concentrations in children with juvenile rheumatoid arthritis undergoing long-term oral gold therapy. Annals of the Rheumatic Diseases. 1984;43(2):228-31.
280. Blocka KL, Paulus HE, Furst DE. Clinical pharmacokinetics of oral and injectable gold compounds. Clin Pharmacokinet. 1986;11(2):133-43.
281. Intoccia AP, Flanagan TL, Walz DT, Gutzait L, Swagzdis JE, Flagiello J, et al. Pharmacokinetics of auranofin in animals. J Rheumatol Suppl. 1982;8:90-8.
282. Furst DE, Dromgoole SH. Comparative pharmacokinetics of triethylphosphine gold (auranofin) and gold sodium thiomalate (GST). Clin Rheumatol. 1984;3 Suppl 1:17-24.
283. Rackham O, Shearwood AM, Thyer R, McNamara E, Davies SM, Callus BA, et al. Substrate and inhibitor specificities differ between human cytosolic and mitochondrial thioredoxin reductases: Implications for development of specific inhibitors. Free Radic Biol Med. 2011;50(6):689-99.
284. Gandin V, Fernandes AP, Rigobello MP, Dani B, Sorrentino F, Tisato F, et al. Cancer cell death induced by phosphine gold(I) compounds targeting thioredoxin reductase. Biochem Pharmacol. 2010;79(2):90-101.
285. Bindoli A, Rigobello MP, Scutari G, Gabbiani C, Casini A, Messori L. Thioredoxin reductase: A target for gold compounds acting as potential anticancer drugs. Coordination Chemistry Reviews. 2009;253(11):1692-707.
286. Rigobello MP, Scutari G, Folda A, Bindoli A. Mitochondrial thioredoxin reductase inhibition by gold(I) compounds and concurrent stimulation of permeability transition and release of cytochrome c. Biochem Pharmacol. 2004;67(4):689-96.

287. Rigobello MP, Folda A, Baldoin MC, Scutari G, Bindoli A. Effect of auranofin on the mitochondrial generation of hydrogen peroxide. Role of thioredoxin reductase. Free Radic Res. 2005;39(7):687-95.
288. Nobili S, Mini E, Landini I, Gabbiani C, Casini A, Messori L. Gold compounds as anticancer agents: chemistry, cellular pharmacology, and preclinical studies. Med Res Rev. 2010;30(3):550-80.
289. Magherini F, Modesti A, Bini L, Puglia M, Landini I, Nobili S, et al. Exploring the biochemical mechanisms of cytotoxic gold compounds: a proteomic study. J Biol Inorg Chem. 2010;15(4):573-82.
290. Gasdaska PY, Oblong JE, Cotgreave IA, Powis G. The predicted amino acid sequence of human thioredoxin is identical to that of the autocrine growth factor human adult T-cell derived factor (ADF): thioredoxin mRNA is elevated in some human tumors. Biochim Biophys Acta. 1994;1218(3):292-6.
291. Lim JY, Yoon SO, Hong SW, Kim JW, Choi SH, Cho JY. Thioredoxin and thioredoxin-interacting protein as prognostic markers for gastric cancer recurrence. World J Gastroenterol. 2012;18(39):5581-8.
292. Nakamura H, Bai J, Nishinaka Y, Ueda S, Sasada T, Ohshio G, et al. Expression of thioredoxin and glutaredoxin, redox-regulating proteins, in pancreatic cancer. Cancer Detect Prev. 2000;24(1):53-60.
293. Wang J, Kobayashi M, Sakurada K, Imamura M, Moriuchi T, Hosokawa M. Possible Roles of an Adult T-Cell Leukemia (ATL)-Derived Factor/Thioredoxin in the Drug Resistance of ATL to Adriamycin. Blood. 1997;89(7):2480-7.
294. Yokomizo A, Ono M, Nanri H, Makino Y, Ohga T, Wada M, et al. Cellular levels of thioredoxin associated with drug sensitivity to cisplatin, mitomycin C, doxorubicin, and etoposide. Cancer Research. 1995;55(19):4293-6.
295. Raninga PV, Di Trapani G, Vuckovic S, Tonissen KF. TrxR1 inhibition overcomes both hypoxia-induced and acquired bortezomib resistance in multiple myeloma through NF-small ka, Cyrillicbeta inhibition. Cell Cycle. 2016;15(4):559-72.
296. Fiskus W, Saba N, Shen M, Ghias M, Liu J, Gupta SD, et al. Auranofin induces lethal oxidative and endoplasmic reticulum stress and exerts potent preclinical activity against chronic lymphocytic leukemia. Cancer Res. 2014;74(9):2520-32.
297. Chen X, Shi X, Zhao C, Li X, Lan X, Liu S, et al. Anti-rheumatic agent auranofin induced apoptosis in chronic myeloid leukemia cells resistant to imatinib through both Bcr/Abl-dependent and -independent mechanisms. Oncotarget. 2014;5(19):9118-32.
298. Cox AG, Brown KK, Arner ES, Hampton MB. The thioredoxin reductase inhibitor auranofin triggers apoptosis through a Bax/Bak-dependent process that involves peroxiredoxin 3 oxidation. Biochem Pharmacol. 2008;76(9):1097-109.
299. Wang J, Wang J, Lopez E, Guo H, Zhang H, Liu Y, et al. Repurposing auranofin to treat TP53-mutated or PTEN-deleted refractory B-cell lymphoma. Blood Cancer J. 2019;9(12):95.
300. Kim NH, Park HJ, Oh MK, Kim IS. Antiproliferative effect of gold(I) compound auranofin through inhibition of STAT3 and telomerase activity in MDA-MB 231 human breast cancer cells. BMB Rep. 2013;46(1):59-64.
301. Liu N, Li X, Huang H, Zhao C, Liao S, Yang C, et al. Clinically used antirheumatic agent auranofin is a proteasomal deubiquitinase inhibitor and inhibits tumor growth. Oncotarget. 2014;5(14):5453-71.

302. Kim SJ, Ju JS, Kang MH, Eun JW, Kim YH, Raninga PV, et al. RNA-binding protein NONO contributes to cancer cell growth and confers drug resistance as a theranostic target in TNBC. Theranostics. 2020;10(18):7974-92.
303. Li H, Hu J, Wu S, Wang L, Cao X, Zhang X, et al. Auranofin-mediated inhibition of PI3K/AKT/mTOR axis and anticancer activity in non-small cell lung cancer cells. Oncotarget. 2016;7(3):3548-58.
304. Yan X, Zhang X, Wang L, Zhang R, Pu X, Wu S, et al. Inhibition of Thioredoxin/Thioredoxin Reductase Induces Synthetic Lethality in Lung Cancers with Compromised Glutathione Homeostasis. Cancer Res. 2019;79(1):125-32.
305. Cui XY, Park SH, Park WH. Anti-Cancer Effects of Auranofin in Human Lung Cancer Cells by Increasing Intracellular ROS Levels and Depleting GSH Levels. Molecules. 2022;27(16).
306. Cui XY, Park SH, Park WH. Auranofin inhibits the proliferation of lung cancer cells via necrosis and caspase-dependent apoptosis. Oncol Rep. 2020;44(6):2715-24.
307. Marzano C, Gandin V, Folda A, Scutari G, Bindoli A, Rigobello MP. Inhibition of thioredoxin reductase by auranofin induces apoptosis in cisplatin-resistant human ovarian cancer cells. Free Radic Biol Med. 2007;42(6):872-81.
308. Guidi F, Landini I, Puglia M, Magherini F, Gabbiani C, Cinellu MA, et al. Proteomic analysis of ovarian cancer cell responses to cytotoxic gold compounds. Metallomics. 2012;4(3):307-14.
309. Wang Y, Hill KS, Fields AP. PKCiota maintains a tumor-initiating cell phenotype that is required for ovarian tumorigenesis. Mol Cancer Res. 2013;11(12):1624-35.
310. Park SH, Lee JH, Berek JS, Hu MC. Auranofin displays anticancer activity against ovarian cancer cells through FOXO3 activation independent of p53. Int J Oncol. 2014;45(4):1691-8.
311. Marzo T, Massai L, Pratesi A, Stefanini M, Cirri D, Magherini F, et al. Replacement of the Thiosugar of Auranofin with Iodide Enhances the Anticancer Potency in a Mouse Model of Ovarian Cancer. ACS Med Chem Lett. 2019;10(4):656-60.
312. Kim NH, Lee MY, Park SJ, Choi JS, Oh MK, Kim IS. Auranofin blocks interleukin-6 signalling by inhibiting phosphorylation of JAK1 and STAT3. Immunology. 2007;122(4):607-14.
313. Park N, Chun YJ. Auranofin promotes mitochondrial apoptosis by inducing annexin A5 expression and translocation in human prostate cancer cells. J Toxicol Environ Health A. 2014;77(22-24):1467-76.
314. Baek HS, Park N, Kwon YJ, Ye DJ, Shin S, Chun YJ. Annexin A5 suppresses cyclooxygenase-2 expression by downregulating the protein kinase C-zeta-nuclear factor-kappaB signaling pathway in prostate cancer cells. Oncotarget. 2017;8(43):74263-75.
315. Liu N, Guo Z, Xia X, Liao Y, Zhang F, Huang C, et al. Auranofin lethality to prostate cancer includes inhibition of proteasomal deubiquitinases and disrupted androgen receptor signaling. Eur J Pharmacol. 2019;846:1-11.
316. Shin DW, Kwon YJ, Ye DJ, Baek HS, Lee JE, Chun YJ. Auranofin Suppresses Plasminogen Activator Inhibitor-2 Expression through Annexin A5 Induction in Human Prostate Cancer Cells. Biomol Ther (Seoul). 2017;25(2):177-85.
317. Li L, Fath MA, Scarbrough PM, Watson WH, Spitz DR. Combined inhibition of glycolysis, the pentose cycle, and thioredoxin metabolism selectively increases cytotoxicity and oxidative stress in human breast and prostate cancer. Redox Biol. 2015;4:127-35.
318. Onodera T, Momose I, Adachi H, Yamazaki Y, Sawa R, Ohba SI, et al. Human pancreatic cancer cells under nutrient deprivation are vulnerable to redox system inhibition. J Biol Chem. 2020;295(49):16678-90.

319. Pessetto ZY, Chen B, Alturkmani H, Hyter S, Flynn CA, Baltezor M, et al. In silico and in vitro drug screening identifies new therapeutic approaches for Ewing sarcoma. Oncotarget. 2017;8(3):4079-95.
320. Mirabelli CK, Johnson RK, Sung CM, Faucette L, Muirhead K, Crooke ST. Evaluation of the in vivo antitumor activity and in vitro cytotoxic properties of auranofin, a coordinated gold compound, in murine tumor models. Cancer research. 1985;45(1):32-9.
321. Goenka S, Simon SR. Organogold drug Auranofin exhibits anti-melanogenic activity in B16F10 and MNT-1 melanoma cells. Arch Dermatol Res. 2020;312(3):213-21.
322. You BR, Shin HR, Han BR, Kim SH, Park WH. Auranofin induces apoptosis and necrosis in HeLa cells via oxidative stress and glutathione depletion. Mol Med Rep. 2015;11(2):1428-34.
323. Van Loenhout J, Freire Boullosa L, Quatannens D, De Waele J, Merlin C, Lambrechts H, et al. Auranofin and Cold Atmospheric Plasma Synergize to Trigger Distinct Cell Death Mechanisms and Immunogenic Responses in Glioblastoma. Cells. 2021;10(11).
324. Szeliga M, Rola R. Menadione Potentiates Auranofin-Induced Glioblastoma Cell Death. Int J Mol Sci. 2022;23(24).
325. Krabbendam IE, Honrath B, Bothof L, Silva-Pavez E, Huerta H, Penaranda Fajardo NM, et al. SK channel activation potentiates auranofin-induced cell death in glio- and neuroblastoma cells. Biochem Pharmacol. 2020;171:113714.
326. Stafford WC, Peng X, Olofsson MH, Zhang X, Luci DK, Lu L, et al. Irreversible inhibition of cytosolic thioredoxin reductase 1 as a mechanistic basis for anticancer therapy. Sci Transl Med. 2018;10(428).
327. Arner ESJ. Targeting the Selenoprotein Thioredoxin Reductase 1 for Anticancer Therapy. Adv Cancer Res. 2017;136:139-51.
328. Zou P, Chen M, Ji J, Chen W, Chen X, Ying S, et al. Auranofin induces apoptosis by ROS-mediated ER stress and mitochondrial dysfunction and displayed synergistic lethality with piperlongumine in gastric cancer. Oncotarget. 2015;6(34):36505-21.
329. Dai B, Yoo SY, Bartholomeusz G, Graham RA, Majidi M, Yan S, et al. KEAP1-dependent synthetic lethality induced by AKT and TXNRD1 inhibitors in lung cancer. Cancer Res. 2013;73(17):5532-43.
330. Arrigo A, Regua AT, Najjar MK, Lo HW. Tumor Suppressor Candidate 2 (TUSC2): Discovery, Functions, and Cancer Therapy. Cancers (Basel). 2023;15(9).
331. Hou GX, Liu PP, Zhang S, Yang M, Liao J, Yang J, et al. Elimination of stem-like cancer cell side-population by auranofin through modulation of ROS and glycolysis. Cell Death Dis. 2018;9(2):89.
332. Kaczmarek LK, Aldrich RW, Chandy KG, Grissmer S, Wei AD, Wulff H. International Union of Basic and Clinical Pharmacology. C. Nomenclature and Properties of Calcium-Activated and Sodium-Activated Potassium Channels. Pharmacol Rev. 2017;69(1):1-11.
333. Zhang X, Selvaraju K, Saei AA, D'Arcy P, Zubarev RA, Arner ES, et al. Repurposing of auranofin: Thioredoxin reductase remains a primary target of the drug. Biochimie. 2019;162:46-54.
334. Busker S, Qian W, Haraldsson M, Espinosa B, Johansson L, Attarha S, et al. Irreversible TrxR1 inhibitors block STAT3 activity and induce cancer cell death. Sci Adv. 2020;6(12):eaax7945.
335. Kast RE, Boockvar JA, Bruning A, Cappello F, Chang WW, Cvek B, et al. A conceptually new treatment approach for relapsed glioblastoma: coordinated undermining of survival paths with nine repurposed drugs (CUSP9) by the International Initiative for Accelerated Improvement of Glioblastoma Care. Oncotarget. 2013;4(4):502-30.

336. Skaga E, Skaga IO, Grieg Z, Sandberg CJ, Langmoen IA, Vik-Mo EO. The efficacy of a coordinated pharmacological blockade in glioblastoma stem cells with nine repurposed drugs using the CUSP9 strategy. J Cancer Res Clin Oncol. 2019;145(6):1495-507.
337. Halatsch M-E, Kast R, Karpel-Massler G, Mayer B, Zolk O, Schmitz B, et al. CTNI-04. Recurrent Glioblastoma Long-Term Survivors Treated With CUSP9v3. Neuro-Oncology. 2021;23(Supplement_6):vi59-vi.
338. Bailey HH. L-S,R-buthionine sulfoximine: historical development and clinical issues. Chem Biol Interact. 1998;111-112:239-54.
339. Dorr RT, Liddil JD, Soble MJ. Cytotoxic effects of glutathione synthesis inhibition by L-buthionine-(SR)-sulfoximine on human and murine tumor cells. Invest New Drugs. 1986;4(4):305-13.
340. Cruz A, Mota P, Ramos C, Pires RF, Mendes C, Silva JP, et al. Polyurea Dendrimer Folate-Targeted Nanodelivery of l-Buthionine sulfoximine as a Tool to Tackle Ovarian Cancer Chemoresistance. Antioxidants (Basel). 2020;9(2).
341. Sun G, Hu W, Zhang J, Jing S. Study on effect of BSO on esophageal cancer cell line TE-1. The Chinese-German Journal of Clinical Oncology. 2012;11(11):638-43.
342. Lee M, Jo A, Lee S, Kim JB, Chang Y, Nam JY, et al. 3-bromopyruvate and buthionine sulfoximine effectively kill anoikis-resistant hepatocellular carcinoma cells. PLoS One. 2017;12(3):e0174271.
343. Anderson CP, Tsai JM, Meek WE, Liu R-M, Tang Y, Forman HJ, et al. Depletion of Glutathione by Buthionine Sulfoximine Is Cytotoxic for Human Neuroblastoma Cell Lines via Apoptosis. Experimental Cell Research. 1999;246(1):183-92.
344. Révész L, Edgren MR, Wainson AA. Selective toxicity of buthionine sulfoximine (BSO) to melanoma cells in vitro and in vivo. International Journal of Radiation Oncology*Biology*Physics. 1994;29(2):403-6.
345. Griffith OW, Meister A. Potent and specific inhibition of glutathione synthesis by buthionine sulfoximine (S-n-butyl homocysteine sulfoximine). J Biol Chem. 1979;254(16):7558-60.
346. Griffith OW. Mechanism of action, metabolism, and toxicity of buthionine sulfoximine and its higher homologs, potent inhibitors of glutathione synthesis. J Biol Chem. 1982;257(22):13704-12.
347. Son MH, Kang KW, Lee CH, Kim SG. Potentiation of cadmium-induced cytotoxicity by sulfur amino acid deprivation through activation of extracellular signal-regulated kinase1/2 (ERK1/2) in conjunction with p38 kinase or c-jun N-terminal kinase (JNK). Complete inhibition of the potentiated toxicity by U0126 an ERK1/2 and p38 kinase inhibitor. Biochem Pharmacol. 2001;62(10):1379-90.
348. Watanabe T, Sagisaka H, Arakawa S, Shibaya Y, Watanabe M, Igarashi I, et al. A novel model of continuous depletion of glutathione in mice treated with L-buthionine (S,R)-sulfoximine. J Toxicol Sci. 2003;28(5):455-69.
349. Martensson J, Jain A, Stole E, Frayer W, Auld PA, Meister A. Inhibition of glutathione synthesis in the newborn rat: a model for endogenously produced oxidative stress. Proc Natl Acad Sci U S A. 1991;88(20):9360-4.
350. Villablanca JG, Volchenboum SL, Cho H, Kang MH, Cohn SL, Anderson CP, et al. A Phase I New Approaches to Neuroblastoma Therapy Study of Buthionine Sulfoximine and Melphalan With Autologous Stem Cells for Recurrent/Refractory High-Risk Neuroblastoma. Pediatr Blood Cancer. 2016;63(8):1349-56.

351. Curtis J, Hedley DW, Minden MD, Moore MA, McCulloch EA, editors. Antileukemic Effects of Buthionine Sulfoximine (BSO) (NSC 326231) in Vivo: A Pilot Study in Acute Myeloblastic Leukemia. Acute Leukemias VIII; 2001 2001//; Berlin, Heidelberg: Springer Berlin Heidelberg.
352. Bailey HH, Mulcahy RT, Tutsch KD, Arzoomanian RZ, Alberti D, Tombes MB, et al. Phase I clinical trial of intravenous L-buthionine sulfoximine and melphalan: an attempt at modulation of glutathione. Journal of Clinical Oncology. 1994;12(1):194-205.
353. Anderson CP, Reynolds CP. Synergistic cytotoxicity of buthionine sulfoximine (BSO) and intensive melphalan (L-PAM) for neuroblastoma cell lines established at relapse after myeloablative therapy. Bone Marrow Transplant. 2002;30(3):135-40.
354. Lane DP. Cancer. p53, guardian of the genome. Nature. 1992;358(6381):15-6.
355. Hernández Borrero LJ, El-Deiry WS. Tumor suppressor p53: Biology, signaling pathways, and therapeutic targeting. Biochimica et Biophysica Acta (BBA) - Reviews on Cancer. 2021;1876(1):188556.
356. Perdrix A, Najem A, Saussez S, Awada A, Journe F, Ghanem G, et al. PRIMA-1 and PRIMA-1(Met) (APR-246): From Mutant/Wild Type p53 Reactivation to Unexpected Mechanisms Underlying Their Potent Anti-Tumor Effect in Combinatorial Therapies. Cancers (Basel). 2017;9(12).
357. Leroy K, Haioun C, Lepage E, Le Metayer N, Berger F, Labouyrie E, et al. p53 gene mutations are associated with poor survival in low and low-intermediate risk diffuse large B-cell lymphomas. Ann Oncol. 2002;13(7):1108-15.
358. Zhang Y, Dube C, Gibert M, Jr., Cruickshanks N, Wang B, Coughlan M, et al. The p53 Pathway in Glioblastoma. Cancers (Basel). 2018;10(9).
359. Peng Y, Chen L, Li C, Lu W, Chen J. Inhibition of MDM2 by hsp90 contributes to mutant p53 stabilization. J Biol Chem. 2001;276(44):40583-90.
360. Rivlin N, Brosh R, Oren M, Rotter V. Mutations in the p53 Tumor Suppressor Gene: Important Milestones at the Various Steps of Tumorigenesis. Genes Cancer. 2011;2(4):466-74.
361. Grombacher T, Eichhorn U, Kaina B. p53 is involved in regulation of the DNA repair gene O6-methylguanine-DNA methyltransferase (MGMT) by DNA damaging agents. Oncogene. 1998;17(7):845-51.
362. Patyka M, Sharifi Z, Petrecca K, Mansure J, Jean-Claude B, Sabri S. Sensitivity to PRIMA-1MET is associated with decreased MGMT in human glioblastoma cells and glioblastoma stem cells irrespective of p53 status. Oncotarget. 2016;7(37):60245-69.
363. Amelio I, Melino G. Context is everything: extrinsic signalling and gain-of-function p53 mutants. Cell Death Discovery. 2020;6(1):16.
364. Wang G, Wang J, Li B, Sun Y, Ding Z, Ding C, editors. p53-Induced ROS-accumulation induces programmed cell death in C6 glioma cells. 2014 International Conference on Information Science, Electronics and Electrical Engineering; 2014 26-28 April 2014.
365. Wojnarowicz PM, Oros KK, Quinn MC, Arcand SL, Gambaro K, Madore J, et al. The genomic landscape of TP53 and p53 annotated high grade ovarian serous carcinomas from a defined founder population associated with patient outcome. PLoS One. 2012;7(9):e45484.
366. Matulonis UA, Sood AK, Fallowfield L, Howitt BE, Sehouli J, Karlan BY. Ovarian cancer. Nat Rev Dis Primers. 2016;2:16061.
367. Jayson GC, Kohn EC, Kitchener HC, Ledermann JA. Ovarian cancer. Lancet. 2014;384(9951):1376-88.
368. Cancer Genome Atlas Research N. Integrated genomic analyses of ovarian carcinoma. Nature. 2011;474(7353):609-15.

369. Xue W, Zender L, Miething C, Dickins RA, Hernando E, Krizhanovsky V, et al. Senescence and tumour clearance is triggered by p53 restoration in murine liver carcinomas. Nature. 2007;445(7128):656-60.
370. Ventura A, Kirsch DG, McLaughlin ME, Tuveson DA, Grimm J, Lintault L, et al. Restoration of p53 function leads to tumour regression in vivo. Nature. 2007;445(7128):661-5.
371. Martins CP, Brown-Swigart L, Evan GI. Modeling the therapeutic efficacy of p53 restoration in tumors. Cell. 2006;127(7):1323-34.
372. Bykov VJ, Issaeva N, Shilov A, Hultcrantz M, Pugacheva E, Chumakov P, et al. Restoration of the tumor suppressor function to mutant p53 by a low-molecular-weight compound. Nat Med. 2002;8(3):282-8.
373. Bykov VJ, Issaeva N, Zache N, Shilov A, Hultcrantz M, Bergman J, et al. Reactivation of mutant p53 and induction of apoptosis in human tumor cells by maleimide analogs. J Biol Chem. 2005;280(34):30384-91.
374. Foster BA, Coffey HA, Morin MJ, Rastinejad F. Pharmacological rescue of mutant p53 conformation and function. Science. 1999;286(5449):2507-10.
375. Bykov VJ, Wiman KG. Mutant p53 reactivation by small molecules makes its way to the clinic. FEBS Lett. 2014;588(16):2622-7.
376. Martinez JD. Restoring p53 tumor suppressor activity as an anticancer therapeutic strategy. Future Oncol. 2010;6(12):1857-62.
377. Brown CJ, Cheok CF, Verma CS, Lane DP. Reactivation of p53: from peptides to small molecules. Trends Pharmacol Sci. 2011;32(1):53-62.
378. Khoo KH, Verma CS, Lane DP. Drugging the p53 pathway: understanding the route to clinical efficacy. Nat Rev Drug Discov. 2014;13(3):217-36.
379. Weinmann L, Wischhusen J, Demma MJ, Naumann U, Roth P, Dasmahapatra B, et al. A novel p53 rescue compound induces p53-dependent growth arrest and sensitises glioma cells to Apo2L/TRAIL-induced apoptosis. Cell Death Differ. 2008;15(4):718-29.
380. Wischhusen J, Naumann U, Ohgaki H, Rastinejad F, Weller M. CP-31398, a novel p53-stabilizing agent, induces p53-dependent and p53-independent glioma cell death. Oncogene. 2003;22(51):8233-45.
381. Zandi R, Selivanova G, Christensen CL, Gerds TA, Willumsen BM, Poulsen HS. PRIMA-1Met/APR-246 induces apoptosis and tumor growth delay in small cell lung cancer expressing mutant p53. Clin Cancer Res. 2011;17(9):2830-41.
382. Shen J, Vakifahmetoglu H, Stridh H, Zhivotovsky B, Wiman KG. PRIMA-1MET induces mitochondrial apoptosis through activation of caspase-2. Oncogene. 2008;27(51):6571-80.
383. Bykov VJ, Zache N, Stridh H, Westman J, Bergman J, Selivanova G, et al. PRIMA-1(MET) synergizes with cisplatin to induce tumor cell apoptosis. Oncogene. 2005;24(21):3484-91.
384. Bykov VJ, Zhang Q, Zhang M, Ceder S, Abrahmsen L, Wiman KG. Targeting of Mutant p53 and the Cellular Redox Balance by APR-246 as a Strategy for Efficient Cancer Therapy. Front Oncol. 2016;6:21.
385. Supiot S, Zhao H, Wiman K, Hill RP, Bristow RG. PRIMA-1(met) radiosensitizes prostate cancer cells independent of their MTp53-status. Radiother Oncol. 2008;86(3):407-11.
386. Bao W, Chen M, Zhao X, Kumar R, Spinnler C, Thullberg M, et al. PRIMA-1Met/APR-246 induces wild-type p53-dependent suppression of malignant melanoma tumor growth in 3D culture and in vivo. Cell Cycle. 2011;10(2):301-7.

387. Lehmann S, Bykov VJ, Ali D, Andren O, Cherif H, Tidefelt U, et al. Targeting p53 in vivo: a first-in-human study with p53-targeting compound APR-246 in refractory hematologic malignancies and prostate cancer. J Clin Oncol. 2012;30(29):3633-9.
388. von Euler M, Wiman KG, Gabra H, Brenton JD, Basu B, Vergote I, et al. Abstract CT204: Preliminary results from PiSARRO, a phase Ib/II study of APR-246, a mutant p53 reactivating small molecule, in combination with standard chemotherapy in platinum-sensitive ovarian cancer. Cancer Research. 2015;75(15_Supplement):CT204-CT.
389. Lehmann S, Bykov VJN, Ali D, Andrén O, Cherif H, Tidefelt U, et al. Targeting p53 in Vivo: A First-in-Human Study With p53-Targeting Compound APR-246 in Refractory Hematologic Malignancies and Prostate Cancer. Journal of Clinical Oncology. 2012;30(29):3633-9.
390. Lambert JM, Gorzov P, Veprintsev DB, Soderqvist M, Segerback D, Bergman J, et al. PRIMA-1 reactivates mutant p53 by covalent binding to the core domain. Cancer Cell. 2009;15(5):376-88.
391. Zhang Q, Bykov VJN, Wiman KG, Zawacka-Pankau J. APR-246 reactivates mutant p53 by targeting cysteines 124 and 277. Cell Death Dis. 2018;9(5):439.
392. Wassman CD, Baronio R, Demir O, Wallentine BD, Chen CK, Hall LV, et al. Computational identification of a transiently open L1/S3 pocket for reactivation of mutant p53. Nat Commun. 2013;4:1407.
393. Blough MD, Zlatescu MC, Cairncross JG. O6-methylguanine-DNA methyltransferase regulation by p53 in astrocytic cells. Cancer Res. 2007;67(2):580-4.
394. Bocangel D, Sengupta S, Mitra S, Bhakat KK. p53-Mediated down-regulation of the human DNA repair gene O6-methylguanine-DNA methyltransferase (MGMT) via interaction with Sp1 transcription factor. Anticancer Research. 2009;29(10):3741-50.
395. Liu DS, Duong CP, Haupt S, Montgomery KG, House CM, Azar WJ, et al. Inhibiting the system x(C)(-)/glutathione axis selectively targets cancers with mutant-p53 accumulation. Nat Commun. 2017;8:14844.
396. Ceder S, Eriksson SE, Cheteh EH, Dawar S, Corrales Benitez M, Bykov VJN, et al. A thiol-bound drug reservoir enhances APR-246-induced mutant p53 tumor cell death. EMBO Mol Med. 2021;13(2):e10852.
397. Peng X, Zhang MQ, Conserva F, Hosny G, Selivanova G, Bykov VJ, et al. APR-246/PRIMA-1MET inhibits thioredoxin reductase 1 and converts the enzyme to a dedicated NADPH oxidase. Cell Death Dis. 2013;4(10):e881.
398. Yoshikawa N, Kajiyama H, Nakamura K, Utsumi F, Niimi K, Mitsui H, et al. PRIMA-1MET induces apoptosis through accumulation of intracellular reactive oxygen species irrespective of p53 status and chemo-sensitivity in epithelial ovarian cancer cells. Oncol Rep. 2016;35(5):2543-52.
399. Tessoulin B, Descamps G, Moreau P, Maiga S, Lode L, Godon C, et al. PRIMA-1Met induces myeloma cell death independent of p53 by impairing the GSH/ROS balance. Blood. 2014;124(10):1626-36.
400. Mohell N, Alfredsson J, Fransson A, Uustalu M, Bystrom S, Gullbo J, et al. APR-246 overcomes resistance to cisplatin and doxorubicin in ovarian cancer cells. Cell Death Dis. 2015;6(6):e1794.
401. Ali D, Mohammad DK, Mujahed H, Jonson-Videsater K, Nore B, Paul C, et al. Anti-leukaemic effects induced by APR-246 are dependent on induction of oxidative stress and the NFE2L2/HMOX1 axis that can be targeted by PI3K and mTOR inhibitors in acute myeloid leukaemia cells. Br J Haematol. 2016;174(1):117-26.

402. Fujihara KM, Corrales Benitez M, Cabalag CS, Zhang BZ, Ko HS, Liu DS, et al. SLC7A11 Is a Superior Determinant of APR-246 (Eprenetapopt) Response than TP53 Mutation Status. Mol Cancer Ther. 2021;20(10):1858-67.
403. Wallis B, Bowman KR, Lu P, Lim CS. The Challenges and Prospects of p53-Based Therapies in Ovarian Cancer. Biomolecules. 2023;13(1).
404. Ropolo M, Daga A, Griffero F, Foresta M, Casartelli G, Zunino A, et al. Comparative analysis of DNA repair in stem and nonstem glioma cell cultures. Mol Cancer Res. 2009;7(3):383-92.
405. Bonm A, Kesari S. DNA Damage Response in Glioblastoma: Mechanism for Treatment Resistance and Emerging Therapeutic Strategies. Cancer J. 2021;27(5):379-85.
406. Leonetti C, Biroccio A, Graziani G, Tentori L. Targeted therapy for brain tumours: role of PARP inhibitors. Curr Cancer Drug Targets. 2012;12(3):218-36.
407. Isabelle M, Moreel X, Gagne JP, Rouleau M, Ethier C, Gagne P, et al. Investigation of PARP-1, PARP-2, and PARG interactomes by affinity-purification mass spectrometry. Proteome Sci. 2010;8:22.
408. Smith SJ, Long A, Barrow JH, Macarthur DC, Coyle B, Grundy RG, et al. Pediatric high-grade glioma: identification of poly(ADP-ribose) polymerase as a potential therapeutic target. Neuro Oncol. 2011;13(11):1171-7.
409. Galia A, Calogero AE, Condorelli R, Fraggetta F, La Corte A, Ridolfo F, et al. PARP-1 protein expression in glioblastoma multiforme. Eur J Histochem. 2012;56(1):e9.
410. Schreiber V, Dantzer F, Ame JC, de Murcia G. Poly(ADP-ribose): novel functions for an old molecule. Nat Rev Mol Cell Biol. 2006;7(7):517-28.
411. Scalia M, Satriano C, Greca R, Stella AM, Rizzarelli E, Spina-Purrello V. PARP-1 inhibitors DPQ and PJ-34 negatively modulate proinflammatory commitment of human glioblastoma cells. Neurochem Res. 2013;38(1):50-8.
412. Higuchi F, Nagashima H, Ning J, Koerner MVA, Wakimoto H, Cahill DP. Restoration of Temozolomide Sensitivity by PARP Inhibitors in Mismatch Repair Deficient Glioblastoma is Independent of Base Excision Repair. Clin Cancer Res. 2020;26(7):1690-9.
413. Dungey FA, Loser DA, Chalmers AJ. Replication-dependent radiosensitization of human glioma cells by inhibition of poly(ADP-Ribose) polymerase: mechanisms and therapeutic potential. Int J Radiat Oncol Biol Phys. 2008;72(4):1188-97.
414. Venere M, Hamerlik P, Wu Q, Rasmussen RD, Song LA, Vasanji A, et al. Therapeutic targeting of constitutive PARP activation compromises stem cell phenotype and survival of glioblastoma-initiating cells. Cell Death Differ. 2014;21(2):258-69.
415. Lugli N, Kamileri I, Halazonetis TD. PARP inhibitors and IR join forces to strike glioblastoma-initiating cells. Cell Death Differ. 2014;21(2):192-3.
416. Farmer H, McCabe N, Lord CJ, Tutt AN, Johnson DA, Richardson TB, et al. Targeting the DNA repair defect in BRCA mutant cells as a therapeutic strategy. Nature. 2005;434(7035):917-21.
417. Bryant HE, Schultz N, Thomas HD, Parker KM, Flower D, Lopez E, et al. Specific killing of BRCA2-deficient tumours with inhibitors of poly(ADP-ribose) polymerase. Nature. 2005;434(7035):913-7.
418. McEllin B, Camacho CV, Mukherjee B, Hahm B, Tomimatsu N, Bachoo RM, et al. PTEN loss compromises homologous recombination repair in astrocytes: implications for glioblastoma therapy with temozolomide or poly(ADP-ribose) polymerase inhibitors. Cancer Res. 2010;70(13):5457-64.

419. Sulkowski PL, Corso CD, Robinson ND, Scanlon SE, Purshouse KR, Bai H, et al. 2-Hydroxyglutarate produced by neomorphic IDH mutations suppresses homologous recombination and induces PARP inhibitor sensitivity. Sci Transl Med. 2017;9(375).
420. Lu Y, Kwintkiewicz J, Liu Y, Tech K, Frady LN, Su YT, et al. Chemosensitivity of IDH1-Mutated Gliomas Due to an Impairment in PARP1-Mediated DNA Repair. Cancer Res. 2017;77(7):1709-18.
421. IDH-Mutant Tumors Vulnerable to PARP Inhibition. Cancer Discov. 2017;7(4):OF4.
422. Lord CJ, Ashworth A. The DNA damage response and cancer therapy. Nature. 2012;481(7381):287-94.
423. Bochum S, Berger S, Martens UM. Olaparib. In: Martens UM, editor. Small Molecules in Oncology. Cham: Springer International Publishing; 2018. p. 217-33.
424. Montemorano L, Lightfoot MD, Bixel K. Role of Olaparib as Maintenance Treatment for Ovarian Cancer: The Evidence to Date. Onco Targets Ther. 2019;12:11497-506.
425. Zhu T, Zheng JY, Huang LL, Wang YH, Yao DF, Dai HB. Human PARP1 substrates and regulators of its catalytic activity: An updated overview. Front Pharmacol. 2023;14:1137151.
426. Ledermann JA, Drew Y, Kristeleit RS. Homologous recombination deficiency and ovarian cancer. Eur J Cancer. 2016;60:49-58.
427. Kondrashova O, Topp M, Nesic K, Lieschke E, Ho GY, Harrell MI, et al. Methylation of all BRCA1 copies predicts response to the PARP inhibitor rucaparib in ovarian carcinoma. Nat Commun. 2018;9(1):3970.
428. Zhang S, Royer R, Li S, McLaughlin JR, Rosen B, Risch HA, et al. Frequencies of BRCA1 and BRCA2 mutations among 1,342 unselected patients with invasive ovarian cancer. Gynecol Oncol. 2011;121(2):353-7.
429. Arora S, Balasubramaniam S, Zhang H, Berman T, Narayan P, Suzman D, et al. FDA Approval Summary: Olaparib Monotherapy or in Combination with Bevacizumab for the Maintenance Treatment of Patients with Advanced Ovarian Cancer. Oncologist. 2021;26(1):e164-e72.
430. Banerjee S, Moore KN, Colombo N, Scambia G, Kim BG, Oaknin A, et al. Maintenance olaparib for patients with newly diagnosed advanced ovarian cancer and a BRCA mutation (SOLO1/GOG 3004): 5-year follow-up of a randomised, double-blind, placebo-controlled, phase 3 trial. Lancet Oncol. 2021;22(12):1721-31.
431. DiSilvestro P, Banerjee S, Colombo N, Scambia G, Kim BG, Oaknin A, et al. Overall Survival With Maintenance Olaparib at a 7-Year Follow-Up in Patients With Newly Diagnosed Advanced Ovarian Cancer and a BRCA Mutation: The SOLO1/GOG 3004 Trial. J Clin Oncol. 2023;41(3):609-17.
432. Ray-Coquard I, Leary A, Pignata S, Cropet C, Gonzalez-Martin A, Marth C, et al. Olaparib plus bevacizumab first-line maintenance in ovarian cancer: final overall survival results from the PAOLA-1/ENGOT-ov25 trial. Ann Oncol. 2023;34(8):681-92.
433. Sim HW, Galanis E, Khasraw M. PARP Inhibitors in Glioma: A Review of Therapeutic Opportunities. Cancers (Basel). 2022;14(4).
434. Cairns RA, Mak TW. Oncogenic isocitrate dehydrogenase mutations: mechanisms, models, and clinical opportunities. Cancer Discov. 2013;3(7):730-41.
435. Bao S, Wu Q, McLendon RE, Hao Y, Shi Q, Hjelmeland AB, et al. Glioma stem cells promote radioresistance by preferential activation of the DNA damage response. Nature. 2006;444(7120):756-60.

436. Carruthers RD, Ahmed SU, Ramachandran S, Strathdee K, Kurian KM, Hedley A, et al. Replication Stress Drives Constitutive Activation of the DNA Damage Response and Radioresistance in Glioblastoma Stem-like Cells. Cancer Res. 2018;78(17):5060-71.
437. Ali M, Kamjoo M, Thomas HD, Kyle S, Pavlovska I, Babur M, et al. The clinically active PARP inhibitor AG014699 ameliorates cardiotoxicity but does not enhance the efficacy of doxorubicin, despite improving tumor perfusion and radiation response in mice. Mol Cancer Ther. 2011;10(12):2320-9.
438. Tentori L, Lacal PM, Muzi A, Dorio AS, Leonetti C, Scarsella M, et al. Poly(ADP-ribose) polymerase (PARP) inhibition or PARP-1 gene deletion reduces angiogenesis. Eur J Cancer. 2007;43(14):2124-33.
439. Albert JM, Cao C, Kim KW, Willey CD, Geng L, Xiao D, et al. Inhibition of poly(ADP-ribose) polymerase enhances cell death and improves tumor growth delay in irradiated lung cancer models. Clin Cancer Res. 2007;13(10):3033-42.
440. Appelboom G, Detappe A, LoPresti M, Kunjachan S, Mitrasinovic S, Goldman S, et al. Stereotactic modulation of blood-brain barrier permeability to enhance drug delivery. Neuro Oncol. 2016;18(12):1601-9.
441. Hanna C, Kurian KM, Williams K, Watts C, Jackson A, Carruthers R, et al. Pharmacokinetics, safety, and tolerability of olaparib and temozolomide for recurrent glioblastoma: results of the phase I OPARATIC trial. Neuro Oncol. 2020;22(12):1840-50.
442. Bindra RS. Penetrating the brain tumor space with DNA damage response inhibitors. Neuro Oncol. 2020;22(12):1718-20.
443. Sun K, Mikule K, Wang Z, Poon G, Vaidyanathan A, Smith G, et al. A comparative pharmacokinetic study of PARP inhibitors demonstrates favorable properties for niraparib efficacy in preclinical tumor models. Oncotarget. 2018;9(98):37080-96.
444. Fulton B, Short SC, James A, Nowicki S, McBain C, Jefferies S, et al. PARADIGM-2: Two parallel phase I studies of olaparib and radiotherapy or olaparib and radiotherapy plus temozolomide in patients with newly diagnosed glioblastoma, with treatment stratified by MGMT status. Clin Transl Radiat Oncol. 2018;8:12-6.
445. Chen J, Li Y, Yu TS, McKay RM, Burns DK, Kernie SG, et al. A restricted cell population propagates glioblastoma growth after chemotherapy. Nature. 2012;488(7412):522-6.
446. Lan X, Jorg DJ, Cavalli FMG, Richards LM, Nguyen LV, Vanner RJ, et al. Fate mapping of human glioblastoma reveals an invariant stem cell hierarchy. Nature. 2017;549(7671):227-32.
447. Liau BB, Sievers C, Donohue LK, Gillespie SM, Flavahan WA, Miller TE, et al. Adaptive Chromatin Remodeling Drives Glioblastoma Stem Cell Plasticity and Drug Tolerance. Cell Stem Cell. 2017;20(2):233-46 e7.
448. Cloughesy TF, Yoshimoto K, Nghiemphu P, Brown K, Dang J, Zhu S, et al. Antitumor activity of rapamycin in a Phase I trial for patients with recurrent PTEN-deficient glioblastoma. PLoS Med. 2008;5(1):e8.
449. Zhu H, Acquaviva J, Ramachandran P, Boskovitz A, Woolfenden S, Pfannl R, et al. Oncogenic EGFR signaling cooperates with loss of tumor suppressor gene functions in gliomagenesis. Proc Natl Acad Sci U S A. 2009;106(8):2712-6.
450. Mukasa A, Wykosky J, Ligon KL, Chin L, Cavenee WK, Furnari F. Mutant EGFR is required for maintenance of glioma growth in vivo, and its ablation leads to escape from receptor dependence. Proc Natl Acad Sci U S A. 2010;107(6):2616-21.
451. Ghosh D, Nandi S, Bhattacharjee S. Combination therapy to checkmate Glioblastoma: clinical challenges and advances. Clin Transl Med. 2018;7(1):33.

452. Fabro F, Lamfers MLM, Leenstra S. Advancements, Challenges, and Future Directions in Tackling Glioblastoma Resistance to Small Kinase Inhibitors. Cancers (Basel). 2022;14(3).
453. Stein GH. T98G: an anchorage-independent human tumor cell line that exhibits stationary phase G1 arrest in vitro. J Cell Physiol. 1979;99(1):43-54.
454. Langdon SP, Lawrie SS, Hay FG, Hawkes MM, McDonald A, Hayward IP, et al. Characterization and properties of nine human ovarian adenocarcinoma cell lines. Cancer Res. 1988;48(21):6166-72.
455. Jean-Claude B, Rachid Z, Brahimi F. Combi-molecules having EGFR and DNA targeting properties. Google Patents; 2011.
456. Forgie BN, Prakash R, Goyeneche AA, Telleria CM. Vitality, viability, long-term clonogenic survival, cytotoxicity, cytostasis and lethality: what do they mean when testing new investigational oncology drugs? Discov Oncol. 2024;15(1):5.
457. Tada H, Shiho O, Kuroshima K, Koyama M, Tsukamoto K. An improved colorimetric assay for interleukin 2. J Immunol Methods. 1986;93(2):157-65.
458. Freeburg EM, Goyeneche AA, Seidel EE, Telleria CM. Resistance to cisplatin does not affect sensitivity of human ovarian cancer cell lines to mifepristone cytotoxicity. Cancer Cell Int. 2009;9:4.
459. Franken NA, Rodermond HM, Stap J, Haveman J, van Bree C. Clonogenic assay of cells in vitro. Nat Protoc. 2006;1(5):2315-9.
460. Michalski R, Thiebaut D, Michalowski B, Ayhan MM, Hardy M, Ouari O, et al. Oxidation of ethidium-based probes by biological radicals: mechanism, kinetics and implications for the detection of superoxide. Sci Rep. 2020;10(1):18626.
461. Chou TC, Talalay P. Quantitative analysis of dose-effect relationships: the combined effects of multiple drugs or enzyme inhibitors. Adv Enzyme Regul. 1984;22:27-55.
462. Abdalbari FH, Martinez-Jaramillo E, Forgie BN, Tran E, Zorychta E, Goyeneche AA, et al. Auranofin Induces Lethality Driven by Reactive Oxygen Species in High-Grade Serous Ovarian Cancer Cells. Cancers (Basel). 2023;15(21).
463. Gamberi T, Chiappetta G, Fiaschi T, Modesti A, Sorbi F, Magherini F. Upgrade of an old drug: Auranofin in innovative cancer therapies to overcome drug resistance and to increase drug effectiveness. Med Res Rev. 2022;42(3):1111-46.
464. Rigobello MP, Scutari G, Boscolo R, Bindoli A. Induction of mitochondrial permeability transition by auranofin, a gold(I)-phosphine derivative. Br J Pharmacol. 2002;136(8):1162-8.
465. Seo MJ, Kim IY, Lee DM, Park YJ, Cho MY, Jin HJ, et al. Dual inhibition of thioredoxin reductase and proteasome is required for auranofin-induced paraptosis in breast cancer cells. Cell Death Dis. 2023;14(1):42.
466. Sze JH, Raninga PV, Nakamura K, Casey M, Khanna KK, Berners-Price SJ, et al. Anticancer activity of a Gold(I) phosphine thioredoxin reductase inhibitor in multiple myeloma. Redox Biol. 2020;28:101310.
467. You BR, Park WH. Auranofin induces mesothelioma cell death through oxidative stress and GSH depletion. Oncol Rep. 2016;35(1):546-51.
468. Kalyanaraman B. NAC, NAC, Knockin' on Heaven's door: Interpreting the mechanism of action of N-acetylcysteine in tumor and immune cells. Redox Biol. 2022;57:102497.
469. Prigent SA, Nagane M, Lin H, Huvar I, Boss GR, Feramisco JR, et al. Enhanced tumorigenic behavior of glioblastoma cells expressing a truncated epidermal growth factor receptor is mediated through the Ras-Shc-Grb2 pathway. J Biol Chem. 1996;271(41):25639-45.

470. Liu N, Huang H, Dou QP, Liu J. Inhibition of 19S proteasome-associated deubiquitinases by metal-containing compounds. Oncoscience. 2015;2(5):457-66.
471. Habermann KJ, Grunewald L, van Wijk S, Fulda S. Targeting redox homeostasis in rhabdomyosarcoma cells: GSH-depleting agents enhance auranofin-induced cell death. Cell Death Dis. 2017;8(10):e3067.
472. Han Y, Chen P, Zhang Y, Lu W, Ding W, Luo Y, et al. Synergy between Auranofin and Celecoxib against Colon Cancer In Vitro and In Vivo through a Novel Redox-Mediated Mechanism. Cancers (Basel). 2019;11(7).
473. Toledano MB, Delaunay-Moisan A, Outten CE, Igbaria A. Functions and cellular compartmentation of the thioredoxin and glutathione pathways in yeast. Antioxid Redox Signal. 2013;18(13):1699-711.
474. Du Y, Zhang H, Zhang X, Lu J, Holmgren A. Thioredoxin 1 is inactivated due to oxidation induced by peroxiredoxin under oxidative stress and reactivated by the glutaredoxin system. J Biol Chem. 2013;288(45):32241-7.
475. Muri J, Thut H, Heer S, Krueger CC, Bornkamm GW, Bachmann MF, et al. The thioredoxin-1 and glutathione/glutaredoxin-1 systems redundantly fuel murine B-cell development and responses. Eur J Immunol. 2019;49(5):709-23.
476. Gencheva R, Arnér ESJ. Thioredoxin Reductase Inhibition for Cancer Therapy. Annu Rev Pharmacol Toxicol. 2022;62:177-96.
477. Lei XG, Zhu JH, Cheng WH, Bao Y, Ho YS, Reddi AR, et al. Paradoxical Roles of Antioxidant Enzymes: Basic Mechanisms and Health Implications. Physiol Rev. 2016;96(1):307-64.
478. Fan Z, Wirth AK, Chen D, Wruck CJ, Rauh M, Buchfelder M, et al. Nrf2-Keap1 pathway promotes cell proliferation and diminishes ferroptosis. Oncogenesis. 2017;6(8):e371.
479. Rojo de la Vega M, Chapman E, Zhang DD. NRF2 and the Hallmarks of Cancer. Cancer Cell. 2018;34(1):21-43.
480. Wang J, Li M, Cui X, Lv D, Jin L, Khan M, et al. Brevilin A promotes oxidative stress and induces mitochondrial apoptosis in U87 glioblastoma cells. Onco Targets Ther. 2018;11:7031-40.
481. Schonberg SA, Rudra PK, Noding R, Skorpen F, Bjerve KS, Krokan HE. Evidence that changes in Se-glutathione peroxidase levels affect the sensitivity of human tumour cell lines to n-3 fatty acids. Carcinogenesis. 1997;18(10):1897-904.
482. Marengo B, De Ciucis C, Verzola D, Pistoia V, Raffaghello L, Patriarca S, et al. Mechanisms of BSO (L-buthionine-S,R-sulfoximine)-induced cytotoxic effects in neuroblastoma. Free Radic Biol Med. 2008;44(3):474-82.
483. Armstrong JS, Steinauer KK, Hornung B, Irish JM, Lecane P, Birrell GW, et al. Role of glutathione depletion and reactive oxygen species generation in apoptotic signaling in a human B lymphoma cell line. Cell Death Differ. 2002;9(3):252-63.
484. Zhu Z, Du S, Du Y, Ren J, Ying G, Yan Z. Glutathione reductase mediates drug resistance in glioblastoma cells by regulating redox homeostasis. J Neurochem. 2018;144(1):93-104.
485. Mendoza MC, Er EE, Blenis J. The Ras-ERK and PI3K-mTOR pathways: cross-talk and compensation. Trends Biochem Sci. 2011;36(6):320-8.
486. Pearson JRD, Regad T. Targeting cellular pathways in glioblastoma multiforme. Signal Transduct Target Ther. 2017;2:17040.
487. Jackman DM, Holmes AJ, Lindeman N, Wen PY, Kesari S, Borras AM, et al. Response and resistance in a non-small-cell lung cancer patient with an epidermal growth factor receptor

mutation and leptomeningeal metastases treated with high-dose gefitinib. J Clin Oncol. 2006;24(27):4517-20.
488. Zeng YD, Liao H, Qin T, Zhang L, Wei WD, Liang JZ, et al. Blood-brain barrier permeability of gefitinib in patients with brain metastases from non-small-cell lung cancer before and during whole brain radiation therapy. Oncotarget. 2015;6(10):8366-76.
489. Bykov VJN, Eriksson SE, Bianchi J, Wiman KG. Targeting mutant p53 for efficient cancer therapy. Nat Rev Cancer. 2018;18(2):89-102.
490. Walz DT, DiMartino MJ, Griswold DE, Intoccia AP, Flanagan TL. Biologic actions and pharmacokinetic studies of auranofin. Am J Med. 1983;75(6A):90-108.
491. Karsa M, Kosciolek A, Bongers A, Mariana A, Failes T, Gifford AJ, et al. Exploiting the reactive oxygen species imbalance in high-risk paediatric acute lymphoblastic leukaemia through auranofin. Br J Cancer. 2021;125(1):55-64.
492. Jakstys B, Ruzgys P, Tamosiunas M, Satkauskas S. Different Cell Viability Assays Reveal Inconsistent Results After Bleomycin Electrotransfer In Vitro. J Membr Biol. 2015;248(5):857-63.
493. Patwardhan RS, Sharma D, Sandur SK. Thioredoxin reductase: An emerging pharmacologic target for radiosensitization of cancer. Transl Oncol. 2022;17:101341.
494. Zhang SP, Zhou J, Fan QZ, Lv XM, Wang T, Wang F, et al. Discovery of hydroxytyrosol as thioredoxin reductase 1 inhibitor to induce apoptosis and G(1)/S cell cycle arrest in human colorectal cancer cells via ROS generation. Exp Ther Med. 2021;22(2):829.
495. Lee SR, Kwon KS, Kim SR, Rhee SG. Reversible inactivation of protein-tyrosine phosphatase 1B in A431 cells stimulated with epidermal growth factor. J Biol Chem. 1998;273(25):15366-72.
496. Reynolds AR, Tischer C, Verveer PJ, Rocks O, Bastiaens PI. EGFR activation coupled to inhibition of tyrosine phosphatases causes lateral signal propagation. Nat Cell Biol. 2003;5(5):447-53.
497. Meng TC, Fukada T, Tonks NK. Reversible oxidation and inactivation of protein tyrosine phosphatases in vivo. Mol Cell. 2002;9(2):387-99.
498. Dagnell M, Pace PE, Cheng Q, Frijhoff J, Ostman A, Arner ESJ, et al. Thioredoxin reductase 1 and NADPH directly protect protein tyrosine phosphatase 1B from inactivation during H(2)O(2) exposure. J Biol Chem. 2017;292(35):14371-80.
499. Mohapatra B, Ahmad G, Nadeau S, Zutshi N, An W, Scheffe S, et al. Protein tyrosine kinase regulation by ubiquitination: critical roles of Cbl-family ubiquitin ligases. Biochim Biophys Acta. 2013;1833(1):122-39.
500. Swaminathan G, Tsygankov AY. The Cbl family proteins: ring leaders in regulation of cell signaling. J Cell Physiol. 2006;209(1):21-43.
501. Khan EM, Heidinger JM, Levy M, Lisanti MP, Ravid T, Goldkorn T. Epidermal growth factor receptor exposed to oxidative stress undergoes Src- and caveolin-1-dependent perinuclear trafficking. J Biol Chem. 2006;281(20):14486-93.
502. Ravid T, Heidinger JM, Gee P, Khan EM, Goldkorn T. c-Cbl-mediated ubiquitinylation is required for epidermal growth factor receptor exit from the early endosomes. J Biol Chem. 2004;279(35):37153-62.
503. Ravid T, Sweeney C, Gee P, Carraway KL, 3rd, Goldkorn T. Epidermal growth factor receptor activation under oxidative stress fails to promote c-Cbl mediated down-regulation. J Biol Chem. 2002;277(34):31214-9.

504. Fazzari F, Chow S, Cheung M, Barghout SH, Schimmer AD, Chang Q, et al. Combined Targeting of the Glutathione and Thioredoxin Antioxidant Systems in Pancreatic Cancer. ACS Pharmacol Transl Sci. 2022;5(11):1070-8.